TECHNISCHE UNIVERSITÄT WIEN

Dissertation

Holographic QCD and the Anomalous Magnetic Moment of the Muon

ausgeführt zum Zwecke der Erlangung des akademischen Grades eines Doktors der technischen Wissenschaften

unter der Anleitung von

Univ.-Prof. Dr. Anton Rebhan
Institut für Theoretische Physik (E136)
TU Wien

eingereicht an der Technischen Universität, Fakultät für Physik

von

Dipl.-Ing. Josef Leutgeb
Matrikelnummer: 1227402

begutachtet von

Prof. Dr. Francesco Bigazzi INFN Florenz	Ass.-Prof. Priv.-Doz. Dr. Massimiliano Procura Universität Wien

Josef Leutgeb

Holographic QCD and the Anomalous Magnetic Moment of the Muon

Gutachter: Francesco Bigazzi und Massimiliano Procura

Betreuer: Anton Rebhan

TU Wien

Institut für Theoretische Physik

Wiedner Hauptstrasse 8-10/E136

A-1040, Wien

To my son Josef.

Kurzfassung

"Was sagt uns die holographische QCD über das anomale magnetische Moment des Myons?"

Vor kurzem hat die Myon $g-2$ Kollaboration am Fermilab eine langjährige Abweichung zwischen dem Experiment und der Vorhersage des Standardmodells der Teilchenphysik bestätigt. Mit 4.2σ steht man mit dieser fesselnden Diskrepanz eventuell kurz vor einer Entdeckung und könnte Beweise für Physik jenseits des Standardmodells finden. Neben experimentellen Verbesserungen wird es entscheidend sein, die Unsicherheiten in der aktuellen theoretischen Vorhersage zu verringern. Während QED und elektroschwache Effekte unter guter Kontrolle sind, wird der Fehler von hadronischen Beiträgen dominiert. Aufgrund der nicht perturbativen Natur der QCD ist eine erste prinzipielle Berechnung dieser Beiträge äußerst schwierig und man muss sich auf Gitter-QCD, den dispersiven Ansatz oder auf Modelle mit hadronischen Freiheitsgraden verlassen.

Eine Klasse besonders interessanter hadronischer Modelle bietet die holographische QCD. Unter Verwendung der stringtheoretisch motivierten Dualität zwischen Eich- und Gravitationstheorien verbindet sie eine stark gekoppelte Quantenfeldtheorie in D-Dimensionen mit einer schwach gekoppelten Gravitationstheorie in $D+1$-Dimensionen. Da bisher kein exaktes Gravitationsdual der QCD bekannt ist, ist man auf Modelle angewiesen, die in bestimmten Eigenschaften der QCD ähneln. Mit einigen der einfacheren holographischen QCD-Modelle ist es möglich, Confinement, chirale Symmetriebrechung, das Spektrum und die Wechselwirkungen von Hadronen und andere nichttriviale Merkmale mit nur einem minimalen Satz freier Parameter mit überraschender Genauigkeit zu beschreiben.

Um die einleitende Frage zu beantworten, berechnen wir mehrere holographische Vorhersagen für das anomale magnetische Moment des Myons. Während holographische Modelle nicht mit der subprozentualen Genauigkeit des dispersiven Ansatzes beim Beitrag der hadronischen Vakuumpolarisation konkurrieren können, gewinnen wir einige wertvolle Einblicke in den Beitrag der hadronischen Licht-an-Licht-Streuung, bei dem der aktuelle Fehler ungefähr 20% beträgt. Mithilfe der holographischen Modelle gelingt es, eine wichtige offene Frage zur Implementierung der von Melnikov und Vainshtein eingeführten Einschränkung für kurze Distanzen zu

lösen, wobei Axialvektormesonen eine zentrale Rolle spielen. Darüber hinaus berechnen wir ohne Einführung zusätzlicher freier Parameter den Beitrag von Glueballs zur Licht-an-Licht-Streuung, der sich selbst nach dem Auffinden überraschend großer Glueball-Photonen-Kopplungen beim aktuellen Präzisionsziel als vernachlässigbar herausstellt.

Abstract

"What does holographic QCD tell us about the anomalous magnetic moment of the muon?"

Recently, the Muon $g-2$ Collaboration at Fermilab has confirmed a long-standing discrepancy between the experiment and the prediction of the Standard Model of particle physics. At 4.2σ, this captivating disagreement is close to a discovery and may give evidence for physics beyond the Standard Model. Besides experimental improvements, it will be crucial to reduce the current uncertainties in the theoretical prediction. While QED and electroweak effects are under good control, the error is dominated by hadronic contributions. Due to the nonperturbative nature of QCD, a first principle calculation of these contributions is exceedingly difficult and one has to rely on lattice QCD, the dispersive approach or on models with hadronic degrees of freedom.

A class of particularly interesting hadronic models is given by holographic QCD. Using the string-theoretically motivated Gauge/Gravity duality, it relates a strongly coupled quantum field theory in D dimensions to a weakly coupled theory of gravity in $D+1$ dimensions. Since up to date no exact gravity dual of QCD is known, one has to rely on models that resemble QCD in certain properties. Using some of the simpler holographic QCD models it is possible to describe confinement, chiral symmetry breaking, the spectrum and interactions of hadrons, and other nontrivial features with only a minimal set of free parameters at a surprising accuracy.

To address the introductory question, we calculate several holographic predictions for the anomalous magnetic moment of the muon. While holographic models cannot compete with the sub percent accuracy of the dispersive approach in the hadronic vacuum polarization contribution, we derive some valuable insights in the hadronic light-by-light scattering contribution, where the current error is roughly 20%. Most importantly, we resolve an open question on the implementation of the short-distance constraint introduced by Melnikov and Vainshtein, emphasizing the role of axial-vector mesons. Furthermore, without introducing additional free parameters, we calculate the contribution of glueballs to light-by-light scattering, which even after finding surprisingly large glueball-photon couplings turns out to be negligible at the current precision goal.

Acknowledgements

Without the support of many remarkable people this thesis would not have been possible. This page is dedicated to them.

First and foremost, I am extremely grateful to my supervisor **Anton Rebhan** who gave me the opportunity to pursue my PhD studies. His relentless support and advice was invaluable.

I would also like to thank **Frederic Brünner** from whom I learned a lot in the beginning of my PhD studies. Likewise, it was a great pleasure to work with **Florian Hechenberger** and **Jonas Mager**.

Thanks also to the **Doktoratskolleg Particles and Interactions – DKPI** for all the benefits I received via the summer schools, retreats, and special travel opportunities such as a three-month stay at INFN Florence. I am very grateful to **Francesco Bigazzi** and **Aldo Cotrone** for making my time in Florence very exciting and enjoyable.

I very much appreciate all the colleagues I shared an office with. **Christian Ecker**, **David Müller**, **Alexander Soloviev**, **Ayan Mukhopadhyay**, **Florian Preis**, **Stephan Stetina** and **Kirill Boguslavski**. Thank you for the stimulating discussions. I also greatly benefited from enlightening discussions with my colleagues **David Andriot**, **Daniel Grumiller**, **Andreas Ipp**, **Jan Lüdtke**, **Massimiliano Procura**, **Harald Skarke**, **Tim Wrase** and **Raphaela Wutte**.

Special thanks also to my collaborators **Lorenzo Bartolini**, **Sven Bjarke Gudnason**, **Piotr Lebiedowicz**, **Otto Nachtmann** and **Antoni Szczurek** for inspiring and fruitful interactions.

Finally, I want to thank my family, most and foremost my mother **Helga Leutgeb** and my partner **Sophie Wagner** for their unrelenting support.

Contents

List of Figures

List of Tables

List of Publications

This thesis is based on the publications:

[I] J. **Leutgeb**, J. **Mager** and A. **Rebhan**
Holographic QCD and the muon anomalous magnetic moment
Eur. Phys. J. C **81** (2021) 1008, [2110.07458]

[II] J. **Leutgeb** and A. **Rebhan**
Hadronic light-by-light contribution to the muon $g-2$ from holographic QCD with massive pions
Phys. Rev. D **104** (2021) 094017, [2108.12345]

[III] P. **Lebiedowicz**, J. **Leutgeb**, O. **Nachtmann**. A. **Rebhan** and A. **Szczurek**
Central exclusive diffractive production of axial-vector $f_1(1285)$ and $f_1(1420)$ mesons in proton-proton collisions
Phys. Rev. D **102** (2020) 114003, [2008.07452]

[IV] J. **Leutgeb** and A. **Rebhan**
Axial vector transition form factors in holographic QCD and their contribution to the anomalous magnetic moment of the muon
Phys. Rev. D **101** (2020) 114015, [1912.01596]

[V] J. **Leutgeb** and A. **Rebhan**
Witten-Veneziano mechanism and pseudoscalar glueball-meson mixing in holographic QCD
Phys. Rev. D **101** (2020) 014006, [1909.12352]

[VI] J. **Leutgeb**, J. **Mager** and A. **Rebhan**
Pseudoscalar transition form factors and the hadronic light-by-light contribution to the anomalous magnetic moment of the muon from holographic QCD
Phys. Rev. D **100** (2019) 094038, [1906.11795]

[VII] F. **Brünner**, J. **Leutgeb** and A. **Rebhan**
A broad pseudovector glueball from holographic QCD
Phys. Lett. B **788** (2019) 431–435, [1807.10164]

Parts of the results have been published in the following conference proceedings articles:

[VIII] P. **Lebiedowicz**, J. **Leutgeb**, O. **Nachtmann**. A. **Rebhan** and A. **Szczurek**
Central exclusive diffractive production of axial-vector f_1 mesons in proton-proton collisions
28th International Workshop on Deep Inelastic Scattering and Related Subjects, 7, 2021, [2107.13940]

[IX] J. **Leutgeb** and A. **Rebhan**
Axial vector transition form factors in holographic QCD and their contribution to the muon $g-2$
PoS **ICHEP2020** (2021) 671, [2012.06514]

[X] P. **Lebiedowicz**, J. **Leutgeb**, O. **Nachtmann**. A. **Rebhan** and A. **Szczurek**
Central exclusive production of axial-vector f_1 mesons in proton-proton collisions
PoS **ICHEP2020** (2021) 492, [2012.03563]

0 Introduction

> *There are only two ways to live your life. One is as though nothing is a miracle. The other is as though everything is a miracle.*
>
> **— Albert Einstein**
> Physicist

SINCE the first measurement with sufficient accuracy at the Brookhaven National Laboratory (BNL) [1], there is a long-standing discrepancy between the theoretical and experimental prediction of the anomalous magnetic moment of the muon $a_\mu = (g-2)_\mu/2$, where the current Standard Model (SM) prediction according to the White Paper of the Muon $g-2$ Theory Initiative [2] is

$$a_\mu^{\text{SM}} = 116\,591\,810(43) \times 10^{-11}. \tag{0.1}$$

The discrepancy was only recently amplified by a measurement of the Fermilab Muon $g-2$ collaboration [3] raising it from 3.7σ to 4.2σ when combined with the earlier BNL result to the experimental average

$$a_\mu^{\text{exp}} = 116\,592\,061(41) \times 10^{-11}. \tag{0.2}$$

Since this discrepancy cannot be explained in the Standard Model, it gives hints at new physics. However, to claim a discovery, it is necessary to improve the significance even further. While there are future prospects of decreasing the experimental uncertainty by additional runs at the Fermilab and by an entirely different approach in the future J-PARC experiment [4], on the theoretical side the focus will be on the two hadronic contributions dominating the error of the prediction.

Out of the two, the larger error is due to the hadronic vacuum polarization (HVP) currently estimated to give the contribution [2]

$$a_\mu^{\text{HVP}} = 6\,845(40) \times 10^{-11}. \tag{0.3}$$

Given its overall size, the estimated error is at only 0.6%, which however has been recently challenged by a lattice calculation [5] claiming a 2% higher value with comparable accuracy. If true, this would reduce the $g-2$ discrepancy to 1.5σ, but very likely give rise to tensions in other sectors of the SM [6, 7, 8, 9].

The second-largest error is in the hadronic light-by-light scattering (HLbL) contribution with a 20% uncertainty

$$a_\mu^{\mathrm{HLbL}} = 92(18) \times 10^{-11}, \tag{0.4}$$

according to Ref. [2]. Since the data-driven approach is limited for this contribution, estimating the various channels also relies on hadronic models.

Holographic QCD is a particularly interesting approach of constructing hadronic models that emerged from one of the most important theoretical developments of the last few decades: the AdS/CFT (Anti-de-Sitter/Conformal Field Theory) correspondence [10]. Realizing a duality between gauge theories and theories of gravity, it allows to study strongly coupled gauge theories by a weakly coupled gravity dual with one additional spacetime dimension. However, since QCD is not conformal, a potential gravity dual needs to, among others, incorporate confinement and chiral symmetry breaking.

The two main approaches to constructing holographic QCD models are the top-down and the bottom-up approach. The top-down approach is based on D-brane configurations in string theory, which are supposed to be dual to theories with certain features of QCD. One of the most popular models, the Sakai-Sugimoto model [11, 12], is based on a 10-dimensional D4-brane solution [13] breaking supersymmetry and conformal invariance. The bottom-up approach, on the other hand, is unconstrained by string theory. Some of the simpler models utilize a 5-dimensional AdS space deformed in the infrared region either by a hard-wall [14, 15] or by a soft-wall cutoff [16] to model nonperturbative effects of QCD.

In this thesis, we apply holographic QCD to study the anomalous magnetic moment of the muon.

Thesis Structure

This thesis is structured in five parts, which will be summarized in the following. Also mentioned are the previous publications of the author on which they are based on.

Part I

The first part will serve as a brief introduction to the anomalous magnetic moment of the muon. After reviewing the status of the anomalous magnetic moment of the electron, the muon and the tauon, we will present the Standard Model prediction for the muon as compiled by the Muon $g-2$ Theory Initiative and introduce important short-distance constraints for the hadronic light-by-light scattering contribution.

Part II

In the second part of this thesis, we will introduce holographic QCD, an application of the gauge/gravity duality. First, we will introduce the AdS/CFT correspondence, mapping strongly coupled gauge theories to weakly coupled theories with gravity. Then we will study applications of this duality to strongly coupled QCD, in particular the Sakai-Sugimoto model and various bottom-up models.

Part III

Based on Refs. [I, II, IV, VI]

The third part will present results obtained from holographic QCD on the anomalous magnetic moment of the muon, in particular on the hadronic light-by-light scattering contribution. To start, we will calculate the pseudoscalar-pole contribution using holographic predictions for the pion transition form factor. Then, we will turn to the contribution of axial-vector mesons and show how they can be used to satisfy a class of important short-distance constraints. Finally, we will consider predictions from holographic models with finite quark masses.

Part IV

Based on Ref. [V]

In the fourth part of this thesis, we will turn to glueballs with the eventual aim of estimating their effect on the anomalous magnetic moment of the muon. To do so, we will consider the Sakai-Sugimoto model, which has a clear realization of glueballs reviewed in the first chapter. Then, we will study the pseudoscalar glueball, which plays an important role in the Witten-Veneziano mechanism, and calculate its decay rates. Next, we will use the model's vector meson dominance to study glueball-photon interactions and finally to estimate their contribution to the anomalous magnetic moment of the muon.

Part V - Appendices

Based on Refs. [III, VII]

The fifth part will not only collect all the appendices of the previous parts, but will also present two of the author's publications not fitting into the main theme of the thesis but presenting experimentally testable predictions that result from the same sector of the Sakai-Sugimoto model that is responsible for the photon-photon-pseudoscalar glueball interaction. The first one concerns decay rates of the pseudovector glueball, while the second one studies central exclusive production of axial-vector mesons in proton-proton scattering.

Part I

Anomalous Magnetic Moment of the Muon

In this part of the thesis, we will briefly introduce the anomalous magnetic moment of leptons and review their status. For the currently most interesting case of the muon, we will then present the Standard Model contributions and predictions as compiled by the Muon $g-2$ Theory Initiative. For the hadronic light-by-light scattering contribution, which contributes the second-largest error to the final estimate and will be studied holographically in the following, we will furthermore introduce important short-distance constraints from perturbative QCD.

1 Lepton Magnetic Moments and their Status

> *There is a theory which states that if ever anyone discovers exactly what the Universe is for and why it is here, it will instantly disappear and be replaced by something even more bizarre and inexplicable.*
>
> *There is another theory which states that this has already happened.*
>
> **— Douglas Adams**
> The Restaurant at the End of the Universe

WHAT is the anomalous magnetic moment of the muon? To answer this question, we first look at the general properties of a lepton. The Standard Model (SM) of particle physics has three charged leptons: the electron (e^-), the muon (μ^-) and the tauon (τ^-), see Fig. 1.1. As charged leptons, they are elementary spin-$1/2$ fermions with electric charge -1 in units of the positron charge e and have flavor-independent coupling constants to gauge bosons. However, electrons, muons, and tauons are not free but interact with other particles which due to their significantly different masses $m_e = 0.511$ MeV, $m_\mu = 105.658$ MeV, and $m_\tau = 1776.99$ MeV effectively leads to very distinct behavior. For example, the electron is a stable particle, the μ is unstable and has a short lifetime of $\tau_\mu = 2.197 \times 10^{-6}$s and the τ is even less stable with $\tau_\tau = 2.906 \times 10^{-13}$s. The μ^- decays almost exclusively into an electron and two neutrinos ($e^-\overline{\nu}_e\nu_\mu$), while the τ^- decays to roughly 65% into hadronic states ($\pi^-\nu_\tau, \pi^-\pi^0\nu_\tau, \dots$) and to about 35% into the two main leptonic decay channels $e^-\overline{\nu}_e\nu_\tau$ and $\mu^-\overline{\nu}_\mu\nu_\tau$ [17].

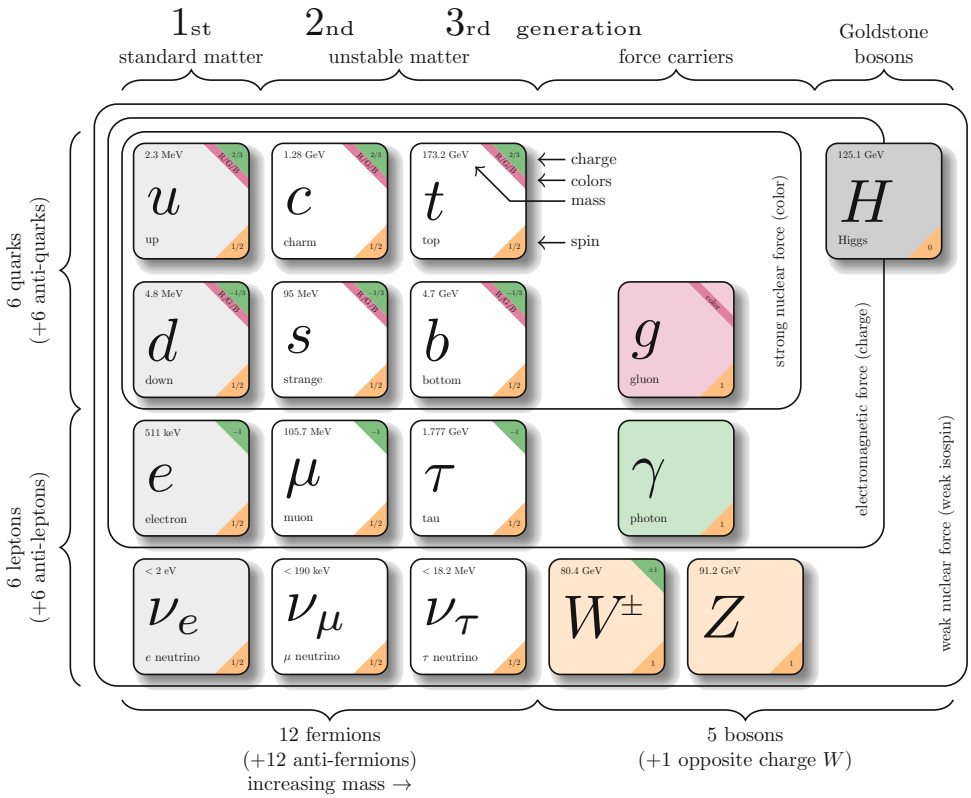

Figure 1.1. – Particles of the Standard Model. Illustration from Ref. [18].

Two other very interesting properties of charged leptons, the magnetic, and electric dipole moments, describe their behavior in electromagnetic fields. This is described by the effective electromagnetic interaction Hamiltonian

$$\mathcal{H} = -\boldsymbol{\mu}_m \cdot \boldsymbol{B} - \boldsymbol{d}_e \cdot \boldsymbol{E}, \tag{1.1}$$

where the magnetic dipole moment $\boldsymbol{\mu}_m$ and the electric dipole moment $\boldsymbol{d}_e$ interact with the magnetic and electric field strengths $\boldsymbol{B}$ and $\boldsymbol{E}$, respectively. However, to use this Hamiltonian the moments have to be known, e.g., by calculating them from first principles.

As an example for a physical effect, let us look at the magnetic dipole moment of an atom where the orbiting lepton with electric charge e, mass m, position $\boldsymbol{r}$ and velocity $\boldsymbol{v}$ creates the orbital magnetic dipole moment

$$\boldsymbol{\mu}_{\text{orbital}} = \frac{e}{2mc}\boldsymbol{L}, \tag{1.2}$$

with the angular momentum $\boldsymbol{L} = m\boldsymbol{r} \times \boldsymbol{v}$. A second contribution to the magnetic dipole moment comes from the spin of the lepton described by the spin operator

$$\boldsymbol{S} = \frac{\hbar\boldsymbol{\sigma}}{2}, \tag{1.3}$$

where σ_i are the Pauli spin matrices and gives the contribution

$$\boldsymbol{\mu}_{\text{spin}} = g_l \frac{e}{2mc}\boldsymbol{S}, \tag{1.4}$$

with the gyromagnetic ratio g_l for the lepton $l = e, \mu, \tau$. Combining the two contributions, the magnetic interaction realizes the (anomalous) Zeeman effect and splits the levels of the atomic spectrum according to

$$\Delta E = \frac{e}{2mc}(\boldsymbol{L} + g_l\boldsymbol{S}) \cdot \boldsymbol{B}. \tag{1.5}$$

This energy difference can be measured in the experiment and can be used to determine the value of g_l, which differs slightly from the classical value of $g_l = 2$. This anomalous contribution is parametrized by

$$a_l \equiv \frac{g_l - 2}{2}, \tag{1.6}$$

the anomalous magnetic moment of the lepton l.

Another effect where the anomalous magnetic moment plays an important role and that is currently used by the $g-2$ Collaboration at Fermilab [3] to measure a_μ is

the Larmor precession of the direction of the lepton spin in electromagnetic fields described by the angular frequency

$$\boldsymbol{\omega}_a = \frac{e}{m}\left[a_\mu \boldsymbol{B} - \left(a_\mu - \frac{1}{\gamma^2 - 1}\right)\boldsymbol{\beta} \times \boldsymbol{E}\right]. \tag{1.7}$$

In the experimental setup, the muons are exposed to a uniform magnetic field $\boldsymbol{B}$ such that they move in a circle and stay confined in a doughnut-shaped storage ring, where an electric quadrupole field $\boldsymbol{E}$ additionally focuses the beam. However, at the so-called magic energy of ~ 3.1 GeV the relativistic Lorentz factor $\gamma_{\text{mag}} \equiv \sqrt{(1+a_\mu)/a_\mu} \approx 29.378$ cancels the effect of the electric field on the precession frequency. This energy also boosts the short muon lifetime $\tau_\mu \approx 2.197 \times 10^{-6}$s by a factor of γ_{mag} and allows for a reasonably sized storage ring with 14m diameter.

1.1 Experimental and Theoretical Status of a_l

Although in the SM the couplings of leptons to gauge bosons are flavor-independent, this lepton universality is broken by quantum effects, such that $a_e \neq a_\mu \neq a_\tau$. In the following, we will briefly review the current status of the three lepton anomalous magnetic moments.

Status of a_e

Currently, the best measurement of a_e, the anomalous magnetic moment of the electron, was performed at Harvard [19] using a Penning trap and yields

$$a_e^{\text{exp}} = 1\,159\,652\,180.73(28) \times 10^{-12}. \tag{1.8}$$

This is likely one of the most precisely known physical quantities [20]. To predict this quantity at a comparable accuracy from theory, one has to include tenth-order QED terms with coefficients $(\alpha/\pi)^5$ to obtain the result [21]:

$$a_e(\alpha_{\text{Cs}}) = 1\,159\,652\,181.606\,(11)(12)(229) \times 10^{-12}. \tag{1.9}$$

The first error comes from the tenth-order QED terms, the second one from hadronic terms, and the last and largest error comes from the uncertainty in determining the fine-structure constant α using atomic interferometry of the Cs atom [22]. Recently, a measurement using the Rb atom [23] improved the accuracy of the fine structure

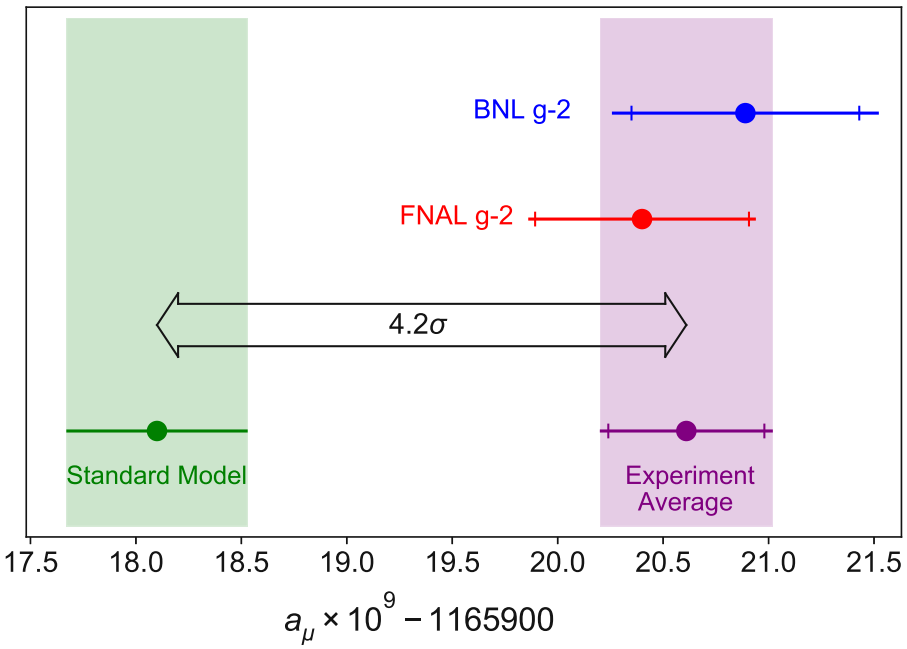

Figure 1.2. – Illustration of the 4.2σ discrepancy between the SM prediction and the experimental average of $(g-2)_\mu$ [3].

constant by a factor of 2.4 and revealed a 5.4σ discrepancy with the Cs measurement. Using this new value of α leads to

$$a_e(\alpha_{\text{Rb}}) = 1\,159\,652\,180.252\,(95) \times 10^{-12}, \tag{1.10}$$

which reduces the discrepancy to the experiment to $\delta a_e \equiv a_e^{\text{exp}} - a_e(\alpha_{\text{Rb}}) = (4.8 \pm 3.0) \times 10^{-13}\,(+1.6\sigma)$ compared to the previous $\delta a_e' \equiv a_e^{\text{exp}} - a_e(\alpha_{\text{Cs}}) = (-8.8 \pm 3.6) \times 10^{-13}\,(-2.4\sigma)$.

Status of a_μ

While the theoretical calculation of the anomalous magnetic moment of the electron is largely dominated by QED contributions, this is no longer true for the much heavier muon ($m_\mu/m_e \approx 200$) since quantum fluctuations including heavier particles with mass M scale as

$$\frac{\delta a_l}{a_l} \propto \frac{m_l^2}{M^2}, \qquad (M \gg m_l). \tag{1.11}$$

To obtain the current theoretical prediction

$$a_\mu^{\text{th}} = 116\,591\,810(43) \times 10^{-11} \tag{1.12}$$

established in the 2020 White Paper of the Muon $g-2$ Theory Initiative [3], it is necessary to consider contributions from the whole Standard Model as will be reviewed in the next chapter.

Comparing this prediction with the recently obtained result

$$a_\mu^{\text{exp}}(\text{FNAL+BNL}) = 116\,592\,061(41) \times 10^{-11} \tag{1.13}$$

of the $g-2$ Collaboration at Fermilab [3] confirms a long-standing discrepancy between the SM and the first experiment with sufficient precision, the E821/BNL experiment [1]. While the Fermilab result on its own reduces the discrepancy from 3.7σ to 3.3σ, combining the two experimental results to the quoted value (1.13) enhances the discrepancy to 4.2σ, see Fig. 1.2.

Since this discrepancy cannot be explained within the Standard Model, it hints to new physics beyond the Standard Model. However, to claim a discovery, it is necessary to establish a 5σ discrepancy. Experimentally, this will be pursued by upcoming improvements of the Fermilab experiment and by an alternative experiment using ultra-cold muons at J-PARC [4] in Japan. Additionally, it will be crucial to improve the SM prediction where the error is dominated by hadronic effects.

Status of a_τ

Given the prospects of a_μ to discover physics beyond the SM, a_τ with the even higher mass of the tauon would in principle be a far more sensitive observable. However, due to its very short lifetime, a precise measurement of the tauons anomalous magnetic moment is currently beyond experimental possibilities.

The current experimental limit from the LEP experiments OPAL and L3 [24, 25] reads

$$-0.052 < a_\tau^{\text{exp}} < 0.013 \tag{1.14}$$

at 95% C.L. and is in agreement with the SM prediction [26]

$$a_\tau^{\text{th}} = 117\,721(5) \times 10^{-8}. \tag{1.15}$$

2 Standard Model Prediction

> *When you have eliminated all which is impossible, then whatever remains, however improbable, must be the truth.*
>
> **— Arthur Conan Doyle**
> The Case-Book of Sherlock Holmes

CURRENTLY, the most interesting lepton magnetic moment is the one of the muon, where a 4.2σ discrepancy between the Standard Model prediction and the experiment could soon give evidence for new physics, while the one of the electron agrees almost perfectly with the SM. Besides experimental improvements, lowering the uncertainty in the theoretical prediction can help to establish a possible discovery. In the Standard Model, the anomalous magnetic moment of the muon may be calculated by considering the T-matrix element

$$\langle \mu^-(p_2)|j^\mu_{\text{em}}(0)|\mu^-(p_1)\rangle. \tag{2.1}$$

It can be written in the relativistic covariant decomposition

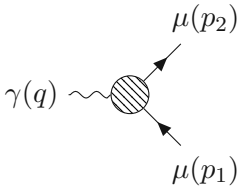

$$= (-ie)\bar{u}(p_2)\left[\gamma^\mu F_E(q^2) + i\frac{\sigma^{\mu\nu}q_\nu}{2m_\mu}F_M(q^2)\right]u(p_1), \tag{2.2}$$

where $u(p)$ are Dirac spinors and momentum conservation determines $q = p_2 - p_1$. The electric or Dirac form factor $F_E(q^2)$ and the magnetic or Pauli form factor $F_M(q^2)$ have the static limits

$$F_E(0) = 1, \qquad F_M(0) = a_\mu, \tag{2.3}$$

where the first equation is the charge renormalization condition and the second equation gives the prediction for the anomalous magnetic moment of the muon $a_\mu \equiv (g-2)_\mu/2$.

The contributions from the SM can be divided into electromagnetic, hadronic and electroweak contributions

$$a_\mu = a_\mu^{\text{QED}} + a_\mu^{\text{had}} + a_\mu^{\text{EW}} \,, \tag{2.4}$$

where the relevant hadronic contributions can be furthermore divided into hadronic vacuum polarization (HVP) and hadronic light-by-light (HLbL) scattering contributions. The electromagnetic contribution contains all possible charged lepton and photon loops. Quark and gluon loops, due to their strongly coupled nature, have to be described by hadronic degrees of freedom and are collected in the hadronic contribution. The last contribution is due to the weak interaction and includes the $W^\pm, Z$ bosons, neutrinos, and the Higgs particle H.

In the following, we will briefly review all these contributions and their current status according to the White Paper of the Muon $g-2$ Theory Initiative [2].

2.1 Electromagnetic Contribution

The electromagnetic or QED contribution to $(g-2)_\mu$ includes loops of charged leptons and photons. The contribution is further divided by the lepton-mass dependence, according to

$$a_\mu^{\text{QED}} = A_1 + A_2(m_\mu/m_e) + A_2(m_\mu/m_\tau) + A_3(m_\mu/m_e, m_\mu/m_\tau) \,, \tag{2.5}$$

where the lepton-mass independent term A_1 is universal for all leptons. Individual contributions are then calculated in a perturbative expansion in the small fine-structure constant $\alpha = 1/137.035...$

$$A_i = \left(\frac{\alpha}{\pi}\right) A_i^{(2)} + \left(\frac{\alpha}{\pi}\right)^2 A_i^{(4)} + \left(\frac{\alpha}{\pi}\right)^3 A_i^{(6)} + \cdots \,, \qquad \text{for } \; i = 1, 2, 3 \,. \tag{2.6}$$

The first coefficient $A_1^{(2)} = 1/2$ corresponds to the Feynman diagram 2.1 and was calculated by Schwinger in 1947 [27]. It exclusively contributes the leading three digits to a_μ. By now the entire tenth-order contribution, i.e. $\mathcal{O}(\alpha^5)$, is necessary to match the experimental precision.

Summing all these terms, the QED contribution reads [28, 21]

$$a_\mu^{\text{QED}}(\alpha(\text{Cs})) = 116\,584\,718.931(7)(17)(6)(100)(23)[104] \times 10^{-11} \,, \tag{2.7}$$

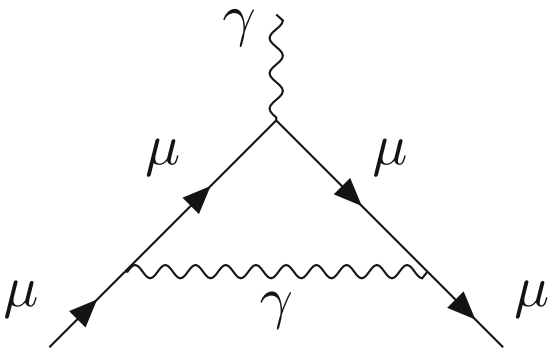

Figure 2.1. – Feynman diagram of the Schwinger term, which gives the leading contribution $a_\mu^{(2)} = 1/(2\pi\alpha) = 0.00116....$

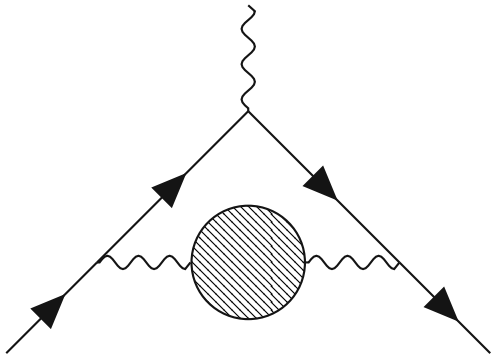

Figure 2.2. – Leading-order HVP contribution to $g-2$. The shaded blob represents the HVP two-point function.

where the uncertainties are due to the τ-lepton mass, the eighth-order, tenth-order, and an estimate for the twelfth-order QED contributions. The fifth error comes from the measurement of the fine-structure constant α using atomic interferometry of the Cs atom [22]. The final error is the sum in quadrature of the individual errors and is dominated by the estimate of the $\mathcal{O}(\alpha^6)$ contribution. It is, however, negligible compared to the uncertainty in the hadronic contribution discussed next.

2.2 Hadronic Vacuum Polarization Contribution

The biggest hadronic effect is given by the $\mathcal{O}(\alpha^2)$ hadronic vacuum polarization term, as depicted in Fig. 2.2. Fortunately, this contribution can be calculated in the dispersive approach by relating it to measurements of the $e^+e^- \to$ hadrons cross-section. The current conservative estimate reads [29, 30, 31, 32, 33, 34]

$$a_\mu^{\text{HVP, LO}} = 6931(40) \times 10^{-11}\,, \tag{2.8}$$

Contribution	Value $\times 10^{11}$
HVP LO (e^+e^-)	6931(40)
HVP NLO (e^+e^-)	−98.3(7)
HVP NNLO (e^+e^-)	12.4(1)
HVP (e^+e^-, LO + NLO + NNLO)	6845(40)

Table 2.1. – Summary of the contributions to a_μ^{HVP} [2].

with a relative uncertainty of only 0.6%, which to a big part comes from a tension between the BABAR and KLOE data sets on the 2π channel. At higher order in the perturbative expansion, the diagram 2.2 may contain additional photon or lepton loops, or additional HVP insertions. These effects are considered with the values

$$a_\mu^{\text{HVP, NLO}} = -98.3(7) \times 10^{-11} [34]\,, \qquad a_\mu^{\text{HVP, NNLO}} = 12.4(1) \times 10^{-11} [35]\,, \tag{2.9}$$

and are combined to the final prediction in Table 2.1.

On the side of lattice QCD, calculations have only recently achieved a comparable precision with the result of the BMW collaboration [5]

$$a_\mu^{\text{HVP, LO}}(\text{BMW}) = 7075(55) \times 10^{11}, \tag{2.10}$$

at 0.8% accuracy. Surprisingly, this is by about 2.1σ higher than the data-driven evaluation and would move the WP result much closer to the experimental value of a_μ. However, even if the discrepancy in a_μ would be eliminated by a change in the HVP contribution, this would very likely lead to a tension in other parts of the SM like the EW-fit as discussed in Ref. [6, 7, 8, 9]. Anyhow, the discrepancy between the two approaches needs further investigation.

2.3 Hadronic Light-by-Light Scattering Contribution

After HVP, the HLbL scattering contribution gives the second-largest uncertainty of the SM prediction to $(g-2)_\mu$. Similar to the HVP contribution, one cannot use perturbation theory to calculate this effect, but one has to rely on lattice QCD or data-driven evaluations. Compared to the vacuum polarization described by a two-point function, the more complicated light-by-light scattering amplitude is described by a four-point function and is suppressed by an additional power of the fine-structure constant α. The total contribution is therefore suppressed by two

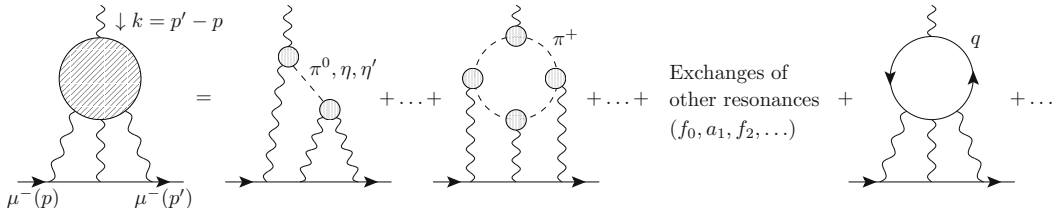

Figure 2.3. – Expansion of the HLbL scattering amplitude. Figure from Ref. [36].

Contribution	Value $\times 10^{11}$
π^0, η, η'-poles	93.8(4.0)
π, K-loops/boxes	−16.4(0.2)
S-wave $\pi\pi$ rescattering	−8(1)
scalars and tensors	−1(3)
axial vectors	6(6)
u, d, s-loops / short-distance	15(10)
c-loop	3(1)
total	92(19)

Table 2.2. – Summary of the contributions to the phenomenological estimate of the LO HLbL contribution [2].

orders of magnitude, and it suffices to have an error of about 10% to meet current precision goals.

As depicted in Fig. 2.3, the HLbL amplitude can be expanded in diagrams with an exchange of a single meson, diagrams with a loop of charged mesons, a quark loop diagram, and other subleading diagrams. It is important to note that the identification of the individual terms in this expansion is model dependent, and the only unambiguous definition can be given within the dispersive framework [2].

In Table 2.2 we list the current phenomenological estimate of the individual contributions obtained by the Muon $g-2$ Theory Initiative [2]. The first three contributions from single-pseudoscalar poles [37, 38, 39] and from two-pion intermediate states [40] are calculated with the dispersive approach, while the estimates for scalars, tensors and axial-vector mesons [41, 42, 20, 43, 44, 45] are model-dependent. The contributions of quark loops are based on Refs. [46, 47, 48].

While in the large-energy or short-distance regime the quark loop can be calculated perturbatively, it is important to avoid a possible double-counting at low energies where quarks are replaced by mesonic degrees of freedom. For increasing virtualities of the photons, heavier and heavier intermediate states can contribute. Summing an infinite number of these intermediate states should reproduce all short-distance constraints (SDC) from perturbative QCD. Therefore, these constraints play an

Contribution	Value $\times 10^{11}$
HLbL (phenomenology)	92(19)
HLbL NLO (phenomenology)	2(1)
HLbL (lattice, uds)	79(35)
HLbL (phenomenology + lattice + NLO)	92(18)

Table 2.3. – Summary of the contributions to a_μ^{HLbL} [2].

important role in the estimate of the error in the HLbL contribution, and will be discussed in more detail in the next subsection.

The full SM HLbL prediction displayed in Table 2.3 is obtained by performing a weighted average of the lattice QCD result [50] with the phenomenological result for light quarks of Table 2.2. Afterwards, the c quark contribution and an estimate for the NLO contribution based on Ref. [49] are added. The final error is about 20% but a reduction to 10%, meeting the precision goal of the Fermilab experiment, seems feasible [2].

2.3.1 Short-Distance Constraints

To formulate the HLbL SDCs, we first have to introduce some notation. The HLbL scattering amplitude is described by the polarization tensor

$$\begin{aligned}\Pi^{\alpha\beta\mu\nu}(q_1,q_2,q_3) \;&:=\; -i\int d^4x\, d^4y\, d^4z\, e^{-i(q_1x+q_2y+q_3z)}\\ &\quad\times\langle\Omega|T\{J^\alpha(x)J^\beta(y)J^\mu(z)J^\nu(0)\}|\Omega\rangle,\end{aligned}\tag{2.11}$$

with the electromagnetic quark currents $J^\mu(x)=e\bar{\psi}_0 Q\gamma^\mu\psi_0$, where ψ_0 is the bare quark multiplet and Q is the quark charge matrix. Following Bardeen, Tung [51], and Tarrach [52] (BTT), this tensor can be decomposed into 54 tensor structures

$$\Pi^{\alpha\beta\mu\nu}=\sum_i^{54} T_i^{\alpha\beta\mu\nu}\Pi_i,\tag{2.12}$$

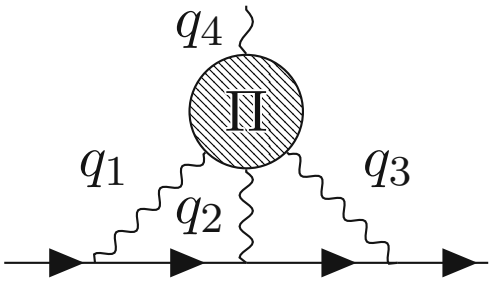

Figure 2.4. – Momentum labels in the leading-order HLbL contribution to $g-2$.

without kinematic singularities or zeros. The HLbL contribution in Fig. 2.4 then takes the form

$$\begin{aligned} a_\mu^{\text{HLbL}} = &-\frac{e^6}{48m_\mu}\int\frac{d^4q_1}{(2\pi)^4}\frac{d^4q_2}{(2\pi)^4}\frac{1}{q_1^2q_2^2(q_1+q_2)^2}\frac{1}{(p+q_1)^2-m_\mu^2}\frac{1}{(p-q_2)^2-m_\mu^2} \\ &\times \text{Tr}\left((\not{p}+m_\mu)[\gamma^\rho,\gamma^\sigma](\not{p}+m_\mu)\gamma^\mu(\not{p}+\not{q}_1+m_\mu)\gamma^\lambda(\not{p}-\not{q}_2+m_\mu)\gamma^\nu\right) \\ &\times\sum_{i=1}^{54}\left(\frac{\partial}{\partial q_4^\rho}T^i_{\mu\nu\lambda\sigma}(q_1,q_2,q_4-q_1-q_2)\right)\Big|_{q_4=0}\Pi_i(q_1,q_2,-q_1-q_2)\,, \end{aligned} \tag{2.13}$$

and can be further simplified to the master formula

$$\begin{aligned} a_\mu^{\text{HLbL}} \;=\; &\frac{2\alpha^3}{3\pi^2}\int_0^\infty dQ_1\int_0^\infty dQ_2\int_{-1}^1 d\tau\sqrt{1-\tau^2}Q_1^3Q_2^3 \\ &\times\sum_{i=1}^{12}T_i(Q_1,Q_2,\tau)\bar{\Pi}_i(Q_1,Q_2,\tau), \end{aligned} \tag{2.14}$$

by using the technique of Gegenbauer polynomials [53]. The integration variables are the norms of the Euclidean momenta $Q_{1,2} := |Q_{1,2}|$ and τ, the cosine of the angle between the two momenta. The 12 basis elements $\bar{\Pi}_i$ are linear combinations of the Π_i functions and T_i are known kernel functions.

For the HLbL scattering, there are two kinds of interesting SDCs. First there are constraints on the form factors describing the coupling of hadrons to photons, and then there are constraints on the full four-point function (2.11).

SDCs on the Form Factor

As a specific example, let us look at the transition form factor (TFF) $\mathcal{F}_P$ of the pion[1], which is relevant for the largest HLbL contribution. The TFF is defined by

$$i\int d^4x e^{iq_1x}\langle\Omega|T\{J^\mu(x)J^\nu(0)\}|P(q_1+q_2)\rangle = \varepsilon^{\mu\nu\alpha\beta}(q_1)_\alpha(q_2)_\beta\mathcal{F}_P(q_1^2,q_2^2). \quad (2.15)$$

Using the operator product expansion (OPE), Refs. [55, 56] have obtained the SDC in the symmetric limit

$$\lim_{Q\to\infty} Q^2\mathcal{F}_P(-Q^2,-Q^2) = \frac{2f_\pi}{3}, \quad (2.16)$$

where f_π is the pion decay constant. The corresponding single-virtual SDC has been obtained by Brodsky and Lepage (BL) in Refs. [57, 58, 59] and reads

$$\lim_{Q\to\infty} Q^2\mathcal{F}_P(-Q^2,0) = 2f_\pi. \quad (2.17)$$

SDCs on the Four-Point Function

For the kinematics in the HLbL contribution, one of the four photons in the four-point function has to be on-shell and soft, and we are left with two interesting short-distance regimes.

In the first regime one takes one of the q_i^2, e.g. q_3^2, much smaller than the other two, which implies $q_1^2 \sim q_2^2$. The corresponding SDC has been derived by Melnikov and Vainshtein (MV) [46] and reads

$$\lim_{Q_3\to\infty}\lim_{Q\to\infty} Q_3^2Q^2\bar{\Pi}_1(Q,Q,Q_3) = -\frac{2}{3\pi^2}, \quad (2.18)$$

in terms of the BTT basis (2.12). In the large-N_c and chiral limit one can even drop the Q_3-limit and the result holds for any Q_3.

The second regime has all three q_i^2 large. In the symmetric limit $q_1^2 \sim q_2^2 \sim q_3^2$, the leading-order behavior of the SDC is identical to the perturbative quark loop and reads [46, 47]

$$\lim_{Q\to\infty} Q^4\bar{\Pi}_1(Q,Q,Q) = -\frac{4}{9\pi^2}. \quad (2.19)$$

Interestingly, if we only consider a finite number of intermediate meson states in the expansion of the HLbL four-point function, the form factor SDCs result in too strong

[1] Other examples can be found in Ref. [54].

a falloff, and we cannot fulfill the SDCs on the four-point function. As an illustration, let us consider the contribution of the neutral pion in the pion-pole approximation

$$\bar{\Pi}_1 = \frac{\mathcal{F}(q_1^2, q_2^2)\mathcal{F}(q_3^2, 0)}{q_3^2 - m_\pi^2} \sim \mathcal{O}(Q_3^{-4} Q^{-4}), \tag{2.20}$$

which is suppressed by an additional factor of Q_3^{-2}. The same holds true for any other single particle intermediate state.

Currently, there are only three known ways to satisfy the SDCs on the four-point function with hadronic degrees of freedom:

- By an ad hoc replacement of the single virtual TFF $\mathcal{F}(q_3^2, 0)$ to be momentum-independent. This was suggested in Ref. [46] and leads to a sizeable increase in the pseudoscalar pole contributions.
- By summing an infinite number of excited pseudoscalar mesons in the Regge model of Ref. [60, 48].
- By summing an infinite number of axial-vector mesons in holographic QCD models [I, II, IV, 61].

Currently, only the Regge model estimate is included in the short-distance contribution to HLbL scattering, as listed in Table 2.2. The holographic models hint to slightly larger values. This will be discussed in more detail in Part III.

2.4 Electroweak Contribution

The electroweak (EW) contribution to a_μ contains all SM diagrams not contained in the pure QED, HVP, or HLbL contributions. The diagrams therefore include at least one W or Z boson, or the Higgs. Their heavy masses strongly suppress the EW contribution, such that it is comparable in size to the HLbL correction. Some one-loop diagrams are shown in Fig. 2.5.

Currently, the EW contribution is calculated to two loops, but also estimates of the leading logarithmic contribution beyond that are included in the estimate [62, 63]

$$a_\mu^{\text{EW}} = 153.6(1.0) \times 10^{-11}\,. \tag{2.21}$$

At two-loop level this contribution also contains hadronic loops, and they dominate the uncertainty, which is still negligible compared to the one of the HVP and HLbL contribution.

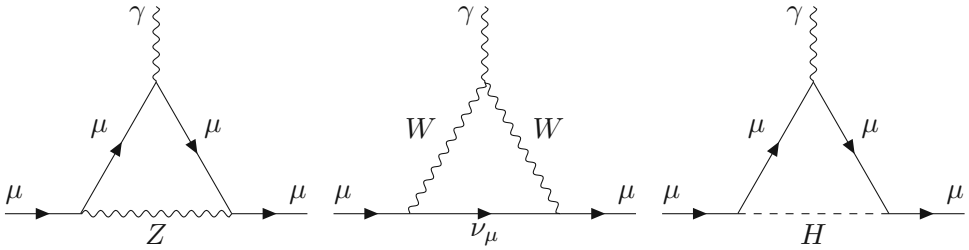

Figure 2.5. – Sample one-loop Feynman diagrams relevant for a_μ^{EW}.

Contribution	Value $\times 10^{11}$
QED	116 584 718.931(104)
HVP (e^+e^-, LO + NLO + NNLO)	6845(40)
HLbL (phenomenology + lattice + NLO)	92(18)
Electroweak	153.6(1.0)
Total SM Value	116 591 810(43)
Experiment (E821+E989)	116 592 061(41)
Difference: $\Delta a_\mu := a_\mu^{\text{exp}} - a_\mu^{\text{SM}}$	251(59)

Table 2.4. – Summary of the contributions to a_μ^{SM} [2].

2.5 Combined Standard Model Prediction

According to the White Paper of the Muon $g-2$ Theory Initiative [2], summing the SM contributions to the muon anomalous magnetic moment yields

$$\begin{aligned} a_\mu^{\text{SM}} &= a_\mu^{\text{QED}} + a_\mu^{\text{EW}} + a_\mu^{\text{HVP, LO}} + a_\mu^{\text{HVP, NLO}} + a_\mu^{\text{HVP, NNLO}} + a_\mu^{\text{HLbL}} + a_\mu^{\text{HLbL, NLO}} \\ &= 116\,591\,810(43) \times 10^{-11}\,, \end{aligned} \tag{2.22}$$

where the total error estimate is dominated by hadronic effects, see Table 2.4. The largest uncertainty comes from HVP, where the relative error is already below 0.6%. HLbL contributes the second-largest uncertainty, with an almost 20% relative error.

Comparing to the experimental average [1, 3]

$$a_\mu^{\text{exp}}(\text{FNAL+BNL}) = 116\,592\,061(41) \times 10^{-11}\,, \tag{2.23}$$

the difference

$$\Delta a_\mu := a_\mu^{\text{exp}} - a_\mu^{\text{SM}} = 251(59) \times 10^{-11}\,, \tag{2.24}$$

amounts to a 4.2σ discrepancy.

Part II

Holographic QCD

In this part of the thesis, we will explore gauge/gravity duality and its application to QCD. We will start with a brief introduction to the AdS/CFT correspondence, which tries to describe strongly coupled gauge theories by their gravity duals. We will then focus on applying this duality to strongly coupled QCD by introducing the Sakai-Sugimoto model and various bottom-up models, as well as reviewing some key concepts and calculations.

3 Gauge/Gravity Duality and the Holographic Principle

> *May it be a light to you in dark places, when all other lights go out.*
>
> **— J.R.R. Tolkien**
> The Fellowship of the Ring

BEFORE we can discuss holographic QCD, we have to first understand its underlying principle, gauge/gravity duality. As a duality, it states that two seemingly distinct theories are actually equivalent. Their Lagrangians or other physical descriptions may differ, but their observables and dynamics are the same. Unlike other known dualities, which typically link string theories to string theories or quantum field theories to quantum field theories, gauge/gravity duality relates quantum field theories to string theories. In particular, this suggests that one can find a quantum field theory dual to a promising candidate for quantum gravity.

Gauge/gravity duality realizes the holographic principle, stating that the number of degrees of freedom in a given volume scales as its surface area. In this picture, the quantum field theory can be thought of as living on the boundary of the theory of gravity. This principle is motivated by the Bekenstein bound, which implies that for a given volume, a black hole has maximal entropy proportional to its surface area.

The most famous realization of this duality is the AdS/CFT correspondence, discovered by Maldacena in 1997 [10]. It relates a theory of quantum gravity in Anti-de Sitter space with a quantum field theory invariant under conformal transformations. In its most useful form, this duality is a strong-weak duality [65, 66], relating a strongly coupled quantum field theory to a weakly coupled theory of gravity, or vice versa.

If gauge/gravity duality is a general feature of nature, it would be fascinating to construct a gravity dual to QCD that would allow one to recast strongly coupled QCD calculations into weakly coupled gravity calculations. However, no exact dual to QCD has yet been discovered, so one has to rely on duals of effective theories that

only describe certain features of QCD. Examples of these holographic QCD models will be presented in the following two chapters.

In this chapter, we will follow Refs. [67, 68] in giving a brief introduction to the AdS/CFT correspondence. The AdS/CFT correspondence will be defined first, followed by a heuristic derivation from string theory. We will go over the field-operator map, also known as the holographic dictionary, before we will discuss the steps required to construct a holographic dual of QCD.

3.1 The AdS/CFT Correspondence

Let us start with a definition of the AdS_5/CFT_4 correspondence [10], which is the most well-known example of the AdS/CFT correspondence. In its strongest form, it states [67]:

> $\mathcal{N} = 4$ Super Yang-Mills theory
> with gauge group $SU(N)$ and Yang-Mills coupling constant g_{YM}
>
> is **dynamically equivalent** to
>
> type IIB superstring theory
> with string length $l_s = \sqrt{\alpha'}$ and coupling constant g_s
> on $AdS_5 \times S^5$ with curvature radius L and N units of $F_{(5)}$ flux on S^5.
>
> The two free parameters on the field theory side, i.e., g_{YM} and N, are mapped to the free parameters g_s and $L/\sqrt{\alpha'}$ on the string theory side by
>
> $$g_{\text{YM}}^2 = 2\pi g_s \qquad \text{and} \qquad 2g_{\text{YM}}^2 N = L^4/\alpha'^2. \tag{3.1}$$

The maximally supersymmetric ($\mathcal{N} = 4$) Super Yang-Mills theory, which is conformal and 4-dimensional, provides the field theory side of this duality. It is therefore denoted as CFT_4 or CFT side. It has two free parameters: the rank N of the gauge group and the coupling constant g_{YM}.[1] On the other hand, we have the AdS side given by the type IIB superstring theory on $AdS_5 \times S^5$. After the Kaluza-Klein reduction on the S^5, this theory is 5-dimensional. Of the two length scales in this theory, only the dimensionless ratio $L/\sqrt{\alpha'}$ is of physical importance. The second free parameter is

[1] In holographic QCD applications, we are mostly interested in describing the strong interaction where the rank of the gauge group is the number of colors N_c. Furthermore, the convention in the relation (3.1) is based on the normalization $-\frac{1}{4g_{\text{YM}}^2}\text{Tr}\, F_{\mu\nu}F^{\mu\nu}$ of the Yang-Mills action and is related by $g^2 = 2g_{\text{YM}}^2$ to the conventional QCD coupling constant.

the string coupling constant g_s. After identifying the free parameters according to Eq. (3.1), the two sides of the duality should be dynamically equivalent and describe the same physics. If this correspondence holds, it links a theory with gravity on the AdS side to a theory without gravitational degrees of freedom on the CFT side.

At this point, it is important to stress that the AdS_5/CFT_4 correspondence in its strongest form is only a conjecture. The difficulty in constructing a proof and doing explicit calculations is, among others, due to the difficulty of quantum string theory in curved backgrounds. To avoid this issue, it is possible to take the weak coupling limit $g_s \ll 1$ of the string theory, while keeping the ratio $L/\sqrt{\alpha'}$ fixed. This results in the strong form of the correspondence, where we have classical string theory at leading order. On the CFT side, the corresponding limit is $g_{\text{YM}} \ll 1$ and $g^2_{\text{YM}}N$ fixed, according to the identification (3.1). This is achieved by the large-N limit $N \to \infty$. Defining the ´t Hooft coupling $\lambda \equiv g^2_{\text{YM}}N$, we see that this limit corresponds to the planar limit of the gauge theory. Keeping λ fixed, the relation $1/N \propto g_s$ implies that the $1/N$ expansion of the gauge theory corresponds to the expansion in the genus of the string worldsheet.

Another useful form, the weak form, is obtained by taking additionally the point-particle limit $\alpha'/L \to 0$. The string length l_s is then negligible compared to the curvature radius L, and the type IIB string theory is replaced by type IIB super gravity. On the CFT side, this corresponds to the strong coupling limit $\lambda \to \infty$. Since in this form the correspondence is a strong/weak duality, i.e., it maps a strongly coupled theory to a weakly coupled one, we can use perturbative supergravity calculations to get insights into the nonperturbative behavior of strongly coupled gauge theories.

3.2 Heuristic Derivation

Even though there are some very non-trivial checks of the AdS/CFT correspondence, there is no proof of it. There is, however, a heuristic derivation of the weak form of the correspondence, following from two different descriptions of D-branes [69].

3.2.1 Open String Perspective

The first description, the open string perspective, views D-branes as higher-dimensional objects on which open strings can end. For simplicity, we will restrict ourselves to D3-branes, with their $(3+1)$-dimensional worldvolumes in $(9+1)$-dimensional

spacetime. The open string endpoints can only move in these four directions, while closed strings can move freely in all directions, see Fig. 3.1a. The open and closed string spectrum consists of a finite number of massless modes and an infinite amount of excited massive states. By restricting to low energies $E \ll \alpha'^{-1/2}$, we can neglect the massive states and the D3 brane and open string dynamics are described by the Dirac-Born-Infeld (DBI) action and Chern-Simons (CS) term

$$S_{D3} = -T_3 \int d^4x\, e^{-\phi} \sqrt{-\det\left(P[g]_{ab} + 2\pi\alpha' F_{ab}\right)} + S_{CS}, \tag{3.2}$$

where $e^{-\phi}$ is the dilaton field, $P[g]_{ab}$ is the induced metric on the D3-brane, F_{ab} is a field-strength on the 4-dimensional worldvolume, and T_3 is the brane tension

$$T_3 = \frac{1}{(2\pi)^3 g_s l_s^4} = \frac{1}{(2\pi)^3 g_s \alpha'^2}. \tag{3.3}$$

Fluctuations of the embedding are described by six real scalar fields ϕ^i, one for each transverse direction to the D3 brane worldvolume. Together with the four gauge fields A_a, these six scalar fields describe the bosonic massless spectrum of open strings. The fermionic degrees of freedom are described by four Weyl fermions Ψ^I.

The closed string spectrum is described by fluctuations of type IIB supergravity in 10-dimensional Minkowski space, most prominently fluctuations of the metric and the dilaton. Through the brane action, these fluctuations then induce interactions between the closed and open strings. In the Maldacena limit

$$\alpha' \to 0 \qquad \text{with} \qquad u = \frac{r}{\alpha'} \quad \text{kept fixed}, \tag{3.4}$$

where r is any distance, these interactions vanish and we can use the open string perspective where branes and geometry decouple.

Let us now study the case of N_c stacked branes. The open string endpoints are then confined to one particular brane, see Fig. 3.1b. This is described by giving the open string modes an additional $U(N_c)$ symmetry. This symmetry can be factored into $U(N_c) = SU(N_c) \times U(1)$, where $U(1)$ corresponds to center of mass motion and due to global translation invariance can be decoupled from the theory. The open string sector then realizes $\mathcal{N} = 4$ $SU(N_c)$ Yang-Mills theory in $(3+1)$-dimensional spacetime.

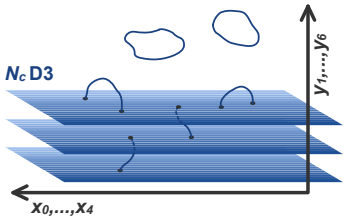

(a) $(3+1)$D worldvolume of N_c D3 branes in $(9+1)$D spacetime.

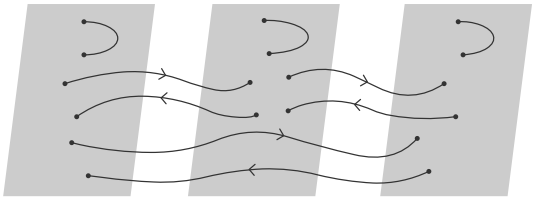

(b) Open strings endpoints on N_c D3 branes.

Figure 3.1. – D3 branes in 10-dimensional spacetime. Figure from Ref. [68].

3.2.2 Closed String Perspective

For the second description of D-branes, we consider them as massive, charged solitonic objects of supergravity. As such, they source supergravity fields and curve the spacetime. The corresponding type IIB supergravity solution of N_c D3 branes extremizes the action (omitting the supergravity fermions)

$$S = \frac{1}{(2\pi)^7 l_s^8} \int d^{10}x\sqrt{-g}\left(e^{-2\phi}(R + 4(\nabla\varphi)^2) - \frac{2}{5!}F_5^2\right), \tag{3.5}$$

with the black hole type metric

$$ds^2 = f(r)^{-1/2}\eta^{\mu\nu}dx_\mu dx_\nu + f(r)^{1/2}\left(dr^2 + r^2\, d\Omega_5^2\right), \tag{3.6}$$

where $d\Omega_5$ is the 5-sphere metric and

$$f(r) = 1 + \frac{L^4}{r^4}, \tag{3.7}$$

is a blackening factor with the horizon radius

$$L^2 = \sqrt{4\pi g_s N_c}\alpha' = \sqrt{4\pi g_s N_c} l_s^2\,. \tag{3.8}$$

The D3 brane solution is furthermore charged under the self-dual $*F_5 = F_5$ field strength of the Ramond-Ramond (RR) four-form potential. This field strength is normalized to

$$\int_{S^5} *F_5 = N_c. \tag{3.9}$$

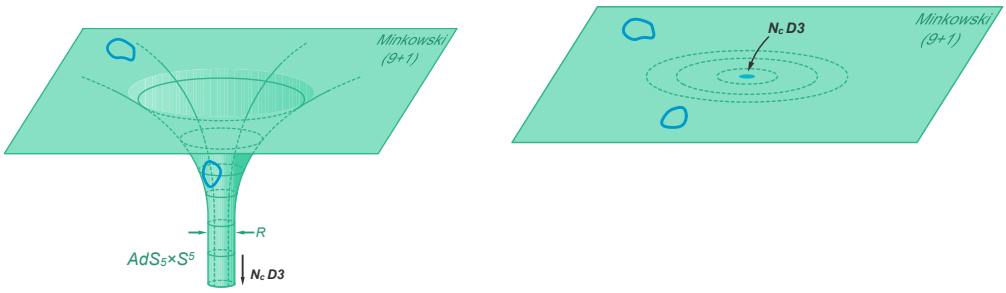

(a) Black hole type geometry of N_c D3 branes with $AdS_5 \times S^5$ as near-horizon geometry.

(b) Asymptotic region for $r \gg l$ is flat.

Figure 3.2. – Black hole type geometry of N_c D3 branes. Figure from Ref. [68].

We can now separate two different regions of the spacetime (3.6), the near-horizon region $r \ll L$ and the asymptotic region $r \gg L$. In the former limit, the near-horizon geometry is $AdS_5 \times S^5$, with the metric

$$ds^2 = \frac{r^2}{L^2}\eta^{\mu\nu}dx_\mu dx_\nu + \frac{L^2}{r^2}\left(dr^2 + r^2 d\Omega_5^2\right), \tag{3.10}$$

as depicted in Fig. 3.2a. While in the asymptotic region, the blackening factor approaches $f(r) \approx 1$ and the geometry reduces to 10-dimensional flat space, see Fig. 3.2b. In the Maldacena limit (3.4), closed strings propagating in these two regions decouple from each other [67] and the theory reduces to type IIB supergravity on $AdS_5 \times S^5$ plus type IIB supergravity on $\mathbb{R}^{9,1}$.

3.2.3 Combining the Perspectives

To conclude this heuristic derivation, one conjectures that the open string and closed string perspective describe the same physics and are, in fact, dual to each other. In the above-mentioned limits, both of them have two decoupled effective theories. The open string perspective is described by $\mathcal{N} = 4$ $SU(N_c)$ Yang-Mills theory in $(3+1)$-dimensional spacetime and type IIB supergravity on $\mathbb{R}^{9,1}$. The closed string perspective, on the other hand, is described by type IIB supergravity on $AdS_5 \times S^5$ and type IIB supergravity on $\mathbb{R}^{9,1}$. The two theories are then only equivalent if $\mathcal{N} = 4$ $SU(N_c)$ Yang-Mills theory is dual to type IIB supergravity on $AdS_5 \times S^5$, as was conjectured by Maldacena in Ref. [10]. As a first non-trivial check of this correspondence, one can compare the symmetries of the two theories and finds that, indeed, in both cases they are given by the group $PSU(2,2|4)$. The bosonic part of this group is given by $SO(4,2)$ and $SO(6)$, which nicely agrees with the

isometry group of AdS_5 and S^5, respectively. The fermionic part is generated by sixteen Poincaré supercharges and sixteen superconformal supercharges.

3.3 Field-Operator Map

Having formulated and motivated the AdS/CFT correspondence, we now want to specify the duality by giving the one-to-one map, or holographic dictionary, that relates field theory operators to string states. Since both theories have the same symmetry group, objects in a common representation should be mapped to each other. On the CFT side, let us look at gauge invariant composite operators

$$\mathcal{O}_\Delta(x) = \mathrm{Str}\left(\phi^{i_1}(x)\phi^{i_2}(x)\dots\phi^{i_\Delta}(x)\right), \tag{3.11}$$

where Δ is the conformal scaling dimension, and Str denotes the symmetrized trace over the color indices of the elementary scalar fields ϕ^i.

In the weak form of the duality, the dual string states are given by linearized fluctuations of type IIB supergravity fields. We split these fluctuations φ into a field living on the AdS_5 space and a part living on the S^5

$$\varphi(x,z,\Omega_5) = \sum_{I=0}^{\infty} \varphi^I(x,z)Y^I(\Omega_5). \tag{3.12}$$

The equations of motion for the S^5 spherical harmonics $Y^I(\Omega_5)$ are

$$\Box_{S^5} Y^I = -\frac{1}{L^2} l(l+4) Y^I, \tag{3.13}$$

while the ones for the AdS field $\varphi^I(x,z)$ depend on which fluctuations we are looking at. Scalar fluctuations of the metric and the self-dual five-form field F_5 are coupled and can be diagonalized by taking linear combinations. One of these combinations we call $s^I(z,x)$ and we find its equation of motion to be

$$\Box_{AdS_5} s^I(z,x) = \frac{1}{L^2} l(l-4) s^I(z,x). \tag{3.14}$$

By identifying $l = \Delta$, we can check that $s^I(z,x)$ is in the same representation as $\mathcal{O}_\Delta(x)$ and that they should be mapped to each other.

To make this mapping more precise, we have to study the supergravity fields near the AdS boundary at $z \to 0$. But first, let us generalize the Klein-Gordon equation (3.14) to the general case of d dimensions:

$$\Box_{\mathrm{AdS}_{d+1}}\phi = \frac{1}{L^2}\Delta(\Delta - d)\phi \Longrightarrow m^2L^2 = \Delta(\Delta - d). \tag{3.15}$$

This equation of motion has two linear independent solutions, which we characterize by their behavior near $z \to 0$. We find the asymptotic solution

$$\phi(z,x)|_{z\to 0} \sim \phi_{(0)}(x)z^{d-\Delta} + \phi_{+}(x)z^{\Delta} + \dots . \tag{3.16}$$

Evaluating the action on this solution at quadratic order, we find that the contribution of $\phi_{(0)}(x)z^{d-\Delta}$ diverges and is non-normalizable, while the contribution of $\phi_{+}(x)z^{\Delta}$ converges and is normalizable.[2] Using dimensional analysis, the holographic dictionary identifies the normalizable mode $\phi_{+}(x)$ with the expectation value of the field theory operator $\mathcal{O}_{\Delta}$ and the non-normalizable mode with its source. This map further leads to the identification of the generating functional for connected Green's function $W[\phi_{(0)}]$ and the classical supergravity action, according to

$$W[\phi_{(0)}] = S_{\text{sugra}}\left[\phi\right]|_{\lim_{z\to 0}\left(\phi(z,x)z^{\Delta-d}\right)=\phi_{(0)}(x)}. \tag{3.17}$$

This identification can be used to holographically calculate correlation functions of field theory operators by varying the generating functional with respect to the sources

$$\left\langle \mathcal{O}_1\left(x_1\right)\mathcal{O}_2\left(x_2\right)\dots\mathcal{O}_n\left(x_n\right)\right\rangle_{\mathrm{CFT}} = -\left.\frac{\delta^n W}{\delta\phi^1_{(0)}\left(x_1\right)\delta\phi^2_{(0)}\left(x_2\right)\dots\delta\phi^n_{(0)}\left(x_n\right)}\right|_{\phi^i_{(0)}=0}. \tag{3.18}$$

3.4 Towards a Holographic Dual of QCD

Up to know, we have studied gauge/gravity duality for conformal systems with supersymmetry. These large symmetry groups allow one to match representations on both sides of the duality and construct the field-operator map. In the weak form, this duality is an interesting tool for studying strongly coupled gauge theories, for which conventional calculations are often difficult. In the following chapters, we are interested in extending this duality to non-supersymmetric gauge theories like QCD,

[2] Note that this behavior depends on the value of Δ and has to be interchanged in some special cases [67].

the theory of strong interactions. Unfortunately, a gravity dual of QCD is not known and one has to rely on theories that only resemble QCD in certain limits. There are two different strategies to construct such theories: the top-down and the bottom-up approach.

The top-down approach tries to deform the AdS/CFT correspondence within the framework of string theory. Important steps are the mechanisms of supersymmetry breaking, conformal symmetry breaking, introduction of flavor degrees of freedom and chiral symmetry breaking. Achieving all of this within string theory is highly non-trivial and restricts the theory considerably. The most prominent example of top-down holographic QCD, the Sakai-Sugimoto model, will be introduced in the next chapter.

In the bottom-up approach, one considers gauge/gravity duality as a fundamental principle of nature and assumes that it holds for any field theory. One starts by selecting characteristic properties of the field theory, like the field content and symmetries, and constructs the corresponding gravity dual by hand. It is clear that this strategy has more freedom than the top-down approach and allows for a lot of flexibility in modelling physical systems. This freedom, however, may come at the cost of numerous free parameters and limit the predictivity of bottom-up models. In Chapter 5, we study some easier bottom-up models that still have a relatively low number of free parameters.

4 The Sakai-Sugimoto Model

> *Eppur si muove.*
> *(And yet it moves.)*
>
> — **Galileo Galilei**
> Physicist

THE Sakai-Sugimoto (SS) model [11, 12] is one of the most successful holographic QCD models. As a top-down holographic model, it is based on a 10-dimensional string construction where the background is a deformed AdS space, breaking conformal symmetry and modelling confinement. To break supersymmetry, fermions get anti-periodic boundary conditions with respect to an additional spatial dimension. Flavor degrees of freedom are introduced by embedding probe branes in this background. For $N_f \ll N_c$, their backreactions can be ignored.

Using this model, one can derive an effective action describing low-energy QCD. However, it is again critical to note that this model is not real QCD, but only an approximation to its low-energy limit. The top-down nature of this model is a significant advantage, as it limits the degrees of freedom in its construction. Besides mesons, this model also nicely describes glueballs and baryons.

This chapter is structured as follows: First, we will review the brane construction of the model. Then, we will show how mesonic degrees of freedom are described as eigenmodes of functions in the holographic direction, how we can fit the parameters of the model to low-energy observables, and how we can calculate simple decay widths. Finally, we will couple the model to photons, show how vector meson dominance is realized, and how one can calculate form factors.

4.1 D4/D8/$\overline{\text{D8}}$ Brane System

The Sakai-Sugimoto model is based on a brane construction consisting of N_c D4 branes and N_f D8 and anti-D8 ($\overline{\text{D8}}$) branes.

	0	1	2	3	(4)	5	6	7	8	9
D4	○	○	○	○	○					
D8-$\overline{\text{D8}}$	○	○	○	○		○	○	○	○	○

Table 4.1. – The D4/D8/$\overline{\text{D8}}$ brane intersection in $(9+1)$-dimensional flat space.

Open string picture

To illustrate the setup, let us start with the open-string picture, where the branes are embedded in 10-dimensional flat space according to Table 4.1. The direction x^4 is compactified on a circle S^1 of radius M_{KK}^{-1} with anti-periodic boundary conditions for fermions (the gauginos). They therefore acquire a mass and can be neglected at low energies, completely breaking supersymmetry. At low energies, we will only consider massless string modes.

Depending on the endpoints of the strings, we can give them different interpretations. The massless modes of strings beginning and ending on the D4 brane (4-4 strings) consist of the gauge fields $A_\mu^{(D4)}$ $(\mu = 0, 1, 2, 3)$ and $A_4^{(D4)}$ along the D4 brane and scalar fields Φ^i $(i = 5, \cdots, 9)$ transverse to the D4 worldvolume. The scalar fields $A_4^{(D4)}$ and Φ^i get mass terms via one-loop corrections and can be neglected. We are therefore left with a 4-dimensional $U(N_c)$ gauge theory described by $A_\mu^{(D4)}$.

The strings with one end on the D4 brane and the other end on the D8 or $\overline{\text{D8}}$ brane are not subjected to the anti-periodic boundary conditions for the fermions. The massless modes include N_f flavors of massless fermions in the fundamental representation of $U(N_c)$ which we interpret as quarks. The $U(N_f)_{D8} \times U(N_f)_{\overline{D8}}$ gauge symmetry of the flavor branes then corresponds to the chiral symmetry of QCD.

By separating the D8 and $\overline{\text{D8}}$ branes in the x^4 direction, the 8-$\overline{8}$ strings get a mass proportional to the distance Δx^4 and are excluded from the theory.

We are therefore left with 4-dimensional $U(N_c)$ gauge fields and N_f flavors of massless fermions. Exactly the field content of QCD.

Closed string picture

In the closed string picture, one uses the supergravity description of D-branes. There is, however, no known gravity solution for the setup in Table 4.1, but one instead uses the assumption $N_f \ll N_c$ under which one can neglect the backreaction of the

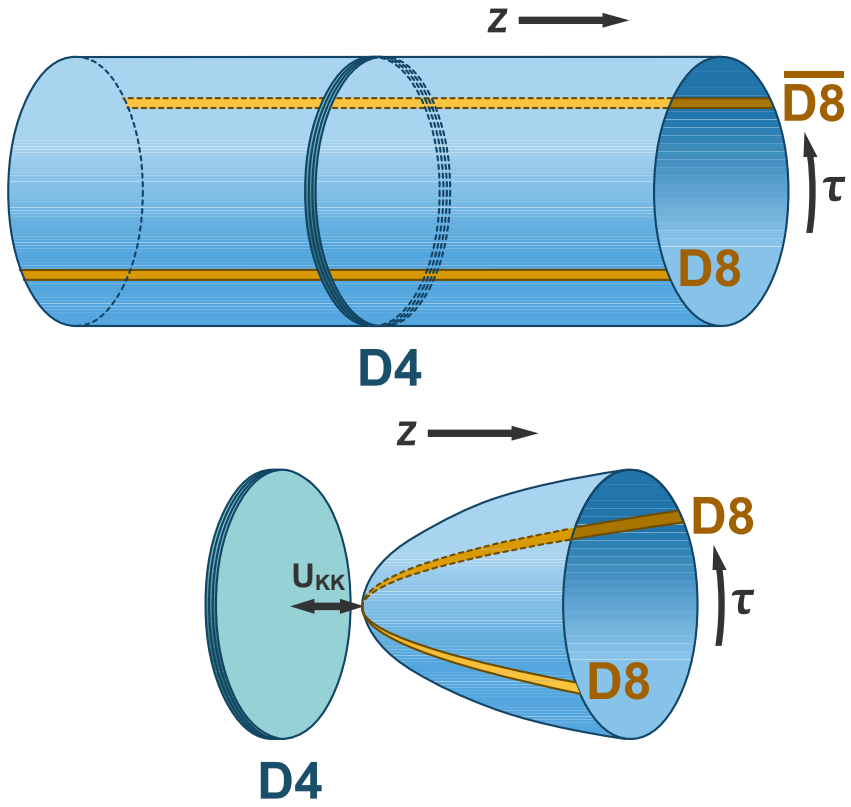

Figure 4.1. – Brane configuration in the $\tau - z$ subspace corresponding to the directions $4-5$ in Table 4.1. The upper and lower visualization correspond to the open and closed string picture respectively. Figure from Ref. [68].

flavor branes to the geometry, and the supergravity solution is simply the one of the D4 brane. The D8 branes are then considered as probes and follow the geometry as depicted in Fig. 4.1. As will be presented in the following, for maximal separation, the D8 branes join at the tip of the cigar-shaped bulk space and geometrically realize chiral symmetry breaking.

4.1.1 D4 Background

Following the notation of Ref. [70], the type IIA supergravity background dual to N_c D4-branes, with one of its four spatial worldvolume directions compactified on a superysymmetry breaking circle S^1, takes the form

$$ds^2 = \left(\frac{U}{R}\right)^{3/2}\left(\eta_{\mu\nu}dx^\mu dx^\nu + f(U)d\tau^2\right) + \left(\frac{R}{U}\right)^{3/2}\left(\frac{dU^2}{f(U)} + U^2 d\Omega_4^2\right),$$
$$e^\phi = g_s\left(\frac{U}{R}\right)^{3/4}, \quad F_4 = dC_3 = \frac{2\pi N_c}{V_4}\epsilon_4\,, \quad f(U) = 1 - \frac{U_{\rm KK}^3}{U^3}\,, \tag{4.1}$$

where x^μ ($\mu = 0,1,2,3$) are the four directions of our physical spacetime and together with the S^1 coordinate τ (denoted by (4) in Table 4.1) span the worldvolume of the D4-brane. The parameter R is proportional to the curvature radius and is related to the string coupling constant g_s and the string length l_s by $R^3 = \pi g_s N_c l_s^3$. The 4-form field strength F_4 is proportional to the volume form ϵ_4 of a unit S^4 sphere with line-element $d\Omega_4^2$ and volume $V_4 = 8\pi^2/3$. The radial coordinate U in the 5-directions transverse to the D4-branes is bounded from below by $U \geq U_{\rm KK}$. To not get a conical singularity at $U = U_{\rm KK}$, the period of the S^1 must satisfy

$$\tau \sim \tau + \delta\tau\,, \quad \delta\tau \equiv \frac{4\pi}{3}\frac{R^{3/2}}{U_{\rm KK}^{1/2}}\,, \tag{4.2}$$

which can be used to define the Kaluza-Klein mass as

$$M_{\rm KK} = \frac{2\pi}{\delta\tau} = \frac{3}{2}\frac{U_{\rm KK}^{1/2}}{R^{3/2}}\,, \tag{4.3}$$

specifying the energy scale below which the compactified direction is negligible, and the dual gauge theory is given by a 4-dimensional Yang-Mills theory. The coupling constant of the dual Yang-Mills theory is given by $g_{\rm YM}^2 = 2\pi g_s l_s M_{\rm KK}$.

One can check that the effective action written in terms of $M_{\rm KK}$ and $g_{\rm YM}$ is actually independent of the string length l_s. Without loss of generality, one can then choose units in which

$$M_{\rm KK} = 1\,, \quad R^3 = \frac{9}{4}\,, \quad U_{\rm KK} = 1\,, \quad \frac{1}{g_s l_s^3} = \frac{4\pi}{9}N_c\,, \quad \lambda^{-1} = \frac{2}{9}l_s^2. \tag{4.4}$$

The last two equations show that the α' expansion in the DBI action and loop expansions in string theory ($1/g_s$) correspond to $1/\lambda$ and $N_c/\lambda^{3/2}$ expansions in the Yang-Mills theory, respectively.

4.1.2 Probe D8-Branes

In the brane configuration of Table 4.1, the embedding of a probe D8-brane in the D4 background (4.1) is described by $U = U(\tau)$ and the induced metric

$$\begin{aligned} ds^2_{D8} &= \left(\frac{U}{R}\right)^{3/2} \eta_{\mu\nu} dx^\mu dx^\nu + \left(\left(\frac{U}{R}\right)^{3/2} f(U) + \left(\frac{R}{U}\right)^{3/2} \frac{U'^2}{f(U)}\right) d\tau^2 \\ &\quad + \left(\frac{R}{U}\right)^{3/2} U^2 d\Omega_4^2, \end{aligned} \tag{4.5}$$

with $U' = \frac{d}{d\tau} U$. The embedding is found by minimizing the D8-brane action proportional to

$$\begin{aligned} S_{D8} &\propto \int d^4x d\tau\, \epsilon_4\, e^{-\phi} \sqrt{-\det(g_{D8})} \\ &\propto \int d^4x d\tau\, U^4 \sqrt{f(U) + \left(\frac{R}{U}\right)^3 \frac{U'^2}{f(U)}}\,, \end{aligned} \tag{4.6}$$

yielding the equation of motion

$$\frac{d}{d\tau}\left(\frac{U^4 f(U)}{\sqrt{f(U) + \left(\frac{R}{U}\right)^3 \frac{U'^2}{f(U)}}}\right) = 0\,. \tag{4.7}$$

With the initial conditions $U(0) = U_0$ and $U'(0) = 0$ at $\tau = 0$ the solution reads

$$\tau(U) = U_0^4 f(U_0)^{1/2} \int_{U_0}^{U} \frac{dU}{\left(\frac{U}{R}\right)^{3/2} f(U) \sqrt{U^8 f(U) - U_0^8 f(U_0)}}\,, \tag{4.8}$$

and for $U_0 = U_{\mathrm{KK}}$ we obtain the easiest configuration depicted in Fig. 4.1, where the D8 and $\overline{\mathrm{D8}}$ are maximally separated at antipodal points on the S^1 and join at the tip U_{KK} of the cigar-shaped subspace. In the following, we will always use this antipodal embedding.

4.2 Mesonic Degrees of Freedom

Through the holographic principle, mesonic degrees of freedom are described by fluctuations of the probe D8-brane characterized by the nine components of the gauge field A_μ ($\mu = 0, 1, 2, 3$), A_U and A_α ($\alpha = 5, 6, 7, 8$, the coordinates on the S^4) and one transverse scalar field ϕ_τ. We are only interested in the lowest spherical

harmonics on the S^4 and S^1, so that the non-vanishing gauge fields to A_μ and A_U only have x^μ and U dependence. The scalar field ϕ_τ is excluded due to its negative τ-parity [71]. This quantum number does not exist in QCD and is therefore excluded from the spectrum.

4.2.1 Equations of Motion

To study these fluctuations, the relevant action is a sum of the Dirac-Born-Infeld (DBI) action and the Chern-Simons (CS) term

$$\begin{aligned} S_{D8} &= -T \int d^9x \,\mathrm{Tr}\, e^{-\phi} \sqrt{-\det(g_{MN} + 2\pi\alpha' F_{MN})} + S_{CS} \\ &= \kappa \int d^4x dZ \,\mathrm{Tr}\left[\frac{1}{2} K^{-1/3} F_{\mu\nu}^2 + K M_{\mathrm{KK}}^2 F_{\mu Z}^2\right] + \mathcal{O}(F^3) \,, \end{aligned} \tag{4.9}$$

where $T = 1/((2\pi)^8 l_s^9)$ is the D8 brane tension, $\kappa \equiv \lambda N_c/(216\pi^3)$ and Tr denotes the trace over flavor indices. The radial direction along the D8 brane is rewritten as

$$K(Z) \equiv 1 + Z^2 \equiv \left(\frac{U}{U_{\mathrm{KK}}}\right)^3 , \tag{4.10}$$

such that Z runs from $-\infty$ to $+\infty$ and $Z = 0$ corresponds to $U = U_{\mathrm{KK}}$.

For the gauge fields, we make the separation ansatz

$$A_\mu(x^\mu, Z) = \sum_{n=1}^{\infty} B_\mu^{(n)}(x^\mu)\psi_n(Z) \,, \tag{4.11}$$

$$A_Z(x^\mu, Z) = \sum_{n=0}^{\infty} \varphi^{(n)}(x^\mu)\phi_n(Z) \,, \tag{4.12}$$

in terms of the complete sets $\{\psi_n(Z)\}$ and $\{\phi_n(Z)\}$.

Setting $\varphi^{(n)} = 0$ for the moment, we obtain the equation of motion

$$-K^{1/3}\,\partial_Z\left(K\,\partial_Z\psi_n\right) = \lambda_n\psi_n \,, \tag{4.13}$$

with eigenvalues λ_n. By demanding the normalization condition[1]

$$\kappa \int dZ K^{-1/3}\,\psi_n\psi_m = \delta_{nm} \,, \tag{4.14}$$

we obtain the 4-dimensional action

$$S_{D8} = \int d^4x \sum_{n=1}^{\infty} 2\,\mathrm{Tr}\left[\frac{1}{4}F_{\mu\nu}^{(n)}F^{\mu\nu(n)} + \frac{1}{2}m_n^2\,B_\mu^{(n)}B^{\mu(n)}\right] + \mathcal{O}(F^3)\,, \tag{4.15}$$

with finite masses $m_n^2 \equiv \lambda_n M_{\mathrm{KK}}^2$ for all $n \geq 1$.

Including non-vanishing modes $\varphi^{(m)}$, it can be shown that the radial functions are related by $\phi_n = m_n^{-1}\,\dot{\psi}_n$ $(n \geq 1)$, and from

$$F_{\mu Z} \;=\; \partial_\mu\varphi^{(0)}\phi_0 + \sum_{n\geq 1}\left(m_n^{-1}\partial_\mu\varphi^{(n)} - B_\mu^{(n)}\right)\dot{\psi}_n\,, \tag{4.16}$$

one can see that $\partial_\mu\varphi^{(n)}$ can be absorbed into $B_\mu^{(n)}$. The action then becomes

$$S_{D8} = -\int d^4x\,2\,\mathrm{Tr}\left[\frac{1}{2}\,\partial_\mu\varphi^{(0)}\partial^\mu\varphi^{(0)} + \sum_{n\geq 1}\left(\frac{1}{4}F_{\mu\nu}^{(n)}F^{\mu\nu(n)} + \frac{1}{2}m_n^2\,B_\mu^{(n)}B^{\mu(n)}\right)\right] + \mathcal{O}(F^3), \tag{4.17}$$

with the zero mode $\phi_0 = 1/(\sqrt{\kappa\pi}K)$, satisfying the normalization condition

$$\kappa\int dZ K\phi_0^2 = \frac{1}{\pi}\int_\infty^\infty dZ\frac{1}{1+Z^2} = 1. \tag{4.18}$$

4.2.2 Meson Spectrum

To obtain the spectrum of the spin-1 mesons contained in the mode expansion (4.11), we have to solve the differential equation (4.13), which is only possible numerically. Since Eq. (4.13) is invariant under the transformation $Z \to -Z$, we can assume that ψ_n is an even or odd function, for which we choose the boundary conditions

$$\partial_Z\psi_n(0) = 0 \;\text{ or }\; \psi_n(0) = 0\,, \tag{4.19}$$

respectively. To get a normalizable solution, we furthermore demand the boundary condition $\psi_n(\pm\infty) = 0$. The resulting spectrum reads

$$\lambda_n^{CP} = \;0.67^{--}\,,\;\; 1.6^{++}\,,\;\; 2.9^{--}\,,\;\; 4.5^{++}\,,\;\cdots\,, \tag{4.20}$$

[1] Note that the normalization of the radial modes depend on the normalization of the flavor matrices. Sakai and Sugimoto use the normalization $\mathrm{Tr}\,T^aT^b = \delta^{ab}/2$, while Ref. [72] uses $\mathrm{Tr}\,T^aT^b = \delta^{ab}$. The mode $\psi_n(Z)B_\mu^{(n)a}(x^\mu)T^a$ should be independent of the convention. Therefore, Ref. [72] uses the normalization condition $2\kappa\int\ldots$, which results in radial modes smaller by a factor $1/\sqrt{2}$ than the ones obtained by Sakai and Sugimoto.

where C and P stand for charge conjugation and parity transformation quantum numbers, respectively. Parity is associated with the 5-dimensional proper Lorentz transformation $(x^1, x^2, x^3, Z) \to (-x^1, -x^2, -x^3, -Z)$, under which $B_\mu^{(n)}$ behaves as a vector when ψ_n is an even function or as an axial vector for odd functions. Charge conjugation implies an interchange of the D8 and $\overline{\text{D8}}$ branes, corresponding to the transformation $Z \to -Z$ and additionally flipping the orientation of the string. This flip amounts to taking the transpose of the gauge fields. $B_\mu^{(n)}$ is then again odd or even when $\psi_n(Z)$ is even or odd, respectively. Ordering the modes by eigenvalue, we find that all ψ_{2k} are odd and all ψ_{2k+1} are even; the lightest λ_1 corresponds to a vector meson and λ_2 to an axial-vector meson, and so on. Comparing ratios of eigenvalues, we find $\sqrt{\lambda_2/\lambda_1} \approx 1.53$ very close to the experimental ratio $m_{a_1}/m_\rho \approx 1.59$. Identifying the second-lightest vector meson with the $\rho(1450)$, we get $\sqrt{\lambda_3/\lambda_1} \approx 2.07$, which is in reasonable agreement with the experimental value $m_{\rho^*}/m_\rho \approx 1.86$.

The massless spin-0 meson $\varphi^{(0)}$ turns out to have quantum numbers $J^{PC} = 0^{-+}$ and is interpreted as a pseudoscalar meson, the Goldstone boson of chiral symmetry breaking. For $N_f = 3$ it consists of pions, kaons, η and η' mesons. In the chiral limit, the η' meson gets a mass due to the anomalous breaking of the axial $U(1)_A$ symmetry. In the large-N_c limit, however, the anomaly is subleading and the symmetry is restored. The η' meson becomes massive only for large but finite N_c. The holographic realization of the $U(1)_A$ anomaly and the η' mass was already discovered in Ref. [11], but we will only review it later in Chapter 10.

The pseudoscalar sector of the DBI action can be rewritten in the familiar form of the chiral Lagrangian, coinciding with the Skyrme model

$$S = \int d^4x \left(\frac{f_\pi^2}{4} \text{Tr} \left(U^{-1} \partial_\mu U \right)^2 + \frac{1}{32 e_S^2} \text{Tr} \left[U^{-1} \partial_\mu U, U^{-1} \partial_\nu U \right]^2 \right) , \tag{4.21}$$

where we use the path-ordered holonomy

$$U = \text{P} \exp \left[i \int_{-\infty}^{\infty} dZ A_Z \right] , \tag{4.22}$$

and identify the pion decay constant

$$f_\pi^2 = \frac{1}{54\pi^4} \lambda M_{\text{KK}}^2 N_c = \frac{4}{\pi} M_{\text{KK}}^2 \kappa. \tag{4.23}$$

The other parameter e_S is determined by the free parameters of the model, and has the value $e_S^{-2} \approx 30.5 \lambda N_c/(27\pi^7)$ [11].

4.2.3 Choice of Parameters

At this point, it is useful to fix the free parameter M_{KK} and λ of the model. The usual fit of Refs. [11, 12] uses the ρ meson mass and the relation $m_\rho = \sqrt{\lambda_1} M_{\text{KK}} \approx 776$ MeV to fix the Kaluza-Klein mass to $M_{\text{KK}} = 949$ MeV. After fixing the mass scale, this fit then uses the experimental value of the pion decay constant $f_\pi \approx 92.4$ MeV and Eq. (4.23) to fix $\lambda = 16.63$. The resulting masses of vector mesons and axial-vector mesons will be presented in the next chapter.

While the usual fit requires mesonic degrees of freedom, it is also possible to fit λ in the pure YM-theory by fitting the string tension of a Wilson line connecting heavy quarks at the boundary with large spatial separation. In the holographic picture, they are represented by fundamental strings that minimize their energy. Since most of their length is near the minimum of the holographic coordinate, their effective string tension is approximated by

$$\sigma = \frac{1}{2\pi l_s^2} \sqrt{-g_{tt} g_{xx}}\Big|_{U=U_{\text{KK}}} = \frac{2\lambda}{27\pi} M_{\text{KK}}^2. \tag{4.24}$$

By comparing to the large-N_c lattice result $m_\rho/\sqrt{\sigma} = 1.504(50)$ of Ref. [73], we can fit $\lambda = 12.55$. In Part IV of this thesis, we will make use of the range $\lambda \approx 16.63 \ldots 12.55$ to estimate the variability of the predictions of this model.

4.2.4 Interactions

We can now use this model to make quantitative predictions on interactions of mesons. By evaluating the higher-order terms of the brane action (4.9) on the mode ansatz and integrating over the radial direction, we can derive an effective 4-dimensional interaction Lagrangian, first studied in Refs. [11, 12] and shortly presented in Appendix A. The coupling constants are given in terms of radial integrals and can be determined numerically. To compare to experimental data, it is also useful to calculate decay rates. As a sample calculation, let us look at the decay of a ρ meson into two pions, as presented in Ref. [72]. For the lowest vector meson $\rho \equiv v^1$, the interaction terms include

$$\mathcal{L}_{\rho\pi\pi} = -\sqrt{2} g_{\rho\pi\pi} \epsilon_{abc} (\partial_\mu \pi^a) \rho^{b\mu} \pi^c, \quad g_{\rho\pi\pi} = \int dZ \frac{1}{\pi K} \psi_1 = 24.030\, \lambda^{-\frac{1}{2}} N_c^{-\frac{1}{2}}. \tag{4.25}$$

The corresponding amplitude is obtained by variation with respect to the ρ and π fields. In the rest frame of the ρ meson with polarization $\epsilon^\mu = (0, \mathbf{e})$ we get

$$\mathcal{M} = i g_{\rho\pi\pi}\, \epsilon^\mu (p_\mu - q_\mu) = 2 i g_{\rho\pi\pi}\, \mathbf{e}\cdot\mathbf{p}, \tag{4.26}$$

where the pion momenta are $p^\mu = (|\mathbf{p}|, \mathbf{p})$ and $q^\mu = (|\mathbf{p}|, -\mathbf{p})$. The decay rate then reads

$$\Gamma_\rho/m_\rho = \frac{1}{4\pi}\int d\Omega \frac{|\mathcal{M}|^2}{16\pi m_\rho^2} = \frac{g_{\rho\pi\pi}^2}{48\pi} \approx \frac{7.659}{\lambda N_c} \approx \begin{cases} 0.1535\ (\lambda = 16.63) \\ 0.2034\ (\lambda = 12.55) \end{cases}, \tag{4.27}$$

which brackets the experimental value $\Gamma_\rho/m_\rho = 0.191(1)$ from Ref. [74].

4.3 Vector Meson Dominance

In this section, we follow Ref. [12] in introducing external gauge fields $(A_{L\mu}, A_{R\mu})$ by weakly gauging the $U(N_f)_L \times U(N_f)_R$ chiral symmetry. Most importantly, the coupling of mesons to the photon field A_μ^{em} can be introduced by the combination

$$A_{L\mu} = A_{R\mu} = eQA_\mu^{\text{em}}\,, \tag{4.28}$$

where e is the charge of the electron and Q is the electric quark charge matrix given by

$$Q = \frac{1}{3}\begin{pmatrix} 2 & & \\ & -1 & \\ & & -1 \end{pmatrix}, \tag{4.29}$$

for $N_f = 3$. According to the holographic principle, the external gauge fields then appear as the asymptotic values of the gauge field A_μ as

$$\lim_{Z\to+\infty} A_\mu(x^\mu, Z) = A_{L\mu}(x^\mu)\,, \quad \lim_{Z\to-\infty} A_\mu(x^\mu, Z) = A_{R\mu}(x^\mu)\,, \tag{4.30}$$

which changes the mode expansion (4.11) to

$$A_\mu(x^\mu, Z) = A_{L\mu}(x^\mu)\psi_+(Z) + A_{R\mu}(x^\mu)\psi_-(Z) + \sum_{n=1}^{\infty} B_\mu^{(n)}(x^\mu)\psi_n(Z)\,, \tag{4.31}$$

where the non-normalizable zero modes of Eq. (4.13) appear as

$$\psi_\pm(Z) \equiv \frac{1}{2}(1 \pm \psi_0(Z))\,, \quad \psi_0(Z) \equiv \frac{2}{\pi}\arctan Z\,. \tag{4.32}$$

Interestingly, we have $\partial_Z \psi_\pm(Z) \propto \phi_0(Z)$, which can be thought of as a continuation of the identity $\partial_Z \psi_n \propto \phi_n$ $(n \geq 1)$ obtained in the previous section.

The modes $\psi_\pm(Z)$ have non-vanishing values at the boundaries $Z \to \pm\infty$ and are thus non-normalizable. The kinetic terms of $A_{L\mu}$ and $A_{R\mu}$ therefore diverge and have to be regulated. However, we are only interested in interactions of mesons with external gauge fields and ignore this issue [12].

To make apparent the distinction between vector and axial-vector fields, we redefine the modes as

$$\mathcal{V}_\mu \equiv \frac{1}{2}(A_{L\mu} + A_{R\mu}) \,, \;\; \mathcal{A}_\mu \equiv \frac{1}{2}(A_{L\mu} - A_{R\mu}) \,, \;\; v_\mu^n \equiv B_\mu^{(2n-1)} \,, \;\; a_\mu^n \equiv B_\mu^{(2n)} \,. \tag{4.33}$$

By inserting the mode expansion (4.31) in the quadratic action (4.9), we obtain an action with a mixed kinetic term[2]

$$\begin{aligned} \mathcal{L}_{D8} \;\supset\; & \frac{1}{2}\mathrm{Tr}\left(\partial_\mu v_\nu^n - \partial_\nu v_\mu^n\right)^2 + \frac{1}{2}\mathrm{Tr}\left(\partial_\mu a_\nu^n - \partial_\nu a_\mu^n\right)^2 \\ & + a_{\mathcal{V}v^n}\mathrm{Tr}\left(\partial^\mu \mathcal{V}^\nu - \partial^\nu \mathcal{V}^\mu\right)\left(\partial_\mu v_\nu^n - \partial_\nu v_\mu^n\right) + a_{\mathcal{A}a^n}\mathrm{Tr}\left(\partial^\mu \mathcal{A}^\nu - \partial^\nu \mathcal{A}^\mu\right)\left(\partial_\mu a_\nu^n - \partial_\nu a_\mu^n\right) \\ & + \mathrm{Tr}\left(i\partial_\mu \Pi + f_\pi \mathcal{A}_\mu\right)^2 + m_{v^n}^2 \mathrm{Tr}\left(v_\mu^n\right)^2 + m_{a^n}^2 \mathrm{Tr}\left(a_\mu^n\right)^2 \,, \end{aligned} \tag{4.34}$$

where the mixing parameters are given by overlap integrals of the radial modes

$$a_{\mathcal{V}v^n} \equiv \kappa \int dZ\, K^{-1/3} \psi_{2n-1} \,, \quad a_{\mathcal{A}a^n} \equiv \kappa \int dZ\, K^{-1/3} \psi_{2n} \psi_0 \,. \tag{4.35}$$

The mixed kinetic terms can be diagonalized by the non-unitary field redefinition

$$\widetilde{v}_\mu^n \;\equiv\; v_\mu^n + a_{\mathcal{V}v^n} \mathcal{V}_\mu \,, \tag{4.36}$$

$$\widetilde{a}_\mu^n \;\equiv\; a_\mu^n + a_{\mathcal{A}a^n} \mathcal{A}_\mu \,. \tag{4.37}$$

One possible way to proceed is to apply this field redefinition to all terms in the action. However, this entails a lot of bookkeeping for individual terms that will eventually cancel with each other anyway. A far more elegant approach is to restart at the mode expansion, which after the field redefinition takes the form

$$A_\mu = \mathcal{V}_\mu \, \psi_v + \mathcal{A}_\mu \psi_a + \sum_{n=1}^{\infty} \widetilde{v}_\mu^n \, \psi_{2n-1} + \sum_{n=1}^{\infty} \widetilde{a}_\mu^n \, \psi_{2n} \,, \tag{4.38}$$

[2] Note again that we use the convention $\mathrm{Tr}\, T^a T^b = \delta^{ab}/2$, so we actually have canonically normalized kinetic terms.

where the non-normalizable modes formally take the form

$$\psi_v \equiv 1 - \sum_{n=1}^{\infty} a_{\mathcal{V}v^n} \psi_{2n-1} \ , \quad \psi_a \equiv \psi_0 - \sum_{n=1}^{\infty} a_{\mathcal{A}a^n} \psi_{2n} \ . \tag{4.39}$$

Using the orthonormality condition (4.14) and the completeness relation

$$\kappa \sum_{n=1}^{\infty} K^{-1/3}(Z')\psi_n(Z)\psi_n(Z') = \delta(Z - Z') \ , \tag{4.40}$$

one can check that ψ_v and ψ_a are orthogonal to the basis elements ψ_m of normalizable functions by

$$0 = \int dZ \, K^{-1/3} \psi_v \psi_m = \int dZ \, K^{-1/3} \psi_a \psi_m \ . \tag{4.41}$$

As a result, they are also orthogonal to all normalizable functions $f(z)$

$$0 = \int dZ \, K^{-1/3} \psi_v f = \int dZ \, K^{-1/3} \psi_a f. \tag{4.42}$$

Note that it is not allowed to set $\psi_v = \psi_a = 0$, which would mean that $\mathcal{V}_\mu$ and $\mathcal{A}_\mu$ decouple completely from the theory. This is not the case since in Eq. (4.39) the constant 1 and ψ_0, the radial modes of $\mathcal{V}_\mu$ or $\mathcal{A}_\mu$, are non-normalizable functions and cannot be expressed completely in terms of the basis elements ψ_m. Roughly, one can imagine that $\psi_v = \psi_a = 0$ are 0 everywhere except at the points $Z = \pm\infty$. The only term in the action (4.9) where this is relevant is

$$\begin{aligned} M_{\mathrm{KK}}^2 \kappa \int dZ \, \mathrm{Tr} \left[K F_{Z\nu}^2 \right] \quad &= \quad \mathrm{Tr} \Big[m_{v^n}^2 (\widetilde{v}_\mu^n - a_{\mathcal{V}v^n} \mathcal{V}_\mu)^2 + m_{a^n}^2 (\widetilde{a}_\mu^n - a_{\mathcal{A}a^n} \mathcal{A}_\mu)^2 + \\ &\qquad (i\partial_\mu \Pi + f_\pi \mathcal{A}_\mu)^2 \Big] + \dots \ , \end{aligned} \tag{4.43}$$

where we have used

$$\kappa \int dZ \, K \, \partial_Z \psi_v \, \partial_Z \psi_{2n-1} \quad = \quad -\lambda_{2n-1} a_{\mathcal{V}v^n} \ , \tag{4.44}$$

$$\kappa \int dZ \, K \, \partial_Z \psi_a \, \partial_Z \psi_{2n} \quad = \quad -\lambda_{2n} a_{\mathcal{A}a^n}. \tag{4.45}$$

All the other terms in the action are independent of $\mathcal{V}_\mu$ and $\mathcal{A}_\mu$ due to Eq. (4.42). This nicely realizes the so-called vector meson dominance (VMD) [75, 76], which states that electromagnetic interactions of hadrons are only mediated through the

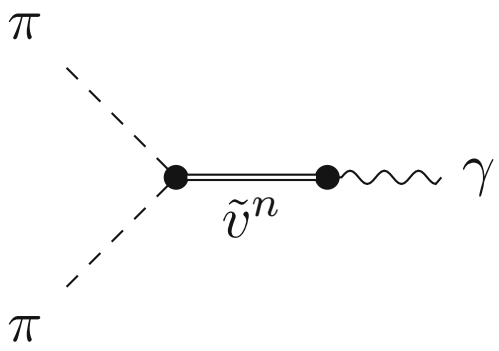

Figure 4.2. – Feynman diagram for the pion form factor using VMD.

exchange of vector mesons. From Eq. (A.4), one can read of the decay constants of the vector and axial-vector mesons as

$$\langle 0|J_\mu^{(V)a}(0)|v^{nb}\rangle = m_{v^n}^2 a_{\mathcal{V}v^n}\delta^{ab}\epsilon_\mu \ , \quad \langle 0|J_\mu^{(A)a}(0)|a^{nb}\rangle = m_{a^n}^2 a_{\mathcal{A}a^n}\delta^{ab}\epsilon_\mu \ . \tag{4.46}$$

Electromagnetic form factors

As a first calculation utilizing VMD, let us calculate the pion form factor $F_\pi(q^2)$ defined by

$$\langle \pi^a(p)|J_\mu^{(V)c}(0)|\pi^b(p')\rangle = f^{abc}(p+p')_\mu F_\pi((p-p')^2) \ , \tag{4.47}$$

where f^{abc} are the $U(N_f)$ structure constants. Due to VMD, we do not have a direct $\pi\pi\mathcal{V}$ coupling but have to combine the $\tilde{v}^n\pi\pi$ and the $\tilde{v}^n\mathcal{V}$ vertex as depicted in Fig. 4.2. Together with the $\tilde{v}^n$ propagator and a sum over all n, we obtain the pion form factor

$$F_\pi(Q^2) = \sum_{n=1}^{\infty} \frac{m_{v^n}^2 a_{\mathcal{V}v^n} g_{v^n\pi\pi}}{Q^2 + m_{v^n}^2} \ . \tag{4.48}$$

As a consistency check, we can set $Q^2 = 0$ and use the sum relation $\sum_{n=1}^{\infty} a_{\mathcal{V}v^n} g_{v^n\pi\pi} = 1$ to calculate $F_\pi(0) = 1$. Additionally, we can use the expansion

$$F_\pi(Q^2) = 1 - \sum_{n=1}^{\infty} \frac{a_{\mathcal{V}v^n} g_{v^n\pi\pi}}{m_{v^n}^2} Q^2 + \mathcal{O}(Q^4) \ , \tag{4.49}$$

to identify the charge radius of the pion [12]

$$\langle r^2\rangle^{\pi^\pm} = 6\sum_{n=1}^{\infty} \frac{a_{\mathcal{V}v^n} g_{v^n\pi\pi}}{m_{v^n}^2} \simeq (0.690 \text{ fm})^2 \ , \tag{4.50}$$

which is independent of λ, making it a particularly sharp prediction in fantastic agreement with the experimental value [74]

$$\langle r^2 \rangle^{\pi^\pm} \Big|_{\text{exp}} \simeq (0.672 \text{ fm})^2 \,. \tag{4.51}$$

Bulk-to-Boundary Propagator

In this section, we have seen how the mode expansion (4.31) introduces external photons and how we can perform explicit calculations including external photons. Now we want to briefly mention an alternative but equivalent approach, which will usually be used in bottom-up models. For this, we start with the momentum dependent mode equation

$$A_\mu(Q, Z) = \mathcal{V}_\mu(Q)\mathcal{J}(Q, Z), \tag{4.52}$$

where $\mathcal{J}(Q, Z)$ is the non-normalizable mode and all mesonic fields $B_\mu^{(n)}$ are set to zero. The non-normalizable mode satisfies the differential equation

$$(1 + Z^2)^{1/3}\partial_Z \left[(1 + Z^2)\partial_Z \mathcal{J}\right] = \frac{Q^2}{M_{\text{KK}}^2}\mathcal{J}, \quad \mathcal{J}(Q, Z = \pm\infty) = 1. \tag{4.53}$$

For real photons, we get $\mathcal{J}(0, Z) = 1$, which is consistent with the previous approach. In a proof similar to the one given for the bottom-up model in the next chapter, one can show that $\mathcal{J}$ satisfies the sum relation

$$\mathcal{J}(Q, Z) = \sum_n \frac{F_n^V \psi_{2n-1}}{Q^2 + m_{v^n}^2}, \tag{4.54}$$

with $F_n^V \equiv m_{v^n}^2 a_{\mathcal{V}v^n}$. In this approach, we directly obtain a $\mathcal{V}\pi\pi$ coupling from the action, and one can easily check that it yields the same result for the pion form factor (4.48). Using the sum relation (4.54) one can see that vector meson interactions can be easily calculated by projecting out poles in the timelike region of the corresponding (off-shell) photon interaction.

5 Bottom-Up Models

> *Everything must be made as simple as possible.*
> *But not simpler.*
>
> — **Albert Einstein**
> Physicist

EVEN before the top-down construction of Sakai and Sugimoto described in the previous chapter, the physics of chiral symmetry breaking and hadrons was studied in holographic bottom-up models. While in the top-down approach, one tries to deform a supersymmetric theory coming from string theory to obtain QCD, the bottom-up approach starts with QCD and tries to construct its 5-dimensional holographic dual by hand. Unfortunately, an exact dual to QCD is not yet known, and the best one can do is to build models that reproduce its characteristic features, like chiral symmetry breaking, and resemble QCD in certain limits. Ideally, the holographic models have few free parameters and can predict a large range of observables. The HW1 model, for example, has four free parameters, which can be fixed to well-measured observables. Stringy physics and the running of the QCD coupling, both of which become important at higher energies, are ignored in the construction of such models.

In this chapter, following the original literature, Ref. [68], and Ref. [II], we will review three of the easier bottom-up holographic QCD models: two hard-wall (HW) models and one soft-wall (SW) model. We will begin with the HW1 model introduced by Erlich et al., and by Da Rold and Pomarol in Refs. [14, 77], respectively. This model is called HW1 to distinguish it from the HW2 model of Hirn and Sanz [15], which will be discussed next. After briefly discussing the SW model of Refs. [78], we will conclude by comparing the spectra of the three bottom-up models and the top-down holographic Sakai-Sugimoto model.

5.1 Hard-Wall 1 Model

As a first step in the construction, we have to choose the field content of the model. The holographic dictionary, using the field-operator map, dictates the 5D field content through the duality between gauge-invariant local operators in the gauge theory and bulk fields on the gravity side. Theoretically, QCD has an infinite number of fields, e.g., composites of quark fields, corresponding to an infinite number of fields in the dual gravity theory. However, we can limit the number of operators to those that are important for chiral dynamics, such as chiral flavor symmetry currents and the chiral order parameter. Their field-operator maps are given by

$$\begin{aligned} &\bar{q}_L \gamma^\mu t^a q_L \leftrightarrow A^a_{L\mu}(x,z)\,, \\ &\bar{q}_R \gamma^\mu t^a q_R \leftrightarrow A^a_{R\mu}(x,z)\,, \\ &\bar{q}^\alpha_R q^\beta_L \leftrightarrow (2/z) X^{\alpha\beta}(x,z)\,, \end{aligned} \tag{5.1}$$

respectively. The 5D bulk mass of these fields is given by the relation $m_5^2 = (\Delta - p)(\Delta + p - 4)$, where Δ is the conformal dimension of the p-form boundary operator. For the currents we have $p = 1$, $\Delta = 3$ and $m_5^2 = 0$, while for the scalar X we have $p = 0$, $\Delta = 3$ and $m_5^2 = -3$.

As a background for these fields, we chose simple AdS_5 with the metric

$$ds^2 = z^{-2}(\eta_{\mu\nu} dx^\mu dx^\nu - dz^2)\,,\ 0 \le z \le z_0\,, \tag{5.2}$$

where the fifth coordinate z is cut off at a finite value z_0 to break the conformal isometry of the AdS space. It can be shown that high-energy QCD physics is reflected in the behavior of the bulk fields close to the AdS boundary $z = 0$, which is therefore referred to as the UV region. The region near the hard-wall cutoff $z = z_0$ is then called the IR region.

The action of the bulk fields (5.1) is given by

$$\begin{aligned} S \;=\; & -\frac{1}{4g_5^2}\int d^4x dz \sqrt{-g}\ \mathrm{Tr}\left(|F_L|^2 + |F_R|^2\right) \\ & + \int d^4x dz \sqrt{-g}\ \mathrm{Tr}\left(|DX|^2 - M_X^2 |X|^2\right) + S_{CS}, \end{aligned} \tag{5.3}$$

where we have introduced the covariant derivative $D_M X = \partial_M X - i A^L_M X + i X A^R_M$ and the Chern-Simons term $S_{CS} = S^L_{CS} - S^R_{CS}$ given by

$$S^{L,R}_{CS} = \frac{N_c}{24\pi^2}\int \mathrm{Tr}\left(AF^2 - \frac{i}{2}A^3 F - \frac{1}{10}A^5\right)^{L,R}, \tag{5.4}$$

up to a potential subtraction of an IR-boundary term discussed in Ref. [79]. We parametrize the bi-fundamental bulk scalar X as

$$X = e^{i\pi^a(x,z)t^a}[\tfrac{1}{2}v(z)]e^{i\pi^a(x,z)t^a}, \tag{5.5}$$

where $\pi^a(x,z)$ is a pseudoscalar field associated to axial transformations [80] and $v(z)/2$ is the vacuum solution

$$v(z) = M_q z + \Sigma\, z^3, \tag{5.6}$$

with the parameters M_q and Σ related to the quark mass matrix and the quark condensate. In the flavor symmetric case, they are proportional to the unit matrix, and we take $\Sigma = \sigma\mathbf{1}$ and $M_q = m_q\mathbf{1}$. With this, we have introduced the four free parameters of the model: m_q, σ, z_0 and g_5.

5.1.1 Vector Sector

The parameter g_5 can be fixed by comparing the result for the vector current two-point function with that of QCD. For the calculation, we introduce the vector field as $V = (A_L + A_R)/2$ and start with the non-normalizable mode in the $V_z = 0$ gauge. It satisfies the equation of motion

$$\partial_z\left[\frac{1}{z}\partial_z\mathcal{J}(Q,z)\right] - \frac{1}{z}Q^2\mathcal{J}(Q,z) = 0. \tag{5.7}$$

With the boundary conditions $\mathcal{J}(Q,0) = 1$ and $\partial_z\mathcal{J}(Q,z_0) = 0$, the solution reads

$$\mathcal{J}(Q,z) = Qz\left[K_1(Qz) + \frac{K_0(Qz_0)}{I_0(Qz_0)}I_1(Qz)\right]. \tag{5.8}$$

Evaluating the action on this solution, we are left with the boundary term

$$S = \frac{1}{2g_5^2}\int d^4x\left(\frac{1}{z}V_\mu^a\partial_z V^{\mu a}\right)_{z=\epsilon}, \tag{5.9}$$

with $V^\mu(q,z) = \mathcal{J}(q,z)V_0^\mu(q)$, where $V_0^\mu(q)$ is the Fourier transform of the source of the vector current $J_\mu^a = \bar{q}\gamma_\mu t^a q$ at the UV boundary. Varying the source V_0, we can derive the vector current two-point function

$$\int_x e^{iqx}\langle J_\mu^a(x)J_\nu^b(0)\rangle = \delta^{ab}(q_\mu q_\nu - q^2 g_{\mu\nu})\Pi_V(Q^2), \tag{5.10}$$

with

$$\Pi_V(Q^2) = -\frac{1}{g_5^2 Q^2}\left(\frac{1}{z}\partial_z \mathcal{J}(Q,z)\right)\Big|_{z\to 0} = -\frac{N_c}{2g_5^2}\ln Q^2. \tag{5.11}$$

Comparing to the calculation of the quark bubble [81]

$$\Pi_V(Q^2) = -\frac{N_c}{24\pi^2}\ln Q^2, \tag{5.12}$$

which is the leading-order diagram in QCD, leads to the identification of the first parameter

$$g_5^2 = \frac{12\pi^2}{N_c}. \tag{5.13}$$

To determine the remaining three parameters, we look at hadron physics, which is described by normalizable modes of the bulk fields. For the vector sector, we use the separation ansatz $V_\mu^a = g_5 \sum_{n=1}^{\infty} v_\mu^a(x)\psi_n(z)$ to get the wave equation

$$\partial_z\left[\frac{1}{z}\partial_z\psi_n(z)\right] + \frac{1}{z}M_n^2\psi_n(z) = 0, \tag{5.14}$$

with boundary conditions $\psi_n(0) = \psi_n'(z_0) = 0$. The solutions $\psi_n(z) \propto zJ_1(M_n z)$ are given by Bessel functions and the discrete eigenvalues $M_n = \gamma_{0,n}/z_0$ determined by the zeros of the Bessel function J_0, denoted by $\gamma_{0,n}$. To get canonically normalized vector mesons upon integrating over the fifth direction in the action, we impose the normalization condition $\int_0^{z_0} dz\, z^{-1}\psi_n(z)^2 = 1$, yielding

$$\psi_n(z) = \sqrt{2}\frac{zJ_1(\gamma_{0,n}z/z_0)}{z_0 J_1(\gamma_{0,n})}. \tag{5.15}$$

We can also define the Green's function or bulk-to-bulk propagator by

$$\frac{1}{z}\left(L_V + q^2\right)G_V(z,z';q) = -\delta(z-z'), \qquad L_V(f) = z\partial_z\left(\frac{1}{z}\partial_z f\right), \tag{5.16}$$

which, in the spectral representation, has the solution

$$G_V(z,z';q) = -\sum_n \frac{\psi_n(z)\psi_n(z')}{q^2 - M_n^2}. \tag{5.17}$$

The bulk-to-bulk and bulk-to-boundary propagator can be related by using Green's 2nd theorem:

$$\begin{aligned}&\int dz\frac{1}{z}\left[\psi\left(L_V + q^2\right)\chi - \chi\left(L_V + q^2\right)\psi\right]\\ &= -\lim_{z'\to 0}\left[\psi(z')\mathcal{D}_{z'}^V\chi(z') - \chi(z')\mathcal{D}_{z'}^V\psi(z')\right],\end{aligned} \tag{5.18}$$

with $\mathcal{D}_z^V = \frac{1}{z}\partial_z$. Choosing $\psi = \mathcal{J}(q,z)$ and $\chi = G_V(z,z';q)$, we get

$$\mathcal{J}(q,z') = \lim_{z\to 0}\frac{1}{z}\partial_z G_V(z,z';q) - G_V(0,z';q). \tag{5.19}$$

Using Eq. (5.17), the second term cancels due to the boundary condition $\psi_n(0) = 0$ and the first term gives the result

$$\mathcal{J}(q,z') = -\sum_n \frac{[\psi_n'(\epsilon)/\epsilon]\psi_n(z')}{q^2 - M_n^2} = -\sum_n \frac{g_5 F_n^V \psi_n(z')}{q^2 - M_n^2}, \tag{5.20}$$

where we have used the vector meson decay constant $F_n^V = \psi_n'(\epsilon)/(g_5\epsilon)$ defined by

$$\langle 0|J_\mu^a(0)|v_n^b(q,\lambda)\rangle = F_n^V \varepsilon_\mu(q,\lambda)\delta^{ab}. \tag{5.21}$$

5.1.2 Axial Sector

In the axial sector, given by $A = (A_L - A_R)/2$ and the pseudoscalar field $\pi(x,z)$ in Eq. (5.5), the Lagrangian reads

$$\mathcal{L}_{axial} = -\frac{1}{4g_5^2 z}(\partial_M A_N - \partial_N A_M)^2 + \frac{\beta(z)}{2g_5^2 z}(\partial_M \pi - A_M)^2, \qquad \beta(z) = g_5^2 v^2/z^2, \tag{5.22}$$

where an implicit contraction with the flat 5D Minkowski metric in mostly minus metric convention is implied. In the gauge $A_z = 0$, we split the gauge field as $A_\mu = A_\mu^\perp + \partial_\mu \phi$ to obtain the coupled equations of motion

$$\partial_z\left(\frac{1}{z}\partial_z\phi\right) + \frac{\beta(z)}{z}(\pi - \phi) = 0, \tag{5.23}$$

$$\partial_z\left(\frac{\beta(z)}{z}\partial_z\pi\right) + \frac{\beta(z)}{z}q^2(\pi - \phi) = 0, \tag{5.24}$$

for the pseudoscalar fields ϕ and π. By defining $y = \partial_z\phi/z$ they can be combined into a single equation [82, 80]:

$$(L_{PS} + q^2)y := \frac{\beta(z)}{z}\partial_z\left(\frac{z}{\beta(z)}\partial_z y\right) - \beta(z)y + q^2 y = 0. \tag{5.25}$$

From Eq. (5.24) we can construct the inverse transformation

$$\partial_z y = \frac{\beta(z)}{z}(\phi - \pi) \tag{5.26}$$

and

$$\partial_z \pi = \frac{q^2}{\beta(z)} z y. \tag{5.27}$$

The normalizable boundary conditions $\phi_n(\epsilon) = 0$, $\pi_n(\epsilon) = 0$ translate to

$$\frac{z}{\beta(z)} \partial_z y_n(z) \Big|_{z=\epsilon} = 0, \tag{5.28}$$

while the non-normalizable boundary conditions $\phi_S(q, \epsilon) = 0$, $\pi_S(q, \epsilon) = -1$ give

$$\frac{z}{\beta(z)} \partial_z y_S(q, z) \Big|_{z=\epsilon} = 1. \tag{5.29}$$

At the infrared boundary $z = z_0$, the boundary conditions have to cancel the boundary term

$$\frac{1}{2g_5^2 z_0} \left(q^2 \phi \partial_z \phi - \beta \pi \partial_z \pi \right)_{z=z_0} = \frac{q^2}{2g_5^2} y(z_0) \left[\phi(z_0) - \pi(z_0) \right] \tag{5.30}$$

in the axial action [II]. The usual choice of Refs. [14, 77] is $\phi'(z_0) = 0$, implying $y(z_0) = 0$. The other choice $[\phi(z_0) - \pi(z_0)] = 0$ implies $\partial_z y|_{z=z_0} = 0$ and is used in the HW3 model of Ref. [II] and Ref. [83].

To get canonically normalized pseudoscalars, we have to normalize the modes by

$$\int_\epsilon^{z_0} dz \frac{z}{\beta(z)} y_n y_m = \int_\epsilon^{z_0} dz \frac{1}{z\beta(z)} \partial_z \phi_n \partial_z \phi_m = \frac{\delta_{mn}}{m_n^2}. \tag{5.31}$$

Plots of the first few mode functions can be seen in Fig. 5.1.

The non-normalizable mode y_S can either be calculated numerically or be expressed by the sum rule [80]

$$y_S(q, z) = \sum_n \frac{m_n^2 y_n(\epsilon) y_n(z)}{q^2 - m_n^2} = -g_5 \sum_{n=1}^{\infty} \frac{f_{\pi_n} m_n^2 y_n(z)}{q^2 - m_n^2}, \tag{5.32}$$

where $f_{\pi_n} = -y_n(\epsilon)/g_5$ are the pion decay constants defined by

$$\langle 0 | J_{\|\mu}^{A,a}(0) | \pi_n^b(q) \rangle = i f_{\pi_n} q_\mu \delta^{ab}. \tag{5.33}$$

Similar to the case of vector mesons, we can also define the pseudoscalar bulk-to-bulk propagator by

$$\frac{z}{\beta(z)} \left(L_{PS} + q^2 \right) G_{PS}(z, z'; q) = -\delta(z - z'), \tag{5.34}$$

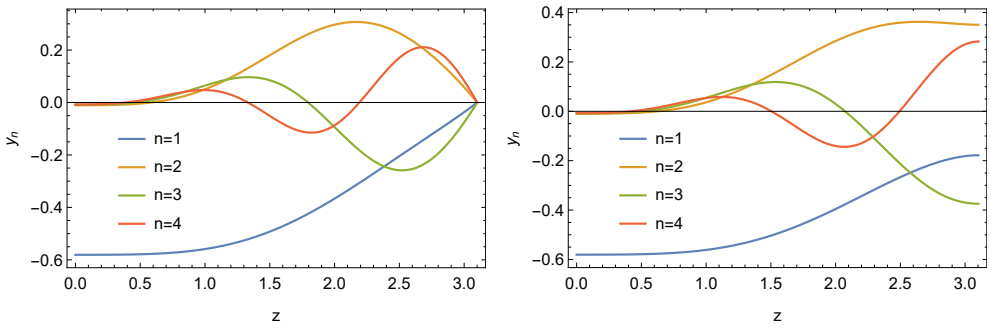

Figure 5.1. – The first four pion mode functions $y_n(z)$ in the HW1 and HW3 model, with $y_n(0) = -g_5 f_{\pi_n}$. Figure from Ref. [II].

which in the spectral representation reads[1]

$$G_{PS}(z, z'; q) = -\sum_n \frac{m_n^2 y_n(z) y_n(z')}{q^2 - m_n^2}. \tag{5.35}$$

Using again Green's 2nd theorem (5.18), but with $\mathcal{D}_z = \frac{z}{\beta(z)}\partial_z$ and choosing $\psi = y_S(q, z)$ and $\chi = G_{PS}(z, z'; q)$, we find a relation between the bulk-to-bulk and bulk-to-boundary propagator

$$y_S(q, z') = \lim_{z\to 0} \frac{z}{\beta(z)} \partial_z G_{PS}(z, z'; q) - G_{PS}(0, z'; q). \tag{5.36}$$

In this case, we can use Eq. (5.35) to see that the first term cancels and the second term results in Eq. (5.32).

For the axial-vector mesons, we make a separation ansatz $A_\mu^\perp = g_5 \sum_{n=1}^\infty a_\mu^{(n)}(x)\psi_n^A(z)$, similar to the one for the vector mesons, to obtain

$$\partial_z \left[\frac{1}{z}\partial_z \psi_n^A(z)\right] + \frac{1}{z}\left[M_{A,n}^2 - \beta(z)\right]\psi_n^A(z) = 0. \tag{5.37}$$

The resulting spectrum differs from the vector sector when $v \neq 0$, even though we choose identical boundary conditions $\psi_n^A(0) = \psi^{A\prime}{}_n(z_0) = 0$. In the HW3 model, one instead chooses the Dirichlet boundary condition $\psi_n^A(z_0)_{\mathrm{HW3}} = 0$, breaking chiral symmetry similarly to the SS or HW2 model.

[1] The unusual m_n^2 is due to the normalization condition (5.31).

5.1.3 Comparison to Experiment

In the following, we will compare the HW1 model to experimental low-energy data. We will keep the parameter g_5 fixed by Eq. (5.13) and then fit the remaining three parameters.

In Ref. [14], two approaches for fitting the three free parameters are described; they are called Model A and B. Model A computes $z_0 = 1/(323\,\text{MeV})$ by fitting the lowest vector meson mass to the physical ρ meson mass. The quark mass m_q and chiral condensate σ are fitted to the experimental values of m_π and f_π, yielding $m_q = 2.29\,\text{MeV}$ and $\sigma = (327\,\text{MeV})^3$. Table 5.1 displays a total of seven different low-energy observables. Model A fits three of them, while the remaining four are model predictions that can be compared to the experiment. The lowest axial-vector mass m_{a_1} and decay constant F_{a_1} slightly overshoot the experimental values, while the ρ meson decay width and its coupling constant to two pions are slightly too low. For these four predictions, the root-mean-square error is 15%.

Model B is given by a global fit over all seven observables listed in Table 5.1 and yields $z_0 = 1/(346\,\text{MeV})$, $m_q = 2.3\,\text{MeV}$ and $\sigma = (308\,\text{MeV})^3$. In this case, we can only compare how close all seven observables are to the experiment, which yields a remarkable root-mean-square error of only 9%. In the following, due to its simplicity, we will mostly use a parameter fit similar to Model A.

A nice comparison of the model with the chiral Lagrangian and the experimental values of its low-energy coefficients L_i at order $\mathcal{O}(p^4)$ can be found in Ref. [77]. By integrating out heavy resonances, one obtains the effective Lagrangian of the pseudo-Goldstone boson

$$\mathcal{L} = \frac{f_\pi^2}{4}\,\text{Tr}\left[D_\mu U^\dagger D^\mu U + U^\dagger\chi + \chi^\dagger U\right] + \mathcal{L}_4 + \mathcal{O}(p^4)\,, \tag{5.38}$$

with

$$U = e^{i\sqrt{2}\,\pi/f_\pi}\,, \qquad \chi = -2\frac{\langle\bar{q}q\rangle}{f_\pi^2}\,(M_q + ip)\,, \qquad M_q = \text{Diag}(m_u, m_d, m_s)\,, \tag{5.39}$$

Observable	Measured (MeV)	Model A (MeV)	Model B (MeV)
m_π	139.6 ± 0.0004 [84]	139.6*	141
m_ρ	775.8 ± 0.5 [84]	775.8*	832
m_{a_1}	1230 ± 40 [84]	1363	1220
f_π	92.4 ± 0.35 [84]	92.4*	84.0
$F_\rho^{1/2}$	345 ± 8 [85]	329	353
$F_{a_1}^{1/2}$	433 ± 13 [86, 87]	486	440
$g_{\rho\pi\pi}$	6.03 ± 0.07 [84]	4.48	5.29

Table 5.1. – Comparison of two different parameter fits of the HW1 model to the experimental values. Model A fits three observables (indicated with *), while Model B is a global fit over all seven observables. Table from Ref. [14].

	Experiment	AdS_5
L_1	0.4 ± 0.3	0.4
L_2	1.4 ± 0.3	0.9
L_3	-3.5 ± 1.1	-2.6
L_4	-0.3 ± 0.5	0.0
L_5	1.4 ± 0.5	1.7
L_6	-0.2 ± 0.3	0.0
L_9	6.9 ± 0.7	5.4
L_{10}	-5.5 ± 0.7	-5.5

Table 5.2. – Holographic predictions for the ten L_i compared to their experimental values [88] at the scale M_ρ in units of 10^{-3} . Table from Ref. [77].

and the fourth-order terms

$$\begin{aligned}
\mathcal{L}_4 &= L_1 \,\mathrm{Tr}^2\left[D_\mu U^\dagger D^\mu U\right] + L_2 \,\mathrm{Tr}\left[D_\mu U^\dagger D_\nu U\right]\mathrm{Tr}\left[D^\mu U^\dagger D^\nu U\right] \\
&+ L_3 \,\mathrm{Tr}\left[D_\mu U^\dagger D^\mu U D_\nu U^\dagger D^\nu U\right] \\
&+ L_4 \,\mathrm{Tr}\left[D_\mu U^\dagger D^\mu U\right]\mathrm{Tr}\left[U^\dagger\chi + \chi^\dagger U\right] + L_5 \,\mathrm{Tr}\left[D_\mu U^\dagger D^\mu U \left(U^\dagger\chi + \chi^\dagger U\right)\right] \\
&+ L_6 \,\mathrm{Tr}^2\left[U^\dagger\chi + \chi^\dagger U\right] + L_7 \,\mathrm{Tr}^2\left[U^\dagger\chi - \chi^\dagger U\right] + L_8 \,\mathrm{Tr}\left[\chi^\dagger U\chi^\dagger U + U^\dagger\chi U^\dagger\chi\right] \\
&- iL_9 \,\mathrm{Tr}\left[F_R^{\mu\nu} D_\mu U D_\nu U^\dagger + F_L^{\mu\nu} D_\mu U^\dagger D_\nu U\right] + L_{10} \,\mathrm{Tr}\left[U^\dagger F_R^{\mu\nu} U F_{L\mu\nu}\right]. \quad (5.40)
\end{aligned}$$

In a similar fit to the Model A in Ref. [14], albeit with slightly different parameters, one finds a nice agreement of the ten coefficients L_i with experimental data displayed in Table 5.2. Given the simplicity of the HW1 model, it is quite remarkable how almost all ten L_i are within the experimental error bars, with the only exceptions being L_2 and L_9, which lie slightly outside.

5.1.4 Chiral Limit

Because all the other models we are looking at are chiral, we also want to introduce the chiral limit for the HW1 model. In this limit, the vector sector remains unchanged, whereas the axial sector changes. As shown below, the axial-vector mesons only get slightly different eigenvalues and eigenmodes, while the pion sector changes significantly.

A useful formula for studying the chiral limit of the pion sector can be derived from the normalization condition (5.31) in which the weight function $z/\beta(z)$ is concentrated at small z values for $M_q \ll \Sigma z_0^2$. The functions y_n are relatively constant for small z and can be pulled out of the integral

$$g_5^2 f_{\pi_n}^2 m_n^2 \int_0^\infty dz \frac{z}{\beta(z)} = 1, \tag{5.41}$$

which after performing the integral yields the Gell-Mann–Oakes–Renner relation

$$f_{\pi_n}^2 m_n^2 \approx 2 M_q \Sigma. \tag{5.42}$$

This implies a vanishing mass in the chiral limit for the ground-state pion with fixed $f_{\pi_1} = f_\pi$. Excited states with $m > 1$ have non-vanishing masses and require $f_{\pi_n} \to 0$. From Eq. (5.32), we can see that the massive pions decouple from the bulk-to-boundary propagator and therefore from the axial-vector current and axial anomaly; the bulk-to-boundary propagator becomes $y_S \to g_5 f_\pi y_1$, $f_\pi = f_{\pi_1}$. The chiral wave function $y_S \equiv \partial_z \Psi / z$ can be given analytically [89, 79] by

$$\Psi(z) = \Gamma(\tfrac{2}{3}) \left(\xi z^3/2\right)^{1/3} \left[I_{-1/3}(\xi z^3) - \frac{I_{2/3}(\xi z_0^3)}{I_{-2/3}(\xi z_0^3)} I_{1/3}(\xi z^3) \right], \tag{5.43}$$

where $\xi = g_5 \sigma / 3$ and $g_5^2 = 12\pi^2 / N_c$. The parameter $\xi = (0.424\,\text{GeV})^3$ is fixed by $f_\pi = 92.4$ MeV.

5.2 Hard-Wall 2 Model

The second hard-wall model studied in this thesis was introduced by Hirn and Sanz [15] and was first called HW2 in Ref. [90]. Compared to the HW1 model, it does not introduce a bi-fundamental scalar field X, but instead breaks chiral symmetry, similarly to the SS model, by introducing different boundary conditions for the vector and axial-vector sector on the hard wall: Neumann for vector and Dirichlet

for axial-vector mesons. The same conditions are applied in the SS model at the point $Z = 0$, the point where the D8 and $\overline{\text{D8}}$ branes join.

Vector mesons and the corresponding bulk-to-boundary propagator describing photons are the same as in the HW1 model and are given by Eq. (5.8) and (5.15). Moreover, the value of z_0 is unchanged, since in the usual fit it is fixed by the ρ meson mass.

Axial-vector mesons are given by the same differential equation as vector mesons (5.14)

$$\partial_z \left[\frac{1}{z}\partial_z \psi_n^A(z)\right] + \frac{1}{z} M_{A,n}^2 \psi_n^A(z) = 0, \tag{5.44}$$

but have different boundary conditions $\psi_n^A(0) = (\psi_n^A)'(z_0) = 0$, leading to the solutions

$$\psi_n^A(z) \propto z J_1(M_n^A z), \quad M_n^A = \gamma_{1,n}/z_0. \tag{5.45}$$

Pions are given by

$$\Psi(z) = 1 - \frac{z^2}{z_0^2}. \tag{5.46}$$

In this model we do not have the parameter σ to fix the pion decay constant, but we have to use the parameter g_5 and the equation

$$g_5^2 = \frac{2}{f_\pi^2 z_0^2}, \tag{5.47}$$

instead. This fit yields $g_5 \approx 4.932$ for $f_\pi = 92.4$. By changing the value of g_5, it is clear that this model does not produce the correct asymptotics of the vector current two-point function.

5.3 Soft-Wall Model

A common issue of the holographic QCD models described up to now is that they do not correctly describe (radially) excited mesons. The holographic eigenvalues are similar to a particle in a box, where the Schrödinger equation gives a spectrum of squared masses m_n^2 growing as n^2 for large n. The data of meson masses, however, suggests a spectrum $m_n^2 \sim n$.

This correct Regge-type spectrum can be achieved in soft-wall (SW) models, as was first shown in Ref. [16]. As bottom-up models, they combine by hand a background similar to the HW models with a nontrivial background dilaton field $\Phi(z) = \kappa^2 z^2$.

This leads to the vector meson spectrum $M_n^2 = 4\kappa^2(n+1)$ with $\kappa = m_\rho/2$ and implements confinement by a soft cutoff as $z \to \infty$. This cutoff, however, leads to an unsatisfactory realization of spontaneous symmetry breaking where the parameters of spontaneous and explicit symmetry breaking are not independent.[2]

We follow Ref. [90] in therefore not considering the original soft-wall model [16] but instead consider the more heuristic model of Ref. [78], where the pion wave function takes the Gaussian form

$$\Psi(z) = e^{-\kappa^2 z^2} \tag{5.48}$$

and axial-vector mesons are absent.

In this model, the bulk-to-boundary propagator has the analytic form

$$\mathcal{J}(Q,\kappa,z) = \frac{U(\frac{Q^2}{4\kappa^2},0,(\kappa z)^2)}{U(\frac{Q^2}{4\kappa^2},0,0)} = \Gamma(1+\tfrac{Q^2}{4\kappa^2})U(\tfrac{Q^2}{4\kappa^2},0,(\kappa z)^2), \tag{5.49}$$

given by confluent hypergeometric functions of the second kind $U(a,b,z)$.

5.4 Comparison of Spectra

In Table 5.3 and 5.4 we compare the holographic masses of the lowest three vector and axial-vector masses to experimental values. We also include the HW2(UV-fit) model, which is basically the HW2 model but not with $g_5 \approx 4.932$ fitted to the pion decay constant (a low-energy observable), but with $g_5 = 2\pi$, to reproduce the correct vector current two-point function (a high-energy observable). However, this change of parameter comes at the cost of bad IR fits, e.g., the ρ mass has 987.2 MeV. The vector meson masses clearly show that the SS, HW1 and HW2 models have the wrong Regge behavior and grow too quickly. The SW model grows slower, but also fails to give a good fit of the excited vector meson masses. For axial-vector mesons, the SS, HW1 and HW2 model give decent values for the lowest mass, while they are absent in the considered SW model of Ref. [78].

[2] The axial sector of the original SW model [16] is worked out in Ref. [82], leading to unphysically high axial-vector meson masses. See also Ref. [91] for improved SW models.

	m_V	m_{V^*}	$m_{V^{**}}$
SS	775	1606.0	2379.3
HW1,2	775	1778.9	2788.8
HW2(UV-fit)	987.2	2266.1	3552.6
SW	775	1096.0	1342.3
m_ρ (exp.)	775.26(25)	1465(25)	1720(20)
m_ω (exp.)	782.65(12)	1425(25)	1670(30)
m_ϕ (exp.)	1019.461(19)	1680(20)	

Table 5.3. – Comparison of the holographic masses of the lowest three vector mesons with the experimental values [92]. Table from Ref. [IV].

	m_A	m_{A^*}	$m_{A^{**}}$
SS	1186.5	2019.8	2843.2
HW1	1375.5	2154.2	2995.1
HW2	1234.8	2260.9	3278.6
HW2(UV-fit)	1573.0	2880.1	4176.4
m_{a_1} (exp.)	1230(40)	1655(16)	$1930(^{+30}_{-70})$
m_{f_1} (exp.)	1281.9(0.5)	1670(30)	1971(15)
$m_{f_1'}$ (exp.)	1426.3(0.9)		

Table 5.4. – Comparison of the holographic masses of the lowest three axial-vector mesons with the experimental values [92]. Table from Ref. [IV].

Part III

Holographic Predictions for a_μ^{HLbL}

In this part of the thesis, we will present the main results of Refs. [I, II, IV, VI] on holographic predictions for the HLbL contribution to the anomalous magnetic moment of the muon. We will start with the calculation of the pseudoscalar-pole contribution, where the crucial pion transition form factor will be studied in some detail. Next, we will study the contribution of axial-vector mesons and their relevance in satisfying short-distance constraints. We will end this part by extending our results to holographic models with massive quarks and a brief discussion.

6 Pion Contribution to HLbL

> *It's a dangerous business, Frodo, going out your door. You step onto the road, and if you don't keep your feet, there's no knowing where you might be swept off to.*
>
> **— J.R.R. Tolkien**
> The Lord of the Rings

EVEN though in recent years the formulation of a dispersive approach for HLbL reduced the uncertainty in the pseudoscalar-pole contribution considerably, it is still interesting to consider model-dependent calculations of this quantity. This is in particular true for holographic QCD models that can describe with a minimal set of free parameters HLbL contributions from different intermediate states. After benchmarking the models by comparing to model-independent results for the pseudoscalar sector, they may also be used to make predictions for the axial-vector sector, where up to now the dispersive approach cannot be used.

We will consider the holographic QCD models introduced in Part II, where we already mentioned that holographic QCD is not real QCD. However, we have also seen that the models often give predictions within a 10% uncertainty, which is well below the current 20% uncertainty in HLbL.

In this chapter, we will present the results obtained in Ref. [VI]. First, we will calculate the pion transition form factor from holographic QCD using the Chern-Simons term. Then, we will compare its low-energy behavior with experimental data from CELLO, CLEO, NA62 and recent preliminary data from BESIII. Further, we will compare to the interpolators of Ref. [90] as well as to new ones introduced in Ref. [93]. Next, we will calculate the high-energy behavior of the transition form factor and compare to short-distance constraints from perturbative QCD and to experimental data from BaBar. Finally, we will compute the pseudoscalar-pole contribution to HLbL using the full 3-dimensional integral formulae of Ref. [94].

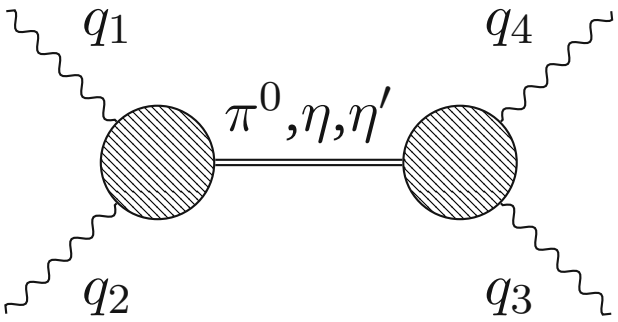

Figure 6.1. – Dominant contributions to the HLbL tensor given by a pseudoscalar meson exchange, where the shaded blobs are described by the pseudoscalar transition form factor.

6.1 Transition Form Factor

The pseudoscalar-pole contribution to HLbL is given by the Feynman diagram 6.1, where the shaded blobs represent the pseudoscalar transition form factor (TFF) defined by

$$\int d^4x e^{-iq_1\cdot x}\langle\pi(q_1+q_2)|T\left\{J_\mu^{e.m.}(x)J_\nu^{e.m.}(0)\right\}|0\rangle = \epsilon_{\mu\nu\rho\sigma}q_1^\rho q_2^\sigma F_{\pi\gamma^*\gamma^*}(Q_1^2,Q_2^2), \quad (6.1)$$

for the pion and similarly for the other pseudoscalar mesons. In the previous part, we have already collected all the necessary ingredients to holographically calculate this TFF.

In all the considered models, it is determined by the universal form of the Chern-Simons term [79, 95, 90, 96] resulting in[1]

$$K(Q_1^2,Q_2^2) \equiv \frac{F(Q_1^2,Q_2^2)}{F(0,0)} = -\int_0^{z_0} \mathcal{J}(Q_1,z)\mathcal{J}(Q_2,z)\partial_z\Psi(z)dz, \quad (6.2)$$

where Ψ and $\mathcal{J}$ are the pion mode and bulk-to-boundary propagator as introduced in Part II for the different models.[2] The normalization of the TFF

$$F_{\pi^0\gamma^*\gamma^*}(0,0) = \frac{N_c}{12\pi^2 f_\pi} \quad (6.3)$$

[1] We use F as a shorthand notation for $F_{\pi\gamma^*\gamma^*}$.
[2] In the SS model the pion mode was called ψ_0.

Model	$\hat{\alpha}[\text{GeV}^{-2}]$	$\hat{\beta}[\text{GeV}^{-4}]$	$\hat{\gamma}[\text{GeV}^{-4}]$
SS	-2.043	4.56	3.55
HW1	-1.595	3.01	2.63
HW2	-1.805	3.65	3.06
SW	-1.665	3.56	2.76
DIP1	-1.760	3.33	3.78
DIP2	-1.760	3.33	3.88
DRV4	-1.742	∞	3.04
DRV9	-1.637	∞	2.68

Table 6.1. – Comparison of the IR behavior of the pion TFF. Table from Ref. [VI].

is fixed by the axial anomaly. In the HW1 model one additionally needs to subtract a boundary term and the result reads [79]

$$K^{\text{HW1}}(Q_1^2, Q_2^2) = -\int_0^{z_0} \mathcal{J}(Q_1, z)\mathcal{J}(Q_2, z)\partial_z\Psi(z)dz + \mathcal{J}(Q_1, z_0)\mathcal{J}(Q_2, z_0)\Psi(z_0). \tag{6.4}$$

6.1.1 Low-Energy Behavior

For the HLbL contribution, the low-energy regime below virtualities of $1\,\text{GeV}^2$ is crucial. It is therefore interesting to compare the low-energy behavior of our TFFs, parametrized in the Taylor series

$$K(Q_1^2, Q_2^2) = 1 + \hat{\alpha}(Q_1^2 + Q_2^2) + \hat{\beta}Q_1^2Q_2^2 + \hat{\gamma}(Q_1^4 + Q_2^4) + O(Q^6), \tag{6.5}$$

with each other and the experiment.

In Table 6.1 the corresponding coefficients are collected. Unfortunately, there is only experimental data on the slope parameter $\hat{\alpha}$ for which the current world average of $\hat{\alpha} = -1.84(17)\,\text{GeV}^{-2}$ [92] is a combination of the CELLO collaboration result $\hat{\alpha} = -1.76(22)\,\text{GeV}^{-2}$ [97] and the recent result $\hat{\alpha} = -2.02(31)\,\text{GeV}^{-2}$ [98] from an analysis of Dalitz decays of π^0 from NA62.

The other lines in the Table 6.1 correspond to the DIP1 and DIP2 interpolators constructed in Ref. [90] to fit the average of $\hat{\alpha}$ and $\hat{\beta}$, and the DRV4 and DRV9 interpolators of [93] considering experimental data up to 4 GeV or 9 GeV, respectively.

In Fig. 6.2 we compare the holographic models to spacelike π^0 TFF data at $Q^2 \leq 4\,\text{GeV}^2$ as compiled in Fig. 3 of Ref. [93], which includes data from CELLO, CLEO and preliminary data from BESIII. Near $Q^2 = 0$ and up to the first data point at 0.3

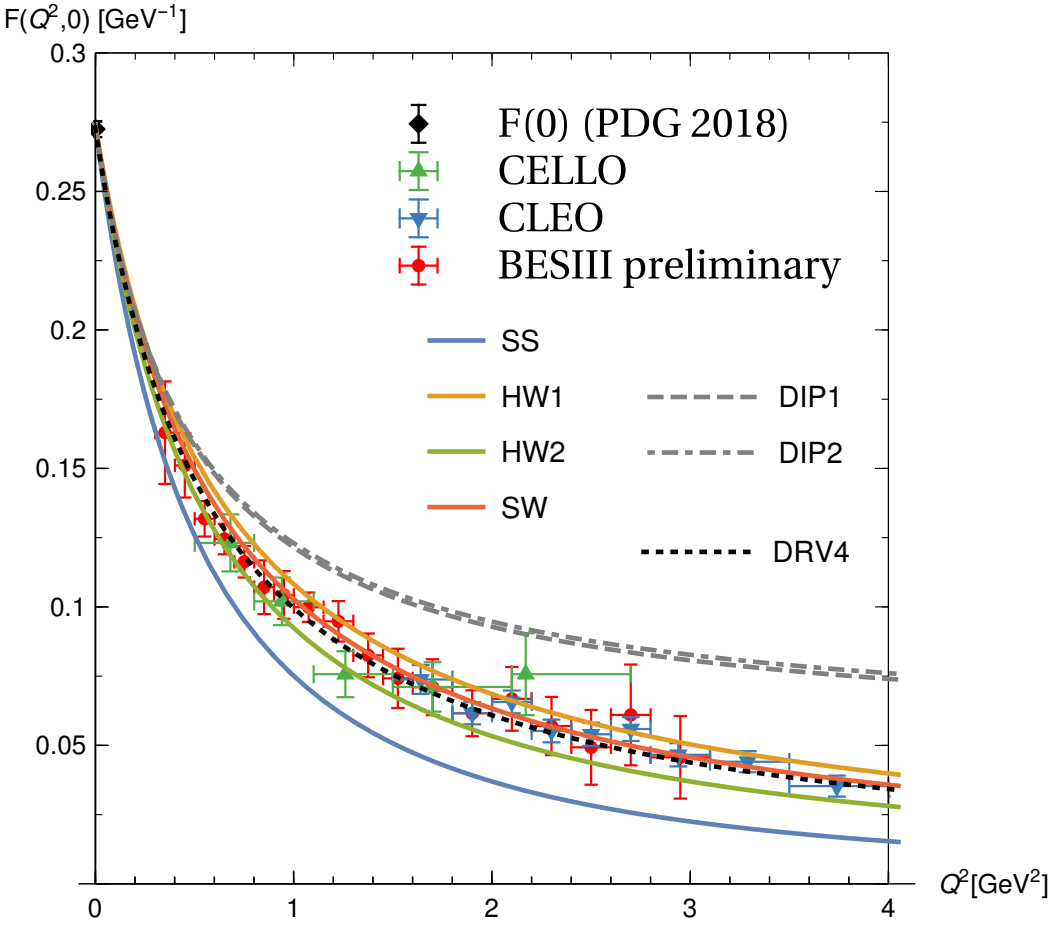

Figure 6.2. – Comparison of the holographic pion TFF to data from CELLO, CLEO and BESIII-preliminary as compiled in Ref. [93]. Figure from Ref. [VI].

GeV^2, all holographic models lie within the error bound. However, at higher energies, the SS model falls off too quickly. The bottom-up models all agree remarkably well with the experimental data points.

6.1.2 High-Energy Behavior

In the high-energy regime, one can use perturbative QCD to study the pion TFF, which factorizes into a perturbatively calculable hard-scattering kernel and a non-perturbative pion distribution amplitude [58, 59, 57, 99]. To leading order, this consideration yields [93]

$$K^{\infty}(Q_1^2, Q_2^2) = \frac{8\pi^2 f_\pi^2}{Q_1^2 + Q_2^2} f(w) \tag{6.6}$$

with $w = (Q_1^2 - Q_2^2)/(Q_1^2 + Q_2^2)$ and

$$f(w) = \frac{1}{w^2} - \frac{1-w^2}{2w^3} \ln \frac{1+w}{1-w}; \tag{6.7}$$

a generalization of the BL (2.17) and OPE-SDC (2.16)

$$F^{\infty}(Q^2, 0) = \frac{2f_\pi}{Q^2}, \qquad F^{\infty}(Q^2, Q^2) = \frac{2f_\pi}{3Q^2}. \tag{6.8}$$

In Ref. [79], it was shown that, for the usual parameter fit of σ, the HW1 pion TFF has an asymptotic limit completely reproducing the LO pQCD result (6.7) with the exact w-dependence for large virtualities

$$\begin{aligned} K^{\mathrm{HW1}}(Q_1^2, Q_2^2) \;&\to\; \frac{8\pi^2 f_\pi^2}{Q_1^2 + Q_2^2} \sqrt{1-w^2} \int_0^\infty d\xi\, \xi^3 K_1(\xi\sqrt{1+w}) K_1(\xi\sqrt{1-w}) \\ &= \frac{8\pi^2 f_\pi^2}{Q_1^2 + Q_2^2} f(w), \end{aligned} \tag{6.9}$$

using the dimensionless variable $\xi = Qz$.

The other bottom-up models also have the same functional form $f(w)$, which is a direct consequence of the asymptotic AdS_5 geometry [90]. The coefficient may however change: in the HW2 model $8\pi^2 f_\pi^2$ is replaced by $4/z_0^2$, and in the SW model by $4\kappa^2$. This corresponds to approximately 61.6% and 89.3% of the LO pQCD result, respectively. The asymptotic behaviors of the individual models are listed in Table 6.2.

In Refs. [90, 61], a different fit for the HW2 model (called HW2(UV-fit) in the following) is suggested. It does not fit z_0 to the ρ-meson mass, a low-energy observable, but instead uses $z_0 = 1/(\sqrt{2}\pi f_\pi)$ fitting the LO pQCD result to 100%. However, this comes at the cost of increasing the ρ-meson mass to 987 MeV.

Model	$\bar{F}(0,\infty)$	$\bar{F}(\infty,\infty)$
SS	0	0
HW1	1.00	1.00
HW2	0.62	0.62
SW	0.89	0.89
DIP1	∞	1.00
DIP2	∞	1.00
DRV4	0.85	0.85
DRV9	0.90	0.90

Table 6.2. – Comparison of the UV behavior of the pion TFF, where $\bar{F} = F/F^{\infty}$ and F^{∞} is the LO pQCD result (6.8). Table from Ref. [VI].

The top-down SS model does not reproduce the correct asymptotic behavior, since the result

$$K^{\text{SS}}(Q_1^2, Q_2^2) \to \frac{16}{9\pi}\left(\frac{2M_{\text{KK}}^2}{Q_1^2+Q_2^2}\right)^{\frac{3}{2}} \frac{2+5\sqrt{1-w^2}}{(\sqrt{1-w}+\sqrt{1+w})^5}. \tag{6.10}$$

falls off too quickly for large virtualities. This weakness is due to the higher dimensional nature of the model, which begins to show above the Kaluza-Klein scale M_{KK}. The model can only make meaningful predictions in the low-energy regime; at high energies, it is instead the dual of a 5-dimensional superconformal QFT.

In Figs. 6.3, 6.4 and 6.5, we compare the asymptotic behavior of the symmetric and asymmetric single and double-virtual TFFs to the result of the dispersion relation study [38], data from BaBar [100] and the result from the recent lattice extrapolation [39]. The HW1 and SW model fit best with dispersion relation and the lattice studies. For the double-virtual plots in Fig. 6.5, these two holographic models fit even better than the DRV9 fit, suggesting that the functional form of the holographic TFFs could be taken as an improvement of the DRV interpolators.

6.2 Contribution to $g-2$

In Chapter 2, we have discussed the expansion of the HLbL contribution and the dominant pseudoscalar pole contribution according to Fig. 2.3. The three possible

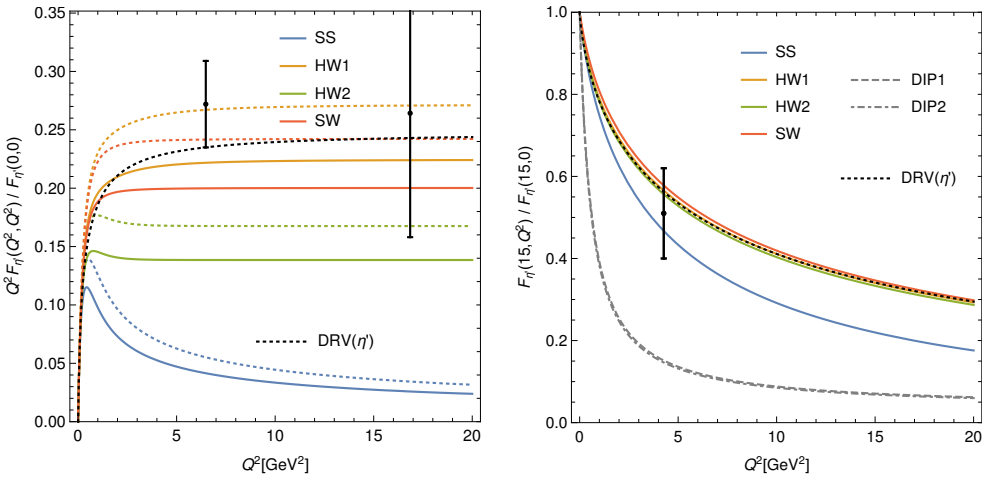

Figure 6.3. – Comparison of the symmetric and asymmetric double-virtual TFFs with DRV(η') from [93] and experimental data from BaBar [100]. Dotted lines correspond to an 10% upscaling of the mass scale within $K(Q_1^2, Q_2^2)$. Figure from Ref. [VI]

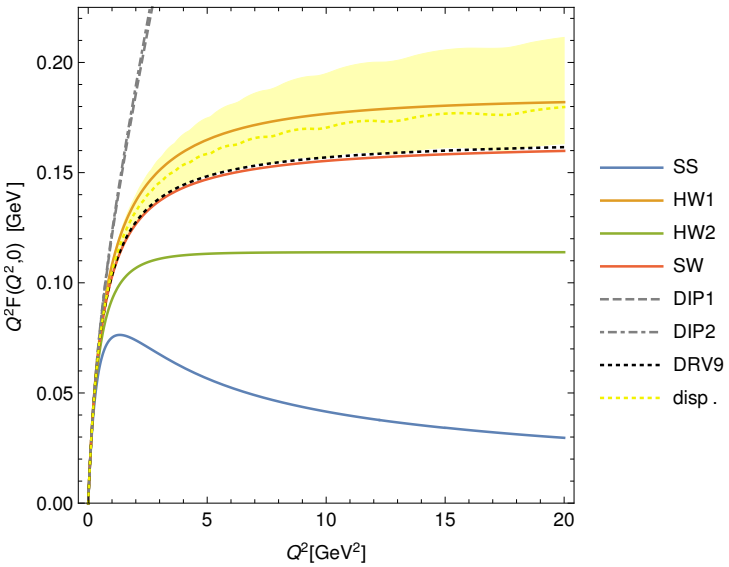

Figure 6.4. – Comparison of the holographic single-virtual pion TFF and the DIP1 and DIP2 interpolators of [90] with the experimental DRV9 interpolators of [93] and the dispersion relation study [38]. The yellow area corresponds to the estimated error of the dispersion result. Figure from Ref. [VI]

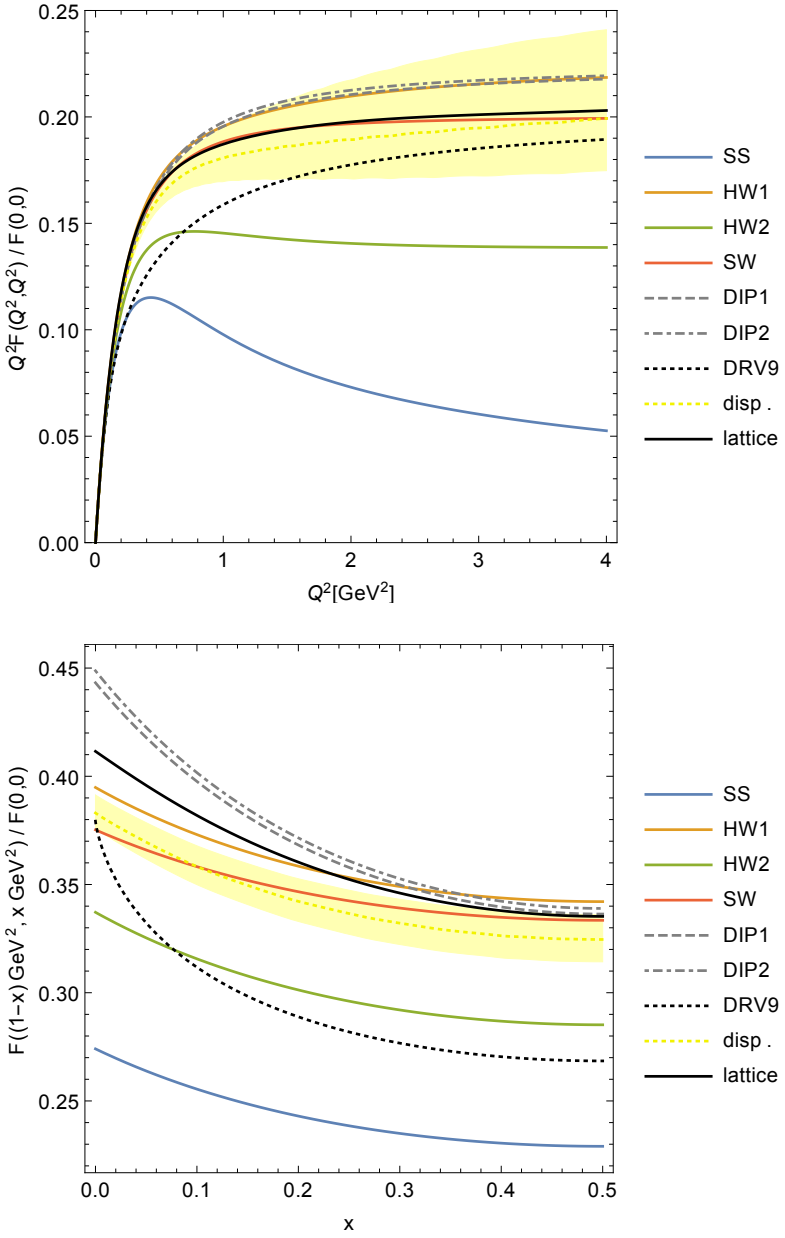

Figure 6.5. – Comparison of the symmetric double-virtual TFF (upper plot) and its dependence on the asymmetry x (lower plot) to the recent lattice extrapolation [39] and the dispersion relation result [38] (yellow band). Figure from Ref. [VI],

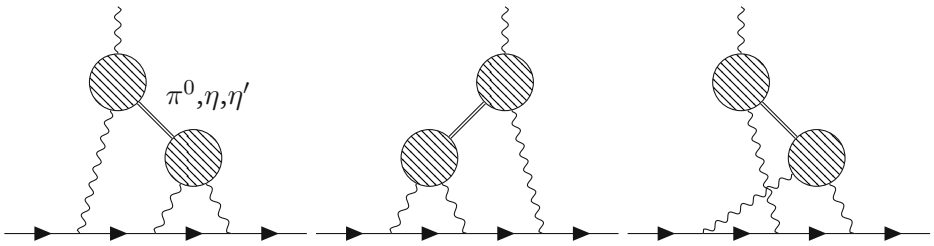

Figure 6.6. – Dominant contributions to the a_μ^{HLbL} given by a pseudoscalar meson exchange. In the pion-pole approximation the shaded blobs represent the transition form factor $F_{P\gamma^*\gamma^*}(q_1^2, q_2^2)$.

diagrams are shown in Fig. 6.6 where the shaded blobs stand for the pseudoscalar TFF (6.1). According to Ref. [101], the contribution can be expressed as

$$a_\mu^{\mathrm{HLbL};\pi^0} = \left(\frac{\alpha}{\pi}\right)^3 \left[a_\mu^{\mathrm{HLbL};\pi^0(1)} + a_\mu^{\mathrm{HLbL};\pi^0(2)}\right], \tag{6.11}$$

$$a_\mu^{\mathrm{HLbL};\pi^0(1)} = \int \frac{d^4q_1}{(2\pi)^4}\frac{d^4q_2}{(2\pi)^4} \frac{1}{q_1^2 q_2^2 (q_1+q_2)^2 [(p+q_1)^2 - m_\mu^2][(p-q_2)^2 - m_\mu^2]} \times \frac{F_{\pi^0\gamma^*\gamma^*}(q_1^2, (q_1+q_2)^2)\ F_{\pi^0\gamma^*\gamma^*}(q_2^2, 0)}{q_2^2 - m_\pi^2}\, \tilde{T}_1(q_1, q_2; p)\,, \tag{6.12}$$

$$a_\mu^{\mathrm{HLbL};\pi^0(2)} = \int \frac{d^4q_1}{(2\pi)^4}\frac{d^4q_2}{(2\pi)^4} \frac{1}{q_1^2 q_2^2 (q_1+q_2)^2 [(p+q_1)^2 - m_\mu^2][(p-q_2)^2 - m_\mu^2]} \times \frac{F_{\pi^0\gamma^*\gamma^*}(q_1^2, q_2^2)\ F_{\pi^0\gamma^*\gamma^*}((q_1+q_2)^2, 0)}{(q_1+q_2)^2 - m_\pi^2}\, \tilde{T}_2(q_1, q_2; p)\,, \tag{6.13}$$

where the kinematic functions $\tilde{T}_{1,2}(q_1, q_2; p)$ are presented in Appendix B. The first and second diagram in Fig. 6.6 give identical contributions described by $\tilde{T}_1$, while the third diagram is described by $\tilde{T}_2$.

Using the method of Gegenbauer polynomials, this 8-dimensional 2-loop integral can be reduced to a 3-dimensional one. A simple formula can be found in Ref. [94] and reads

$$a_\mu^{\mathrm{HLbL};\pi^0(1)} = \int_0^\infty dQ_1 \int_0^\infty dQ_2 \int_{-1}^1 d\tau\ w_1(Q_1, Q_2, \tau) \times F_{\pi^0\gamma^*\gamma^*}(-Q_1^2, -(Q_1+Q_2)^2)\ F_{\pi^0\gamma^*\gamma^*}(-Q_2^2, 0), \tag{6.14}$$

$$a_\mu^{\mathrm{HLbL};\pi^0(2)} = \int_0^\infty dQ_1 \int_0^\infty dQ_2 \int_{-1}^1 d\tau\ w_2(Q_1, Q_2, \tau) \times F_{\pi^0\gamma^*\gamma^*}(-Q_1^2, -Q_2^2)\ F_{\pi^0\gamma^*\gamma^*}(-(Q_1+Q_2)^2, 0), \tag{6.15}$$

with weight functions w_1 and w_2 again given in Appendix B.

Model	$a_\mu^{\pi^0}$	a_μ^{η}	$a_\mu^{\eta'}$	sum
SS	48.3	11.7	7.8|9.5	69.4
SW	59.2	15.9	11.2|13.4	88.5
HW1	65.2	18.2	13.2|15.6	99.0
HW2	56.6	14.8	10.3|12.4	83.7
$\text{HW2}_{\text{UV-fit}}$	75.4	21.9	16.1|19.0	119.4
DIP1	65.4	19.0	14.4|16.9	101.4
DIP2	65.8	19.2	14.6|17.1	102.2
DRV [93]	56(2)	15(1)	13(1)	84(4)
WP [2]	63.6(2.7)	16.3(1.4)	14.5(1.9)	94.3(5.3)

Table 6.3. – Holographic results for the pseudoscalar pole contribution to a_μ^{HLbL} in multiples of 10^{-11}. The three bottom-up models (SW, HW1 & HW2) nicely bracket the WP result. Table from Ref. [VI].

This formula with the holographic TFF of the pion can be used to holographically predict the pion-pole contribution to a_μ^{HLbL}. The various predictions for the holographic models are collected in Table 6.3. For estimating a_μ^{η} and $a_\mu^{\eta'}$ we include the experimental masses for η and η', keep the pion result for $K(Q_1^2, Q_2^2)$ and simply rescale $F(0,0)$ to the central experimental values quoted in Ref. [93]. In summing the pseudoscalar contributions, we consider a second value for η' that includes an additional upscaling of the mass scale within the TFF by 10%. This is in line with the presumably more realistic higher Λ parameter in Ref. [93].

Compared to the WP result, the DIP interpolators of Ref. [90] as well as the HW2(UV-fit) model severely overestimate the pseudoscalar meson contribution. For the three bottom-up holographic QCD models, the SW, HW1 and HW2 model, bracket the WP result and can be combined to an overall holographic prediction. A more in-depth discussion of the holographic results can be found at the end of Chapter 8.

7 Axial-Vector Contribution to HLbL

> *When the snows fall and the white winds blow,*
> *the lone wolf dies but the pack survives.*
>
> — **George R.R. Martin**
> A Game of Thrones

ALTHOUGH the holographic results for the pseudoscalar-pole contribution to HLbL cannot compete with the dispersive approach, in the previous chapter, we were able to make reasonable predictions bracketing the WP result. By comparing to experimental data on the TFF, we found that some holographic models do even better than model-dependent parameter fits. An additional advantage of the holographic models we will now turn to is that, without introducing additional parameters, we can calculate the contribution of the infinite tower of axial-vector mesons to HLbL.

This chapter, following Ref. [IV], is structured as follows: First, we will construct the holographic axial-vector TFF for the SS model and the HW models and compare them to low-energy data from LHCb and L3, as well as to high-energy constraints from pQCD. Then, we will calculate the axial-vector contribution to the HLbL scattering four-point function and show how the infinite tower of axial-vector mesons satisfies the Melnikov-Vainshtein SDC. Finally, we evaluate the contribution to $g-2$.

7.1 Transition Form Factor

Similar to the pseudoscalar mesons discussed in the previous chapter, axial-vector mesons can couple to two photons and can therefore contribute to the HLbL scatter-

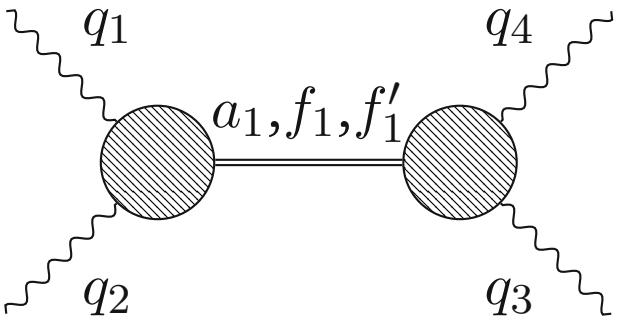

Figure 7.1. – Axial-vector meson contributions to the HLbL tensor, where the shaded blobs are described by the axial-vector transition form factor.

ing amplitude in Fig. 7.1. Again, the crucial ingredient is the TFF, which in the SS model, can be obtained from the Lagrangian[1]

$$\mathcal{L}_{\mathcal{A}\gamma\gamma} = -i\frac{N_c}{12\pi^2}\mathrm{Tr}\,\epsilon^{\mu\nu\rho\sigma}\int_{-\infty}^{\infty} dZ\,\left(a_\mu \mathcal{V}'_\nu \partial_\rho \mathcal{V}_\sigma + \mathcal{V}_\mu a'_\nu \partial_\rho \mathcal{V}_\sigma + \mathcal{V}_\mu \mathcal{V}'_\nu \partial_\rho a_\sigma\right), \tag{7.1}$$

while for the HW models the Z integral is replaced by $2\int_0^{z_0} dz(\ldots)$. Using partial integration, the Lagrangian can be simplified to

$$\mathcal{L}_{\mathcal{A}\gamma\gamma} = -i\frac{N_c}{12\pi^2}\mathrm{Tr}\,\epsilon^{\mu\nu\rho\sigma}\left[\int_{-\infty}^{\infty} dZ\left(-3\mathcal{V}'_\mu a_\nu \partial_\rho \mathcal{V}_\sigma\right) + \mathcal{V}_\mu a_\nu \partial_\rho \mathcal{V}_\sigma\Big|_{Z=-\infty}^{\infty}\right], \tag{7.2}$$

where potentially an unwanted boundary term appears, which would result in a non-vanishing 2-real-photon decay of the axial-vector meson, violating the Landau-Yang theorem [102, 103]. The bulk term automatically satisfies the Landau-Yang theorem by $\mathcal{V}'_\mu = 0$ for $Q^2 \to 0$, since in this limit the bulk-to-boundary propagator becomes constant. The boundary term vanishes automatically in the SS model and the HW2 model due to boundary conditions, but needs to be subtracted by hand in the HW1 model.

The amplitude $\gamma^*(q_1)\gamma^*(q_2) \to \mathcal{A}^a$ can be written as

$$\mathcal{M}^a = i\frac{N_c}{4\pi^2}\mathrm{Tr}\left(\mathcal{Q}^2 t^a\right)\epsilon_1^\mu \epsilon_2^\nu \epsilon_{\mathcal{A}}^{*\rho}\epsilon_{\mu\nu\rho\sigma}\left[q_2^\sigma Q_1^2 A(Q_1^2, Q_2^2) - q_1^\sigma Q_2^2 A(Q_2^2, Q_1^2)\right], \tag{7.3}$$

with the function $A(Q_1^2, Q_2^2)$ given by[2]

$$A^{\mathrm{HW}}(Q_1^2, Q_2^2) = \frac{2}{Q_1^2}\int_0^{z_0} dz\left[\frac{d}{dz}\mathcal{J}(Q_1, z)\right]\mathcal{J}(Q_2, z)\psi^A(z)\Big/\left[g_5^{-2}\int_0^{z_0}\frac{dz}{z}(\psi^A)^2\right]^{1/2}, \tag{7.4}$$

[1] For simplicity, we will restrict to the lightest axial-vector meson mode here. A generalization to the n-th mode is straightforward.

[2] Note that $A(Q_1^2, Q_2^2)$ is not symmetric.

with the axial-vector meson mode defined in Eq. (5.37) or Eq. (5.44) for the HW models and

$$A^{\rm SS}(Q_1^2,Q_2^2)=\frac{1}{Q_1^2}\int_{-\infty}^{\infty}dZ\left[\frac{d}{dZ}\mathcal{J}^{\rm SS}(Q_1,Z)\right]\mathcal{J}^{\rm SS}(Q_2,Z)\psi^A_{\rm SS}(Z)\Big/\left[\kappa\int_{-\infty}^{\infty}\frac{dZ}{Z}(\psi^A_{\rm SS})^2\right]^{1/2} \tag{7.5}$$

for the SS model, where $\psi^A_{\rm SS}\equiv\psi_2$ is defined by Eq. (4.13). The brackets $[\dots]^{1/2}$ make explicit the normalization conditions of the radial modes ψ^A of the axial-vector mesons.

7.1.1 Low-Energy Behavior

Although the Landau-Yang theorem forbids the decay of an axial-vector meson into two real photons, there is experimental data from the L3 Collaboration [104, 105] on the so-called equivalent 2-photon decay width of the lightest f_1 meson. It describes the decay into one off-shell longitudinal photon and one transverse photon [106, 107]

$$\tilde\Gamma_{\gamma\gamma}=\lim_{Q_1^2\to0}\Gamma(\mathcal{A}\to\gamma_L^*\gamma_T)M_A^2/(2Q_1^2). \tag{7.6}$$

This is related to the axial TFF as

$$\tilde\Gamma_{\gamma\gamma}=\frac{\pi\alpha^2M_A}{12}[F^{(1)}_{\mathcal{A}\gamma^*\gamma^*}(0,0)]^2, \tag{7.7}$$

with

$$M_A^{-2}F^{(1)}_{\mathcal{A}\gamma^*\gamma^*}(0,0)=\frac{N_c}{4\pi^2}{\rm Tr}\,(\mathcal{Q}^2t^a)A(0,0). \tag{7.8}$$

The experimental results $\tilde\Gamma_{\gamma\gamma}=3.5(8)$ keV for $f_1(1285)$ [104] and $3.2(9)$ keV for $f_1(1420)$ [105] translate to the universal value

$$|A(0,0)|^{\rm exp.}\simeq15(2){\rm GeV}^{-2}, \tag{7.9}$$

with the mixing angle $\phi_f\approx20.4^\circ$, which is close to $\phi_f=\pm(24\pm3)^\circ$, the recent LHCb result [108] as well as to other results obtained in Refs. [109, 110] pointing to the range $+(20\dots30)^\circ$.

To calculate $A(0,0)$ holographically, we can use that $\frac{d}{dz}\mathcal{J}(Q_1,z)$ vanishes like Q_1^2 for small virtualities. In the HW2 model we get

$$A(0,0)=-4\sqrt{2}\frac{J_0(\gamma_{1,1})-1}{\gamma_{1,1}^3J_0(\gamma_{1,1})}g_5z_0^2=-0.3502g_5z_0^2=-16.633\,{\rm GeV}^{-2}\quad\text{(HW2)}, \tag{7.10}$$

in the HW1 model

$$A(0,0) = -0.3478 g_5 z_0^2 = -21.043\,\text{GeV}^{-2} \quad \text{(HW1)} \tag{7.11}$$

and in the SS model

$$A(0,0) = -1.2379 \kappa^{-1/2} M_{\text{KK}}^{-2} = -15.926\,\text{GeV}^{-2} \quad \text{(SS)}. \tag{7.12}$$

The results for the SS and HW2 models agree quite well with the experimental data of f_1, while the HW1 model overestimates the amplitude by about 40%.[3]

In Figure 7.2 and 7.3 we compare the single-virtual and double-virtual axial-vector TFF from holographic models to the experimental fit of the L3 data [41]. In the double-virtual case they deviate rather strongly since the holographic models manage to have the same asymptotic power-law as in the single-virtual case, while the dipole fit decays too quickly.

7.1.2 High-Energy Behavior

To study the asymptotic behavior, we use the parametrization

$$\begin{aligned} Q_{1,2}^2 &= r_{1,2}^2 Q^2 \equiv (1 \pm w) Q^2, \\ Q^2 &= \frac{1}{2}(Q_1^2 + Q_2^2), \quad w = (Q_1^2 - Q_2^2)/(Q_1^2 + Q_2^2), \end{aligned} \tag{7.13}$$

with which we obtain for both HW models the result

$$\begin{aligned} A^{\text{HW}}(Q_1^2, Q_2^2) \;\to\; & \frac{a A(0,0)}{(z_0 Q)^4} r_1^{-1} r_2 \int_0^\infty d\xi\, \xi^3 \left[K_1(r_1\xi) + r_1 \xi K_1'(r_1\xi)\right] K_1(r_2\xi) \\ &= \frac{a A(0,0)}{(z_0 Q)^4} \frac{1}{w^4} \left[w(3-2w) + \frac{1}{2}(w+3)(1-w) \ln \frac{1-w}{1+w} \right], \end{aligned} \tag{7.14}$$

where a is a dimensionless constant depending on the model and the particular axial-vector mode. After its holographic derivation in Ref. [IV], it was shown in Ref. [54] to agree with pQCD in the Brodsky-Lepage formalism.

[3] In Ref. [II] instead of the value (7.9), we compare to $|A(0,0)|^{\text{exp.}}_{f_1(1285)} \simeq 16.6(1.5)\text{GeV}^{-2}$, which takes into account $SU(3)$ flavor breaking of our flavor-symmetric models and reduces the discrepancy to below 30%.

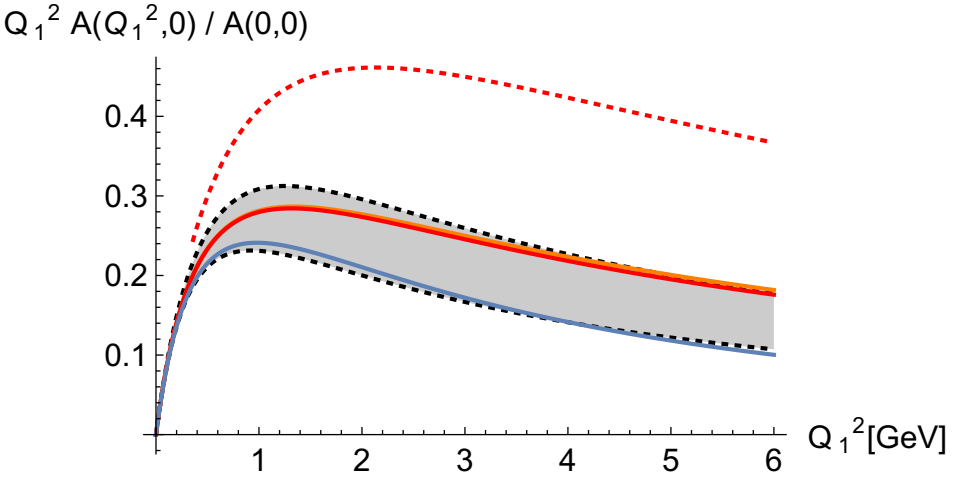

Figure 7.2. – Comparison of the single-virtual axial-vector TFF from holographic models (SS: blue, HW1: orange, HW2: red, HW2(UV-fit): red dashed) to the dipole fit of the L3 data for $f_1(1285)$ (gray band). Figure from Ref. [IV].

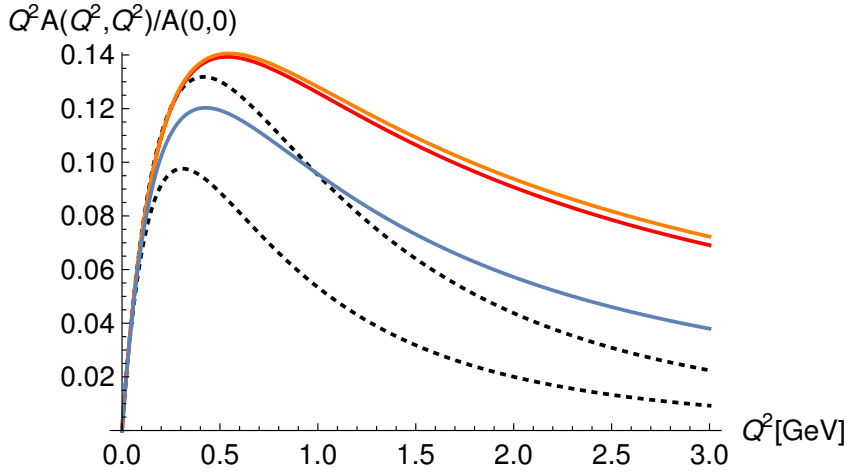

Figure 7.3. – Comparison of the symmetric double-virtual axial-vector TFF from holographic models (SS: blue, HW1: orange, HW2: red), to the extrapolation of the L3 data with a dipole model [41] (black dashed). Figure from Ref. [IV].

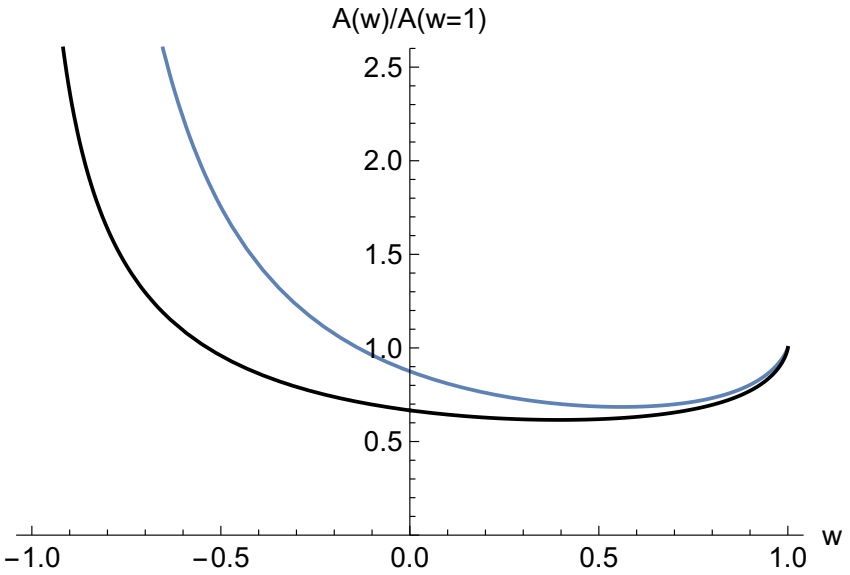

Figure 7.4. – Comparison of the short-distance behavior of $A(Q_1^2, Q_2^2)$ for different asymmetry parameters w. The bottom-up HW models (black) agree with pQCD, while the top-down SS model (blue) deviates from it. Figure from Ref. [IV].

The SS model, showing its higher-dimensional origin, does not agree with pQCD and gives the result

$$\begin{aligned} A^{\text{SS}}(Q_1^2, Q_2^2) \quad &\to \quad \frac{a^{\text{SS}} A^{\text{SS}}(0,0) M_{\text{KK}}^5}{Q^5} r_1^{-1} \int_0^\infty d\xi\, \xi^4 (1 + 3r_2) e^{-3(r_1\xi + r_2\xi)} \\ &= \frac{a^{\text{SS}} A^{\text{SS}}(0,0) M_{\text{KK}}^5}{Q^5} \frac{8}{81} \frac{6\sqrt{1-w} + \sqrt{1+w}}{\sqrt{1+w}(\sqrt{1-w} + \sqrt{1+w})^6}. \end{aligned} \tag{7.15}$$

In particular, here the large momentum scaling is $A^{\text{SS}} \sim 1/Q^5$, while in the HW models and pQCD we have $A \sim 1/Q^4$. The qualitatively different w-dependence is displayed in Figure 7.4.

7.2 High-Energy Behavior of the Four-Point Function

In this section, we will show how the short-distance constraint by Melnikov and Vainshtein [46] (MV-SDC) is satisfied in the HW models by summing the infinite tower of axial-vector mesons.

As discussed in Chapter 2, the MV-SDC can be expressed as [60, 48]

$$\lim_{Q_3 \to \infty} \lim_{Q \to \infty} Q^2 Q_3^2 \bar{\Pi}_1(Q, Q, Q_3) = -\frac{2}{3\pi^2}. \tag{7.16}$$

In the previous chapter, we encountered the contribution of the pion to $\bar{\Pi}_1(Q, Q, Q_3)$, which however scales as $\sim 1/(Q_3^4 Q^2)$ and therefore does not contribute to the SDC. Another contribution comes from the longitudinal part of the axial-vector mesons and reads

$$\begin{aligned}\bar{\Pi}_1 &= -\frac{g_5^2}{2\pi^4}\sum_{n=1}^{\infty}\int_0^{z_0} dz \left[\frac{d}{dz}\mathcal{J}(Q,z)\right]\mathcal{J}(Q,z)\psi_n^A(z)\frac{1}{(M_n^A Q_3)^2} \\ &\quad\times\int_0^{z_0} dz' \left[\frac{d}{dz'}\mathcal{J}(Q_3,z')\right]\psi_n^A(z'). \end{aligned} \tag{7.17}$$

From (7.14) and (7.4), we can see that at large virtualities the first integral behaves as $1/Q^2$, while the second as $1/Q_3^2$. Together with the $1/Q_3^2$ from the propagator, this shows that any single axial-vector meson does not contribute. It is only after summing the infinite number of axial-vector contributions that one gets a finite contribution. This holds true for both HW models, but for simplicity let us only look at the HW2 model, where $\mathcal{J}$ and ψ^A are given in terms of Bessel functions.[4] Recalling Chapter 5, the wave functions are solutions of

$$\partial_z\left[\frac{1}{z}\partial_z\psi_n^A(z)\right] + \frac{1}{z}M_{A,n}^2\psi_n^A(z) = 0, \tag{7.18}$$

and are given by

$$\psi_n^A(z) = \sqrt{2}zz_0^{-1}J_1(\gamma_{1,n}z/z_0)/|J_0(\gamma_{1,n})|. \tag{7.19}$$

They are normalized to $\int_0^{z_0} dz z^{-1}(\psi^A(z))_n^2 = 1$ and satisfy the completeness relation

$$\sum_{n=1}^{\infty}\psi_n^A(z)\psi_n^A(z') = z\delta(z-z'). \tag{7.20}$$

The Green's function or bulk-to-bulk propagator of (5.44) reads

$$G^A(Q;z,z') = zz'\left[K_1(Qz_>)I_1(Qz_0) - I_1(Qz_>)K_1(Qz_0)\right]I_1(Qz_<)/I_1(Qz_0), \tag{7.21}$$

where $z_< = \min(z,z')$ and $z_> = \max(z,z')$. An alternative form is given by the spectral representation

$$G^A(Q;z,z') = \sum_{n=1}^{\infty}\frac{\psi_n^A(z)\psi_n^A(z')}{Q^2+(M_n^A)^2}, \tag{7.22}$$

[4] A similar calculation for the HW1 model with quark masses will be presented in the next chapter.

which for $Q = 0$ reduces to the sum $\sum_{n=1}^{\infty} \psi_n^A(z)\psi_n^A(z')/(M_n^A)^2$. The same expression as appears in Eq. (7.17). In this limit, the analytic form reduces to the simple result

$$G^A(0; z, z') = \frac{z_<^2(z_0^2 - z_>^2)}{2z_0^2}. \tag{7.23}$$

In the limit $Q^2 \gg Q_3^2$, we use the parametrization $Qz = \xi$, $Q_3 z' = \xi'$ to obtain

$$\begin{aligned} &-\frac{g_5^2}{2\pi^4}\frac{1}{2Q_3^2}\int_0^\infty d\xi \int_0^\infty d\xi' \xi K_1(\xi)\frac{d}{d\xi}[\xi K_1(\xi)]\frac{d}{d\xi'}[\xi' K_1(\xi')]\xi^2/Q^2 \\ &= \frac{g_5^2}{2\pi^4}\frac{1}{2Q_3^2}\int_0^\infty d\xi \xi K_1(\xi)\frac{d}{d\xi}[\xi K_1(\xi)]\xi^2/Q^2 = -\frac{2}{\pi^2}\frac{1}{2Q_3^2}\frac{2}{3Q^2}. \end{aligned} \tag{7.24}$$

In the last step we have set $g_5^2 = 4\pi^2$ at $N_c = 3$ to exactly[5] reproduce the MV-SDC (8.14). Figure 7.5 illustrates the summation over the infinite tower.

In the large-N_c and chiral limit, one can show that the MV-SDC (8.14) is stronger and holds for all values of Q_3

$$\lim_{Q\to\infty} Q^2 \bar{\Pi}_1(Q, Q, Q_3) = -\frac{g_5^2}{(2\pi)^2}\frac{2}{3\pi^2 Q_3^2}. \tag{7.25}$$

This is also realized in the HW2 model, where the pion gives the additional contribution.

7.3 Contribution to $g - 2$

With the method of Gegenbauer polynomials, we can again reduce the 8-dimensional integral of the 2-loop diagram to a 3-dimensional one of the form[6]

$$a_\mu^{\mathrm{AV}} = \int_0^\infty dQ_1 \int_0^\infty dQ_2 \int_{-1}^1 d\tau\, \rho_a(Q_1, Q_2, \tau). \tag{7.26}$$

The total contribution from all the axial-vector mesons is, as expected, dominated by the lowest modes. This is illustrated in Figure 7.6, where the contribution of the infinite sum is almost exclusively given by the ground state. The numerical results for the considered models are collected in Table 7.1.

[5] This is not the usual choice of parameters for the HW2 model and corresponds to HW2(UV-fit). The usual choice (5.47) only reaches 62% of the MV-SDC.
[6] The explicit formula is given in Appendix B.

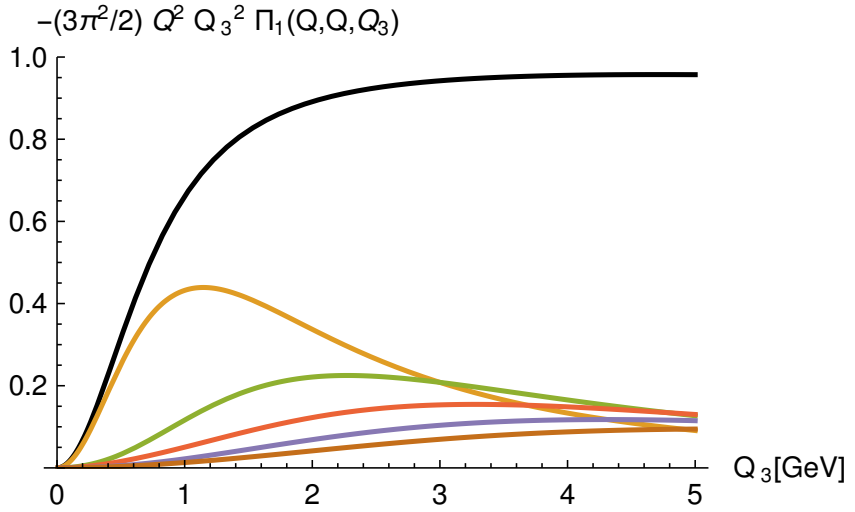

Figure 7.5. – Axial-vector meson contribution to $Q_3^2 Q^2 \bar{\Pi}_1(Q,Q,Q_3)$ at $Q = 50$ GeV and normalized to the asymptotic value (8.14). The first 5 axial-vector mesons (colored) decay too fast. It takes the infinite sum (black) to get the correct asymptotic value. Figure from Ref. [IV].

	$j=1$	$j\leq 2$	$j\leq 3$	$j\leq 4$	$j\leq 5$	a_μ^{AV}
HW1	31.4	36.2	37.9	39.1	39.6	40.6×10^{-11}
HW2	23.0	26.2	27.4	27.9	28.2	28.7×10^{-11}
HW2(UV-fit)	23.7	26.9	28.1	28.6	28.9	29.4×10^{-11}
SS	13.8	14.5	14.7	14.8	14.8	14.8×10^{-11}

Table 7.1. – Holographic results for the contribution of the infinite tower of axial-vector mesons to a_μ^{AV}. Table from Ref. [IV].

The combined holographic prediction for the pseudoscalar plus axial-vector pole contributions are displayed in Table 7.2. For the realization of the MV-SDC, only the longitudinal polarization of the axial-vector meson is relevant. It is responsible for $57-58\%$ of the total contribution and can be compared to the short-distance contribution in Table 2.2. Numerically, our result is significantly smaller than what is obtained by the simple MV model, but comparable in size to the WP result of $a_\mu^{\mathrm{WP,SDC}} = 15(10)\times 10^{-11}$. Comparing the axial-vector contribution $a_\mu^{\mathrm{WP,axials}} = 6(6)\times 10^{-11}$ to our result for transverse axial-vector mesons suggests that it has been underestimated so far.

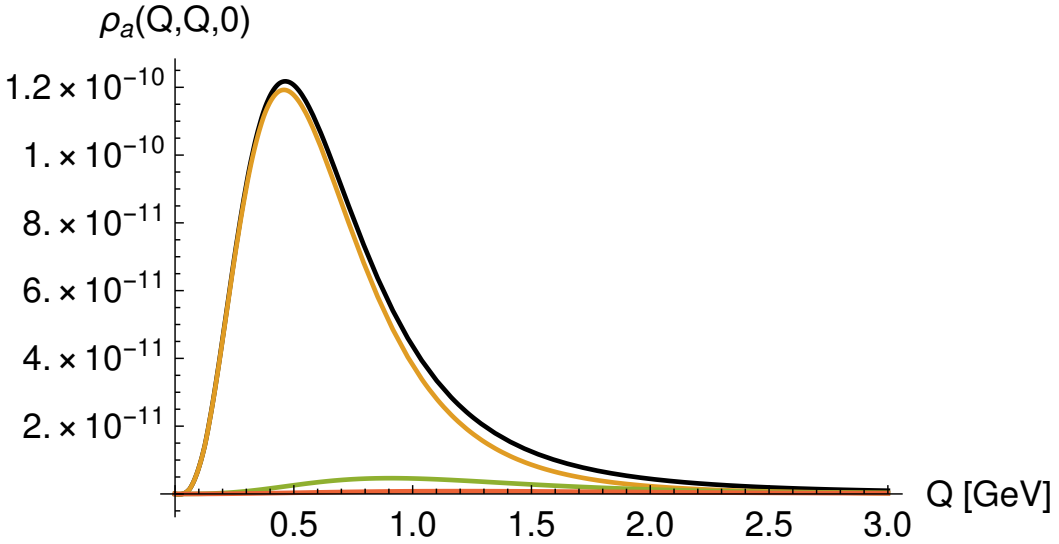

Figure 7.6. – The integrand $\rho_a(Q_1, Q_2, \tau)$ of Eq. (7.26) for the slice $Q_1 = Q_2$ and $\tau = 0$. The infinite sum (black) is almost exclusively given by the ground state (orange). Figure from Ref. [IV].

	HW1	HW2
$a_\mu^{\mathrm{PS}}[\pi^0 + \eta + \eta'] \times 10^{11}$	$99.0[65.2 + 18.2 + 15.6]$	$83.7[56.6 + 14.8 + 12.4]$
$a_\mu^{\mathrm{AV}}[L + T] \times 10^{11}$	$40.6[23.2 + 17.4]$	$28.7[16.6 + 12.0]$
$a_\mu^{\mathrm{PS+AV}} \times 10^{11}$	140	112

Table 7.2. – Combination of the pseudoscalar pole contribution of Chapter 6 and the infinite tower of axial-vector mesons. Table from Ref. [IV].

8 Massive Pion Contribution to HLbL

> *Life is like a box of chocolates. You never know what you're gonna get.*
>
> — **Forrest Gump**
> Forrest Gump

In the previous two chapters, we have considered predictions of chiral holographic models to a_μ^{HLbL} and found that the tower of axial-vector mesons is responsible for satisfying the MV-SDC. In the chiral limit, excited pseudoscalars decouple from the axial-vector current and the axial anomaly and were therefore not considered. However, in the light of the Regge model of Ref. [60, 48] where an infinite tower of pseudoscalars is responsible for the MV-SDC, the question arises what role they play in holographic models.

Excited pions are most easily implemented in the HW1 model, where they are even present in the chiral limit, but can also be studied with massive quarks described by the vacuum expectation value (5.6) of the bifundamental scalar field X. To get a range of predictions and to not only work with one model, it is possible to also consider different variants of the HW1 model. Two possible modifications are considering the second set of possible boundary conditions (5.30) giving rise to what we call the HW3 model, and generalizing the scaling dimensions of the chiral condensate and the quark mass described by the bulk mass M_X^2 of the bifundamental scalar field.

In this chapter, we will address the role of massive pions following Ref. [II]. First, we will introduce the different variants of the HW1 model with quark masses we are considering. Next, we will present the necessary change of the CS-term when leaving the chiral limit and derive an interesting and, as far as we know, novel sum relation. Then, we will analytically derive the contribution of axial-vector mesons and pions to the MV-SDC. Finally, we will calculate the contributions to $g-2$ and end with a brief discussion of the holographic predictions for the hadronic contribution to the anomalous magnetic moment of the muon.

8.1 Model Variants

So far, we have only considered chiral models in this part of the thesis. The model with the easiest implementation of quark masses is the HW1 model, in which, as explained in Chapter 5, quark masses and chiral condensates are described by the vacuum solution (5.6) of the scalar field X. Following Ref. [83], we also consider a generalization away from the usual choice $M_X^2 = -3$ to get the vacuum solution

$$v(z) = M_q z_0 (z/z_0)^{\Delta^-} + \Sigma\, z_0^3 (z/z_0)^{\Delta^+}, \tag{8.1}$$

with the scaling dimensions

$$\Delta^\pm = 2 \pm \sqrt{4 + M_X^2} \equiv 2 \pm \alpha, \tag{8.2}$$

and the admissible range $-4 < M_X^2 < 0$ [83]. The additional free parameter M_X^2 can then be used to fit the mass of the lowest axial-vector meson or the first excited pion. This also generalizes the Gell-Mann–Oakes–Renner relation to

$$f_{\pi_n}^2 m_n^2 \approx 2\alpha M_q \Sigma, \tag{8.3}$$

which implies that the $n > 1$ massive pions have vanishing decay constants in the chiral limit.

As a second generalization of the HW1 model, we change the chiral symmetry preserving boundary conditions $F_{z\mu}^{L,R}(z_0) = 0$ to chiral symmetry breaking ones $(A_\mu^L - A_\mu^R)(z_0) = 0$ and $(F_{z\mu}^L + F_{z\mu}^R)(z_0) = 0$, as was suggested in Ref. [83]. This variant we call HW3. We therefore consider four different HW models with non-vanishing quark masses.

HW1m: is the original HW1 model as was introduced by Erlich, Katz, Son and Stephanov [14], although we are using a slightly different parameter fit. In the chiral limit, this coincides with the HW1 model considered in Refs. [IV, VI].

HW1m': generalizes the HW1m model in the choice of M_X^2 to additionally fit the mass of the a_1 meson. This also lowers the mass of the first excited pion to a more physical value, but it cannot be fitted exactly.

HW3m: is similar to the HW1 model, but has changed IR boundary conditions, as proposed in Ref. [83]. In the HW3 models, no manual subtraction of the infrared boundary in the CS term is necessary.

	m_{π_2} [MeV]	f_{π_2} [MeV]	$\lvert F_{\pi_2\gamma\gamma}\rvert$ [GeV^{-1}]	m_{a_1} [MeV]	F_{a_1}/m_{a_1} [MeV]
Experiment	1300(100)	2.20(46)	$< 0.0544(71)$	1230(40)	168(7)
HW1(chiral)	1899	0	0.202	1375	177
HW1m	1892	1.56	0.203	1367	175
HW1m'	1591	1.59	0.250	1230*	148
HW3m	1715	1.56	0.196	1431	195
HW3m'	1300*	1.92	0.206	1380	186

Table 8.1. – Comparison of the most relevant masses and decay constants in the axial sector. Experimental values are from Refs. [113][114][48][113][112], respectively. Fitted values are denoted with *. A more detailed comparison of the model values is given in Appendix C.

HW3m': generalizes the HW3m model by using M_X^2 to fit the mass of the $\pi(1300)$ meson. This model is similar to the one of Domènech, Panico, and Wulzer in Ref. [83] and deviates from it only in the parameter fit.

As can be seen in Table 8.1, the mass of the first excited pion is too high in all models, except in the HW3m' model, where it is fitted exactly. This fit also raises the value of f_{π_2} to be consistent with the experimental bound. For the amplitude $|F_{\pi_2\gamma\gamma}|$ there is at present no direct measurement available, but we can compare to the upper bound of Ref. [48], which holographic results strongly overestimate. The masses of the axial-vector mesons do not vary as widely as the masses of the first excited pion, and are somewhere between the experimental values $M_{a_1(1260)} = 1230(40)$ MeV and $M_{f_1(1420)} = 1426.3(9)$ MeV. For the decay constant of the axial-vector meson, we define F_{a_1} such that it corresponds to $F_A^{a=3} m_A$ and $F_A^{a=3} m_A/\sqrt{2}$ in [54, 111] and [112], respectively. The ballpark $(148 \ldots 195)$ MeV is roughly consistent with the result $168(7)$ MeV inferred from light-cone sum rules [111, 112].

8.2 Axial Anomaly and Massive Pions

To construct the TFF for massive pions, it turns out that we can no longer use the CS term resulting in

$$F_{\pi_1\gamma^*\gamma^*}(Q_1^2, Q_2^2) = \frac{N_c}{12\pi^2 f_\pi} K^{\text{HW1,3}}(Q_1^2, Q_2^2). \tag{8.4}$$

with

$$K^{\text{HW1,3}}(Q_1^2, Q_2^2) = -\int_0^{z_0} \mathcal{J}(Q_1, z)\mathcal{J}(Q_2, z)\partial_z \Psi(z) dz + \mathcal{J}(Q_1, z_0)\mathcal{J}(Q_2, z_0)\Psi(z_0), \tag{8.5}$$

and $\Psi = \phi - \pi$ as was introduced in Ref. [79] and used in Ref. [VI]. This is obvious by looking at

$$K^{\text{HW1,3}}(0,0) = -\Psi(z)|_0^{z_0} + \Psi(z_0) = \Psi(0) = 1, \tag{8.6}$$

which is only correct in the chiral limit, where the pion mode is proportional to the bulk-to-boundary propagator (as demonstrated in Chapter 5) and therefore $\Psi_1(0) \equiv \Psi(0) = 1$. With quark masses, the boundary conditions instead imply $\Psi_n(0) = 0$ resulting in the wrong axial anomaly.

In Ref. [II] we instead show that the correct expression is given by

$$F_{\pi_n \gamma^* \gamma^*}(Q_1^2, Q_2^2) = \frac{N_c}{12\pi^2} g_5 K_n(Q_1^2, Q_2^2), \tag{8.7}$$

with

$$\begin{aligned} K_n(Q_1^2, Q_2^2) &= -\int_0^{z_0} dz\, \mathcal{J}(Q_1, z)\mathcal{J}(Q_2, z) z y_n(z) \\ &\quad + \mathcal{J}(Q_1, z_0)\mathcal{J}(Q_2, z_0) \left(\frac{z}{\beta}\partial_z y_n(z)\right)_{z \to z_0}. \end{aligned} \tag{8.8}$$

Expressed in terms of the ϕ and π modes the TFF reads

$$\begin{aligned} K_n(Q_1^2, Q_2^2) &= -\int_0^{z_0} dz\, \mathcal{J}(Q_1, z)\mathcal{J}(Q_2, z)\partial_z \phi_n(z) \\ &\quad + \mathcal{J}(Q_1, z_0)\mathcal{J}(Q_2, z_0) \left[\phi_n(z_0) - \pi_n(z_0)\right], \end{aligned} \tag{8.9}$$

which implies

$$K_n(0,0) = -\pi_n(z_0). \tag{8.10}$$

In the chiral limit our definition agrees with Eq. (8.5) since $\pi_1(z) \equiv -1/(g_5 f_{\pi_1})$ and hence $\partial_z \Psi = \partial_z \phi_1$.

With non-vanishing quark masses the sum rule (5.32) implies $y_S(0, z) = g_5 \sum_{n=1}^{\infty} f_{\pi_n} y_n(z)$ and consequently

$$g_5 \sum_{n=1}^{\infty} f_{\pi_n} K_n(0,0) = 1, \tag{8.11}$$

or equivalently

$$\sum_{n=1}^{\infty} f_{\pi_n} F_{\pi_n \gamma\gamma} = \frac{N_c}{12\pi^2}, \tag{8.12}$$

which is an interesting generalization of the well-known chiral result $f_\pi F_{\pi\gamma\gamma} = \frac{N_c}{12\pi^2}$ following from the axial anomaly.

For the high-energy behavior of the pion TFF, we obtain the result

$$F_{\pi_n\gamma^*\gamma^*}(Q_1^2, Q_2^2) \to \frac{g_5^2 N_c}{12\pi^2} \frac{4 f_{\pi_n}}{Q_1^2 + Q_2^2} \left[\frac{1}{w^2} - \frac{1-w^2}{2w^3} \ln \frac{1+w}{1-w} \right], \tag{8.13}$$

as a generalization of Eq. (6.9).

8.3 High-Energy Behavior of the Four-Point Function

One of the main motivations for Ref. [II] was to investigate the role of massive pions in the high-energy behavior of the HLbL four-point function. In the previous chapter following Ref. [IV], we have seen that in the chiral HW1 model 100% of the MV-SDC [60, 48]

$$\lim_{Q_3\to\infty} \lim_{Q\to\infty} Q^2 Q_3^2 \bar{\Pi}_1(Q, Q, Q_3) = -\frac{2}{3\pi^2} \tag{8.14}$$

is satisfied by the tower of axial-vector mesons. In light of the Regge model of Ref. [60, 48], where the tower of massive pions is responsible for 100% of the MV-SDC, it seems natural to ask how it is realized in the massive HW1 model with an infinite tower of axial-vector mesons and pions.

Furthermore, it is interesting to consider the symmetric SDC [46, 47],

$$\lim_{Q\to\infty} \lim_{Q\to\infty} Q^4 \bar{\Pi}_1(Q, Q, Q) = -\frac{4}{9\pi^2}, \tag{8.15}$$

related to the perturbative quark loop and for which axial-vector mesons only contribute around 80% to the coefficient [61, II]. It would be intriguing to also realize the remaining 20% within holographic models.

8.3.1 Axial-Vector Contribution

In the previous chapter, we have sketched the derivation of the short-distance behavior of

$$\bar{\Pi}_1^{\mathrm{AV}} = -\frac{g_5^2}{2\pi^4 Q_3^2} \int_0^{z_0} dz \int_0^{z_0} dz' \mathcal{J}'(Q, z) \mathcal{J}(Q, z) \mathcal{J}'(Q_3, z') G_A(0; z, z'), \tag{8.16}$$

for the HW2 model, where we have an analytic expression for the Green's function G_A. In the HW1 model, the defining differential equation

$$\left(z\partial_z\frac{1}{z}\partial_z-\beta(z)\right)G_A(0;z,z')=-z\delta(z-z') \tag{8.17}$$

can only be solved numerically. For large virtualities $Q, Q_3 \gg m_\rho$, the integrals in Eq. (8.16) are dominated by the region $z, z' \ll z_0$ and we can use the leading-order solution

$$G_A(0,z,z')=\frac{1}{2}\left(\min(z,z')\right)^2\left(1+\mathcal{O}(Q^{-n})+\mathcal{O}(Q_3^{-n})\right), \quad n>0, \tag{8.18}$$

where n is a positive function of the scaling dimension Δ_-, to calculate the MV-SDC

$$\begin{aligned}
&\lim_{Q_3\to\infty}\lim_{Q\to\infty}Q^2Q_3^2\bar{\Pi}_1^{\text{AV}}(Q,Q,Q_3)\\
&=-\frac{g_5^2}{2\pi^4}\int_0^\infty d\xi\int_0^\infty d\xi'\xi K_1(\xi)\frac{d}{d\xi}[\xi K_1(\xi)]\frac{d}{d\xi'}[\xi' K_1'(\xi')]\frac{1}{2}\xi^2\\
&=\frac{g_5^2}{(2\pi)^2}\frac{1}{2\pi^2}\int_0^\infty d\xi\xi^2\frac{d}{d\xi}[\xi K_1(\xi)]^2=-\frac{2}{3\pi^2},
\end{aligned} \tag{8.19}$$

using $z=\xi/Q$ and $z'=\xi'/Q_3$. Since the behavior is dominated by the UV-region, this result holds for all HW1 and HW3 models regardless of quark masses, value of M_X^2, or IR-boundary conditions. The only exception is at the border $M_X^2=0$ of the allowed values, where $\Delta_-=0$ and $n=0$. Giving 100% of the MV-SDC, this result implies that the infinite tower massive pions should not contribute. This will be checked in the next subsection.

For now, let us continue by calculating the symmetric SDC

$$\begin{aligned}
&\lim_{Q\to\infty}Q^4\bar{\Pi}_1^{\text{AV}}(Q,Q,Q)\\
&=-\frac{g_5^2}{2\pi^4}\int_0^\infty d\xi\int_0^\infty d\xi'\frac{1}{2}\frac{d}{d\xi}[\xi K_1(\xi)]^2\frac{d}{d\xi'}[\xi' K_1'(\xi')]\frac{1}{2}[\min(\xi,\xi')]^2\\
&=-\frac{g_5^2}{(2\pi)^2\pi^2}\int_0^\infty d\xi\int_0^\infty d\xi'[\xi K_1(\xi)]^2[\xi' K_1'(\xi')]\xi\delta(\xi-\xi')\\
&=-\frac{g_5^2}{(2\pi)^2\pi^2}\int_0^\infty d\xi\,\xi[\xi K_1(\xi)]^3=-0.361\frac{1}{\pi^2},
\end{aligned} \tag{8.20}$$

which is again valid for all here considered models and accounts for roughly 81% of the desired result $4/(9\pi^2)$ in Eq. 2.19.

8.3.2 Pseudoscalar Contribution

Due to the boundary term in the pion TFF (8.8), the pion-pole contribution takes the slightly more complicated form

$$\begin{aligned}\bar{\Pi}_1^{(\pi)} &= -\sum_{n=1}^{\infty}\frac{F_{\pi_n\gamma^*\gamma^*}(Q_1^2,Q_2^2)F_{\pi_n\gamma^*\gamma}(Q_3^2)}{Q_3^2+m_n^2}\\ &= -\frac{1}{4\pi^2}\sum_n\frac{1}{Q_3^2+m_n^2}\Big\{\mathcal{J}(Q_1,z_0)\mathcal{J}(Q_2,z_0)\mathcal{J}(Q_3,z_0)\left(\frac{z}{\beta}\partial_z y_n(z)\right)^2_{z\to z0}\\ &\quad -\mathcal{J}(Q_1,z_0)\mathcal{J}(Q_2,z_0)\left(\frac{z}{\beta}\partial_z y_n(z)\right)_{z\to z0}\int_0^{z_0}dz\mathcal{J}(Q_3,z)zy_n(z)\\ &\quad -\mathcal{J}(Q_3,z_0)\left(\frac{z}{\beta}\partial_z y_n(z)\right)_{z\to z0}\int_0^{z_0}dz\mathcal{J}(Q_1,z)\mathcal{J}(Q_2,z)zy_n(z)\\ &\quad +\int_0^{z_0}dz\mathcal{J}(Q_1,z)\mathcal{J}(Q_2,z)zy_n(z)\int_0^{z_0}dz'\mathcal{J}(Q_3,z')z'y_n(z')\Big\},\end{aligned}\tag{8.21}$$

where the first three terms, however, vanish in the large-Q limit due to $\lim_{Q\to\infty}\mathcal{J}(Q,z_0)=0$ and $\lim_{Q\to\infty}Q^2\mathcal{J}(Q,z_0)=0$. The last term can then be formally written as

$$\begin{aligned}&-\frac{1}{4\pi^2}\sum_{n=1}^{\infty}\int_0^{z_0}dzdz'\mathcal{J}(Q_1,z)\mathcal{J}(Q_2,z)\mathcal{J}(Q_3,z')zz'y_n(z')(Q_3^2-L_{PS})^{-1}y_n(z)\\ =\;&-\frac{1}{4\pi^2}\int_0^{z_0}dzdz'\mathcal{J}(Q_1,z)\mathcal{J}(Q_2,z)\mathcal{J}(Q_3,z')z'z(Q_3^2-L_{PS})^{-1}G_{PS}(z,z';0),\end{aligned}\tag{8.22}$$

where L_{PS} is the defining y_n differential operator (5.25) and G_{PS} the corresponding bulk-to-bulk propagator (5.34). In the limit of the MV-SDC, we can use $z'\gg z$ and $L_{PS}G_{PS}(z,z';0)=0$ to obtain

$$\bar{\Pi}_1^{(\pi)}\big|_{Q\gg Q_3\gg m_\rho}\to-\frac{1}{4\pi^2Q_3^2}\int_0^{z_0}dzdz'\mathcal{J}(Q_1,z)\mathcal{J}(Q_2,z)\mathcal{J}(Q_3,z')z'zG_{PS}(z,z';0).\tag{8.23}$$

To find the bulk-to-bulk propagator, we then use

$$\partial_z\frac{z}{\beta(z)}\partial_z G_{PS}(0;z,z')=-\delta(z-z'),\quad \beta(z)\sim M_q^2(z/z_0)^{2-2\Delta_-},\tag{8.24}$$

for parametrically small z.

For $M_X^2=-3$ we get

$$G_{PS}(0;z,z')\to -M_q^2\ln\left(\max(z,z')\right)+\text{const.},\tag{8.25}$$

leading to the MV-SDC contribution

$$\begin{aligned} -Q^2Q_3^2\bar{\Pi}_1^{(\pi)}(Q,Q,Q_3) &\sim \frac{M_q^2}{4\pi^2}\frac{\ln(Q_3)}{Q_3^2}\int_0^\infty d\xi\xi^3[K_1(\xi)]^2\int_0^\infty d\xi'\xi'^2K_1(\xi') \\ &= \frac{M_q^2}{6\pi^2}\frac{\ln(Q_3^2)}{Q_3^2}\to 0, \end{aligned} \tag{8.26}$$

for large $Q \gg Q_3 \gg m_\rho$. As was the case for the axial-vector contribution, summing the infinite tower enhances the scaling $1/Q_3^2$ of a single meson, but in this case only by $\ln(Q_3^2)$, which is not enough to contribute to the MV-SDC. Graphically, the behavior of $P_1 \equiv -Q^2Q_3^4\bar{\Pi}_1^{(\pi)}(Q,Q,Q_3)$ is displayed in the left panels of Fig. 8.1. Since the logarithmic behavior is not visible, as it is suppressed by the prefactor $M_q^2/(3\pi^2) \sim 3\cdot 10^{-6}\,\text{GeV}^2$, we artificially enhance the quark mass by a factor 25 in Fig. 8.2, where the slow build-up of the logarithm becomes visible.

In the case $M_X^2 < -3$, relevant for the HW1m' and HW3m' models, the logarithmic enhancement disappears, and we get $Q^2Q_3^2\bar{\Pi}_1^{(\pi)}(Q,Q,Q_3) \sim Q_3^{-2}$. For completeness, let us also consider $-3 < M_X^2 < 0$, where $1 > \Delta_- > 0$ and we obtain

$$G_{PS}(0;z,z') \to \frac{M_q^2}{2(1-\Delta_-)}\left(\frac{z_0}{z'}\right)^{2(1-\Delta_-)} \propto Q_3^{2(1-\Delta_-)} \tag{8.27}$$

leading to the contribution

$$Q^2Q_3^2\bar{\Pi}_1^{(\pi)}(Q,Q,Q_3) \sim -\frac{2^{2\Delta^- -3}\Gamma(\Delta^-)\Gamma(1+\Delta^-)}{3\pi^2}\frac{M_q^2}{Q_3^2}\frac{(z_0Q_3)^{2(1-\Delta^-)}}{1-\Delta^-} \propto Q_3^{-2\Delta^-}. \tag{8.28}$$

Interestingly, massive pions also contribute in the chiral limit, where they decouple from the axial-vector current. In this case, the bulk-to-boundary propagator

$$G_{PS}(0;z,z')_{\text{chiral}} \to \text{const.} + \frac{\Sigma^2 z_0^4}{2(1-\Delta_+)}\left(\frac{z_0}{z'}\right)^{2(1-\Delta_+)} \propto \text{const.} + Q_3^{-2-2\alpha}, \tag{8.29}$$

produces no enhancement and does not contribute to the MV-SDC, regardless of the value of M_X^2.

The massive pion contribution to the symmetric SDC (8.15) is also given by Eq. (8.22), but we cannot use the succeeding arguments to derive an analytic result. Numerically, we did not find any evidence for an enhancement of the asymptotic behavior beyond the asymmetric case, as can be seen in the right panels of Figs. 8.1 and 8.2.

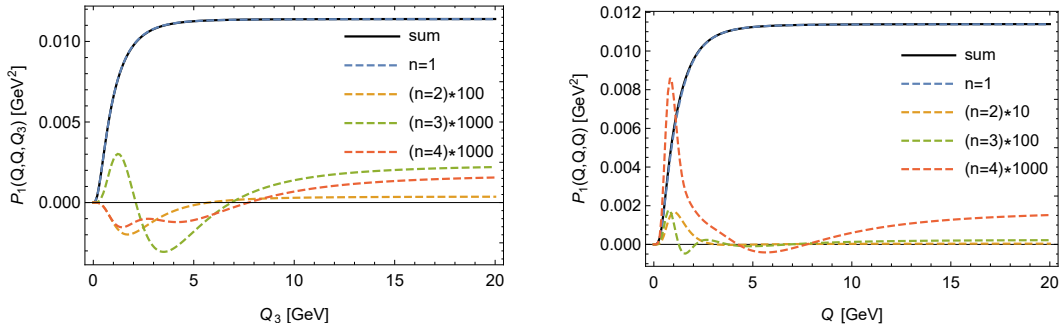

Figure 8.1. – Contribution of the first four pion modes to $P_1(Q,Q,Q_3) = -Q^2Q_3^4\Pi_1^{(\pi)}(Q,Q,Q_3)$ in the HW1m model with $Q = 200$ GeV on the left and $Q_3 = Q$ on the right. The sum is still suppressed by $1/Q_3^2$ as compared to the MV-SDC and does not contribute. The logarithmic enhancement is not visible. Figure from Ref. [II].

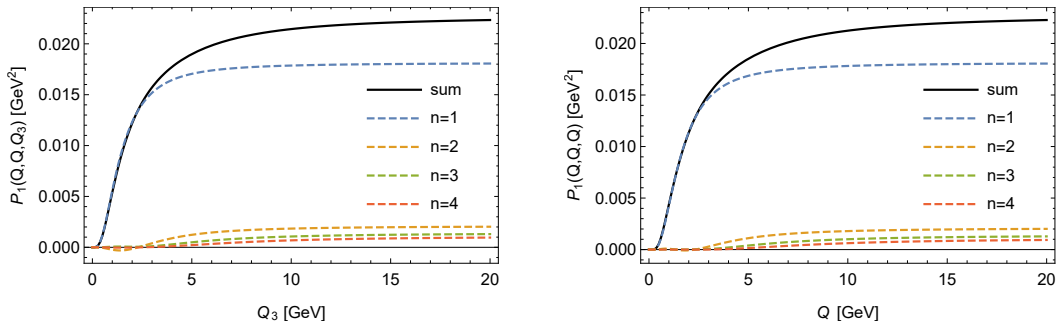

Figure 8.2. – Similar to Figure 8.1, but with quark masses increased by a factor of 25, such that the build-up of the logarithmic enhancement becomes visible. Figure from Ref. [II].

Model	$a_\mu^{\pi^0}$	a_μ^{π}	$a_\mu^{\pi\cup a_1}$	$a_{\mu(L)}^{\pi^*\cup a_1}$	$a_{\mu(L)}^{\pi^*\cup a_1^*}$	$a_\mu^{\mathrm{P}^*}$	$a_\mu^{\mathrm{A}}[L+T]$	$a_\mu^{\mathrm{A+P}^*}$
HW1(chiral)	65.2	66.1	76.2	6.6	2.2	3.5	$40.6[23.2+17.4]$	44.0
HW1m	66.0	66.8	77.0	6.7	2.2	3.5	$40.8[23.3+17.5]$	44.3
HW1m'	64.3	66.1	77.0	8.1	3.7	7.2	$43.3[25.0+18.3]$	50.5
HW3m	66.6	67.4	77.4	6.5	1.9	3.4	$39.9[22.7+17.2]$	43.3
HW3m'	66.0	67.5	77.8	7.4	2.7	6.1	$41.2[23.5+17.7]$	47.3

Table 8.2. – Partial sums of contributions to a_μ^{HLbL}, where (L) denotes the longitudinal contribution, π and a_1 the entire towers, and π^* and a_1^* only the excited modes. The flavor multiplet is collected in $a_\mu^{\mathrm{A}} \equiv 4a_\mu^{a_1}$ and $a_\mu^{\mathrm{P}^*} \equiv 4a_\mu^{\pi^*}$, valid in the flavor-symmetric case. Numerical results for single modes can be found in Appendix C. Table from Ref. [II].

8.4 Contribution to $g-2$

The calculation of the contribution to a_μ^{HLbL} is analogous to the previous two chapters, only with changed TFFs and masses. The detailed results are listed in Appendix C and presented in partial sums of contributions in Table 8.2. We find that the chiral result $a_\mu^{\pi^0} = 65.2 \times 10^{-11}$, also obtained in Chapter 6, is remarkably close to the massive HW models with the range $a_\mu^{\pi^0} = (64.3 \ldots 66.6) \times 10^{-11}$. For the contribution of massive pions[1], we find the range $a_\mu^{\pi^*} = (0.8 \ldots 1.8) \times 10^{-11}$. For the tower of axial-vector mesons, we obtain the total contribution in the range $a_\mu^{\mathrm{A}} = (39.3 \ldots 43.3) \times 10^{-11}$. Although in Chapter 6 we have worked out the η and η' contributions in the chiral HW1 mode, here we assume a flavor-symmetric setup for the massive HW models. Contributions of the flavor asymmetry and the $U(1)_A$ anomaly will be studied in a future work.

One weakness of the here considered HW models is that they do not have a running coupling constant. As a result, the TFF might reach their SDCs too quickly, whereas at large but not excessively large momenta perturbative corrections also contribute. As an attempt to account for this and to make extrapolations to real QCD, we consider a reduction of the coupling constant g_5^2 by 10% and by 15% roughly corresponding to the perturbative corrections in Refs. [115, 116]. The resulting increase in the vector-vector-correlator function Π_V (5.11) is then also consistent with the next-to-leading order result in Ref. [81]. The coupling constant reductions modify $A_1(0,0)$ and the contributions to a_μ^{HLbL} according to the factors in Table 8.3 estimated from the chiral HW1 model.

[1] Even though massive pions decouple from the axial-vector current in the chiral HW1 mode, they still have a non-vanishing two photon coupling and contribute to the HLbL scattering amplitude.

$\frac{g_5^2 N_c}{12\pi^2}$	$R(A(0,0)_{n=1})$	$R(a_\mu^{P_1,P})$	$R(a_\mu^{A_1})$	$R(a_\mu^{A})$
0.90	0.93	0.96	0.91	0.95
0.85	0.90	0.94	0.87	0.92

Table 8.3. – Reduction factors R to various quantities due to the coupling constant reduction of g_5^2 by 10% and by 15% as estimated from the chiral HW model. Table from Ref. [II].

As a conservative estimate, we apply these reduction factors to the lower values in our results according to

$$\begin{aligned} a_\mu^{\pi^0} &= (R(a_\mu^{P_1})_{0.85} \times 64.3 \ldots 66.6) \times 10^{-11} \\ &= (60.5 \ldots 66.6) \times 10^{-11}, \end{aligned} \tag{8.30}$$

and analogously for the other contributions to obtain our final predictions

$$\begin{aligned} a_\mu^{P^*} &= (3.2 \ldots 7.2) \times 10^{-11}, \\ a_{\mu(L)}^{A} &= (20.8 \ldots 25.0) \times 10^{-11}, \\ a_\mu^{A} &= (36.6 \ldots 43.3) \times 10^{-11}, \\ a_\mu^{A+P^*} &= (39.8 \ldots 50.5) \times 10^{-11}. \end{aligned} \tag{8.31}$$

8.5 Discussion

In this part of the thesis, we have seen how holographic QCD can be used to make predictions for the anomalous magnetic moment of the muon, particularly for the HLbL contribution with its current theoretical uncertainty of 20% and even 100% in the axial-vector contribution. The holographic pseudoscalar and axial-vector TFF satisfy important SDC from pQCD and the OPE, and the infinite tower of axial-vector mesons can be used to implement the MV-SDC on the HLbL scattering four-point function. Besides fitting other low-energy observables, this is achieved with only three free parameters in the chiral HW1 model.

As the primary contribution, we find a remarkable agreement of our prediction (8.30) for the pion-pole contribution to the result $a_\mu^{\pi^0} = 62.6^{+3.0}_{-2.5} \times 10^{-11}$ of the data-driven dispersive approach [38]. To compare the remaining contribution of the axial sector, we combine the axial sector and SDC contributions $a_\mu^{\mathrm{WP,axials}} = 6(6) \times 10^{-11}$ and $a_\mu^{\mathrm{WP,SDC}} = 15(10) \times 10^{-11}$ of the WP [2] with linearly added errors to $21(16) \times 10^{-11}$. This is significantly smaller than the corresponding holographic prediction $a_\mu^{A+P^*}$ in

Eq. 8.31. Since the holographic and the SM estimates for the SDC contributions are compatible [117, 118], this points to an extra contribution of $\gtrsim 20 \times 10^{-11}$ in the (transverse) axial-vector meson sector.

Apart from the axial-sector, holographic QCD models can also be used to consider other hadronic contributions to a_μ. Recently, the holographic scalar meson contribution to a_μ^{HLbL} was calculated in Ref. [119], albeit by introducing different sets of parameters for the considered $f_0(500)$, $f_0(990)$, and the $a_0(980)$ mesons. Another, not yet considered, contribution is mediated by glueballs, which are nicely implemented in holographic models as will be discussed in the next part of this thesis.

For completeness, let us also comment on holographic predictions for HVP, as were first calculated in Ref. [120] and recently in [121]. In contrast to HLbL, holographic QCD is not precise enough to help with the unresolved discrepancy between lattice and data-driven approaches, which differ by only 2%. Further discussion and possible ways to improve the holographic models will be discussed in Ref. [122].

Part IV

Holographic Glueballs

In this part of the thesis, we will extend the holographic SS model to include glueballs, which allows us to study their effect on the anomalous magnetic moment of the muon. We will start with a general introduction to glueballs in the SS model and calculate the spectrum. Next, we will in detail consider the pseudoscalar glueball and its role in the Witten-Veneziano mechanism, leading to an interesting mixing with the singlet component of the η mesons which introduces otherwise absent interactions such as photon couplings. Finally, we calculate radiative glueball decays and give an estimate on the contribution to HLbL.

9 Glueballs in the Sakai-Sugimoto Model

> *Don't underestimate the force.*
>
> **— Darth Vader**
> Star Wars: Episode IV - A New Hope

Up to this point in the thesis, we have concentrated on the physics of flavor degrees of freedom, but as it turns out, there are also a multitude of interesting observables in the color sector. Since the strong force is self-interacting, gluons may bind together to form particles known as glueballs [123, 124, 125]. However, the strong coupling makes it difficult to study these states from first principles. Mathematically, glueballs manifest in the spectrum of pure Yang-Mills theory as a mass gap. Proving the existence of this mass gap is an important open issue and is one of the Millennium Problems formulated by the Clay Mathematics Institute [126].

Not only is the theoretical description of glueballs difficult, but also, experimentally, no glueball state has been identified unambiguously. One difficulty is that glueball states are difficult to distinguish from other meson states with which they can mix. Since the states are characterized by their mass and decay products, one depends upon theoretical predictions of these quantities to identify whether the state is a glueball or not. Future experiments, such as the PANDA experiment at FAIR [127], will provide new data and will hopefully make it possible to identify glueballs more clearly.

Besides lattice QCD, a promising description of glueballs is given by holographic QCD, where glueballs are dual to fluctuations of the geometry. In this chapter, we will review glueballs in the Sakai-Sugimoto model, where they are given as fluctuations of the Witten background, which determines the spectrum. By considering the D-brane action in this fluctuating background, glueball-meson interactions can be calculated. Using VMD, this fixes the interaction of glueballs with photons and correspondingly the contribution to HLbL [128].

States from G_{MN}				States from A_{MNL}		
$G_{\mu\nu}$	$G_{\mu,11}$	$G_{11,11}$	Eq.	$A_{\mu\nu,11}$	$A_{\mu\nu\rho}$	Eq.
G_{ij} 2^{++}	C_i $1^{++}_{(-)}$	ϕ 0^{++}	T_4	B_{ij} 1^{+-}	C_{123} $0^{+-}_{(-)}$	N_4
$G_{i\tau}$ $1^{-+}_{(-)}$	C_τ 0^{-+}		V_4	$B_{i\tau}$ $1^{--}_{(-)}$	$C_{ij\tau}$ 1^{--}	M_4
$G_{\tau\tau}$ 0^{++}			S_4	G^α_α State 0^{++}		L_4

Table 9.1. – Classification of glueball fluctuations following Ref. [129]. Quantum numbers correspond to J^{PC}, with $P_\tau = -1$ indicated as subscript.

This chapter is structured as follows: First we will construct the possible glueball states in the Witten background, find the corresponding mode equations, and assign parity and charge conjugation quantum numbers. After a comparison of the resulting glueball spectrum to lattice QCD, we will finish this chapter with a review of some selected glueball interactions. The presentation will follow the study of Brower, Mathur, and Tan [129], with some notation and results from Ref. [72] and Refs. [V, VII].

9.1 The Glueball Spectrum in Witten's Background

As discussed in Chapter 4, the Sakai-Sugimoto model is based on 10-dimensional supergravity. Even though the background (4.1) looks relatively simple, with only a dilaton, a metric and a 3-form field, studying its fluctuations involves many other fields. By reformulating this background in terms of 11-dimensional supergravity, as described in Appendix D, the calculation simplifies significantly. In this higher-dimensional theory, the field content is given by a single multiplet: the supergraviton, whose two bosonic fields are the graviton G_{MN} and a 3-form field A_{MNL}. Upon compactifying the 11th direction, we get back to 10-dimensional supergravity. The 11-dimensional graviton then gives rise to a dilaton ϕ and a Ramond-Ramond 1-form field C_1. The 11-dimensional 3-form field yields a Kalb-Ramond 2-form field B_2 and a Ramond-Ramond 3-form field C_3. This classification is presented in Table 9.1 for the specific case of an $AdS_7 \times S^4$ spacetime.

In studying fluctuations of these fields, we will ignore Kaluza-Klein excitations in the compactified directions since they would correspond to charges and quantum numbers not realized in nature; therefore, fluctuations depend solely on their 4-momentum and the radial coordinate.

Metric Fluctuations

Let us start with fluctuations of the 11-dimensional geometry. As discussed in Appendix D, the Witten background can be given by the 11-dimensional line-element

$$ds^2 = \frac{r^2}{L^2}\left(f(r)dx_4^2 + \eta_{\mu\nu}dx^\mu dx^\nu + dx_{11}^2\right) + \frac{L^2}{r^2}\frac{dr^2}{f(r)} + \frac{L^2}{4}d\Omega_4^2. \tag{9.1}$$

It is useful to classify the metric fluctuations

$$G_{MN} \to G_{MN} + \delta G_{MN} \tag{9.2}$$

by the form of their polarization tensor h_{MN} at $r \to \infty$, where the dual field theory is living. Constructing the polarization tensor in the rest frame of the graviton, the indices can take values among $(x_1, x_2, x_3, \tau, x_{11})$. Considering that the polarization tensor should be traceless, we can count $(5\times 6)/2 - 1 = 14$ independent components of the polarization tensor.

The warp factor $f(r)$ in the line-element (9.1) singles out the τ-direction, and we can divide the polarization tensor's 14 independent components into $9{+}4{+}1$ components, which correspond to the irreducible representations of $SO(4)$. The mode equations of the metric fluctuations follow this classification, and the corresponding radial wave equations are called T_4, V_4 and S_4, respectively.

Since the 11th direction is compactified, the identification of the spin is only due to the $SO(3)$ symmetry in (x_1, x_2, x_3). This breaks the representations further, and results in degenerate spectra for fields with different spin [129]:

- the 9-dimensional representation breaks into $5+3+1$ under $SO(3)$,

$$\begin{aligned} G_{ij}: &\quad h_{ij} - \frac{1}{3}\delta_{ij}h_{kk} \neq 0 \quad \to \quad \text{spin-2}, \\ C_i: &\quad h_{i,11} = h_{11,i} \neq 0 \quad \to \quad \text{spin-1}, \\ \phi: &\quad h_{11,11} = -3h_{11} = -3h_{22} = -3h_{33} \neq 0 \quad \to \quad \text{spin-0}, \end{aligned} \tag{9.3}$$

- the 4-dimensional representation breaks into $3+1$ under $SO(3)$,

$$\begin{aligned} G_{i\tau}: &\quad h_{\tau i} = h_{i\tau} \neq 0 \quad \to \quad \text{spin-1}, \\ C_\tau: &\quad h_{\tau,11} = h_{0\tau} \neq 0 \quad \to \quad \text{spin-0}, \end{aligned} \tag{9.4}$$

- the 1-dimensional representation is singlet under $SO(3)$,

$$G_{\tau\tau}: \quad h_{\tau\tau} = -4h_{11} = -4h_{22} = -4h_{33} = -4h_{11,11} \neq 0 \quad \rightarrow \quad \text{spin-0}. \tag{9.5}$$

Additionally, there is the volume fluctuation of the S^4 sphere given by G^α_α with mode equation L_4.

3-Form Fluctuations

For fluctuations of the antisymmetric 3-form field A_{MNL}, a similar counting gives ten independent components, which split into $4+6$ components under $SO(4)$. The corresponding mode equations are called N_4 and M_4, respectively. Identifying the spin, we find [129]:

- a 4-dimensional representation which breaks into $3+1$ under $SO(3)$,

$$\begin{aligned} B_{ij}: \quad & A_{ij,11} \neq 0 \rightarrow \quad \text{spin-1}, \\ C_{123}: \quad & A_{ijk} \neq 0 \rightarrow \quad \text{spin-0}, \end{aligned} \tag{9.6}$$

- a 6-dimensional representation which breaks into $3+3$ under $SO(3)$,

$$\begin{aligned} B_{i\tau}: \quad & A_{i\tau,11} \neq 0 \rightarrow \quad \text{spin-1}\ , \\ C_{ij\tau}: \quad & A_{ij\tau} \neq 0 \rightarrow \quad \text{spin-1}\ . \end{aligned} \tag{9.7}$$

Mode Equation and Spectrum

For the glueball fields we make a similar separation ansatz as for the mesonic degrees of freedom considered in the previous chapters. The exact form of this ansatz is

Mode J^{PC}	S_4 0^{++}	T_4 $0^{++}/2^{++}$	V_4 0^{-+}	N_4 1^{+-}	M_4 1^{--}	L_4 0^{++}
$n=0$	7.30835	22.0966	31.9853	53.3758	83.0449	115.002
$n=1$	46.9855	55.5833	72.4793	109.446	143.581	189.632
$n=2$	94.4816	102.452	126.144	177.231	217.397	277.283
$n=3$	154.963	162.699	193.133	257.959	304.531	378.099
$n=4$	228.709	236.328	273.482	351.895	405.011	492.171

Table 9.2. – Glueball spectrum in the Witten background in units of $M_{\rm KK}^2/9$, according to Ref. [72].

presented in Appendix E. According to the counting of representations, we get six distinct eigenvalue equations[1], which read

$$\begin{aligned}
&\frac{d}{dr}(r^7 - r\, r_{\rm KK}^6)\frac{d}{dr}T_4(r) + L^4 m^2 r^3 T_4(r) = 0\,,\\
&\frac{d}{dr}(r^7 - r\, r_{\rm KK}^6)\frac{d}{dr}V_4(r) + \left(L^4 m^2 r^3 - \frac{9\, r_{\rm KK}^{12}}{r(r^6 - r_{\rm KK}^6)}\right)V_4(r) = 0\,,\\
&\frac{d}{dr}(r^7 - r\, r_{\rm KK}^6)\frac{d}{dr}S_4(r) + \left(L^4 m^2 r^3 + \frac{432 r^5 r_{\rm KK}^{12}}{(5r^6 - 2r_{\rm KK}^6)^2}\right)S_4(r) = 0\,,\\
&\frac{d}{dr}(r^7 - r\, r_{\rm KK}^6)\frac{d}{dr}N_4(r) + \left(L^4 m^2 r^3 - 27 r^5 + \frac{9 r_{\rm KK}^6}{r}\right)N_4(r) = 0\,,\\
&\frac{d}{dr}(r^7 - r\, r_{\rm KK}^6)\frac{d}{dr}M_4(r) + \left(L^4 m^2 r^3 - 27 r^5 - \frac{9 r^5 r_{\rm KK}^6}{r^6 - r_{\rm KK}^6}\right)M_4(r) = 0\,,\\
&\frac{d}{dr}(r^7 - r\, r_{\rm KK}^6)\frac{d}{dr}L_4(r) + (L^4 m^2 r^3 - 72 r^5)L_4(r) = 0\,.
\end{aligned} \tag{9.8}$$

With normalizable boundary conditions, the six distinct towers of eigenvalues can be calculated. The resulting spectra are displayed in Table 9.2.

Parity and Charge Conjugation Assignment

In Table 9.1, we have already assigned the quantum numbers J^{PC} corresponding to spin, parity, and charge conjugation to the glueball fluctuations. In the following, we will motivate this assignment. We start by defining the action of symmetry

[1] Three follow from the AdS_7-metric, one from the S^4-metric, and two from the 3-form field fluctuations.

transformations on the gauge fields. Usual 3-dimensional parity transformation acts as

$$\begin{aligned} P:\ & A_0\left(x^0,x^i,\tau\right)\to A_0\left(x^0,-x^i,\tau\right), \\ P:\ & A_i\left(x^0,x^i,\tau\right)\to -A_i\left(x^0,-x^i,\tau\right), \\ P:\ & A_\tau\left(x^0,x^i,\tau\right)\to A_\tau\left(x^0,-x^i,\tau\right). \end{aligned} \tag{9.9}$$

There is also a parity transformation in the compactified τ direction. It is defined by

$$\begin{aligned} P_\tau:\ & A_0\left(x^0,x^i,\tau\right)\to A_0\left(x^0,x^i,-\tau\right), \\ P_\tau:\ & A_i\left(x^0,x^i,\tau\right)\to A_i\left(x^0,x^i,-\tau\right), \\ P_\tau:\ & A_\tau\left(x^0,x^i,\tau\right)\to -A_\tau\left(x^0,x^i,-\tau\right). \end{aligned} \tag{9.10}$$

As stated before, we are truncating our fluctuations to fluctuations independent of the compactified directions. Fluctuations with $P_\tau=-1$ quantum numbers should therefore be excluded [129, 71]. Finally, charge conjugation is defined by

$$\begin{aligned} C:\ & A_0\left(x^0,x^i,\tau\right)\to -A_0^T\left(x^0,x^i,\tau\right), \\ C:\ & A_i\left(x^0,x^i,\tau\right)\to -A_i^T\left(x^0,x^i,\tau\right), \\ C:\ & A_\tau\left(x^0,x^i,\tau\right)\to -A_\tau^T\left(x^0,x^i,\tau\right). \end{aligned} \tag{9.11}$$

Using these definitions, we can determine the quantum numbers P and C of a glueball fluctuation by requiring that the D4 brane action at $r\to\infty$

$$\begin{aligned} S_{D4} \;=\; & -\mathrm{STr}\int d^5x\,\sqrt{-\det\left[G_{ab}+e^{-\frac{\phi}{2}}\left(B_{ab}+F_{ab}\right)\right]} \\ & +\int d^5x\,\left(C_1\wedge F\wedge F+C_3\wedge F+C_5\right), \end{aligned} \tag{9.12}$$

is invariant. By expanding this action in terms of fluctuations we find, among others, the term

$$h_{ab}\mathrm{Tr}\left(F^{ac}F^b_{\ c}\right)=h_{ij}\mathrm{Tr}\left(F^{ic}F^j_{\ c}\right). \tag{9.13}$$

It is invariant for the quantum numbers

$$h_{ij}\to 2^{++}\left(P_\tau=+\right). \tag{9.14}$$

The results for the other fluctuations are collected in Table 9.1.

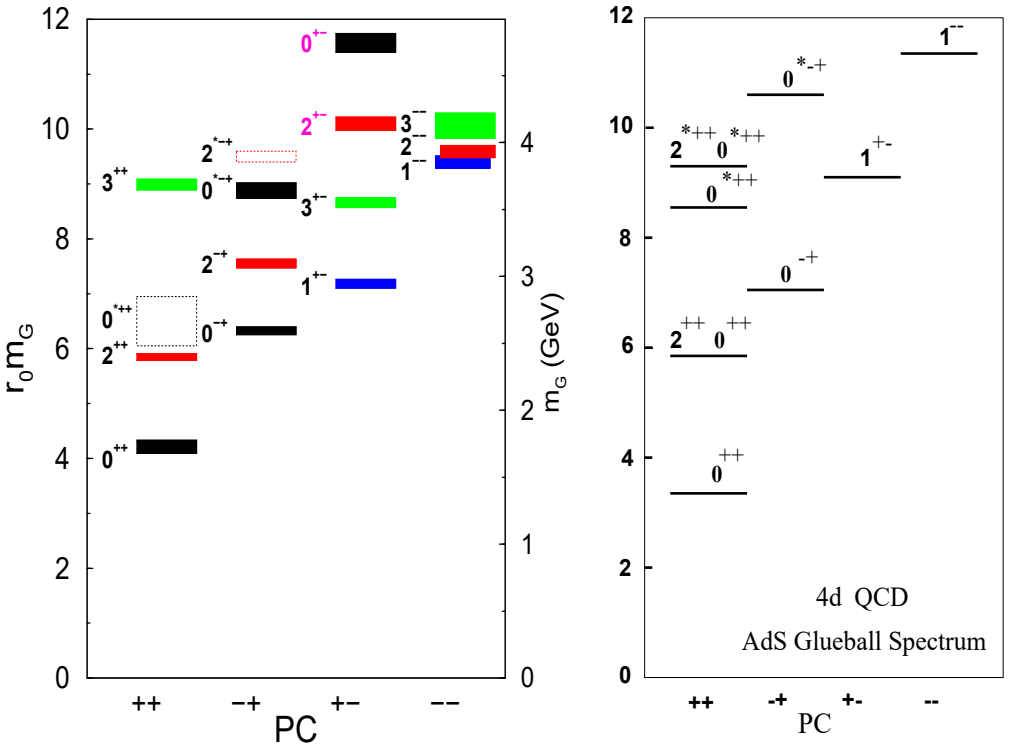

Figure 9.1. – Comparison of the lattice glueball spectrum of Ref. [130] to the holographic glueball spectrum of Ref. [129].

9.2 Comparison to the Lattice Glueball Spectrum

At this point, it is interesting to compare the glueball spectrum of the Witten background to results from lattice QCD. In Fig. 9.1 we compare the lattice result of Ref. [130] to the holographic result of Ref. [129], where the tensor glueball mass is used to fix the mass scale. Both spectra begin with a scalar glueball and are followed by a tensor glueball and a pseudoscalar glueball. While the second-lightest scalar glueball on the lattice is an excited state, the holographic model's second-lightest scalar glueball is an independent mode. As one can see from Table 9.2, most of the glueball spectrum is above the Kaluza-Klein mass scale and is therefore in a region where the holographic model begins to show its higher-dimensional nature. The two spectra deviate correspondingly. In addition to this disagreement, the lattice result also contains higher-spin modes and other quantum number combinations that are absent in the holographic spectrum. This is due to the supergravity approximation; higher-spin modes could be included by considering stringy excitations.

9.3 Glueball Interactions

Even though the SS model uses the probe approximation for the flavor branes in which the background does not feel the flavor branes, the reverse is certainly not true. Fluctuating the background does change the flavor brane action given by the DBI and CS action (4.9). This induces interactions of glueball states with mesons. To study this effect, we have to first reduce the 11-dimensional glueball fluctuations to ten dimensions. As described in Appendix D, this is achieved by

$$ds^2 = G_{\hat{M}\hat{N}} dx^{\hat{M}} dx^{\hat{N}} = e^{-2\phi/3} g_{MN} dx^M dx^N + e^{4\phi/3} dx_{11}^2, \tag{9.15}$$

where 11D and 10D indices are denoted with and without hats, respectively. For the Witten background (4.1), this gives the relation

$$\begin{aligned}
g_{\mu\nu} &= \frac{r^3}{L^3}\left[\left(1+\frac{L^2}{2r^2}\delta G_{11,11}\right)\eta_{\mu\nu} + \frac{L^2}{r^2}\delta G_{\mu\nu}\right], \\
g_{44} &= \frac{r^3 f}{L^3}\left(1+\frac{L^2}{2r^2}\delta G_{11,11} + \frac{L^2}{r^2 f}\delta G_{44}\right), \\
g_{rr} &= \frac{L}{rf}\left(1+\frac{L^2}{2r^2}\delta G_{11,11} + \frac{r^2 f}{L^2}\delta G_{rr}\right), \\
g_{r\mu} &= \frac{r}{L}\delta G_{r\mu}, \\
g_{\Omega\Omega} &= \frac{r}{L}\left(\frac{L}{2}\right)^2\left(1+\frac{L^2}{2r^2}\delta G_{11,11}\right), \\
e^{4\phi/3} &= \frac{r^2}{L^2}\left(1+\frac{L^2}{r^2}\delta G_{11,11}\right).
\end{aligned} \tag{9.16}$$

Using these identities with the explicit glueball fluctuations given in Appendix E, we can calculate the induced metric on the D8 brane action (4.9) to obtain interaction terms between glueballs and mesons.

As a specific example, let us study scalar glueball decays into two pions as calculated in Ref. [72]. From Table 9.2 one can see that the SS model has three towers of 0^{++} glueballs. The L_4 scalar, arising from fluctuations of the 4-sphere volume, is quite heavy and is usually neglected. The T_4 and S_4 scalars come from two

distinct polarizations of the AdS_7 metric: the dilatonic (D) and an "exotic" [131] (E) polarization.[2] For the former, we obtain the relevant interaction Lagrangian

$$\mathcal{L}^{G_D\to\pi\pi} = \frac{1}{2}d_1 \mathrm{Tr}\,\partial_\mu\pi\partial_\nu\pi\left(\eta^{\mu\nu} - \frac{\partial^\mu\partial^\nu}{M_D^2}\right)G_D, \tag{9.17}$$

where the coupling constant is given by

$$d_1 = \int dZ \frac{H_D}{\pi K}. \tag{9.18}$$

For the exotic polarization, we get interactions

$$\mathcal{L}^{G_E\to\pi\pi} = -\mathrm{Tr}\left[\frac{1}{2}c_1\partial_\mu\pi\partial_\nu\pi\frac{\partial^\mu\partial^\nu}{M_E^2}G_E + \frac{1}{2}\check{c}_1\partial_\mu\pi\partial^\mu\pi\, G_E\right], \tag{9.19}$$

where the two coupling constants are given by

$$c_1 = \int dZ\left[\frac{1}{4} + \frac{3}{5K-2}\right]\frac{H_E}{\pi K}, \qquad \check{c}_1 = \int dZ\frac{H_E}{4\pi K}. \tag{9.20}$$

From these interaction Lagrangians, we can easily calculate the corresponding amplitudes in the center of mass frame

$$|\mathcal{M}_D| = |d_1\mathbf{p}\cdot\mathbf{q}| = |d_1|\frac{M_D^2}{4}, \tag{9.21}$$

$$|\mathcal{M}_E| = |(c_1+\check{c}_1)p_0q_0 - \check{c}_1\mathbf{p}\cdot\mathbf{q}| = |c_1+2\check{c}_1|\frac{M_E^2}{4}, \tag{9.22}$$

where p^μ and q^μ are the four-momenta of the pions with $p_0 = q_0 = |\mathbf{p}| = |\mathbf{q}| = M_{D,E}/2$. The decay widths then read

$$\Gamma_{G_{D,E}\to\pi\pi} = \frac{3|\mathbf{p}|}{16\pi M_{D,E}^2}|\mathcal{M}_{D,E}|^2, \tag{9.23}$$

with the numerical results

$$\begin{aligned}\Gamma_{G_E\to\pi\pi}/M_E &= \frac{3|c_1+2\check{c}_1|^2M_E^2}{512\pi} \approx \frac{13.79}{\lambda N_c^2} \approx 0.092 \quad (M_E \approx 855\text{MeV}),\\ \Gamma_{G_D\to\pi\pi}/M_D &= \frac{3|d_1|^2M_D^2}{512\pi} \approx \frac{1.359}{\lambda N_c^2} \approx 0.009 \quad (M_D \approx 1487\text{MeV}),\end{aligned} \tag{9.24}$$

where we have used the usual parameters $\lambda = 16.63$ and $M_{\mathrm{KK}} = 949$.

[2] The term "exotic" mode was introduced in Ref. [131] and refers to its holographic origin as a metric fluctuation dominated by $\delta G_{\tau\tau}$ and not to any exotic J^{PC} quantum numbers.

Similarly, one can calculate decays of the scalar glueball into other mesons, or one can study decay rates of the other glueball fluctuations listed in Table 9.1. Some results and observations are summarized in the following:

Scalar Glueball (0^{++})

The experimental status of the lightest scalar glueball state is ambiguous. There are phenomenological models which identify the isoscalar meson $f_0(1500)$ as predominantly a glueball state and the $f_0(1710)$ as a $q\bar{q}$ state, and other models with a reverse identification [132, 133, 134, 135, 136, 137, 138, 139, 140, 141, 142]. Comparing the results for the scalar glueball decay rates to the experimental data of the two scalar glueball candidates, Ref. [72] finds that the exceedingly light exotic glueball does not agree well with the experimental candidates. After an artificial increase of the glueball mass, this still holds true, and it is suggested that one should exclude the exotic glueball state from the physical spectrum.

The dilaton glueball state has a mass of around 1.5 GeV and only needs a slight extrapolation to be compared to the experimental candidate states. The decay rates are found to agree better with $f_0(1710)$ than with $f_0(1500)$, and it is concluded that $f_0(1710)$ should be considered as a glueball state. This conclusion is corroborated by the studies [143, 144], where effects of finite quark masses are considered. Radiative scalar glueball decays are presented in Chapter 11.

Tensor Glueball (2^{++})

In the SS model, the tensor glueball has the same mass of 1487 MeV as the dilaton glueball. Unfortunately, this is far too light compared to the lattice value of 2.4 GeV and the experimental candidates around 2 GeV [145, 146]. Extrapolating the tensor glueball mass to 2 GeV, Ref. [72] finds a marginal agreement with the potential glueball candidate $f_2(1950)$. When increasing the mass to 2.4 GeV, the glueball state turns out to be very broad. Decays including one or two photons are discussed in Chapter 11. In Ref. [III] and Appendix F, we use the tensor glueball fluctuation to study central exclusive production of the f_1 meson in proton-proton collisions. There the pomeron, the Regge trajectory starting with the tensor glueball, plays an important role.

Pseudoscalar Glueball (0^{-+})

The pseudoscalar glueball fluctuation plays a crucial role in the identification of the QCD theta term and in generating the Witten-Veneziano mass, as demonstrated in Ref. [V]. The crucial anomalous mixing of the Ramond-Ramond C_1 field with the singlet component of the pseudoscalar meson also induces new decay rates of the pseudoscalar glueball previously missed in Ref. [147]. After extrapolating the glueball mass to 2.6 GeV, as indicated by (quenched) lattice results, the pseudoscalar glueball fluctuation is a rather broad resonance. The pseudoscalar glueball will be discussed in more detail in Chapter 10 and 11.

Pseudovector Glueball (1^{+-})

Decay rates of the pseudovector glueball are calculated in Ref. [VII] and will be presented in Appendix G. The main observation is that holographic QCD predicts a very broad state ($\Gamma/M \approx 1$) for which establishing experimental evidence will be difficult.

10 Pseudoscalar Glueball and Witten-Veneziano Mechanism

> *Shaken, not stirred.*
>
> — **James Bond**
> Goldfinger

THE $U(1)_A$ part of the QCD flavor symmetry $U(N_f)_L \times U(N_f)_R$ plays an important role in the generation of the η' mass. Since this part is broken by the axial anomaly, only the remaining $U(1)_V \times SU(N_f)_L \times SU(N_f)_R \to U(N_f)_V$ symmetry can be spontaneously broken and therefore lead only to $N_f^2 - 1$ pseudoscalar Goldstone bosons whose masses are proportional to the quark mass according to the Gell-Mann–Oakes–Renner relation.[1] The $U(1)_A$ pseudoscalar meson, regarded as the η' meson, is too heavy to be a Goldstone boson [148]. The explanation of 't Hooft [149, 150] that this mass is due to instantons does not work in the large-N_c limit, where these effects are exponentially suppressed. Instead, Veneziano [151] and Witten [152] proposed a mechanism using the nontrivial θ-dependence of large-N_c pure Yang-Mills theory to generate the mass term $m_0^2 = 2N_f\chi_g/f_\pi^2$, proportional to the chiral susceptibility χ_g, for the singlet η_0.

In the Witten model [13], the background of the SS model, this mechanism is indeed realized and was first discussed in Ref. [153] using a model with flavor D6 branes and later by Sakai and Sugimoto [11, 12] for the SS model. A detailed derivation of the Witten-Veneziano mechanism in the SS model is given in Ref. [154]. In this chapter, we will review the alternative derivation of Ref. [V] and its implications on the mixing of the singlet η_0 with the pseudoscalar glueball. Compared to the very narrow pseudoscalar glueball resonance of Ref. [147], this mixing leads to additional interaction terms and a rather broad resonance.

This chapter is structured as follows: First, we will review the realization of the θ parameter and the pseudoscalar glueball fluctuation in the Witten model. Next, we will

[1] In the strict large-N_c limit, the $U(1)_A$ anomaly is a subleading effect in the $1/N_c$ expansion. We therefore consider only large but finite N_c.

include flavor degrees of freedom and study how the $U(1)_A$ anomaly generates the Witten-Veneziano mass of the η_0 meson. Considering the most general pseudoscalar glueball fluctuation, we will derive an effective action with a mixed kinetic term whose diagonalization introduces a mixing of the η_0 meson with the pseudoscalar glueball. We will finish this chapter by calculating the resulting decay rates of the pseudoscalar glueball.

10.1 Theta Parameter

To start, let us look at the Witten model [13] of low-energy pure Yang-Mills theory, as introduced in Chapter 9. It is based on a stack of N_c D4 branes in type IIA supergravity, described by the D4 brane action

$$\begin{aligned} S^{\text{D4}} &= -T_4 \text{Tr} \int d^4x d\tau e^{-\phi} \sqrt{-g_{(5)}} (\mathbf{1} + \frac{1}{2}(2\pi\alpha')^2 |F_{\text{YM}}|^2 + \dots) \\ &\quad + T_4 (2\pi\alpha')^2 \int C_1 \wedge F_{\text{YM}} \wedge F_{\text{YM}} + \dots . \end{aligned} \tag{10.1}$$

Through compactifying the theory on the supersymmetry breaking circle S_τ with radius M_{KK}^{-1} it is dual to pure $(3+1)$-dimensional YM-theory. Taking the UV limit $U \to \infty$, we get

$$\mathcal{L} = -\frac{1}{2g_{\text{YM}}^2} \text{Tr}\, |F_{\text{YM}}|^2 + \frac{\theta}{8\pi^2} \text{Tr}\, F_{\text{YM}} \wedge F_{\text{YM}}, \tag{10.2}$$

where we have used the D4 brane tension $T_4 = (2\pi)^{-4} l_s^{-5}$ and $\alpha' = l_s^2$ to define

$$g_{\text{YM}}^2 = 2\pi g_s l_s M_{\text{KK}}, \quad \theta + 2\pi k = \frac{1}{l_s} \int_{S_\tau} C_1. \tag{10.3}$$

The θ parameter is therefore fixed[2] by the one-form field $C_\tau d\tau$, which in the Witten background vanishes. However, non-normalizable fluctuations of C_τ can give rise to a local spacetime dependent θ parameter. Normalizable modes are usually interpreted as pseudoscalar glueballs [129].

These fluctuations are described by the quadratic action

$$\begin{aligned} S_{\text{R}} \supset & -\frac{1}{4\kappa_{10}^2} \int d^{10}x \sqrt{-g} \left(|F_2|^2 \right) \\ = & -\frac{2\pi R_4 V_4}{64\kappa_{10}^2} \int d^4x \int_{r_{\text{KK}}}^{\infty} dr \left(\frac{r^3 L}{f(r)} \eta^{\mu\nu} \partial_\mu C_\tau \partial_\nu C_\tau + \frac{r^7}{L^3} \left(\partial_r C_\tau\right)^2 \right), \end{aligned} \tag{10.4}$$

[2] Up to $2\pi k$, where k is an integer. We will work in the $k = 0$ branch.

which directly follows from type IIA supergravity in the Ramond-Ramond sector. By varying this action, we easily find the mode equation[3]

$$\partial_r \left(\frac{r^7}{L^3} \partial_r C_\tau \right) + \frac{r^3 L}{f(r)} M_G^2 C_\tau = 0, \tag{10.5}$$

which is solved by the massless non-normalizable mode

$$C_\tau^{(0)} = \frac{l_s}{2\pi R_4} f(r) \vartheta(x), \tag{10.6}$$

where the prefactor is chosen such that the action evaluated on this solution reads

$$S_{\mathrm{R}} = -\frac{\chi_g}{2} \int d^4x\, \theta^2, \qquad \chi_g = \frac{\lambda^3 M_{\mathrm{KK}}^4}{4(3\pi)^6}, \tag{10.7}$$

and χ_g is the topological susceptibility. In the current case of pure Yang-Mills theory, we have set $\vartheta(x) = \theta$. However, after including flavor fields, this identification will be modified.

The normalizable solutions $C_\tau^{(2)}$, with normalizable boundary conditions $C_\tau^{(2)}(r = \infty) = C_\tau^{(2)}(r = r_{\mathrm{KK}}) = 0$, of the mode equation (10.5) are only available numerically. The obtained spectrum agrees with the one listed in Table 9.2 where the lightest state has a mass of 1789 MeV when using the usual parameter fit.

10.2 Witten-Veneziano Mechanism and the $U(1)_A$ Anomaly

In this section, we will see how the identification of the θ parameter changes after including flavor degrees of freedom in the Witten model. To demonstrate this, we will start with the 9-dimensional CS term

$$S_{\mathrm{CS}} = T_8 \,\mathrm{Tr} \int_{D8} e^{2\pi\alpha' \mathcal{F}_2} \wedge \sum_j C_{2j+1}. \tag{10.8}$$

In the Witten model only the 3-form field $F_4 = dC_3$ is nonzero; it gives rise to the Wess-Zumino-Witten term crucial for almost every preceding chapter. In studying the pseudoscalar glueball fluctuations in C_1 also other terms are relevant.

[3] For pseudoscalar glueball fluctuations it is easier to study 10-dimensional supergravity instead of using the 11-dimensional formulation. Up to an overall factor, this equation of motion is related to the 11-dimensional one in Eq. (9.8) by the substitution $C_\tau(r, x) \to f(r)^{1/2} V_4(r) G(x)$.

We will describe the C_1 field in terms of C_7 by making use of the Hodge duality $dC_7 = F_8 = \star F_2$, to find

$$\begin{aligned} S_{\rm CS} &\supset T_8 2\pi\alpha' \int_{\rm D8} {\rm Tr}\,(\mathcal{F}_2 \wedge C_7) \\ &= T_8 2\pi\alpha' \int {\rm Tr}\,(\mathcal{A}_1) \wedge \star F_2 \wedge \omega_\tau \\ &= T_8 2\pi\alpha' \int dx^{10} \sqrt{|g_{10}|}\,[\delta(\tau) + \delta(\tau-\pi)] \\ &\quad \times \left({\rm Tr}\,(\mathcal{A}_r)\, g^{rr} g^{\tau\tau} \partial_r C_\tau + g^{\mu\nu} g^{\tau\tau} {\rm Tr}\,(\mathcal{A}_\mu)\, \partial_\nu C_\tau\right), \end{aligned} \tag{10.9}$$

where we have defined $\omega_\tau = [\delta(\tau) + \delta(\tau-\pi)]\, d\tau$ to extend the 9-dimensional worldvolume integral of the D8 brane to the entire 10-dimensional bulk spacetime. From this bilinear term, we see that the bulk field C_τ mixes with the Abelian part of the flavor field $\hat{\mathcal{A}} := N_f^{-1} {\rm Tr}\,\mathcal{A}$.

The equations of motion for C_τ get an additional term

$$\begin{aligned} \frac{1}{32\kappa_{10}^2} \partial_r \left(\frac{r^7}{L^3} \partial_r C_\tau \right) &= 2\pi\alpha' T_8 \partial_r \left(\sqrt{-g} g^{rr} g^{\tau\tau}\, {\rm Tr}\,(\mathcal{A}_r) \right) (\delta(\tau) + \delta(\tau-\pi)) \\ &= 2\pi\alpha' T_8 \partial_r \left(\frac{r^7}{2^4 L^3} N_f \hat{\mathcal{A}}_r \right) (\delta(\tau) + \delta(\tau-\pi)), \end{aligned} \tag{10.10}$$

which we solve by an additional localized fluctuation, satisfying

$$\partial_r C_\tau^{(\delta)} = 4\pi\alpha' \kappa_{10}^2 T_8 N_f \hat{\mathcal{A}}_r\, (\delta(\tau) + \delta(\tau-\pi)), \tag{10.11}$$

and $\Box C_\tau^{(\delta)} = 0$.

Similar to the previous section, we can identify the θ parameter by

$$\begin{aligned} \theta &= l_s^{-1} \int_{S_\tau} C_1 = l_s^{-1} \int dr d\tau\, \partial_r (C_\tau^{(0)} + C_\tau^{(\delta)}) \\ &= \vartheta(x) + \frac{2\pi\alpha' 4\kappa_{10}^2 T_8 \sqrt{N_f}}{\sqrt{2} f_\pi l_s} \eta_0(x) = \vartheta(x) + \frac{\sqrt{2N_f}}{f_\pi} \eta_0(x), \end{aligned} \tag{10.12}$$

where now an additional term proportional to η_0 appears.

We are only interested in the $\theta = 0$ case, corresponding to

$$\vartheta(x) = -\frac{\sqrt{2N_f}}{f_\pi} \eta_0(x). \tag{10.13}$$

This is a fundamental result in the realization of the Witten-Veneziano mechanism in the SS model. It states that to have a vanishing θ parameter, the meson field η_0

has to appear in the non-normalizable mode of $C_\tau^{(0)}$. Again evaluating the action on this non-normalizable solution, we get the extra mass term

$$m_0^2 = \frac{2N_f}{f_\pi^2}\chi_g, \tag{10.14}$$

in agreement with the Witten-Veneziano formula [152, 151].

10.3 Pseudoscalar Glueball-Meson Mixing

Using the most general fluctuation $C_\tau = C_\tau^{(0)} + C_\tau^{(\delta)} + C_\tau^{(2)}$, we see that the η_0 meson also mixes with the pseudoscalar glueball $\tilde{G}$. At leading order in N_f/N_c we get the mixed kinetic terms[4]

$$S_{\mathrm{R}}^{(\mathrm{kin.})} = \int d^4x \left(\zeta_1 \partial_\mu \eta_0 \partial^\mu \eta_0 + \zeta_2 \partial_\mu \eta_0 \partial^\mu \tilde{G} - \frac{1}{2}\partial_\mu \tilde{G} \partial^\mu \tilde{G}\right), \tag{10.15}$$

and the effective mass terms

$$S_{\mathrm{R}}^{(\mathrm{mass})} = -\frac{1}{2}m_0^2\eta_0^2 - \frac{1}{2}M_{\tilde{G}}^2\tilde{G}^2. \tag{10.16}$$

The coupling constants are defined by

$$\zeta_1 = -\frac{\pi^3}{12\kappa_{10}^2 M_{\mathrm{KK}}}\int_{r_{\mathrm{KK}}}^\infty dr \frac{r^3 L}{f(r)}\left(C_\tau^{(0)} + 2C_\tau^{(\delta)}\right) C_\tau^{(0)}/\eta_0^2 =: \frac{N_f}{N_c}\bar{\zeta}_1, \tag{10.17}$$

and

$$\begin{aligned}\zeta_2 &= -\frac{\pi^3}{12\kappa_{10}^2 M_{\mathrm{KK}}}\int_{r_{\mathrm{KK}}}^\infty dr \frac{r^3 L}{f(r)}\left(C_\tau^{(0)} + C_\tau^{(\delta)}\right) C_\tau^{(2)}/\left(\eta_0\tilde{G}\right) \\ &\approx 0.011180\sqrt{\frac{N_f}{N_c}}\lambda.\end{aligned} \tag{10.18}$$

The Witten-Veneziano mass of the η_0 meson reads

$$m_0^2 = \frac{\pi V_4}{\kappa_{10}^2 M_{\mathrm{KK}}}\int_{r_{\mathrm{KK}}}^\infty dr \frac{1}{2^4}\frac{r^7}{L^3}\left(\partial_r C_\tau^{(0)}/\eta_0\right)^2 = \frac{\lambda^2 N_f}{27\pi^2 N_c}M_{\mathrm{KK}}^2, \tag{10.19}$$

in agreement with Refs. [11, 12, 154]. An important observation is the scaling behavior $\zeta_2 \propto \sqrt{N_f/N_c}$ and $\zeta_1, m_0^2 \propto N_f/N_c$.

[4] By evaluating the contribution of $(C_\tau^{(\delta)})^2$ we obtain divergent terms proportional to $\delta(0)$ analogous to the calculation of Hořava and Witten [155]. These divergences may presumably be canceled by going beyond the probe approximation and will therefore be dropped in the following.

To diagonalize the action, we perform a non-unitary field redefinition

$$\begin{aligned}\eta_0 &\to (1+\zeta_1)\,\eta_0 + \zeta_2 \tilde{G},\\ \tilde{G} &\to \left(1+\frac{1}{2}\zeta_2^2\right)\tilde{G},\end{aligned} \tag{10.20}$$

resulting in

$$\begin{aligned}\mathcal{L}^{(\text{bilin.})}_{\eta_0,\tilde{G}} &= -\frac{1}{2}(\partial_\mu\eta_0)^2 - \frac{1}{2}(\partial_\mu\tilde{G})^2 - \frac{1}{2}M_G^2(1+\zeta_2^2)\tilde{G}^2 - \frac{1}{2}m_0^2\eta_0^2\\ &\quad + O(N_f^{3/2}/N_c^{3/2}).\end{aligned} \tag{10.21}$$

The mass of the lightest pseudoscalar glueball is therefore changed by

$$\begin{aligned}M_G^2 = (1789.0\,\text{MeV})^2 \quad &\to \quad \left(1+(0.01118\,\lambda)^2 N_f/N_c\right) M_G^2\\ &= (1819.7\ldots 1806.5\,\text{MeV})^2\end{aligned} \tag{10.22}$$

for $\lambda = 16.63\ldots 12.55$.

10.4 Decay Modes

An important feature of the field redefinition (10.20), is that it mixes the η_0 meson with the pseudoscalar glueball $\tilde{G}$. The pseudoscalar glueball therefore inherits all kinds of decays from the η_0 meson. To derive these interactions, it suffices to consider the leading-order transformation

$$\begin{aligned}\eta_0 &\to \eta_0 + \zeta_2\,\tilde{G} = \eta_0 + 0.01118\sqrt{\frac{N_f}{N_c}}\lambda\,\tilde{G},\\ \tilde{G} &\to \tilde{G}.\end{aligned} \tag{10.23}$$

Decay into two vector mesons

The pseudoscalar glueball decay is dominated by the decay channel into two vector mesons which is obtained from the Chern-Simons term and mediated through the η_0 mixing. The interaction reads

$$S^{\text{D8}}_{\text{CS}} \supset k_1 \tilde{G}\epsilon^{\mu\nu\rho\sigma}\text{Tr}\partial_\mu v_\nu \partial_\rho v_\sigma, \tag{10.24}$$

	$\Gamma_p(M_G = 1813 \pm 7\ \text{MeV})$	$\Gamma_p(M_G = 2600\ \text{MeV})$
$\rho\rho$	$36.8 \ldots 45.0$	$190 \ldots 248$
$\omega\omega$	$11.4 \ldots 13.8$	$62 \ldots 81$
$K^*\bar{K}^*$	$2.7 \ldots 1.8$	$189 \ldots 246$
$\phi\phi$	-	$29 \ldots 38$
$a_1 a_1$	-	$3.1 \ldots 4.0$
$\sum_{vv}$	$51 \ldots 61$	$473 \ldots 618$

Table 10.1. – Partial decay widths in MeV for pseudoscalar glueball into two vector mesons, with model parameters $\lambda = 16.63 \ldots 12.55$ and on the left with M_G of Eq. (10.22), and on the right extrapolated to 2600 MeV. Table from Ref. [V].

with the coupling

$$\begin{aligned} k_1 &= \zeta_2 \frac{1}{\sqrt{N_f}} U_{\text{KK}} T_8 \frac{(2\pi\alpha')^3}{2g_s} L^3 \pi^2 \int dZ \phi_0 \psi_1^2 \\ &= 9.8092\, M_{\text{KK}}^{-1} N_c^{-1} \lambda^{-\frac{1}{2}}. \end{aligned} \tag{10.25}$$

After summing over the vector meson polarizations the amplitude squared reads

$$\sum_{\epsilon_1,\epsilon_2} \left| \mathcal{M}(\tilde{G} \to vv) \right|^2 = 8 k_1^2 M^2 \left(\frac{M^2}{4} - m^2 \right). \tag{10.26}$$

The resulting partial decay widths are displayed in Table 10.1. Also presented is an extrapolation of the pseudoscalar glueball mass to the lattice prediction of 2600 MeV, where we have assumed that the relevant coupling parameters ζ_2 scales, like its inverse mass dimension, as M_G^{-1}. Overall, the mixing-induced vertices give bigger contribution than considered in Ref. [72], where the pseudoscalar glueball was found to be a narrow resonance.

Decay into three pseudoscalar mesons

Introducing quark masses to the SS model, one obtains the usual pseudoscalar meson mass term

$$\text{Tr}\,(\mathcal{M}(U + U^\dagger)) \to \text{Tr}\,(\mathcal{M}(U + U^\dagger)) + i\zeta_2 f_\pi^{-1} \sqrt{2/N_f}\, \tilde{G}\, \text{Tr}\,(\mathcal{M}(U - U^\dagger)), \tag{10.27}$$

where the second term gives rise to vertices of the pseudoscalar glueball with $K\bar{K}\pi, K\bar{K}\eta(')$, $\eta(')^3$ and $\eta(')\pi\pi$. Using the mass matrix in the form

$$\mathcal{M} = \text{diag}\left(m_\pi^2,\, m_\pi^2,\, 2m_K^2 - m_\pi^2\right), \tag{10.28}$$

	$\Gamma_p(M_G = 1813 \pm 7\ \text{MeV})$	$\Gamma_p(M_G = 2600\ \text{MeV})$
$K\bar{K}\pi$ (w/o KK^*)	$0.398 \ldots 0.387$	$0.558 \ldots 0.550$
$K\bar{K}\eta$ (w/o $f_0(1710)\eta$ etc.)	$0.0263 \ldots 0.0064$	$0.1092 \ldots 0.0285$
$K\bar{K}\eta'$	-	$0.3303 \ldots 0.3570$
$\pi\pi\eta$	$0.0048 \ldots 0.0061$	$0.0049 \ldots 0.0061$
$\pi\pi\eta'$	$0.0011 \ldots 0.0007$	$0.0021 \ldots 0.0013$
$\eta\eta\eta$	$0.0039 \ldots 0.0007$	$0.0337 \ldots 0.0064$
$\eta\eta\eta'$	-	$0.0564 \ldots 0.0277$
$\eta\eta'\eta'$	-	$0.0047 \ldots 0.0048$
$PP\eta^{(\prime)}$ (w/o $f_0(1710)\eta^{(\prime)}$)	$0.036 \ldots 0.014$	$0.540 \ldots 0.431$
$f_0(1710)\eta^{(\prime)} \to PP\eta^{(\prime)}$ [147]	$0.0068 \ldots 0.015$	$2.5 \ldots 4.3$

Table 10.2. – Partial decay widths in MeV for pseudoscalar glueball decays into three pseudoscalar mesons with $\lambda = 16.63 \ldots 12.55$. Note that these results do not yet include vector-meson resonances like $\tilde{G} \to KK^* \to K\bar{K}\pi$. Table from Ref. [V].

one can easily see that the coupling is directly proportional to the pseudoscalar meson mass and is therefore enhanced, e.g., in $K\bar{K}\pi$ as compared to $\eta(')\pi\pi$. The resulting decay rates are collected in Table 10.2 and the total decay width is visualized in Fig. 10.1.

Decay into a pseudoscalar and one or two vector mesons

The quark mass term further induces a tiny mixing of the pseudoscalar glueball with the η_8 meson, neglected so far. This tiny effect is however the leading-order contribution to decays like

$$\tilde{G} \to KK^*, \pi K^* K^*, KK^*\rho, KK^*\omega, KK^*\phi, \eta(')K^*K^*, \tag{10.29}$$

coming from the commutator terms in the DBI action $\mathrm{Tr}\,(\partial_\mu \Pi, [V^\mu, \Pi])$. The partial decay widths are collected in Table 10.3.

	$\Gamma_p(M_G = 1813 \pm 7\ \text{MeV})$	$\Gamma_p(M_G = 2600\ \text{MeV})$
KK^*	$0.381 \ldots 0.288$	$0.302 \ldots 0.225$
$\pi K^* K^*$	-	$0.0113 \ldots 0.0112$
$KK^*\rho$	-	$(2.50 \ldots 2.47) \times 10^{-3}$
$KK^*\omega$	-	$(0.799 \ldots 0.787) \times 10^{-3}$
$KK^*\phi$	-	$(0.253 \ldots 0.249) \times 10^{-3}$
$\eta K^* K^*$	-	$(0.097 \ldots 0.026) \times 10^{-3}$

Table 10.3. – Partial decay widths in MeV for pseudoscalar glueball decays into one pseudoscalar meson and one or two vector mesons with $\lambda = 16.63 \ldots 12.55$. Table from Ref. [V].

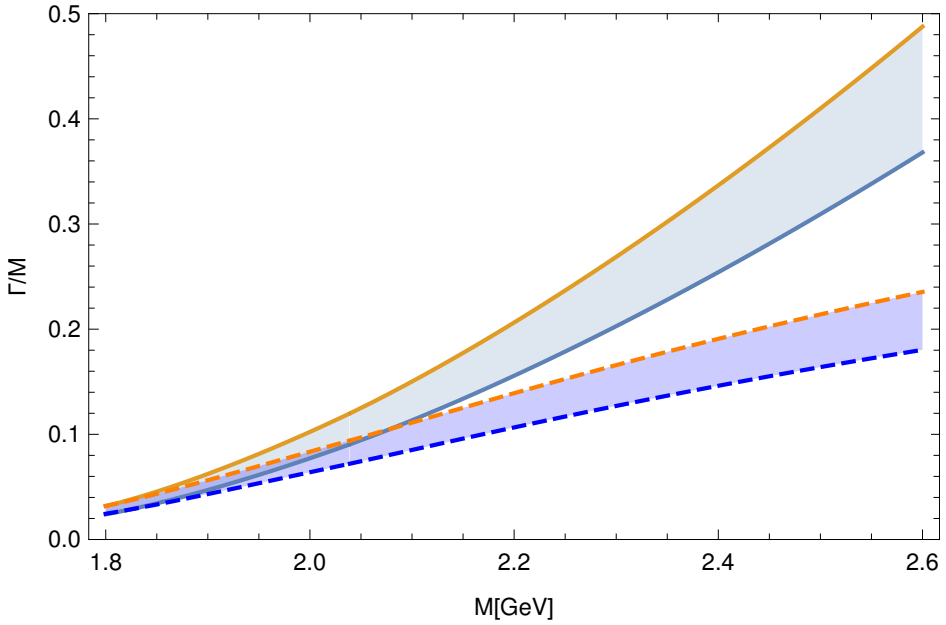

Figure 10.1. – Relative pseudoscalar glueball decay width Γ/M (blue: $\lambda = 16.63$, orange: $\lambda = 12.55$, full line: ζ_2 fixed, dashed line: ζ_2 decreasing like M_{KK}^{-1}). Figure from Ref. [V].

11 Radiative Glueball Decays

> *There is nothing like looking, if you want to find something. You certainly usually find something, if you look, but it is not always quite the something you were after.*
>
> **— J.R.R. Tolkien**
> The Hobbit

An interesting feature of the SS model is that one can naturally combine glueball interaction vertices with VMD to determine the interactions with photons. Particularly interesting are decays into two photons following from the interaction with two vector mesons. This allows us to calculate the TFF of glueballs and to estimate their contribution to $g-2$.

This chapter is organized as follows: First, we will construct radiative interaction terms of the scalar and tensor glueball and calculate the decay widths. Next, we will perform a similar study for the pseudoscalar glueball before estimating the glueball contribution to HLbL.

11.1 Radiative Scalar and Tensor Glueball Decays

Interactions of scalar and tensor glueballs with photons follow straightforwardly, by combining the glueball interactions obtained in Ref. [72] with VMD as discussed in Chapter 4. For simplicity, we will start with the dilatonic glueball G_D and its 2-vector-meson interaction [72]

$$\mathcal{L}_{G_D v^m v^n} = \mathrm{Tr}\left(d_3^{mn}\eta^{\rho\sigma}F^m_{\mu\rho}F^n_{\nu\sigma} + d_2^{mn}M^2_{\mathrm{KK}}v^m_\mu v^n_\nu\right)\left(\eta^{\mu\nu} - \frac{\partial^\mu\partial^\nu}{\Box}\right)G_D, \tag{11.1}$$

where the coupling constants are given by

$$d_2^{mn} = \kappa\int dz\, K\psi'_{2n-1}\psi'_{2m-1}H_D, \qquad d_3^{mn} = \kappa\int dz\, K^{-1/3}\psi_{2n-1}\psi_{2m-1}H_D, \tag{11.2}$$

which for the lightest vector meson take the values

$$d_2^{mm} \approx \{4.3714, ...\} \frac{1}{\lambda^{\frac{1}{2}} N_c M_{\text{KK}}}, \qquad d_3^{mm} \approx \{18.873, ...\} \frac{1}{\lambda^{\frac{1}{2}} N_c M_{\text{KK}}}. \tag{11.3}$$

After applying VMD to one of the two vector mesons to replace it with a photon, we obtain the effective interaction term

$$\mathcal{L}_{G_D \mathcal{V} v^m} = 2 d_3^{m\mathcal{V}} \eta^{\rho\sigma} \text{Tr} \left(F^m_{\mu\rho} F^{\mathcal{V}}_{\nu\sigma} \right) \left(\eta^{\mu\nu} - \frac{\partial^\mu \partial^\nu}{\Box} \right) G_D, \tag{11.4}$$

with the coupling constant

$$d_3^{m\mathcal{V}} \equiv \kappa \int dz \, K^{-1/3} \psi_{2m-1} H_D \approx \{0.468951, ...\} \frac{1}{M_{\text{KK}} \sqrt{N_c}}. \tag{11.5}$$

The other coupling $d_2^{m\mathcal{V}}$ vanishes for on-shell photons since it involves $d\mathcal{J}(0,z)/dz$ with $\mathcal{J}(0,z) \equiv 1$, similar to the holographic realization of the Landau-Yang theorem in Chapter 7.

Replacing also the second vector meson with a photon, we obtain the 2γ-interaction

$$\mathcal{L}_{G_D \mathcal{V}\mathcal{V}} = 2 d_3^{\mathcal{V}\mathcal{V}} \eta^{\rho\sigma} \text{Tr} \left(F^{\mathcal{V}}_{\mu\rho} F^{\mathcal{V}}_{\nu\sigma} \right) \left(\eta^{\mu\nu} - \frac{\partial^\mu \partial^\nu}{\Box} \right) G_D, \tag{11.6}$$

with the coupling constant

$$d_3^{\mathcal{V}\mathcal{V}} \equiv \kappa \int dz \, K^{-1/3} H_D \approx 0.0130195 \lambda^{1/2} M_{\text{KK}}^{-1}. \tag{11.7}$$

A similar derivation for the exotic scalar glueball G_E, where we have five coupling constants instead of the two in Eq. (11.1), is presented in Appendix H.

A comparison of the resulting decay rates for the two holographic scalar glueball modes extrapolated[1] to the two glueball candidate states $f_0(1500)$ and $f_0(1710)$ is presented in Table 11.1.

The interaction vertices for the tensor glueball G_T according to the derivation in Appendix H result in decay rates collected in Table 11.2. For the tensor glueball mass, we follow Ref. [72] in considering the model mass of 1487 MeV, 2000 MeV close to the glueball candidate $f_2(1950)$, and the lattice prediction of 2400 MeV.

[1] To extrapolate the glueball mass, we rescale the mass scale M_{KK} of the theory and the coupling constants according to their scaling with M_{KK}. This rescaling was also used in Ref. [V] and is mostly consistent with Ref. [72] except for the exotic scalar glueball since its coupling constants scale with different powers of M_{KK}.

	M^{exp}[MeV]	Γ_{G_E}[keV]	Γ_{G_D}[keV]
$f_0\,(1500) \to \rho\gamma$	1505	58.3	183
$f_0\,(1500) \to \omega\gamma$	1505	6.62	21.0
$f_0\,(1500) \to \phi\gamma$	1505	2.92	13.7
$f_0\,(1500) \to \gamma\gamma$	1505	$0.306 \ldots 0.231$	$6.97 \ldots 5.26$
$f_0\,(1710) \to \rho\rho$	1722	$(90.5 \ldots 120) \cdot 10^3$	$(55.9 \ldots 74.1) \cdot 10^3$
$f_0\,(1710) \to \omega\omega$	1722	$(28.4 \ldots 37.6) \cdot 10^3$	$(17.4 \ldots 23.0) \cdot 10^3$
$f_0\,(1710) \to \rho\gamma$	1722	99.0	280
$f_0\,(1710) \to \omega\gamma$	1722	11.4	32.3
$f_0\,(1710) \to \phi\gamma$	1722	7.98	29.4
$f_0\,(1710) \to \gamma\gamma$	1722	$0.350 \ldots 0.264$	$7.98 \ldots 6.02$

Table 11.1. – Decay rates of radiative scalar glueball decays for $\lambda = 16.63 \ldots 12.55$.

	Γ_{G_T}[keV] ($M_G = 1487$MeV)	Γ_{G_T}[keV] ($M_G = 2000$MeV)	Γ_{G_T}[keV] ($M_G = 2400$MeV)
$G_T \to \rho\rho$	-	$(270 \ldots 358) \cdot 10^3$	$(382 \ldots 507) \cdot 10^3$
$G_T \to \omega\omega$	-	$(88.2 \ldots 117) \cdot 10^3$	$(127 \ldots 169) \cdot 10^3$
$G_T \to K^*K^*$	-	$(240 \ldots 318) \cdot 10^3$	$(417 \ldots 552) \cdot 10^3$
$G_T \to \phi\phi$	-	-	$(76.7 \ldots 102) \cdot 10^3$
$G_T \to \rho\gamma$	260	522	716
$G_T \to \omega\gamma$	29.9	60.7	83.6
$G_T \to \phi\gamma$	24.0	78.8	123
$G_T \to \gamma\gamma$	$7.35 \ldots 5.55$	$9.89 \ldots 7.46$	$11.9 \ldots 8.95$

Table 11.2. – Decay rates of radiative tensor glueball decays for $\lambda = 16.63 \ldots 12.55$.

In the literature, such as the PDG, one sometimes finds arguments that glueball candidates should have a small 2-photon width somewhere below 1 eV, see also Refs. [156, 157, 135, 145]. For example, the $f_2(2200)$ and the $f_0(1710)$ mesons were ruled out as glueball states due to their large 2γ-coupling by the Belle collaboration in Ref. [158].

The holographic results presented in this chapter, however, indicate the possibility of large 2-photon widths in the keV range for glueballs, which are actually comparable in size to the $\pi^0 \to 2\gamma$ width of roughly 7.7 keV [159]. Additional results and a detailed discussion will be given in Ref. [128].

11.2 Radiative Pseudoscalar Glueball Decays

Couplings of the pseudoscalar glueball to two vector mesons were absent in the considerations of Ref. [147] and only appear through the mixing with the η_0 meson as derived in Ref. [V] and reviewed in Chapter 10.

The coupling was obtained in Eq. (10.24) and reads

$$S_{G_{PS}v^m v^n} = k_1^{v^n v^m} G_{PS} \epsilon^{\mu\nu\rho\sigma} \operatorname{Tr} \partial_\mu v_\nu^m \partial_\rho v_\sigma^n, \tag{11.8}$$

with the coupling constant[2]

$$\begin{aligned} k_1^{v^1 v^1} &\approx 0.00462289 M_{\text{KK}}^{-1} \lambda^{1/2} \int dz K^{-1} \psi_1 \psi_1 \\ &\approx 19.6184 M_{\text{KK}}^{-1} N_c^{-1} \lambda^{-1/2}, \end{aligned} \tag{11.9}$$

where the numerically derived mixing angle appears.

The corresponding photon interactions are obtained by applying VMD resulting in

$$S_{G_{PS}\mathcal{V}v^m} = 2k_1^{\mathcal{V}v^m} G_{PS} \epsilon^{\mu\nu\rho\sigma} \operatorname{Tr} \partial_\mu v_\nu^m \partial_\rho \mathcal{V}_\sigma, \tag{11.10}$$

and

$$S_{G_{PS}\mathcal{V}\mathcal{V}} = 2k_1^{\mathcal{V}\mathcal{V}} G_{PS} \epsilon^{\mu\nu\rho\sigma} \operatorname{Tr} \partial_\mu \mathcal{V}_\nu \partial_\rho \mathcal{V}_\sigma, \tag{11.11}$$

with the coupling constants

$$\begin{aligned} k_1^{\mathcal{V}v^1} &\approx 0.00462289 M_{\text{KK}}^{-1} \lambda^{1/2} \int dz K^{-1} \psi_1 \\ &\approx 0.493557 M_{\text{KK}}^{-1} N_c^{-1/2}, \end{aligned} \tag{11.12}$$

and

$$\begin{aligned} k_1^{\mathcal{V}\mathcal{V}} &\approx 0.00462289 M_{\text{KK}}^{-1} \lambda^{1/2} \int dz K^{-1} \\ &\approx 0.0145232 M_{\text{KK}}^{-1} \lambda^{1/2}. \end{aligned} \tag{11.13}$$

In Table 11.3, we collect the resulting decay widths, which are again in the keV range.

[2] The numerical value differs from Eq. (10.25) due to the different convention of $\operatorname{Tr} T^a T^b$.

	$\Gamma_{G_{PS}}$[keV] ($M_G = 1813 \pm 7$MeV)	$\Gamma_{G_{PS}}$[keV] ($M_G = 2600$MeV)
$G_{PS} \to \rho\rho$	$(36.8 \dots 45.0) \cdot 10^3$	$(190 \dots 248) \cdot 10^3$
$G_{PS} \to \omega\omega$	$(11.3 \dots 13.8) \cdot 10^3$	$(62.2 \dots 81.3) \cdot 10^3$
$G_{PS} \to \phi\phi$	–	$(29.2 \dots 38.1) \cdot 10^3$
$G_{PS} \to K^*K^*$	$(2.69 \dots 1.81) \cdot 10^3$	$(188 \dots 246) \cdot 10^3$
$G_{PS} \to \rho\gamma$	$272 \dots 263$	$536 \dots 528$
$G_{PS} \to \omega\gamma$	$31.5 \dots 30.5$	$62.5 \dots 61.6$
$G_{PS} \to \phi\gamma$	$34.6 \dots 33.2$	$92.7 \dots 91.4$
$G_{PS} \to \gamma\gamma$	$6.98 \dots 5.16$	$9.98 \dots 7.42$

Table 11.3. – Decay rates of radiative pseudoscalar glueball decays for $\lambda = 16.63 \dots 12.55$.

11.3 Contribution to a_μ^{HLbL}

Given the surprisingly large 2γ-decay width of holographic glueballs in the SS model, the question arises whether they may have a larger contribution to a_μ^{HLbL} than expected. As discussed in Part II, the SS model does not do too well in predicting the pion and axial-vector contribution to HLbL, mainly due to its wrong UV-asymptotics. However, compared to the bottom-up models, it has the advantage of a clear implementation of glueballs, which allows us to study their contribution to $g-2$. Since the SS model predicts only rough values for the whole axial sector (25% too small judging from the π_0 contribution), we will only estimate the maximal positive value of the allowed glueball contribution, which, we assume, is given by the pseudoscalar glueball while neglecting the presumably negative contribution from scalar and tensor glueballs.[3]

The pseudoscalar glueball TFF can be easily calculated from the Lagrangian 11.11, and due to the mixing with the η_0 meson is proportional to the pion TFF

$$F_{G_{PS}\gamma\gamma}(Q_1, Q_2) = \frac{4}{3} k_1^{\gamma\gamma} K_{\pi\gamma\gamma}(Q_1, Q_2). \tag{11.14}$$

Using the techniques presented in Chapter 6 we can calculate the contribution[4]

$$a_\mu^{G_{PS}} = 0.155396 \cdot 10^{-11}, \tag{11.15}$$

[3] While a comparison to the contribution of pseudoscalars, and scalar and tensor mesons in the SM prediction, see Table 2.2, indicates an in absolute numbers smaller contribution of scalar and tensor glueballs, the radiative glueball decays calculated in this chapter hint at them having a comparable size.

[4] To calculate the maximal holographic prediction, we use the model mass of 1789 MeV without the NLO mass correction (10.22) and $\lambda = 16.63$.

which is only about 0.2% of the current SM prediction $a_\mu^{\mathrm{HLbL}} = 92(18) \cdot 10^{-11}$. We can therefore conclude that at current precision goals, glueballs can be safely neglected.

12 Conclusion

"What does holographic QCD tell us about the anomalous magnetic moment of the muon?"

THIS was the question posed at the very beginning of this thesis. While there are certainly many more aspects on which holographic QCD can provide valuable insights and that need further research, we were able to shed some light on a few of them. Most importantly, we used holographic QCD to study the hadronic light-by-light scattering contribution to the anomalous magnetic moment of the muon, where we were able to resolve an open question on the implementation of the Melnikov-Vainshtein short-distance constraint.

To study this contribution, we made use of the Sakai-Sugimoto model as well as various bottom-up models. While the former is tightly constrained by its 10-dimensional string-theoretic construction, which actually turned out to be a disadvantage in fitting the UV-asymptotics, the latter allow for more freedom in their construction, which makes them in principle less predictive. We therefore only considered some of the simplest models: one soft-wall and two hard-wall models. One of the hard-wall models turned out to form the first hadronic model where the Melnikov-Vainshtein short-distance constraint can be implemented consistently in the chiral limit.

Since all considered holographic QCD models use some approximations and are not exactly dual to real QCD, one cannot expect that their quantitative predictions are very precise. However, as we have seen, they often lie close to experimental values, which is quite surprising given the simplicity of these models. Without introducing additional free parameters, it is also possible to predict quantities for which there are currently no clear experimental values, such as glueball decay rates, or to predict quantities with relatively large experimental or theoretical uncertainties. One such quantity is the hadronic light-by-light scattering contribution to the anomalous magnetic moment of the muon, where the current error of the Standard Model prediction is roughly 20% and even 100% for the contribution of the axial-vector meson.

To calculate the pseudoscalar and axial-vector meson contribution, one crucial input is the transition form factor, which we have holographically calculated. By comparing its low and high-energy behavior to experimental data and results from perturbative QCD, we found good agreement and in some cases could even do better than other hadronic models. An additional advantage of holographic models is that they contain an infinite tower of excited axial-vector mesons. By summing their contributions to the hadronic light-by-light four-point function, we were able to show that they nicely saturate the Melnikov-Vainshtein short-distance constraint. Since away from the chiral limit it could also be possible to satisfy this constraint with an infinite tower of excited pseudoscalar mesons, we also considered holographic QCD models with quark masses. While we found a certain enhancement of the asymptotic behavior by summing the infinite pseudoscalar tower, it was not enough to contribute at the leading order. The final holographic predictions for $(g-2)_\mu$ agree well with the Standard Model prediction for the pseudoscalar sector, but hint at an extra contribution of roughly 20×10^{-11} in the axial-vector meson sector.

Finally, we performed an estimate of the more exotic glueball contribution. To this end, we considered radiative glueball decays in the Sakai-Sugimoto model and found surprisingly large decay rates in the keV range. This is in stark contrast to the literature, where decay rates above some eV are interpreted as hinting at a large quark admixture. However, even with such large decay rates, we estimated that glueballs will only increase the hadronic light-by-light scattering contribution by 0.2%.

Part V

Appendix

In these appendices, we will collect additional formulas not given explicitly in the main text of this thesis and briefly present the results of Ref. [VII] and [III]. In the first appendix, we will give the effective interaction Lagrangian of the SS model with a definition of the coupling constants. Subsequently, we will state the full expression for the master integral of the pion contribution to HLbL. Third, additional results of the HW models will be presented. In the fourth appendix, we will turn to glueballs and show the relation between 10 and 11-dimensional supergravity. Explicit glueball fluctuations will be given next before presenting the results of Ref. [VII] and [III]. Lastly, we give the photon-glueball couplings of the exotic scalar glueball and the tensor glueball.

A

Meson Couplings in the Sakai-Sugimoto Model

In this appendix, we briefly present the effective 4-dimensional interaction Lagrangian and coupling constants of the SS model, as obtained in Refs. [12].

Let us start with the DBI action (4.9)

$$S_{\rm D8}^{\rm DBI} = \kappa \int d^4x dZ \, {\rm Tr} \left[\frac{1}{2} K^{-1/3} F_{\mu\nu}^2 + K F_{\mu Z}^2 \right] , \tag{A.1}$$

with

$$\kappa \equiv \frac{\lambda N_c}{216\pi^3} , \quad K(Z) \equiv 1 + Z^2 . \tag{A.2}$$

After the field redefinitions (4.36) and (4.37) the first term yields

$$\begin{aligned}
& \kappa \int dZ \, {\rm Tr} \left[\frac{1}{2} K^{-1/3} F_{\mu\nu}^2 \right] \\
= \; & {\rm Tr} \Bigg[\frac{1}{2e^2} \left((F_{\mu\nu}^{A_L})^2 + (F_{\mu\nu}^{A_R})^2 \right) \\
& + \frac{1}{2} (\partial_\mu \widetilde{v}_\nu^n - \partial_\nu \widetilde{v}_\mu^n)^2 + \frac{1}{2} (\partial_\mu \widetilde{a}_\nu^n - \partial_\nu \widetilde{a}_\mu^n)^2 \\
& + (\partial_\mu \widetilde{v}_\nu^n - \partial_\nu \widetilde{v}_\mu^n) ([\widetilde{v}^{p\mu}, \widetilde{v}^{q\nu}] \, g_{v^n v^p v^q} + [\widetilde{a}^{p\mu}, \widetilde{a}^{q\nu}] \, g_{v^n a^p a^q}) \\
& + (\partial_\mu \widetilde{a}_\nu^n - \partial_\nu \widetilde{a}_\mu^n) ([\widetilde{v}^{p\mu}, \widetilde{a}^{q\nu}] - [\widetilde{v}^{q\nu}, \widetilde{a}^{p\mu}]) \, g_{v^p a^n a^q} \\
& + \frac{1}{2} [\widetilde{v}_\mu^m, \widetilde{v}_\nu^n] [\widetilde{v}^{p\mu}, \widetilde{v}^{q\nu}] \, g_{v^m v^n v^p v^q} + \frac{1}{2} [\widetilde{a}_\mu^m, \widetilde{a}_\nu^n] [\widetilde{a}^{p\mu}, \widetilde{a}^{q\nu}] \, g_{a^m a^n a^p a^q} \\
& + ([\widetilde{v}_\mu^m, \widetilde{v}_\nu^n] [\widetilde{a}^{p\mu}, \widetilde{a}^{q\nu}] + [\widetilde{v}_\mu^m, \widetilde{a}_\nu^p] [\widetilde{v}^{n\mu}, \widetilde{a}^{q\nu}] - [\widetilde{v}_\mu^m, \widetilde{a}_\nu^p] [\widetilde{v}^{n\nu}, \widetilde{a}^{q\mu}]) \, g_{v^m v^n a^p a^q} \Bigg] ,
\end{aligned} \tag{A.3}$$

while the second term reads

$$\begin{aligned}
\kappa \int dZ \, {\rm Tr} \left[K F_{Z\nu}^2 \right] \; = \; & {\rm Tr} \Big[m_{v^n}^2 (\widetilde{v}_\mu^n - a_{\mathcal{V}v^n} \mathcal{V}_\mu)^2 + m_{a^n}^2 (\widetilde{a}_\mu^n - a_{\mathcal{A}a^n} \mathcal{A}_\mu)^2 + (i\partial_\mu \Pi + f_\pi \mathcal{A}_\mu)^2 \\
& + 2i g_{a^m v^n \pi} \, \widetilde{a}_\mu^m [\Pi, \widetilde{v}^{n\mu}] - 2 g_{v^n \pi\pi} \, \widetilde{v}_\mu^n [\Pi, \partial^\mu \Pi] \\
& - c_{a^n a^m} [\Pi, \widetilde{a}_\mu^n] [\Pi, \widetilde{a}^{m\mu}] - c_{v^n v^m} [\Pi, \widetilde{v}_\mu^n] [\Pi, \widetilde{v}^{m\mu}] \Big] .
\end{aligned} \tag{A.4}$$

As discussed in Chapter 4 there are no direct couplings to $\mathcal{V}_\mu$ or $\mathcal{A}_\mu$, only mixing terms realizing VMD. The masses

$$m_{v^n}^2 \equiv \lambda_{2n-1} M_{\mathrm{KK}}^2 \,, \quad m_{a^n}^2 \equiv \lambda_{2n} M_{\mathrm{KK}}^2 \,, \tag{A.5}$$

are determined by the eigenvalues of the differential equation (4.13), while the eigenmodes appear in the integrals defining the mixing angles

$$a_{\mathcal{V}v^n} \equiv \kappa \int dz\, K^{-1/3} \psi_{2n-1} \,, \quad a_{\mathcal{A}a^n} \equiv \kappa \int dz\, K^{-1/3} \psi_{2n} \psi_0 \,. \tag{A.6}$$

The normalization of the photon kinetic term

$$e^{-2} \equiv \frac{\kappa}{2} \int dz\, K^{-1/3} \psi_v$$

is divergent and needs some further treatment [12]. However, as we are anyway only interested in the structure of the photon interactions and not the dynamics of the external gauge fields we can simply ignore this issue. The coupling constants are defined by

$$\begin{aligned} g_{v^m \pi\pi} &\equiv \kappa \int dz\, K \phi_0^2 \psi_{2m} \\ &= \frac{1}{\pi} \int dz\, K^{-1} \psi_{2m}, \end{aligned} \tag{A.7}$$

$$\begin{aligned} g_{a^m v^n \pi} &\equiv 2\kappa \int dz\, K \phi_0 \psi_{2m} \partial_z \psi_{2n-1} \\ &= \frac{f_\pi}{M_{\mathrm{KK}}} \int dz\, \psi_{2m} \partial_z \psi_{2n-1} \,, \end{aligned} \tag{A.8}$$

$$\begin{aligned} c_{a^n a^m} &\equiv \kappa \int dz\, K \phi_0^2 \psi_{2n} \psi_{2m} \\ &= \frac{1}{\pi} \int dz\, K^{-1} \psi_{2n} \psi_{2m} \,, \end{aligned} \tag{A.9}$$

$$\begin{aligned} c_{v^n v^m} &\equiv \kappa \int dz\, K \phi_0^2 \psi_{2n-1} \psi_{2m-1} \\ &= \frac{1}{\pi} \int dz\, K^{-1} \psi_{2n-1} \psi_{2m-1} \,, \end{aligned} \tag{A.10}$$

and

$$
\begin{aligned}
g_{v^n v^p v^q} &\equiv \kappa \int dz\, K^{-1/3} \psi_{2n-1}\psi_{2p-1}\psi_{2q-1} \,, \\
g_{v^n a^p a^q} &\equiv \kappa \int dz\, K^{-1/3} \psi_{2n-1}\psi_{2p}\psi_{2q} \,, \\
g_{a^n v^p v^q} &\equiv \kappa \int dz\, K^{-1/3} \psi_{0}\psi_{2n}\psi_{2p-1}\psi_{2q-1} \,, \\
g_{a^n a^p a^q} &\equiv \kappa \int dz\, K^{-1/3} \psi_{0}\psi_{2n}\psi_{2p}\psi_{2q} \,, \\
g_{v^m v^n v^p v^q} &\equiv \kappa \int dz\, K^{-1/3} \psi_{2m-1}\psi_{2n-1}\psi_{2p-1}\psi_{2q-1} \,, \\
g_{a^m a^n a^p a^q} &\equiv \kappa \int dz\, K^{-1/3} \psi_{2m}\psi_{2n}\psi_{2p}\psi_{2q} \,, \\
g_{v^m v^n a^p a^q} &\equiv \kappa \int dz\, K^{-1/3} \psi_{2m-1}\psi_{2n-1}\psi_{2p}\psi_{2q} \,.
\end{aligned}
\tag{A.11}
$$

The CS term containing only the flavor gauge fields reads

$$
S_{\text{D8}}^{\text{CS}} = \frac{N_c}{24\pi^2} \int_{M^4\times\mathbb{R}} \omega_5(A) \,, \tag{A.12}
$$

with the 5-form

$$
\omega_5(A) = \text{Tr}\left(AF^2 - \frac{1}{2}A^3F + \frac{1}{10}A^5 \right) \,. \tag{A.13}
$$

Using the same field redefinitions as for the DBI action, the effective 4-dimensional action reads

$$
\begin{aligned}
S_{\text{D8}}^{\text{CS}} \;=\; & -\frac{N_c}{4\pi^2}\frac{i}{f_\pi} \int_{M^4} \text{Tr}\Big[\Pi\, dB^n dB^m\, c_{nm} \\
& \quad + \Pi\, (dB^m B^n B^p + B^m B^n dB^p)\, c_{mnp} + \Pi\, B^m B^n B^p B^q\, c_{mnpq} \Big] \\
& + \frac{N_c}{24\pi^2} \int_{M^4} \text{Tr}\Big[B^m B^n dB^p\, d_{mn|p} - \frac{3}{2} B^m B^n B^p B^q\, d_{mnp|q} \Big] \,,
\end{aligned}
\tag{A.14}
$$

where the fields are conveniently collected to $B^{2n-1} \equiv \widetilde{v}^n$, $B^{2n} \equiv \widetilde{a}^n$. The coupling constants are defined by

$$
\begin{aligned}
& c_{mn} \equiv \frac{1}{\pi}\int dz\, K^{-1}\psi_m\psi_n \,, \quad c_{mnp} \equiv \frac{1}{\pi}\int dz\, K^{-1}\psi_m\psi_n\psi_p \,, \\
& c_{mnpq} \equiv \frac{1}{\pi}\int dz\, K^{-1}\psi_m\psi_n\psi_p\psi_q \,, \\
& d_{mn|p} \equiv \int dz\, (\psi_n\partial_z\psi_m - \psi_m\partial_z\psi_n)\,\psi_p \,, \quad d_{mnp|q} \equiv \int dz\, \psi_m\psi_n\psi_p\,\partial_z\psi_q \,.
\end{aligned}
\tag{A.15}
$$

The HLbL Master Integral

B

In this appendix, we give additional expressions for the pseudoscalar and axial-vector HLbL master integral as used in Part III, following Refs. [101, 94, 17] and [IV].

B.1 Master Integral for Pseudoscalar Mesons

The kinematic functions in Eq. (6.11) take the explicit form [101]

$$\begin{aligned}\tilde{T}_1(q_1,q_2;p) &= (-64\pi^6)\left[\frac{16}{3}(p\cdot q_1)(p\cdot q_2)(q_1\cdot q_2) - \frac{16}{3}(p\cdot q_2)^2 q_1^2\right.\\ &\quad -\frac{8}{3}(p\cdot q_1)(q_1\cdot q_2)q_2^2 + 8(p\cdot q_2)q_1^2 q_2^2 - \frac{16}{3}(p\cdot q_2)(q_1\cdot q_2)^2\\ &\quad \left.+\frac{16}{3}m_\mu^2 q_1^2 q_2^2 - \frac{16}{3}m_\mu^2(q_1\cdot q_2)^2\right], \qquad \text{(B.1)}\\ \tilde{T}_2(q_1,q_2;p) &= (-64\pi^6)\left[\frac{16}{3}(p\cdot q_1)(p\cdot q_2)(q_1\cdot q_2) - \frac{16}{3}(p\cdot q_1)^2 q_2^2\right.\\ &\quad +\frac{8}{3}(p\cdot q_1)(q_1\cdot q_2)q_2^2 + \frac{8}{3}(p\cdot q_1)q_1^2 q_2^2\\ &\quad \left.+\frac{8}{3}m_\mu^2 q_1^2 q_2^2 - \frac{8}{3}m_\mu^2(q_1\cdot q_2)^2\right]. \qquad \text{(B.2)}\end{aligned}$$

After using the method of Gegenbauer polynomials, the master integrals (6.14) and (6.15) use the weight functions [94, 17]

$$w_1(Q_1,Q_2,\tau) = \left(-\frac{2\pi}{3}\right)\sqrt{1-\tau^2}\,\frac{Q_1^3Q_2^3}{Q_2^2+m_\pi^2}\,I_1(Q_1,Q_2,\tau), \qquad \text{(B.3)}$$

$$w_2(Q_1,Q_2,\tau) = \left(-\frac{2\pi}{3}\right)\sqrt{1-\tau^2}\,\frac{Q_1^3Q_2^3}{(Q_1+Q_2)^2+m_\pi^2}\,I_2(Q_1,Q_2,\tau), \qquad \text{(B.4)}$$

with the functions

$$\begin{aligned} I_1(Q_1,Q_2,\tau) &= X(Q_1,Q_2,\tau)\Big(8\,P_1\,P_2\,(Q_1\cdot Q_2)-2\,P_1\,P_3\,(Q_2^4/m_\mu^2-2\,Q_2^2)\\ &\quad -2\,P_1\,(2-Q_2^2/m_\mu^2+2\,(Q_1\cdot Q_2)\,/m_\mu^2)+4\,P_2\,P_3\,Q_1^2\\ &\quad -4\,P_2-2\,P_3\,(4+Q_1^2/m_\mu^2-2\,Q_2^2/m_\mu^2)+2/m_\mu^2\Big)\\ &\quad -2\,P_1\,P_2\,(1+(1-R_{m1})\,(Q_1\cdot Q_2)\,/m_\mu^2)\\ &\quad +P_1\,P_3\,(2-(1-R_{m1})\,Q_2^2/m_\mu^2)+P_1\,(1-R_{m1})/m_\mu^2\\ &\quad +P_2\,P_3\,(2+(1-R_{m1})^2\,(Q_1\cdot Q_2)\,/m_\mu^2)+3\,P_3\,(1-R_{m1})/m_\mu^2, \end{aligned} \tag{B.5}$$

and

$$\begin{aligned} I_2(Q_1,Q_2,\tau) &= X(Q_1,Q_2,\tau)\Big(4\,P_1\,P_2\,(Q_1\cdot Q_2)+2\,P_1\,P_3\,Q_2^2-2\,P_1+2\,P_2\,P_3\,Q_1^2\\ &\quad -2\,P_2-4P_3-4/m_\mu^2\Big)\\ &\quad -2\,P_1\,P_2-3\,P_1\,(1-R_{m2})/(2m_\mu^2)-3\,P_2\,(1-R_{m1})/(2m_\mu^2)\\ &\quad -P_3\,(2-R_{m1}-R_{m2})/(2m_\mu^2)\\ &\quad +P_1\,P_3\,(2+3\,(1-R_{m2})\,Q_2^2/(2m_\mu^2)+(1-R_{m2})^2\,(Q_1\cdot Q_2)\,/(2m_\mu^2))\\ &\quad +P_2\,P_3\,(2+3\,(1-R_{m1})\,Q_1^2/(2m_\mu^2)+(1-R_{m1})^2\,(Q_1\cdot Q_2)\,/(2m_\mu^2)), \end{aligned} \tag{B.6}$$

where the integration variables

$$Q_3^2 = (Q_1+Q_2)^2 = Q_1^2+2Q_1\cdot Q_2+Q_2^2, \tag{B.7}$$

$$Q_1\cdot Q_2 = Q_1Q_2\tau, \tag{B.8}$$

$$\tau = \cos\theta, \tag{B.9}$$

the photon propagators $P_1^2=1/Q_1^2, P_2^2=1/Q_2^2, P_3^2=1/Q_3^2$ and the definitions

$$X(Q_1,Q_2,\tau) = \frac{1}{Q_1Q_2\,x}\arctan\left(\frac{zx}{1-z\tau}\right), \tag{B.10}$$

$$x = \sqrt{1-\tau^2}, \tag{B.11}$$

$$z = \frac{Q_1Q_2}{4m_\mu^2}\,(1-R_{m1})\,(1-R_{m2})\,, \tag{B.12}$$

$$R_{mi} = \sqrt{1+4m_\mu^2/Q_i^2}, \quad i=1,2, \tag{B.13}$$

were used.

B.2 Master Integral for Axial-Vector Mesons

The master integral for the axial-vector contribution to HLbL takes a similar but more complicated form and was derived independently in Refs. [IV, 61].

As a 3-dimensional integral the master integral may be written as

$$a_\mu^{\mathrm{AV}} = -\frac{2\alpha^3}{3\pi^2}\int_0^\infty dQ_1 dQ_2 \int_{-1}^{+1} d\tau \sqrt{1-\tau^2} Q_1^3 Q_2^3 \left(K_1 + K_2\right), \tag{B.14}$$

with the s-channel integration kernel

$$\begin{aligned}
K_1 =& \frac{A(Q_3^2,0)\left(Q_1^2 A(Q_1^2,Q_2^2)+Q_2^2 A(Q_2^2,Q_1^2)\right)}{2Q_1Q_2Q_3^2 m_\mu^2 M_A^2}\Big[\tau\left(Q_2^2(4\sigma_2^E+\left(\sigma_2^E\right)^2-5)-8m_\mu^2\right)\\
&-4Q_2Q_1\left(-4\left(\tau^2-1\right)Xm_\mu^2+2Q_2^2X-\sigma_1^E-\sigma_2^E+2\right)-8Q_2Q_1^3X+Q_1^2\tau\left(-16Q_2^2X+4\sigma_1^E+\left(\sigma_1^E\right)^2-5\right)\Big]\\
&+\frac{A(Q_1^2,Q_2^2)A(Q_3^2,0)}{2Q_1Q_2^2Q_3^2 m_\mu^2\left(M_A^2+Q_3^2\right)}\Big[Q_2^3Q_1^2\tau\left(-8Q_2^2X+2\sigma_1^E+\left(\sigma_1^E\right)^2-2\sigma_2^E\tau^2+8\sigma_2^E+\left(\sigma_2^E\right)^2\tau^2+\left(\sigma_2^E\right)^2+\tau^2-12\right)\\
&-4m_\mu^2\left(Q_2^3\tau+Q_1^3\left(1-4Q_2^2\tau^2X\right)+Q_2^2Q_1\left(4Q_2^2X+\tau^2\right)-4Q_2Q_1^4\tau X+Q_2Q_1^2\tau\left(4Q_2^2X+3\right)\right)\\
&+2Q_2^4Q_1\left(-2Q_2^2X+\sigma_1^E-\sigma_2^E\tau^2+2\sigma_2^E+\left(\sigma_2^E\right)^2\tau^2-3\right)+2Q_2^2Q_1^3\left(-6Q_2^2X+\sigma_1^E+2\sigma_2^E-3\right)\\
&-4Q_2Q_1^4\tau\left(4Q_2^2X-\sigma_1^E+1\right)+Q_1^5\left(-8Q_2^2X+2\sigma_1^E-2\right)+Q_2^5(\left(\sigma_2^E\right)^2-1)\tau\Big]\\
&+\frac{A(Q_2^2,Q_1^2)A(Q_3^2,0)}{2Q_1^2Q_2Q_3^2 m_\mu^2\left(M_A^2+Q_3^2\right)}\Big[2Q_1^2\left(-2Q_2\tau^2m_\mu^2+Q_2^3\left(8\tau^2Xm_\mu^2+2\sigma_1^E+\sigma_2^E-3\right)-4Q_2^5X\right)-4Q_2Q_1^6X\\
&-2Q_2Q_1^4\left(8Xm_\mu^2+6Q_2^2X+\sigma_1^E\tau^2-2\sigma_1^E-\left(\sigma_1^E\right)^2\tau^2-\sigma_2^E+3\right)\\
&Q_1^3\tau\left(Q_2^2\left(-16Q_2^2X-2\sigma_1^E\left(\tau^2-4\right)+\left(\sigma_1^E\right)^2\left(\tau^2+1\right)+2\sigma_2^E+\left(\sigma_2^E\right)^2+\tau^2-12\right)-4m_\mu^2\left(4Q_2^2X+1\right)\right)\\
&-2Q_2^3\left(2m_\mu^2-Q_2^2(\sigma_2^E-1)\right)+4Q_2^2Q_1\tau\left(m_\mu^2\left(4Q_2^2X-3\right)+Q_2^2(\sigma_2^E-1)\right)-Q_1^5\tau\left(8Q_2^2X-\left(\sigma_1^E\right)^2+1\right)\Big],
\end{aligned} \tag{B.15}$$

and the combined t and u-channel integration kernel,

$$
\begin{aligned}
K_2 = & \frac{A(Q_2^2,0)\left(Q_3^2 A(Q_3^2,Q_1^2)+Q_1^2 A(Q_1^2,Q_3^2)\right)}{Q_1 Q_2 Q_3^2 m_\mu^2 M_A^2}\times \\
& \left(-4\tau m_\mu^2 - 4Q_1Q_2\left(\tau^2-1\right)\left(-4Xm_\mu^2+2Q_2^2X-R_{m1}+1\right)+Q_1^2((R_{m1})^2-1)\tau\right) \\
& + \frac{A(Q_1^2,Q_3^2)A(Q_2^2,0)}{Q_1 Q_2 Q_3^2 m_\mu^2\left(M_A^2+Q_2^2\right)}\Big[2Q_2Q_1^3\left(4Q_2^2\left(\tau^2+1\right)X-4R_{m1}\tau^2+(R_{m1})^2\tau^2-R_{m2}+3\tau^2+1\right) \\
& +Q_2^2Q_1^2\tau(-2R_{m1}+(R_{m1})^2-6R_{m2}-(R_{m2})^2+8)+Q_1^4\tau\left(16Q_2^2X-6R_{m1}+(R_{m1})^2+5\right) \\
& -4m_\mu^2\left(Q_2^2\tau+4Q_2Q_1^3\left(\tau^2+1\right)X+2Q_1^2\tau\left(6Q_2^2X-1\right)+Q_2Q_1\left(4Q_2^2X-1\right)\right) \\
& +2Q_2^3Q_1\left(-2Q_2^2X+R_{m1}-3R_{m2}+2\right)+Q_2^4((R_{m2})^2-1)\tau+4Q_2Q_1^5X\Big] \\
& - \frac{A(Q_2^2,0)A(Q_3^2,Q_1^2)}{Q_1^2 Q_2 Q_3^2 m_\mu^2\left(M_A^2+Q_2^2\right)}\Big[10Q_2^4Q_1(R_{m2}-1)\tau+2Q_2^5(R_{m2}-1)-4Q_2Q_1^6X \\
& +4m_\mu^2\left\{4Q_2Q_1^4\left(\tau^2+1\right)X+2Q_1^3\tau\left(2Q_2^2\left(2\tau^2+3\right)X-1\right)\right. \\
& \qquad \left.+Q_2Q_1^2\left(4Q_2^2\left(3\tau^2+1\right)X-4\tau^2-1\right)+2Q_2^2Q_1\tau\left(2Q_2^2X-1\right)-Q_2^3\right\} \\
& -Q_2^2Q_1^3\tau\left(16Q_2^2\left(\tau^2+1\right)X-2R_{m1}\left(5\tau^2+2\right)+(R_{m1})^2\left(\tau^2+1\right)-10R_{m2}-(R_{m2})^2+9\tau^2+14\right) \\
& -Q_1^5\tau\left(24Q_2^2X-6R_{m1}+(R_{m1})^2+5\right)+2Q_2^3Q_1^2\left(\tau^2\left(-4Q_2^2X+2R_{m1}-9\right)+R_{m2}\left(6\tau^2+2\right)+(R_{m2})^2\tau^2-2\right) \\
& -2Q_2Q_1^4\left(2Q_2^2\left(10\tau^2+1\right)X-8R_{m1}\tau^2+(R_{m1})^2\tau^2-R_{m2}+7\tau^2+1\right)\Big]. \qquad \text{(B.16)}
\end{aligned}
$$

C

Single Mode Contributions to a_μ^{HLbL} from HW Models

In this appendix, we list some data of the single HW modes and their contributions to HLbL as discussed in Chapter 8 and obtained in Ref. [II].

Model	PS	$n=1$	$n=2$	$n=3$
HW1 (chiral)	m_{π_n} [MeV]	$0 \,\text{↱}\, 135$	1899	2887
$M_X^2 = -3$	f_{π_n} [MeV]	92.4*	0	0
	$F_{\pi_n\gamma\gamma}$ [GeV^{-1}]	0.274	−0.202	0.153
	$a_\mu^{\pi_n} \cdot 10^{11}$	65.2	0.7	0.1
HW1m	m_{π_n} [MeV]	135*	1892	2882
$M_X^2 = -3$	f_{π_n} [MeV]	92.4*	1.56	1.25
	$F_{\pi_n\gamma\gamma}$ [GeV^{-1}]	0.276	−0.203	0.154
	$a_\mu^{\pi_n} \cdot 10^{11}$	66.0	0.7	0.1
HW1m'	m_{π_n} [MeV]	135*	1591	2564
$M_X^2 = -3.837$	f_{π_n} [MeV]	92.4*	1.59	0.950
	$F_{\pi_n\gamma\gamma}$ [GeV^{-1}]	0.277	−0.250	0.194
	$a_\mu^{\pi_n} \cdot 10^{11}$	64.3	1.5	0.3
HW3m	m_{π_n} [MeV]	135*	1715	2513
$M_X^2 = -3$	f_{π_n} [MeV]	92.4*	1.56	1.34
	$F_{\pi_n\gamma\gamma}$ [GeV^{-1}]	0.277	−0.196	0.0797
	$a_\mu^{\pi_n} \cdot 10^{11}$	66.6	0.8	0.04
HW3m'	m_{π_n} [MeV]	135*	1300*	2113
$M_X^2 = -3.841$	f_{π_n} [MeV]	92.4*	1.92	1.29
	$F_{\pi_n\gamma\gamma}$ [GeV^{-1}]	0.278	−0.206	0.0474
	$a_\mu^{\pi_n} \cdot 10^{11}$	66.0	1.5	0.01

Table C.1. – Comparison of the various HW model results in the pseudoscalar sector, where * indicates fitted values and ↱ the manual raising of the pion mass in the chiral limit. Table from Ref. [II].

Model	AV	$n=1$	$n=2$	$n=3$	$n=4$	$n=5$
HW1 (chiral)	m_{A_n} [MeV]	1375	2154	2995	3939	4917
$M_X^2=-3$	$F_{\mathrm{A}_n}/m_{\mathrm{A}_n}$ [MeV]	177	204	263	311	351
	$A(0,0)$ [GeV^{-2}]	-21.04	-2.93	0.294	-2.16	0.400
	$a_\mu^{\mathrm{A}_n}\cdot 10^{11}$	31.4	4.7	1.8	1.2	0.5
HW1m	m_{A_n} [MeV]	1367	2141	2987	3934	4914
$M_X^2=-3$	$F_{\mathrm{A}_n}/m_{\mathrm{A}_n}$ [MeV]	175	204	263	311	351
	$A(0,0)$ [GeV^{-2}]	-21.00	-3.21	0.328	-2.16	0.376
	$a_\mu^{\mathrm{A}_n}\cdot 10^{11}$	31.4	4.9	1.8	1.2	0.5
HW1m'	m_{A_n} [MeV]	1230*	1977	2901	3879	4873
$M_X^2=-3.837$	$F_{\mathrm{A}_n}/m_{\mathrm{A}_n}$ [MeV]	148	208	266	312	351
	$A(0,0)$ [GeV^{-2}]	-19.95	-7.29	0.678	-2.18	0.341
	$a_\mu^{\mathrm{A}_n}\cdot 10^{11}$	29.8	8.7	2.0	1.3	0.5
HW3m	m_{A_n} [MeV]	1431	2421	3398	4387	5384
$M_X^2=-3$	$F_{\mathrm{A}_n}/m_{\mathrm{A}_n}$ [MeV]	195	244	291	332	369
	$A(0,0)$ [GeV^{-2}]	-21.27	0.310	-2.09	-0.299	-0.514
	$a_\mu^{\mathrm{A}_n}\cdot 10^{11}$	32.7	3.4	1.7	0.7	0.4
HW3m'	m_{A_n} [MeV]	1380	2355	3345	4345	5350
$M_X^2=-3.841$	$F_{\mathrm{A}_n}/m_{\mathrm{A}_n}$ [MeV]	186	242	291	332	369
	$A(0,0)$ [GeV^{-2}]	-21.29	-0.841	-1.76	-0.440	-0.476
	$a_\mu^{\mathrm{A}_n}\cdot 10^{11}$	33.2	4.1	1.8	0.8	0.4

Table C.2. – Comparison of the various HW model results in the axial-vector sector, where * indicates fitted values. Table from Ref. [II].

D

Reduction of 11-dimensional Supergravity to 10D

In this appendix, we want to present the relation between 10 and 11-dimensional supergravity, as it is crucial for the glueball classification in Chapter 9.

Since we are only interested in the bosonic degrees of freedom, we will drop the fermionic fields and write the 11-dimensional supergravity Lagrangian as [160]

$$\begin{aligned} 2\kappa_{11}^2 \mathcal{L}_{11}^{(b)} &= \sqrt{-g}R - \frac{\sqrt{-g}}{2\cdot 4!} F^{\hat{M}_1\hat{M}_2\hat{M}_3\hat{M}_4} F_{\hat{M}_1\hat{M}_2\hat{M}_3\hat{M}_4} \\ &\quad + \frac{1}{6\cdot 3!\cdot (4!)^2} \epsilon^{\hat{M}_1\ldots\hat{M}_{11}} A_{\hat{M}_1\hat{M}_2\hat{M}_3} F_{\hat{M}_4\ldots\hat{M}_7} F_{\hat{M}_8\ldots\hat{M}_{11}}. \end{aligned} \tag{D.1}$$

As a solution, the Witten model [13] considers the line-element

$$ds^2 = \frac{r^2}{L^2}\left(f(r)dx_4^2 + \eta_{\mu\nu}dx^\mu dx^\mu + dx_{11}^2\right) + \frac{L^2}{r^2}\frac{dr^2}{f(r)} + \frac{L^2}{4}d\Omega_4^2, \tag{D.2}$$

which for $f(r) = 1$ reduces to $AdS_7 \times S^5$, the M5 brane solution [161]. With the blackening factor

$$f(r) = 1 - \frac{r_{\text{KK}}^6}{r^6}, \tag{D.3}$$

the solution describes a doubly Wick-rotated[1] black hole in $AdS_7 \times S^5$.

The equations of motion following from the Lagrangian (D.1)

$$\begin{aligned} \frac{\sqrt{-g}}{2\kappa_{11}^2}\left(R_{\hat{M}\hat{N}} - \frac{1}{2}R\, g_{\hat{M}\hat{N}}\right) = &\frac{\sqrt{-g}}{2\kappa_{11}^2 2\cdot 4!}\Big(4F_{\hat{M}}{}^{\hat{M}_1\hat{M}_2\hat{M}_3} F_{\hat{N}\hat{M}_1\hat{M}_2\hat{M}_3} \\ &- \frac{1}{2}F^{\hat{M}_1\hat{M}_2\hat{M}_3\hat{M}_4} F_{\hat{M}_1\hat{M}_2\hat{M}_3\hat{M}_4}\, g_{\hat{M}\hat{N}}\Big), \end{aligned} \tag{D.4}$$

are not solved by the line-element (D.2) alone, but additionally need the field-strength

$$F_{\alpha\beta\gamma\delta} = \frac{6}{L}\sqrt{g_{S^4}}\epsilon_{\alpha\beta\gamma\delta}, \tag{D.5}$$

proportional to the volume-form of the unit S^4 sphere.

[1] The blackening factor is not in front of the time coordinate, but is moved to the spatial coordinate x_4 by using two Wick rotations.

To get to 10-dimensional supergravity, we use the dimensional reduction

$$x^{11} \simeq x^{11} + 2\pi R_{11}, \quad R_{11} = g_s l_s, \quad l_s^2 = \alpha' \tag{D.6}$$

and rewrite the line-element in the string-frame

$$ds^2 = G_{\hat{M}\hat{N}} dx^{\hat{M}} dx^{\hat{N}} = e^{-2\phi/3} g_{MN} dx^M dx^N + e^{4\phi/3} dx_{11}^2, \tag{D.7}$$

where the M, N indices are 10-dimensional and ϕ is the dilaton, which for the Witten model is given by $e^{\phi} = (r/L)^{3/2}$.

This leads to the type IIA supergravity action

$$S = S_{\mathrm{NS}} + S_{\mathrm{R}} + S_{\mathrm{CS}}, \tag{D.8}$$

where the Neveu-Schwarz, Ramond-Ramond and Chern-Simons term are given by [161]

$$\begin{aligned} S_{\mathrm{NS}} &= \frac{1}{2\kappa_{10}^2} \int d^{10}x \sqrt{-g} e^{-2\phi} \left(R + 4\,\partial_M \phi \partial^M \phi - \frac{1}{2} |dB_2|^2 \right), \\ S_{\mathrm{R}} &= -\frac{1}{4\kappa_{10}^2} \int d^{10}x \sqrt{-g} \left(|F_2|^2 + |F_4|^2 \right), \quad |F_p|^2 = \frac{1}{p!} F_{M\ldots} F^{M\ldots}, \\ S_{\mathrm{CS}} &= -\frac{1}{4\kappa_{10}^2} \int B_2 \wedge F_4 \wedge F_4, \end{aligned} \tag{D.9}$$

with the field identification in Table 9.1 and the coupling constant $2\kappa_{10}^2 = 2\kappa_{11}^2/(2\pi R_{11})$.[2]

[2] As explained in Ref. [V], it is possible to rescale the fields $F_{2,4} \to g_s F_{2,4}$, $e^{-\Phi} \to g_s e^{-\Phi}$ and the coupling constant $\kappa_{10} \to g_s \kappa_{10}$ to obtain the standard D-brane action.

Explicit Glueball Fluctuations

E

In this appendix, let us write out explicitly all glueball fluctuations considered in this thesis and not presented in the main text, i.e., the two scalar and the tensor glueball. The pseudoscalar and pseudovector glueball fluctuations are presented in Chapter 10 and Appendix G, respectively. The vector and L_4 scalar glueball are not considered due to their high masses and not yet calculated decay rates. We follow the notation of Ref. [72].

E.1 Scalar and Tensor Glueball

As can be seen in Table 9.1, the 2^{++} tensor glueball is degenerate with a 0^{++} glueball. The tensor glueball is simply given by transverse traceless polarizations of $\delta G_{\mu\nu}$ such as

$$\delta G_{11} = -\delta G_{22} = -\frac{r^2}{L^2} H_T(r) G_T(x), \tag{E.1}$$

while the scalar is given by the combination

$$\begin{aligned} \delta G_{11,11} &= -3\frac{r^2}{L^2} H_D(r) G_D(x) \\ \delta G_{\mu\nu} &= \frac{r^2}{L^2} H_D(r) \left[\eta_{\mu\nu} - \frac{\partial_\mu \partial_\nu}{\Box}\right] G_D(x). \end{aligned} \tag{E.2}$$

This scalar glueball is often called dilaton glueball, the reason being that it is essentially given by $\delta G_{11,11}$, which upon dimensional reduction becomes the dilaton. Plugging the mode expansion back into the supergravity action

$$S = \frac{1}{2\kappa_{11}^2} (L/2)^4 \Omega_4 \int d^7x \sqrt{-\det G} \left(R(G) + \frac{30}{L^2}\right) \tag{E.3}$$

we obtain the quadratic action[1]

$$\begin{aligned}&\int d^7x\sqrt{-\det G}\left(R(G)+\frac{30}{L^2}\right)\Big|_{H_E^2}\\ =\;& -\mathcal{C}_{D,T}\int dx^{11}\,d^4x\,dx^4\,\frac{1}{2}\left[(\partial_\mu G_{D,T})^2+M_{D,T}^2G_{D,T}^2\right],\end{aligned}\tag{E.4}$$

where $M_D = M_T$ and

$$\mathcal{C}_{D,T}=\int_{r_{\rm KK}}^\infty\frac{dr\,r^3}{L^3}\begin{cases}6H_D(r)^2\\ H_T(r)^2\end{cases}.\tag{E.5}$$

In the derivation we have used partial integration and the mode equations (9.8), with $H_D = H_T = T_4$. Unless stated otherwise, we require the boundary conditions $H'(r_{\rm KK}) = 0$ and $\lim_{r\to\infty} H(r) = 0$. For the lowest eigenmode we obtain

$$\mathcal{C}_T = 0.22547\,[H_T(r_{\rm KK})]^2\frac{r_{\rm KK}^4}{L^3},\tag{E.6}$$

where the overall scale $H_T(r_{\rm KK})$ has to be set by requiring $\mathcal{C}_{D,T}\int dx^{11}\,dx^4 = 1$, leading to

$$[H_{D,T}(r_{\rm KK})]^{-1} = \lambda^{1/2}\,N_c\,M_{\rm KK}\begin{cases}0.033588\\ 0.013712\end{cases}.\tag{E.7}$$

E.2 Exotic Scalar Glueball

The second scalar glueball on the left side of Table 9.1 has the more involved ansatz

$$\begin{aligned}\delta G_{44} &= -\frac{r^2}{L^2}fH_E(r)G_E(x)\\ \delta G_{\mu\nu} &= \frac{r^2}{L^2}H_E(r)\left[\frac{1}{4}\eta_{\mu\nu}-\left(\frac{1}{4}+\frac{3r_{\rm KK}^6}{5r^6-2r_{\rm KK}^6}\right)\frac{\partial_\mu\partial_\nu}{M_E^2}\right]G_E(x),\\ \delta G_{11,11} &= \frac{r^2}{L^2}\frac{1}{4}H_E(r)G_E(x),\\ \delta G_{rr} &= -\frac{L^2}{r^2}f^{-1}\frac{3r_{\rm KK}^6}{5r^6-2r_{\rm KK}^6}H_E(r)G_E(x),\\ \delta G_{r\mu} &= \frac{90\,r^7r_{\rm KK}^6}{M_E^2L^2(5r^6-2r_{\rm KK}^6)^2}H_E(r)\partial_\mu G_E(x),\end{aligned}\tag{E.8}$$

[1] For tensor mesons, this describes only single polarizations. The general form is $\frac{1}{4}T_{\mu\nu}(\Box - M_T^2)T^{\mu\nu}$. Note also that the tensor polarization is normalized to 2 here.

where the dominant contribution δG_{44} has no counterpart in real QCD; this fluctuation is therefore labeled "exotic" scalar glueball [131]. A similar calculation as before with $H_E = S_4$ yields

$$\mathcal{C}_E = \int_{r_{\rm KK}}^{\infty} \frac{dr\, r^3}{L^3} \frac{5}{8} H_E(r)^2, \tag{E.9}$$

where for the lowest eigenmode we obtain

$$\mathcal{C}_E = 0.057395\, [H_E(r_{\rm KK})]^2 \frac{r_{\rm KK}^4}{L^3} \tag{E.10}$$

and

$$[H_E(r_{\rm KK})]^{-1} = 0.0069183\, \lambda^{1/2}\, N_c\, M_{\rm KK}. \tag{E.11}$$

F

Central Exclusive Production of Axial-Vector Mesons

In the main parts of this thesis, we have encountered the important short and long-distance regimes of QCD. In this appendix, we will turn to a soft high-energy scattering process with high center-of-mass energy s but small momentum transfer t, which has contributions from both regimes. A description of many such soft high-energy scattering processes can be given by the Regge model, whose origin is connected to string theory.

As a special example, we want to look at the central exclusive production (CEP) of an f_1 meson in proton-proton scattering

$$p + p \to p + f_1 + p, \tag{F.1}$$

which at high s and low t is mediated by a pomeron $\mathbb{P}$ as depicted in Fig. F.1. As argued in Ref. [III], we treat the pomeron as a rank-2 symmetric tensor, with the lightest particle on its trajectory being the $J^{PC} = 2^{++}$ glueball.

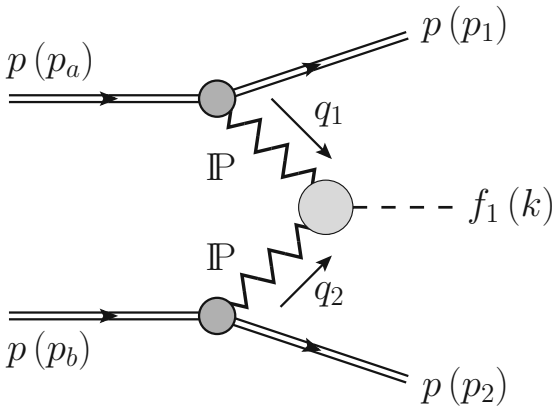

Figure F.1. – CEP of an f_1 meson with double-pomeron exchange [III].

In this appendix, we will briefly present the results obtained in Ref. [III]. First, we will introduce the formalism and the tensor-pomeron approach of Ref. [162] to study CEP. Next, we will construct the crucial pomeron-pomeron-f_1 coupling using either angular-momentum algebra arguments or the holographic Sakai-Sugimoto model. Finally, we will present a comparison of our results with the data points from the WA102 experiment.

F.1 Formalism

In this section, we present the formalism we use to study central exclusive production of f_1 mesons in proton-proton collisions. The process in question is written as

$$p(p_a, \lambda_a) + p(p_b, \lambda_b) \to p(p_1, \lambda_1) + f_1(k, \lambda) + p(p_2, \lambda_2)\,, \tag{F.2}$$

where $p_{a,b}$, $p_{1,2}$ and $\lambda_{a,b}$, $\lambda_{1,2} = \pm\frac{1}{2}$ are the momenta and helicities of the protons, and k and $\lambda = 0, \pm 1$ the corresponding quantities of the f_1 meson. This meson is an axial-vector meson with $J^{PC} = 1^{++}$; we will consider $f_1(1285)$ or $f_1(1420)$.

The main process we are considering is the $\mathbb{PP}$-fusion mechanism, shown at the Born level in Fig. F.1. Other processes, like the $f_{2\mathbb{R}}$ reggeon exchange, which are subdominant in the high-energy limit, are neglected here. The corresponding kinematic variables are

$$\begin{aligned}
&q_1 = p_a - p_1, \quad q_2 = p_b - p_2, \quad k = q_1 + q_2,\\
&t_1 = q_1^2, \quad t_2 = q_2^2, \quad m_{f_1}^2 = k^2,\\
&s = (p_a + p_b)^2 = (p_1 + p_2 + k)^2,\\
&s_1 = (p_a + q_2)^2 = (p_1 + k)^2,\\
&s_2 = (p_b + q_1)^2 = (p_2 + k)^2\,.
\end{aligned} \tag{F.3}$$

The amplitude can be written in the form

$$\begin{aligned}
\mathcal{M}^{(\mathbb{PP}\to f_1)}_{\mu,\,\lambda_a\lambda_b\to\lambda_1\lambda_2 f_1} \;=\; & (-i)\,\bar{u}(p_1,\lambda_1) i\Gamma^{(\mathbb{P}pp)}_{\mu_1\nu_1}(p_1,p_a) u(p_a,\lambda_a)\\
& \times i\Delta^{(\mathbb{P})\,\mu_1\nu_1,\alpha_1\beta_1}(s_1,t_1)\, i\Gamma^{(\mathbb{PP}f_1)}_{\alpha_1\beta_1,\alpha_2\beta_2,\mu}(q_1,q_2)\, i\Delta^{(\mathbb{P})\,\alpha_2\beta_2,\mu_2\nu_2}(s_2,t_2)\\
& \times \bar{u}(p_2,\lambda_2) i\Gamma^{(\mathbb{P}pp)}_{\mu_2\nu_2}(p_2,p_b) u(p_b,\lambda_b)\,,
\end{aligned} \tag{F.4}$$

where $\Delta^{(\mathbb{P})}$ and $\Gamma^{(\mathbb{P}pp)}$ are the effective propagator and proton vertex function for the tensor-pomeron exchange. According to Ref. [162], they are written as

$$\begin{aligned} i\Delta^{(\mathbb{P})}_{\mu\nu,\kappa\lambda}(s,t) &= \frac{1}{4s}\left(g_{\mu\kappa}g_{\nu\lambda}+g_{\mu\lambda}g_{\nu\kappa}-\frac{1}{2}g_{\mu\nu}g_{\kappa\lambda}\right)(-is\alpha'_{\mathbb{P}})^{\alpha_{\mathbb{P}}(t)-1}\,, \\ i\Gamma^{(\mathbb{P}pp)}_{\mu\nu}(p',p) &= -i3\beta_{\mathbb{P}NN}F_1(t)\left\{\frac{1}{2}\left[\gamma_\mu(p'+p)_\nu+\gamma_\nu(p'+p)_\mu\right]-\frac{1}{4}g_{\mu\nu}(\not{p}'+\not{p})\right\}, \end{aligned} \tag{F.5}$$

where $t=(p'-p)^2$, $\beta_{\mathbb{P}NN}=1.87$ GeV^{-1} and $F_1(t)$ is the electromagnetic Dirac form factor of the proton. The pomeron trajectory $\alpha_{\mathbb{P}}(t)$ has the standard linear form

$$\alpha_{\mathbb{P}}(t)=\alpha_{\mathbb{P}}(0)+\alpha'_{\mathbb{P}}\,t\,, \tag{F.6}$$

$$\alpha_{\mathbb{P}}(0)=1.0808\,,\quad \alpha'_{\mathbb{P}}=0.25\ \text{GeV}^{-2}\,. \tag{F.7}$$

All of these quantities are well known from other CEP reactions like

$$p{+}p\to p{+}X{+}p\,,\quad \text{where}\quad X=\eta,\,\eta',\,f_0,\,f_2,\,\pi^+\pi^-,\,4\pi,\,p\bar{p},\,K\bar{K},\,K\bar{K}K\bar{K},\,\rho^0,\,\phi,\,\phi\phi\,, \tag{F.8}$$

studied in Refs. [163, 164, 165]. The main new ingredient in the study of Ref. [III] is the pomeron-pomeron-f_1 vertex $\Gamma^{(\mathbb{P}\mathbb{P}f_1)}$, which will be presented in more detail in the next section. We find two bare couplings Γ' and Γ'', which for realistic applications should be multiplied by a form factor according to

$$i\Gamma^{(\mathbb{P}\mathbb{P}f_1)}_{\kappa\lambda,\rho\sigma,\alpha}(q_1,q_2)=\left(i\Gamma'^{(\mathbb{P}\mathbb{P}f_1)}_{\kappa\lambda,\rho\sigma,\alpha}(q_1,q_2)\,|_{\text{bare}}+i\Gamma''^{(\mathbb{P}\mathbb{P}f_1)}_{\kappa\lambda,\rho\sigma,\alpha}(q_1,q_2)\,|_{\text{bare}}\right)\tilde{F}_{\mathbb{P}\mathbb{P}f_1}(q_1^2,q_2^2,k^2)\,. \tag{F.9}$$

For the form factor we make the factorized ansatz

$$\tilde{F}^{(\mathbb{P}\mathbb{P}f_1)}(q_1^2,q_2^2,k^2)=F_M(q_1^2)F_M(q_2^2)F^{(\mathbb{P}\mathbb{P}f_1)}(k^2)\,, \tag{F.10}$$

where on-shell mesons have $F^{(\mathbb{P}\mathbb{P}f_1)}(m_{f_1}^2)=1$ and we use

$$F_M(t)=\frac{1}{1-t/\Lambda_0^2}\,, \tag{F.11}$$

with $\Lambda_0^2=0.5$ GeV^2 [162, 166]. As an alternative to the factorized ansatz (F.10) we also consider the exponential form

$$\tilde{F}^{(\mathbb{P}\mathbb{P}f_1)}(t_1,t_2,m_{f_1}^2)=\exp\left(\frac{t_1+t_2}{\Lambda_E^2}\right)\,, \tag{F.12}$$

with $k^2=m_{f_1}^2$ and a cutoff constant Λ_E to be fitted to the experimental data.

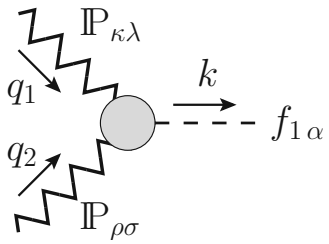

Figure F.2. – Fictitious "real" pomeron coupling to an f_1 meson [III].

To calculate the full amplitude, we also include absorption effects to the Born amplitude in the one-channel-eikonal approach

$$\mathcal{M}_{pp\to ppf_1} = \mathcal{M}^{\text{Born}}_{pp\to ppf_1} + \mathcal{M}^{pp-\text{rescattering}}_{pp\to ppf_1}\,, \tag{F.13}$$

where the second term are "soft" pp-rescattering corrections. The results are presented in Section F.3.

F.2 Pomeron-Pomeron-f_1 Coupling

The strategy used in Refs. [163, 164, 167, 168, 169, 170, 171] to construct pomeron-pomeron-meson couplings is to look at the corresponding couplings of two fictitious "real" pomerons and use the same coupling for CEP. As for an f_1 meson, the fictitious reaction reads

$$\mathbb{P}\,(m,\epsilon_1) + \mathbb{P}\,(m,\epsilon_2) \to f_1\,(m_{f_1},\epsilon)\,, \tag{F.14}$$

where $\mathbb{P}$ are "real pomerons" of mass squared $t > 0$[1], with polarization tensors $\epsilon^{(1)}$ and $\epsilon^{(2)}$, see also Fig. F.2.

Couplings from Angular-Momentum Algebra

As a first approach, we construct the couplings by using elementary angular-momentum algebra [163], where for a given meson we use the orbital angular momentum l and total $\mathbb{PP}$ spin S as guiding principle. According to Ref. [163], the production of a $J^P = 1^+$ meson can have

$$(l,S) = (2,2)\,,\ (4,4)\,, \tag{F.15}$$

[1] In the CEP process (F.2) the two pomerons have invariant masses $t_1 < 0$ and $t_2 < 0$.

and no other values. To construct the coupling, the spin-2 pomeron fields are represented by $\mathbb{P}_{\kappa\lambda}$, while the f_1 vector field U_α is represented by the antisymmetric second-rank tensor field $\partial_\alpha U_\beta - \partial_\beta U_\alpha$. Using some heuristic principles the couplings can be constructed as

$$\begin{aligned}\mathcal{L}^{(2,2)}_{\mathbb{P}\mathbb{P}f_1} &= \frac{g'_{\mathbb{P}\mathbb{P}f_1}}{32M_0^2}\left(\mathbb{P}_{\kappa\lambda}\overset{\leftrightarrow}{\partial}_\mu\overset{\leftrightarrow}{\partial}_\nu\mathbb{P}_{\rho\sigma}\right)\left(\partial_\alpha U_\beta - \partial_\beta U_\alpha\right)\Gamma^{(8)\,\kappa\lambda,\rho\sigma,\mu\nu,\alpha\beta}\,,\\ \mathcal{L}^{(4,4)}_{\mathbb{P}\mathbb{P}f_1} &= \frac{g''_{\mathbb{P}\mathbb{P}f_1}}{24\cdot32\cdot M_0^4}\left(\mathbb{P}_{\kappa\lambda}\overset{\leftrightarrow}{\partial}_{\mu_1}\overset{\leftrightarrow}{\partial}_{\mu_2}\overset{\leftrightarrow}{\partial}_{\mu_3}\overset{\leftrightarrow}{\partial}_{\mu_4}\mathbb{P}_{\rho\sigma}\right)\left(\partial_\alpha U_\beta - \partial_\beta U_\alpha\right)\Gamma^{(10)\,\kappa\lambda,\rho\sigma,\mu_1\mu_2\mu_3\mu_4,\alpha\beta}\,,\end{aligned} \tag{F.16}$$

where the asymmetric derivative $\overset{\leftrightarrow}{\partial}_\mu = \overset{\rightarrow}{\partial}_\mu - \overset{\leftarrow}{\partial}_\mu$ and $M_0 = 1$ GeV are used. The rank 8 and rank 10 tensors $\Gamma^{(8)}$ and $\Gamma^{(10)}$ are combinations of the metric and Levi-Civita symbol, realizing the symmetries of the couplings. Explicitly they read

$$\begin{aligned}\Gamma^{(8)}_{\kappa\lambda,\rho\sigma,\mu\nu,\alpha\beta} \;=\;& g_{\kappa\rho}g_{\mu\sigma}\varepsilon_{\lambda\nu\alpha\beta} + g_{\lambda\rho}g_{\mu\sigma}\varepsilon_{\kappa\nu\alpha\beta} + g_{\kappa\sigma}g_{\mu\rho}\varepsilon_{\lambda\nu\alpha\beta} + g_{\lambda\sigma}g_{\mu\rho}\varepsilon_{\kappa\nu\alpha\beta}\\ &+g_{\kappa\rho}g_{\mu\lambda}\varepsilon_{\sigma\nu\alpha\beta} + g_{\sigma\kappa}g_{\mu\lambda}\varepsilon_{\rho\nu\alpha\beta} + g_{\rho\lambda}g_{\mu\kappa}\varepsilon_{\sigma\nu\alpha\beta} + g_{\sigma\lambda}g_{\mu\kappa}\varepsilon_{\rho\nu\alpha\beta}\\ &-g_{\kappa\lambda}g_{\mu\rho}\varepsilon_{\sigma\nu\alpha\beta} - g_{\kappa\lambda}g_{\mu\sigma}\varepsilon_{\rho\nu\alpha\beta} - g_{\kappa\mu}g_{\rho\sigma}\varepsilon_{\lambda\nu\alpha\beta} - g_{\lambda\mu}g_{\rho\sigma}\varepsilon_{\kappa\nu\alpha\beta}\\ &+(\mu\leftrightarrow\nu)\end{aligned} \tag{F.17}$$

and

$$\begin{aligned}\Gamma^{(10)}_{\kappa\lambda,\rho\sigma,\mu_1\mu_2\mu_3\mu_4,\alpha\beta} \;=\;& \Big\{\Big[\Big(g_{\kappa\mu_1}g_{\lambda\mu_2} - \frac{1}{4}g_{\kappa\lambda}g_{\mu_1\mu_2}\Big)\Big(g_{\rho\mu_3}\varepsilon_{\sigma\mu_4\alpha\beta} - \frac{1}{4}g_{\rho\sigma}\varepsilon_{\mu_3\mu_4\alpha\beta}\Big)\\ &+(\kappa\leftrightarrow\lambda) + (\rho\leftrightarrow\sigma) + (\kappa\leftrightarrow\lambda,\rho\leftrightarrow\sigma)\Big] + (\kappa,\lambda)\leftrightarrow(\rho,\sigma)\Big\}\\ &+ \text{all permutation of } \mu_1,\mu_2,\mu_3,\mu_4\,.\end{aligned} \tag{F.18}$$

Note however that this construction of couplings is not unique.

Couplings from Holographic QCD

As a second approach, we construct the fictitious $\mathbb{P}\mathbb{P}f_1$ couplings in the holographic framework of the Sakai-Sugimoto model [11, 12]. Analogous to the coupling of a singlet pseudoscalar to two tensor glueballs in Ref. [172], we can derive the coupling of a singlet axial-vector meson from the gravitational CS action

$$S_{\text{CS}} \;\supset\; \frac{N_c}{1536\pi^2}\int d^5x\,\epsilon^{MNPQR}\text{Tr}(A_M)R_{NPST}R_{QR}{}^{TS}, \tag{F.19}$$

where R_{NPST} is the induced Riemann tensor on the D8 branes. Using the singlet component of the axial-vector meson $\mathrm{Tr}(A_\mu) = A_\mu^{(0)} = U_\mu(x)\psi(Z)$, we can simplify the action to

$$S_{\mathrm{CS}} \supset \frac{N_c}{384\pi^2}\sqrt{\frac{N_f}{2}}\int d^5x\epsilon^{\mu\nu\rho\sigma}A_\mu^{(0)}R_{Z\nu ST}R_{\rho\sigma}{}^{TS}. \tag{F.20}$$

Evaluating the Riemann tensors to second order in the metric perturbations dual to tensor glueballs and integrating over the radial direction we obtain the coupling Lagrangian

$$\begin{aligned}\mathcal{L}^{\mathrm{CS}} &= \varkappa' U_\alpha \varepsilon^{\alpha\beta\gamma\delta}\mathbb{P}^\mu{}_\beta\,\partial_\delta\mathbb{P}_{\gamma\mu} \\ &\quad + \varkappa'' U_\alpha \varepsilon^{\alpha\beta\gamma\delta}\left(\partial_\nu\mathbb{P}^\mu{}_\beta\right)\left(\partial_\delta\partial_\mu\mathbb{P}^\nu{}_\gamma - \partial_\delta\partial^\nu\mathbb{P}_{\gamma\mu}\right),\end{aligned} \tag{F.21}$$

with the couplings

$$\varkappa' = -\frac{4.872\,\mathcal{N}\sqrt{N_f}}{\sqrt{N_c^3\lambda^3}}, \tag{F.22}$$

$$\varkappa'' = \frac{27.434\,\mathcal{N}\sqrt{N_f}}{M_{\mathrm{KK}}^2\sqrt{N_c^3\lambda^3}}. \tag{F.23}$$

Due to ambiguities in the reggeization of the tensor glueball [172], we leave the normalization constant $\mathcal{N}$ undetermined and consider only the ratio of the two couplings

$$\frac{\varkappa''}{\varkappa'} = -\frac{5.631}{M_{\mathrm{KK}}^2} \tag{F.24}$$

as holographic prediction. As explained in Chapter 4 the parameter M_{KK} is usually fixed by fitting the ρ meson mass, such that $M_{\mathrm{KK}} = 949\,\mathrm{MeV}$. This choice, however, leads to a tensor glueball mass of $M_T \approx 1487\,\mathrm{MeV}$, which is too low compared to the standard pomeron trajectory with $M_T \approx 1917.5\,\mathrm{MeV}$. Lattice gauge theory even predicts $M_T \simeq 2400\,\mathrm{MeV}$ [130]. We therefore consider changing M_{KK} to reproduce the tensor glueball mass as an alternative fit. Respectively these choices lead to $\varkappa''/\varkappa' = -\{6.25, 3.76, 2.44\}\,\mathrm{GeV}^{-2}$.

Comparison of Couplings

To compare the two coupling Lagrangians in Eq. (F.16) and Eq. (F.21), we consider the fusion of two "real" pomerons of mass m in the process

$$\begin{aligned} &\mathbb{P}(q_1, \epsilon^{(1)}) + \mathbb{P}(q_2, \epsilon^{(2)}) \to f_1(k, \epsilon)\,, \\ &q_1 + q_2 = k\,, \quad q_1^2 = q_2^2 = m^2\,. \end{aligned} \tag{F.25}$$

If the two descriptions are equivalent we expect the equivalence relation

$$\mathcal{L}^{\text{CS}} \mathrel{\widehat{=}} \mathcal{L}^{(2,2)} + \mathcal{L}^{(4,4)}. \tag{F.26}$$

After some calculation we indeed find a relation between the coupling parameters

$$\begin{aligned} g'_{\mathbb{P}\mathbb{P}f_1} &= -\varkappa' \frac{M_0^2}{k^2} - \varkappa'' \frac{M_0^2(k^2 - 2m^2)}{2k^2}\,, \\ g''_{\mathbb{P}\mathbb{P}f_1} &= \varkappa'' \frac{2M_0^4}{k^2}\,. \end{aligned} \tag{F.27}$$

Note however that the relation involves the invariant mass squared k^2 of the resonance f_1. Assuming a narrow resonance, we can set $k^2 = m_{f_1}^2 = \text{const.}$ to get a momentum independent linear relation between the couplings $(\varkappa', \varkappa'')$ and $(g'_{\mathbb{P}\mathbb{P}f_1}, g''_{\mathbb{P}\mathbb{P}f_1})$. Otherwise, the relation includes form factors depending on k^2. For small and negative invariant masses of the pomerons $t_{1,2}$, we expect the approximate relation

$$\begin{aligned} g'_{\mathbb{P}\mathbb{P}f_1} &\approx -\varkappa' \frac{M_0^2}{k^2} - \varkappa'' \frac{M_0^2(k^2 - t_1 - t_2)}{2k^2}\,, \\ g''_{\mathbb{P}\mathbb{P}f_1} &\approx \varkappa'' \frac{2M_0^4}{k^2}\,. \end{aligned} \tag{F.28}$$

F.3 Results for the WA102 Experiment

In this section, we present some selected results of Ref. [III] for the $pp \to ppf_1(1285)$ and $pp \to ppf_1(1420)$ reactions, at relatively low c.m. energy $\sqrt{s} = 29.1$ GeV such that we can compare our results to the WA102 experimental data from Ref. [173]. In Ref. [III], we have also performed similar calculations to make predictions for the LHC experiments at $\sqrt{s} = 13$ TeV and the STAR experiment at RHIC at $\sqrt{s} = 200$ GeV [174] and at $\sqrt{s} = 510$ GeV, which however will not be presented here. With a cut

on the meson's Feynman variable $|x_F| \leqslant 0.2$ [2] the WA102 experiment obtains the total cross-sections

$$\begin{aligned} f_1(1285): &\quad \sigma_{\text{exp.}} = (6919 \pm 886)\ \text{nb}\,, \\ f_1(1420): &\quad \sigma_{\text{exp.}} = (1584 \pm 145)\ \text{nb}\,. \end{aligned} \tag{F.29}$$

Furthermore they give distributions in t and ϕ_{pp}, the azimuthal angle between the transverse momentum vectors of the outgoing protons. In Figs. F.3 and F.4 we compare these distributions with different fits of our model parameters. The best fits are found to be

$$\begin{aligned} (l,S) = (2,2)\ \text{term}\quad \text{only}: &\quad g'_{\mathbb{PP}f_1} = 4.89\,,\ g''_{\mathbb{PP}f_1} = 0, \\ (l,S) = (4,4)\ \text{term}\quad \text{only}: &\quad g'_{\mathbb{PP}f_1} = 0\,,\ g''_{\mathbb{PP}f_1} = 10.31, \\ \text{CS}\quad \text{terms}: &\quad \varkappa' = -8.88\,,\ \varkappa''/\varkappa' = -1.0\ \text{GeV}^{-2}\,. \end{aligned} \tag{F.30}$$

For the first two fits it suffices to use either $g'_{\mathbb{PP}f_1}$ or $g''_{\mathbb{PP}f_1}$, while the third fit uses both $\varkappa'$ and $\varkappa''$, where the best-fit ratio $\varkappa''/\varkappa' = -1.0\ \text{GeV}^{-2}$ is outside the estimated ratio $-(6.25\cdots 2.44)\ \text{GeV}^{-2}$. This could indicate that the holographic prediction needs a better understanding of how to reggeize the tensor glueball propagator, as discussed for CEP of η and η' mesons in Ref. [172]. By using the relation (F.28) with $k^2 = m_{f_1}^2 = (1282\ \text{MeV})^2$ and $t_1 = t_2 = -0.1\ \text{GeV}^2$ we find that the third fit corresponds approximately to

$$g'_{\mathbb{PP}f_1} = 0.42\,,\ g''_{\mathbb{PP}f_1} = 10.81\,, \tag{F.31}$$

which agrees closely with the second fit of only fitting $g''_{\mathbb{PP}f_1}$.

[2] This Feynman variable is defined by $x_{F,M} = 2p_{z,M}/\sqrt{s}$, where $p_{z,M}$ is the longitudinal momentum of the outgoing meson in the c.m. frame.

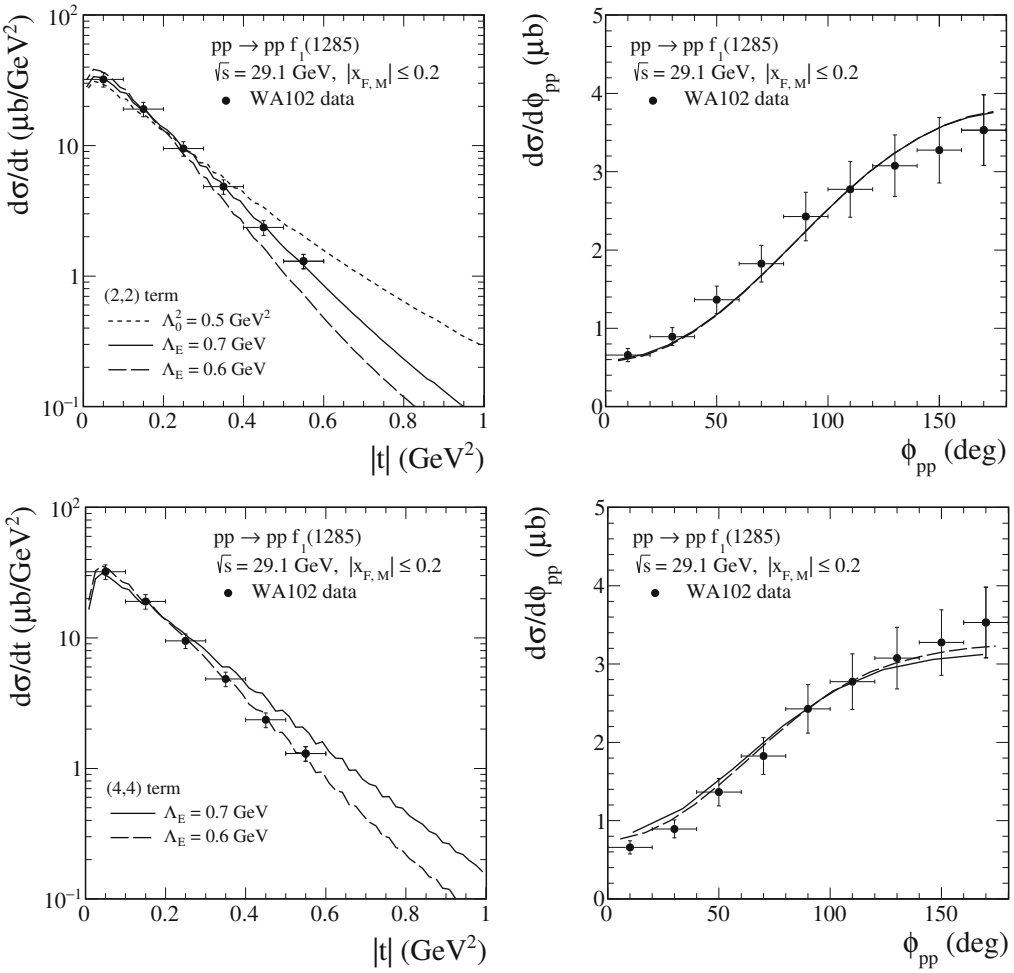

Figure F.3. – Fit to the WA102 data for $|t|$ in the left panels and for ϕ_{pp} in the right panels, normalized to the total cross-section. The upper panels correspond to the fit with only a $(2,2)$ term and $|g'_{\mathbb{PP}f_1}| = 4.89$, while the lower panels correspond to the $(4,4)$ fit with $|g''_{\mathbb{PP}f_1}| = 10.31$. Figures from Ref. [III].

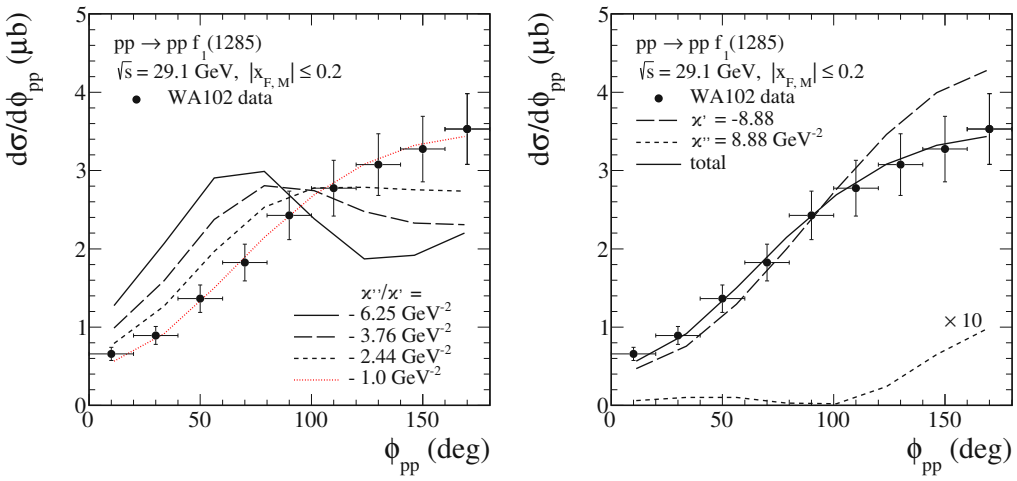

Figure F.4. – Same as Fig. F.3 with $\Lambda_E = 0.7$ GeV, but with different values of $\varkappa''/\varkappa'$. Figures from Ref. [III].

G A Broad Pseudovector Glueball

In Chapter 9, we have discussed the glueball spectrum of the SS model based on the Witten background. By studying the bosonic sector of 11-dimensional supergravity, we obtained towers of glueball states with quantum numbers $J^{PC} = 0^{++}, 2^{++}, 0^{-+}, 1^{+-}, 1^{--}$. In this appendix, we will present the results of Ref. [VII] on decay rates of the 1^{+-} pseudovector glueball. We will start this appendix by introducing the explicit solution of the pseudovector glueball fluctuation. Next, we will construct the dominant interaction vertices contained in the CS term, and we will conclude by presenting predictions for the pseudoscalar glueball decay rates. Finally, the derivation of the negligible vertices from the DBI action will be presented.

G.1 Pseudovector Glueball Fluctuation

As discussed in Ref. [129] and Chapter 9, pseudovector glueballs with quantum numbers 1^{+-} are contained in fluctuations of the three-form field A_3 with one index in the 11th direction. After dimensional reduction, this field reduces to the Kalb-Ramond two-form field B_2 of type IIA string theory, see Table 9.1. The explicit solution of the pseudovector glueball was worked out in Ref. [VII] and reads

$$\begin{aligned} B_{\mu\nu} &= A_{\mu\nu 11} = r^3 N_4(r) \tilde{B}_{\mu\nu}(x^0, \mathbf{x}), \\ & A_{\rho 4 r} = 6 r^2 N_4(r) \epsilon^{\alpha\beta\gamma\delta} \eta_{\rho\alpha} \frac{\partial_\beta}{\Box} \tilde{B}_{\gamma\delta}, \end{aligned} \tag{G.1}$$

where $\tilde{B}_{\mu\nu}$ is antisymmetric and satisfies $\eta^{\rho\mu}\partial_\rho \tilde{B}_{\mu\nu} = 0$. Using this ansatz in the relevant terms of the 11D supergravity action

$$\begin{aligned} 2\kappa_{11}^2 \mathcal{L}_{11}^{(b)} \supset & - \frac{\sqrt{-g}}{2 \cdot 4!} F^{a_1 \ldots a_4} F_{a_1 \ldots a_4} \\ & + \frac{\sqrt{g_{S^4}}}{2 \cdot 4! L} \epsilon^{a_1 \ldots a_7} A_{a_1 \ldots a_3} F_{a_4 \ldots a_7}, \end{aligned} \tag{G.2}$$

where a_i are AdS_7 indices, with the same mode equation as mentioned in Eq. (9.8)

$$\frac{d}{dr}r(r^6 - r_{\rm KK}^6)\frac{d}{dr}N_4(r) - (L^4M^2r^3 - 27r^5 + \frac{9r_{\rm KK}^6}{r})N_4(r) = 0, \tag{G.3}$$

we obtain the mass and kinetic term of the 4-dimensional effective Lagrangian

$$\mathcal{L}_4 = -\frac{1}{4}\mathcal{C}_B\eta^{\rho\mu}\eta^{\sigma\nu}\tilde{B}_{\mu\nu}\left(M^2 - \Box\right)\tilde{B}_{\rho\sigma} + \dots . \tag{G.4}$$

The constant $\mathcal{C}_B$ is defined by an integral over the radial modes

$$\mathcal{C}_B = R_{11}R_4L^7\frac{\pi^4}{3\kappa_{11}^2}\int {\rm d}r\, r^3N_4(r)^2, \tag{G.5}$$

and to get canonically normalized fields, it has to be set to $\mathcal{C}_B = 1$. This fixes the normalization of the radial mode of the ground state with $M \approx 2311$ MeV to

$$[N_4(r_{\rm KK})]^{-1} \approx 0.00983838\, L^3\lambda^{\frac{1}{2}}N_cM_{\rm KK}. \tag{G.6}$$

An alternative form of the action can be derived by expressing the field $\tilde{B}_{\mu\nu}$ as

$$\tilde{B}_{\mu\nu} = \frac{1}{\sqrt{\Box}}\eta^{\lambda\rho}\eta^{\kappa\sigma}\epsilon_{\mu\nu\lambda\kappa}\,\varepsilon_\rho\partial_\sigma G_{PV}^{(\varepsilon)}(x), \tag{G.7}$$

where ε_ρ is a polarization vector. The glueball field $G_{PV}^{(\varepsilon)}(x)$ is then canonically normalized with $\mathcal{L}_4 = -\frac{1}{2}G_{PV}^{(\varepsilon)}\left(M^2 - \Box\right)G_{PV}^{(\varepsilon)} + \dots$.

G.2 Dominant Decays from the CS Term

To calculate interactions of the pseudovector glueball with quark-antiquark states in the SS model, we have to induce the background Kalb-Ramond fluctuation to the D8-$\overline{\rm D8}$-brane system described by the DBI and CS action. The dominant decays follow from the CS action [175]

$$S_{\rm CS} = T_8\ {\rm Tr}\int_{D8} e^{\mathcal{F}_2}\wedge\sum_j C_{2j+1}, \tag{G.8}$$

where the field $\mathcal{F}_{MN} \equiv 2\pi\alpha' F_{MN} + B_{MN}$ contains the $U(N_f)$ field strength F_{MN} and the Kalb-Ramond field B_{MN}. Using the non-vanishing C_3 field and integrating over the S^4 sphere, we obtain the relevant 5-dimensional action

$$S_{\rm CS}^{(B_2)} = \frac{1}{2}(2\pi\alpha')^2\ T_8\ L^3\pi^2g_s^{-1}{\rm Tr}\int A_1\wedge F_2\wedge B_2. \tag{G.9}$$

Inserting the pseudovector fluctuation (G.1), we obtain the interaction terms

$$\begin{aligned}\mathcal{L}^{\rm CS}_{4,\rm int} \supset\ & b_1(\Pi^a\partial_\mu\widetilde{v}^a_\mu + \widetilde{v}^a_\mu\partial_\nu\Pi^a)\,{}^\star\tilde{B}^{\mu\nu} \\ & -ib_2\,\mathrm{Tr}(T^a[T^b,T^c])\,\Pi^a\widetilde{v}^b_\mu\widetilde{v}^c_\nu\,{}^\star\tilde{B}^{\mu\nu},\end{aligned} \tag{G.10}$$

where we use ${}^\star\tilde{B}^{\mu\nu} \equiv \frac{1}{2}\epsilon^{\mu\nu\rho\sigma}\tilde{B}_{\rho\sigma}$ and the $U(N_f)$ fields as introduced in Chapter 4: the pseudoscalar mode Π and the lowest vector meson mode $\widetilde{v}_\mu \equiv \widetilde{v}^1_\mu$. The coupling constants are defined by[1]

$$b_1 \equiv 4C\int r^3\phi_0\psi_1 N_4 dZ = 56.027\,N_c^{-1}\lambda^{-\frac{1}{2}}, \tag{G.11}$$

and

$$b_2 \equiv 6C\int r^3\phi_0\psi_1^2 N_4 dZ = 2571.72\,N_c^{-\frac{3}{2}}\lambda^{-1}, \tag{G.12}$$

with $C = T_8(2\pi l_s^2 r_{\rm KK}L\pi)^2/(16g_s)$. The interaction terms from the DBI action are derived in the next section, where we also show that they are negligible compared to the CS interaction terms.

To calculate decay rates into physical mesons, we use the relation

$$\begin{aligned}\eta &= \eta_8\cos\theta_P - \eta_0\sin\theta_P \\ \eta' &= \eta_8\sin\theta_P + \eta_0\cos\theta_P,\end{aligned} \tag{G.13}$$

with the mixing angle [144]

$$\theta_P = \frac{1}{2}\arctan\frac{2\sqrt{2}}{1-\frac{3}{2}m_0^2/(m_K^2-m_\pi^2)}, \tag{G.14}$$

obtained by considering bare quark masses (realized in the SS model via world-sheet instantons [176, 177, 178]) and the Witten-Veneziano mass m_0. The Witten-Veneziano mass in the SS model is discussed in more detail in Chapter 10, and reads [11]

$$m_0^2 = \frac{N_f}{27\pi^2 N_c}\lambda^2 M_{\rm KK}^2. \tag{G.15}$$

For the vector mesons ω and ϕ, we assume ideal mixing $\theta_V = \arctan(1/\sqrt{2})$ [179]. The resulting 2 and 3-body decay rates are summarized in Table G.1. Combining the results, we conclude that the pseudovector glueball is a very broad state with $\Gamma/M \approx 1$. This suggests that it will be very difficult to experimentally identify this state.

[1] In this appendix, we follow Refs. [VII, 72] in using the convention $\mathrm{Tr}\,T^aT^b = \delta^{ab}$.

decay channel	Γ/M
$\pi\rho$	$0.3624\ldots0.4803$
KK^*	$0.1945\ldots0.2578$
$\eta\omega$	$0.0530\ldots0.0941$
$\eta\phi$	$0.0086\ldots0.0076$
$\eta'\omega$	$0.0168\ldots0.0203$
$\eta'\phi$	$0.0020\ldots0.0079$
$\pi\rho\rho$	$0.2595\ldots0.4556$
πK^*K^*	$0.0213\ldots0.0375$
$KK^*\rho$	$0.0032\ldots0.0056$
$KK^*\omega$	$0.0011\ldots0.0019$
total	$0.9225\ldots1.3685$

Table G.1. – Predictions for the pseudoscalar glueball decay rates into pseudoscalar and vector mesons using $\lambda = 16.63\ldots12.55$. Table from Ref. [VII].

G.3 Subleading Pseudovector Glueball Decays from the DBI Action

In this section, we consider pseudovector glueball decays from the DBI action, and show that the resulting couplings are subleading and can be neglected. We start by expanding the square root of the DBI action as

$$\begin{aligned} S_{\text{DBI}} =& -T_8 \int d^9x e^{-\phi}\, \text{STr}\, \sqrt{-\det\left(g_{MN}+\mathcal{F}_{MN}\right)} \\ =& -T_8 \int d^9x e^{-\phi} \sqrt{-g}\, \text{STr}\left[1+\frac{1}{2}\text{tr}\Big(-\frac{1}{2}\left(g^{-1}\mathcal{F}\right)^2\right. \\ &+\frac{1}{3}\left(g^{-1}\mathcal{F}\right)^3-\frac{1}{4}\left(g^{-1}\mathcal{F}\right)^4\Big) \\ &\left.+\frac{1}{32}\text{tr}\left(\left(g^{-1}\mathcal{F}\right)^2\right)^2\right]+\mathcal{O}\left(\mathcal{F}^5\right). \end{aligned} \tag{G.16}$$

After a similar calculation as was performed for the CS term, we obtain the interaction terms

$$\begin{aligned} \mathcal{L}^{\text{DBI}}_{4,\text{int}} \supset\ & \bar{b}_1 F^{\nu\rho}F_{\rho\sigma}F^{\sigma\mu}\tilde{B}_{\mu\nu}+\bar{b}_2 F^{\rho\sigma}F_{\rho\sigma}F^{\mu\nu}\tilde{B}_{\mu\nu} \\ & \bar{b}_3\partial^\rho\Pi\partial_\rho\Pi F^{\mu\nu}\tilde{B}_{\mu\nu}+\bar{b}_4 V^\rho\partial_\rho\Pi F^{\mu\nu}\tilde{B}_{\mu\nu} \\ & +\bar{b}_5 V^\rho V_\rho F^{\mu\nu}\tilde{B}_{\mu\nu}, \end{aligned} \tag{G.17}$$

with coupling constants

$$\begin{aligned}
\bar{b}_1 &= 36D \int dZ K^{-\frac{5}{6}} \psi_1^3 N_4 \\
&= 0.0000375351\, N_c^{-\frac{3}{2}} \lambda^{-2}, \\
\bar{b}_2 &= -\bar{b}_1/4, \\
\bar{b}_3 &= -\frac{D}{18} M_{\text{KK}}^6 L^6 \int dZ K^{\frac{1}{2}} N_4 \phi_0^2 \psi_1 \\
&= -0.0000168453\, N_c^{-\frac{3}{2}} \lambda^{-2}, \\
\bar{b}_4 &= 2D M_{\text{KK}}^4 L^3 \int dZ K^{\frac{1}{2}} N_4 \phi_0 \partial_Z \psi_1 \\
&= -0.00875721\, N_c^{-\frac{3}{2}} \lambda^{-2}, \\
\bar{b}_5 &= -18 D M_{\text{KK}}^2 \int dZ K^{\frac{1}{2}} N_4 \psi_1 \left(\partial_Z \psi_1\right)^2 \\
&= -1.78464\, N_c^{-\frac{3}{2}} \lambda^{-2},
\end{aligned} \tag{G.18}$$

where $D = L^3 N_c/(576 M_{\text{KK}}^2 \pi^2)$. All the obtained interactions contain three $U(N_f)$ fields and one pseudovector glueball. Comparing the coupling constants to the coupling b_2 in Eq. (G.12), we see that the contributions from the DBI action are suppressed by an additional factor of λ^{-1} as well as by their numerical value.

Photon-Glueball Interactions

H

In this appendix, we collect the interaction terms of the exotic scalar and the tensor glueball with up to two vector mesons and the corresponding photon interactions following from VMD.

H.1 Exotic Scalar Glueball

Following Ref. [72], the exotic scalar glueball G_E has the 2-vector-meson interaction terms

$$\begin{aligned}\mathcal{L}_{G_E v^m v^n} &= -\mathrm{Tr}\left\{ c_2^{mn} M_{\mathrm{KK}}^2 \left[v_\mu^m v_\nu^n \frac{\partial^\mu \partial^\nu}{M_E^2} G_E + \frac{1}{2} v_\mu^m v^{n\mu} \left(1 - \frac{\Box}{M_E^2}\right) G_E \right] \right. \\ &\quad + c_3^{mn} \left[\eta^{\rho\sigma} F_{\mu\rho}^m F_{\nu\sigma}^n \frac{\partial^\mu \partial^\nu}{M_E^2} G_E - \frac{1}{4} F_{\mu\nu}^m F^{n\mu\nu} \left(1 + \frac{\Box}{M_E^2}\right) G_E \right] + \\ &\quad + c_4^{mn} \frac{3}{M_E^2} v_\mu^n F^{m\mu\nu} \partial_\nu G_E \\ &\quad \left. + \breve{c}_2^{mn} M_{\mathrm{KK}}^2 v_\mu^m v^{n\mu} G_E + \frac{1}{2} \breve{c}_3^{mn} F_{\mu\nu}^m F^{n\mu\nu} G_E \right\}, \end{aligned} \tag{H.1}$$

with the five coupling constants

$$\begin{aligned} c_2^{mn} &= \kappa \int dz K \psi'_{2m-1} \psi'_{2n-1} \overline{H}_E, \\ c_3^{mn} &= \kappa \int dz K^{-1/3} \psi_{2m-1} \psi_{2n-1} \overline{H}_E \\ c_4^{mn} &= \kappa M_{\mathrm{KK}}^2 \int dz \, \frac{20 z K}{(5K-2)^2} \psi_{2m-1} \psi'_{2n-1} H_E, \\ \breve{c}_2^{mn} &= \frac{\kappa}{4} \int dz K \psi'_{2m-1} \psi'_{2n-1} H_E \\ \breve{c}_3^{mn} &= \frac{\kappa}{4} \int dz K^{-1/3} \psi_{2m-1} \psi_{2n-1} H_E, \end{aligned} \tag{H.2}$$

where we have defined

$$\overline{H}_E = \left[\frac{1}{4} + \frac{3}{5K-2} \right] H_E. \tag{H.3}$$

Applying VMD once, only three coupling constants survive, and we get

$$\begin{aligned}\mathcal{L}_{G_E\mathcal{V}v^m} &= -\mathrm{Tr}\left\{c_3^{m\mathcal{V}}\left[2\eta^{\rho\sigma}F^m_{\mu\rho}F^{\mathcal{V}}_{\nu\sigma}\frac{\partial^\mu\partial^\nu}{M_E^2}G_E-\frac{1}{2}F^m_{\mu\nu}F^{\mathcal{V}\mu\nu}\left(1+\frac{\Box}{M_E^2}\right)G_E\right]\right.\\ &\left.+c_4^{\mathcal{V}n}\frac{3}{M_E^2}v^n_\mu F^{\mathcal{V}\mu\nu}\partial_\nu G_E+\breve{c}_3^{m\mathcal{V}}F^m_{\mu\nu}F^{\mathcal{V}\mu\nu}G_E\right\},\end{aligned} \tag{H.4}$$

with the couplings

$$\begin{aligned}c_3^{m\mathcal{V}} &= \kappa\int dzK^{-1/3}\psi_{2m-1}\overline{H}_E=\{1.551,...\}\frac{1}{M_{\mathrm{KK}}N_c^{\frac{1}{2}}},\\ c_4^{\mathcal{V}m} &= \kappa M_{\mathrm{KK}}^2\int dz\,\frac{20ZK}{(5K-2)^2}\psi'_{2m-1}H_E=\{-0.262,...\}\frac{M_{\mathrm{KK}}}{N_c^{\frac{1}{2}}},\\ \breve{c}_3^{m\mathcal{V}} &= \frac{\kappa}{4}\int dzK^{-1/3}\psi_{2m-1}H_E=\{0.425,...\}\frac{1}{M_{\mathrm{KK}}N_c^{\frac{1}{2}}}.\end{aligned} \tag{H.5}$$

The 2-photon interaction reads

$$\begin{aligned}\mathcal{L}_{G_E\mathcal{V}\mathcal{V}} &= -\mathrm{Tr}\left\{c_3^{\mathcal{V}\mathcal{V}}\left[2F^{\mathcal{V}}_{\mu\rho}F^{\mathcal{V}\rho}_{\nu}\frac{\partial^\mu\partial^\nu}{M_E^2}G_E-\frac{1}{2}F^{\mathcal{V}}_{\mu\nu}F^{\mathcal{V}\mu\nu}\left(1+\frac{\Box}{M_E^2}\right)G_E\right]\right.\\ &\left.+\breve{c}_3^{\mathcal{V}\mathcal{V}}F^{\mathcal{V}}_{\mu\nu}F^{\mathcal{V}\mu\nu}G_E\right\},\end{aligned} \tag{H.6}$$

where the two coupling constants are defined by

$$c_3^{\mathcal{V}\mathcal{V}}=\kappa\int dzK^{-1/3}\overline{H}_E=\frac{237.587\kappa}{M_{\mathrm{KK}}N_c\lambda^{1/2}}=0.0355\frac{\lambda^{\frac{1}{2}}}{M_{\mathrm{KK}}}, \tag{H.7}$$

and

$$\breve{c}_3^{\mathcal{V}\mathcal{V}}=\frac{\kappa}{4}\int dzK^{-1/3}H_E=\frac{71.18\kappa}{M_{\mathrm{KK}}N_c\lambda^{1/2}}=0.0106\frac{\lambda^{\frac{1}{2}}}{M_{\mathrm{KK}}}. \tag{H.8}$$

H.2 Tensor Glueball

For the tensor glueball, we start with the interaction [72]

$$\mathcal{L}_{G_Tv^mv^n}=\mathrm{Tr}\left[t_2^{mn}M_{\mathrm{KK}}^2v^m_\mu v^n_\nu G_T^{\mu\nu}+t_3^{mn}F^m_{\mu\rho}F^{n\rho}_{\nu}G_T^{\mu\nu}\right], \tag{H.9}$$

where the coupling constants

$$t_2^{mn}=\int dzK\psi'_{2m-1}\psi'_{2n-1}H_T=2\sqrt{3}d_2^{mn}, \tag{H.10}$$

and

$$t_3^{mn} = \int dz K^{-1/3} \psi_{2m-1} \psi_{2n-1} H_T = 2\sqrt{3} d_3^{mn}, \tag{H.11}$$

are related to the couplings of the dilaton scalar glueball.

The photon interactions are given by

$$\mathcal{L}_{G_T v^n \mathcal{V}} = 2 t_3^{\mathcal{V}n} G_T^{\mu\nu} \mathrm{Tr} \left(F_{\mu\rho}^{\mathcal{V}} F_{\nu}^{n\rho} \right), \tag{H.12}$$

and

$$\mathcal{L}_{G_T \mathcal{V}\mathcal{V}} = 2 t_3^{\mathcal{V}\mathcal{V}} G_T^{\mu\nu} \mathrm{Tr} \left(F_{\mu\rho}^{\mathcal{V}} F_{\nu}^{\mathcal{V}\rho} \right), \tag{H.13}$$

with the coupling constants

$$t_3^{\mathcal{V}n} = \int dz K^{-1/3} \psi_{2n-1} H_T = 2\sqrt{3} d_3^{\mathcal{V}n}, \tag{H.14}$$

and

$$t_3^{\mathcal{V}\mathcal{V}} = \int dz K^{-1/3} H_T = 2\sqrt{3} d_3^{\mathcal{V}\mathcal{V}}. \tag{H.15}$$

Bibliography

[1] MUON G-2 collaboration, G. W. Bennett et al., *Final Report of the Muon E821 Anomalous Magnetic Moment Measurement at BNL*, *Phys. Rev. D* **73** (2006) 072003, [hep-ex/0602035].

[2] T. Aoyama et al., *The anomalous magnetic moment of the muon in the Standard Model*, *Phys. Rept.* **887** (2020) 1–166, [2006.04822].

[3] MUON G-2 collaboration, B. Abi et al., *Measurement of the Positive Muon Anomalous Magnetic Moment to 0.46 ppm*, *Phys. Rev. Lett.* **126** (2021) 141801, [2104.03281].

[4] M. Abe et al., *A New Approach for Measuring the Muon Anomalous Magnetic Moment and Electric Dipole Moment*, *PTEP* **2019** (2019) 053C02, [1901.03047].

[5] S. Borsanyi et al., *Leading hadronic contribution to the muon magnetic moment from lattice QCD*, *Nature* **593** (2021) 51–55, [2002.12347].

[6] A. Crivellin, M. Hoferichter, C. A. Manzari and M. Montull, *Hadronic Vacuum Polarization: $(g-2)_\mu$ versus Global Electroweak Fits*, *Phys. Rev. Lett.* **125** (2020) 091801, [2003.04886].

[7] A. Keshavarzi, W. J. Marciano, M. Passera and A. Sirlin, *Muon $g-2$ and $\Delta\alpha$ connection*, *Phys. Rev. D* **102** (2020) 033002, [2006.12666].

[8] B. Malaescu and M. Schott, *Impact of correlations between a_μ and α_{QED} on the EW fit*, *Eur. Phys. J. C* **81** (2021) 46, [2008.08107].

[9] G. Colangelo, M. Hoferichter and P. Stoffer, *Constraints on the two-pion contribution to hadronic vacuum polarization*, *Phys. Lett. B* **814** (2021) 136073, [2010.07943].

[10] J. M. Maldacena, *The Large N limit of superconformal field theories and supergravity*, *Int.J.Theor.Phys.* **38** (1999) 1113–1133, [hep-th/9711200].

[11] T. Sakai and S. Sugimoto, *Low energy hadron physics in holographic QCD*, *Prog.Theor.Phys.* **113** (2005) 843–882, [hep-th/0412141].

[12] T. Sakai and S. Sugimoto, *More on a holographic dual of QCD*, *Prog.Theor.Phys.* **114** (2005) 1083–1118, [hep-th/0507073].

[13] E. Witten, *Anti-de Sitter space, thermal phase transition, and confinement in gauge theories*, *Adv.Theor.Math.Phys.* **2** (1998) 505–532, [hep-th/9803131].

[14] J. Erlich, E. Katz, D. T. Son and M. A. Stephanov, *QCD and a holographic model of hadrons*, *Phys. Rev. Lett.* **95** (2005) 261602, [hep-ph/0501128].

[15] J. Hirn and V. Sanz, *Interpolating between low and high energy QCD via a 5-D Yang-Mills model*, *JHEP* **12** (2005) 030, [hep-ph/0507049].

[16] A. Karch, E. Katz, D. T. Son and M. A. Stephanov, *Linear confinement and AdS/QCD*, *Phys. Rev.* **D74** (2006) 015005, [hep-ph/0602229].

[17] F. Jegerlehner and A. Nyffeler, *The Muon $g-2$*, *Phys. Rept.* **477** (2009) 1–110, [0902.3360].

[18] D. Galbraith and C. Burgard., "Standard Model Diagram." http://davidgalbraith.org/portfolio/ux-standard-model-of-the-standard-model/, 2012.

[19] D. Hanneke, S. Fogwell and G. Gabrielse, *New measurement of the electron magnetic moment and the fine structure constant*, *Physical Review Letters* **100** (Mar, 2008) .

[20] F. Jegerlehner, *The Anomalous Magnetic Moment of the Muon, Second Edition*, *Springer Tracts Mod. Phys.* **274** (2017) pp.1–693.

[21] T. Aoyama, T. Kinoshita and M. Nio, *Theory of the Anomalous Magnetic Moment of the Electron*, *Atoms* **7** (2019) 28.

[22] R. H. Parker, C. Yu, W. Zhong, B. Estey and H. Müller, *Measurement of the fine-structure constant as a test of the Standard Model*, *Science* **360** (2018) 191, [1812.04130].

[23] L. Morel, Z. Yao, P. Cladé and S. Guellati-Khélifa, *Determination of the fine-structure constant with an accuracy of 81 parts per trillion*, *Nature* **588** (2020) 61–65.

[24] OPAL collaboration, K. Ackerstaff et al., *An Upper limit on the anomalous magnetic moment of the tau lepton*, *Phys. Lett. B* **431** (1998) 188–198, [hep-ex/9803020].

[25] L3 collaboration, M. Acciarri et al., *Measurement of the anomalous magnetic and electric dipole moments of the tau lepton*, *Phys. Lett. B* **434** (1998) 169–179.

[26] W. Lohmann, *Electromagnetic and weak moments of the tau-lepton*, *Nucl. Phys. B Proc. Suppl.* **144** (2005) 122–127, [hep-ex/0501065].

[27] J. S. Schwinger, *On Quantum electrodynamics and the magnetic moment of the electron*, *Phys. Rev.* **73** (1948) 416–417.

[28] T. Aoyama, M. Hayakawa, T. Kinoshita and M. Nio, *Complete Tenth-Order QED Contribution to the Muon g-2*, *Phys. Rev. Lett.* **109** (2012) 111808, [1205.5370].

[29] M. Davier, A. Hoecker, B. Malaescu and Z. Zhang, *Reevaluation of the hadronic vacuum polarisation contributions to the Standard Model predictions of the muon $g-2$ and $\alpha(m_Z^2)$ using newest hadronic cross-section data*, *Eur. Phys. J.* **C77** (2017) 827, [1706.09436].

[30] A. Keshavarzi, D. Nomura and T. Teubner, *Muon $g-2$ and $\alpha(M_Z^2)$: a new data-based analysis*, *Phys. Rev.* **D97** (2018) 114025, [1802.02995].

[31] G. Colangelo, M. Hoferichter and P. Stoffer, *Two-pion contribution to hadronic vacuum polarization*, *JHEP* **02** (2019) 006, [1810.00007].

[32] M. Hoferichter, B.-L. Hoid and B. Kubis, *Three-pion contribution to hadronic vacuum polarization*, *JHEP* **08** (2019) 137, [1907.01556].

[33] M. Davier, A. Hoecker, B. Malaescu and Z. Zhang, *A new evaluation of the hadronic vacuum polarisation contributions to the muon anomalous magnetic moment and to $\alpha(m_Z^2)$*, *Eur. Phys. J. C* **80** (2020) 241, [1908.00921].

[34] A. Keshavarzi, D. Nomura and T. Teubner, *$g-2$ of charged leptons, $\alpha(M_Z^2)$, and the hyperfine splitting of muonium*, *Phys. Rev. D* **101** (2020) 014029, [1911.00367].

[35] A. Kurz, T. Liu, P. Marquard and M. Steinhauser, *Hadronic contribution to the muon anomalous magnetic moment to next-to-next-to-leading order*, *Phys. Lett.* **B734** (2014) 144–147, [1403.6400].

[36] A. Nyffeler, *Hadronic light-by-light scattering in the muon $g-2$*, *EPJ Web Conf.* **218** (2019) 01001, [1710.09742].

[37] P. Masjuan and P. Sanchez-Puertas, *Pseudoscalar-pole contribution to the $(g_\mu-2)$: a rational approach*, *Phys. Rev.* **D95** (2017) 054026, [1701.05829].

[38] M. Hoferichter, B.-L. Hoid, B. Kubis, S. Leupold and S. P. Schneider, *Dispersion relation for hadronic light-by-light scattering: pion pole*, *JHEP* **10** (2018) 141, [1808.04823].

[39] A. Gérardin, H. B. Meyer and A. Nyffeler, *Lattice calculation of the pion transition form factor with $N_f = 2 + 1$ Wilson quarks*, *Phys. Rev. D* **100** (2019) 034520, [1903.09471].

[40] G. Colangelo, M. Hoferichter, M. Procura and P. Stoffer, *Dispersion relation for hadronic light-by-light scattering: two-pion contributions*, *JHEP* **04** (2017) 161, [1702.07347].

[41] V. Pauk and M. Vanderhaeghen, *Single meson contributions to the muon's anomalous magnetic moment*, *Eur. Phys. J.* **C74** (2014) 3008, [1401.0832].

[42] I. Danilkin and M. Vanderhaeghen, *Light-by-light scattering sum rules in light of new data*, *Phys. Rev. D* **95** (2017) 014019, [1611.04646].

[43] M. Knecht, S. Narison, A. Rabemananjara and D. Rabetiarivony, *Scalar meson contributions to a μ from hadronic light-by-light scattering*, *Phys. Lett. B* **787** (2018) 111–123, [1808.03848].

[44] G. Eichmann, C. S. Fischer and R. Williams, *Kaon-box contribution to the anomalous magnetic moment of the muon*, *Phys. Rev. D* **101** (2020) 054015, [1910.06795].

[45] P. Roig and P. Sanchez-Puertas, *Axial-vector exchange contribution to the hadronic light-by-light piece of the muon anomalous magnetic moment*, *Phys. Rev. D* **101** (2020) 074019, [1910.02881].

[46] K. Melnikov and A. Vainshtein, *Hadronic light-by-light scattering contribution to the muon anomalous magnetic moment revisited*, *Phys. Rev.* **D70** (2004) 113006, [hep-ph/0312226].

[47] J. Bijnens, N. Hermansson-Truedsson and A. Rodríguez-Sánchez, *Short-distance constraints for the HLbL contribution to the muon anomalous magnetic moment*, *Phys. Lett. B* **798** (2019) 134994, [1908.03331].

[48] G. Colangelo, F. Hagelstein, M. Hoferichter, L. Laub and P. Stoffer, *Longitudinal short-distance constraints for the hadronic light-by-light contribution to $(g-2)_\mu$ with large-N_c Regge models*, *JHEP* **03** (2020) 101, [1910.13432].

[49] G. Colangelo, M. Hoferichter, A. Nyffeler, M. Passera and P. Stoffer, *Remarks on higher-order hadronic corrections to the muon $g-2$*, *Phys. Lett.* **B735** (2014) 90–91, [1403.7512].

[50] T. Blum, N. Christ, M. Hayakawa, T. Izubuchi, L. Jin, C. Jung et al., *Hadronic Light-by-Light Scattering Contribution to the Muon Anomalous Magnetic Moment from Lattice QCD*, *Phys. Rev. Lett.* **124** (2020) 132002, [1911.08123].

[51] W. A. Bardeen and W. K. Tung, *Invariant amplitudes for photon processes*, *Phys. Rev.* **173** (1968) 1423–1433.

[52] R. Tarrach, *Invariant Amplitudes for Virtual Compton Scattering Off Polarized Nucleons Free from Kinematical Singularities, Zeros and Constraints*, *Nuovo Cim. A* **28** (1975) 409.

[53] G. Colangelo, M. Hoferichter, M. Procura and P. Stoffer, *Dispersion relation for hadronic light-by-light scattering: theoretical foundations*, *JHEP* **09** (2015) 074, [1506.01386].

[54] M. Hoferichter and P. Stoffer, *Asymptotic behavior of meson transition form factors*, *JHEP* **05** (2020) 159, [2004.06127].

[55] V. A. Nesterenko and A. V. Radyushkin, *Comparison of the QCD Sum Rule Approach and Perturbative QCD Analysis for $\gamma^*\gamma^* \to \pi^0$ Process*, *Sov. J. Nucl. Phys.* **38** (1983) 284.

[56] V. A. Novikov, M. A. Shifman, A. I. Vainshtein, M. B. Voloshin and V. I. Zakharov, *Use and Misuse of QCD Sum Rules, Factorization and Related Topics*, *Nucl. Phys. B* **237** (1984) 525–552.

[57] S. J. Brodsky and G. P. Lepage, *Large-Angle Two-Photon Exclusive Channels in Quantum Chromodynamics*, *Phys. Rev.* **D24** (1981) 1808.

[58] G. P. Lepage and S. J. Brodsky, *Exclusive Processes in Quantum Chromodynamics: Evolution Equations for Hadronic Wave Functions and the Form-Factors of Mesons*, *Phys. Lett.* **87B** (1979) 359–365.

[59] G. P. Lepage and S. J. Brodsky, *Exclusive Processes in Perturbative Quantum Chromodynamics*, *Phys. Rev.* **D22** (1980) 2157.

[60] G. Colangelo, F. Hagelstein, M. Hoferichter, L. Laub and P. Stoffer, *Short-distance constraints on hadronic light-by-light scattering in the*

anomalous magnetic moment of the muon, *Phys. Rev. D* **101** (2020) 051501, [1910.11881].

[61] L. Cappiello, O. Catà, G. D'Ambrosio, D. Greynat and A. Iyer, *Axial-vector and pseudoscalar mesons in the hadronic light-by-light contribution to the muon* $(g-2)$, *Phys. Rev. D* **102** (2020) 016009, [1912.02779].

[62] A. Czarnecki, W. J. Marciano and A. Vainshtein, *Refinements in electroweak contributions to the muon anomalous magnetic moment*, *Phys. Rev.* **D67** (2003) 073006, [hep-ph/0212229].

[63] C. Gnendiger, D. Stöckinger and H. Stöckinger-Kim, *The electroweak contributions to* $(g-2)_\mu$ *after the Higgs boson mass measurement*, *Phys. Rev.* **D88** (2013) 053005, [1306.5546].

[64] MUON G-2 collaboration, G. Bennett et al., *Final Report of the Muon E821 Anomalous Magnetic Moment Measurement at BNL*, *Phys. Rev. D* **73** (2006) 072003, [hep-ex/0602035].

[65] E. Witten, *Anti-de Sitter space and holography*, *Adv. Theor. Math. Phys.* **2** (1998) 253–291, [hep-th/9802150].

[66] S. S. Gubser, I. R. Klebanov and A. M. Polyakov, *Gauge theory correlators from noncritical string theory*, *Phys. Lett. B* **428** (1998) 105–114, [hep-th/9802109].

[67] M. Ammon and J. Erdmenger, *Gauge/gravity duality: Foundations and applications*. Cambridge University Press, Cambridge, 4, 2015.

[68] Y. Kim and D. Yi, *Holography at work for nuclear and hadron physics*, *Adv. High Energy Phys.* **2011** (2011) 259025, [1107.0155].

[69] J. Polchinski, *String theory. Vol. 2: Superstring theory and beyond*, .

[70] M. Kruczenski, D. Mateos, R. C. Myers and D. J. Winters, *Towards a holographic dual of large* N_c *QCD*, *JHEP* **0405** (2004) 041, [hep-th/0311270].

[71] T. Imoto, T. Sakai and S. Sugimoto, *Mesons as Open Strings in a Holographic Dual of QCD*, *Prog.Theor.Phys.* **124** (2010) 263–284, [1005.0655].

[72] F. Brünner, D. Parganlija and A. Rebhan, *Glueball Decay Rates in the Witten-Sakai-Sugimoto Model*, *Phys. Rev.* **D91** (2015) 106002, [1501.07906].

[73] G. S. Bali, F. Bursa, L. Castagnini, S. Collins, L. Del Debbio et al., *Mesons in large-N QCD*, *JHEP* **1306** (2013) 071, [1304.4437].

[74] Particle Data Group collaboration, K. Olive et al., *Review of Particle Physics*, *Chin.Phys.* **C38** (2014) 090001 and 2015 update.

[75] M. Gell-Mann and F. Zachariasen, *Form-factors and vector mesons*, *Phys. Rev.* **124** (1961) 953–964.

[76] J. J. Sakurai, *Currents and Mesons*, *University of Chicago Press, Chicago, 1969* .

[77] L. Da Rold and A. Pomarol, *Chiral symmetry breaking from five-dimensional spaces*, *Nucl. Phys.* **B721** (2005) 79–97, [hep-ph/0501218].

[78] H. R. Grigoryan and A. V. Radyushkin, *Structure of vector mesons in holographic model with linear confinement*, *Phys. Rev.* **D76** (2007) 095007, [0706.1543].

[79] H. R. Grigoryan and A. V. Radyushkin, *Anomalous Form Factor of the Neutral Pion in Extended AdS/QCD Model with Chern-Simons Term*, *Phys. Rev.* **D77** (2008) 115024, [0803.1143].

[80] Z. Abidin and C. E. Carlson, *Strange hadrons and kaon-to-pion transition form factors from holography*, *Phys. Rev. D* **80** (2009) 115010, [0908.2452].

[81] M. A. Shifman, A. I. Vainshtein and V. I. Zakharov, *QCD and Resonance Physics. Theoretical Foundations*, *Nucl. Phys. B* **147** (1979) 385–447.

[82] H. J. Kwee and R. F. Lebed, *Pion form-factors in holographic QCD*, *JHEP* **01** (2008) 027, [0708.4054].

[83] O. Domènech, G. Panico and A. Wulzer, *Massive Pions, Anomalies and Baryons in Holographic QCD*, *Nucl. Phys. A* **853** (2011) 97–123, [1009.0711].

[84] Particle Data Group collaboration, S. Eidelman et al., *Review of particle physics. Particle Data Group*, *Phys. Lett. B* **592** (2004) 1.

[85] J. F. Donoghue, E. Golowich and B. R. Holstein, *Dynamics of the standard model*, vol. 2. CUP, 2014, 10.1017/CBO9780511524370.

[86] D. T. Son and M. A. Stephanov, *QCD and dimensional deconstruction*, *Phys. Rev. D* **69** (2004) 065020, [hep-ph/0304182].

[87] N. Isgur, C. Morningstar and C. Reader, *The a1 in tau Decay*, *Phys. Rev. D* **39** (1989) 1357.

[88] A. Pich, *Effective field theory: Course*, in *Les Houches Summer School in Theoretical Physics, Session 68: Probing the Standard Model of Particle Interactions*, pp. 949–1049, 6, 1998, hep-ph/9806303.

[89] H. R. Grigoryan and A. V. Radyushkin, *Pion form-factor in chiral limit of hard-wall AdS/QCD model*, *Phys. Rev.* **D76** (2007) 115007, [0709.0500].

[90] L. Cappiello, O. Cata and G. D'Ambrosio, *The hadronic light by light contribution to the $(g-2)_\mu$ with holographic models of QCD*, *Phys. Rev.* **D83** (2011) 093006, [1009.1161].

[91] H. J. Kwee and R. F. Lebed, *Pion Form Factor in Improved Holographic QCD Backgrounds*, *Phys. Rev. D* **77** (2008) 115007, [0712.1811].

[92] M. Tanabashi et al., *Review of Particle Physics*, *Phys. Rev. D* **98** (2018) 030001.

[93] I. Danilkin, C. F. Redmer and M. Vanderhaeghen, *The hadronic light-by-light contribution to the muon's anomalous magnetic moment*, *Prog. Part. Nucl. Phys.* **107** (2019) 20–68, [1901.10346].

[94] A. Nyffeler, *Precision of a data-driven estimate of hadronic light-by-light scattering in the muon $g-2$: Pseudoscalar-pole contribution*, *Phys. Rev.* **D94** (2016) 053006, [1602.03398].

[95] H. R. Grigoryan and A. V. Radyushkin, *Pion in the Holographic Model with 5D Yang-Mills Fields*, *Phys. Rev.* **D78** (2008) 115008, [0808.1243].

[96] A. Stoffers and I. Zahed, *$\gamma^*\gamma^* \to \pi^0$ Form Factor from AdS/QCD*, *Phys. Rev.* **C84** (2011) 025202, [1104.2081].

[97] CELLO collaboration, H. J. Behrend et al., *A Measurement of the π^0, η and η' electromagnetic form-factors*, *Z. Phys.* **C49** (1991) 401–410.

[98] NA62 collaboration, C. Lazzeroni et al., *Measurement of the π^0 electromagnetic transition form factor slope*, *Phys. Lett.* **B768** (2017) 38–45, [1612.08162].

[99] A. V. Efremov and A. V. Radyushkin, *Factorization and Asymptotical Behavior of Pion Form-Factor in QCD*, *Phys. Lett.* **94B** (1980) 245–250.

[100] BABAR collaboration, J. P. Lees et al., *Measurement of the $\gamma^*\gamma^* \to \eta'$ transition form factor*, *Phys. Rev.* **D98** (2018) 112002, [1808.08038].

[101] M. Knecht and A. Nyffeler, *Hadronic light by light corrections to the muon $g-2$: The Pion pole contribution*, *Phys. Rev.* **D65** (2002) 073034, [hep-ph/0111058].

[102] L. D. Landau, *On the angular momentum of a system of two photons*, *Dokl. Akad. Nauk Ser. Fiz.* **60** (1948) 207–209.

[103] C.-N. Yang, *Selection Rules for the Dematerialization of a Particle Into Two Photons*, *Phys. Rev.* **77** (1950) 242–245.

[104] L3 collaboration, P. Achard et al., *$f_1(1285)$ formation in two-photon collisions at LEP*, *Phys. Lett.* **B526** (2002) 269–277, [hep-ex/0110073].

[105] L3 collaboration, P. Achard et al., *Study of resonance formation in the mass region 1400 – 1500 MeV through the reaction $\gamma\gamma \to K^0_S K^\pm \pi^\mp$*, *JHEP* **03** (2007) 018.

[106] G. A. Schuler, F. A. Berends and R. van Gulik, *Meson photon transition form-factors and resonance cross-sections in e^+e^- collisions*, *Nucl. Phys.* **B523** (1998) 423–438, [hep-ph/9710462].

[107] V. Pascalutsa, V. Pauk and M. Vanderhaeghen, *Light-by-light scattering sum rules constraining meson transition form factors*, *Phys. Rev.* **D85** (2012) 116001, [1204.0740].

[108] LHCb collaboration, R. Aaij et al., *Observation of $\bar{B}_{(s)} \to J/\psi f_1(1285)$ Decays and Measurement of the $f_1(1285)$ Mixing Angle*, *Phys. Rev. Lett.* **112** (2014) 091802, [1310.2145].

[109] J. J. Dudek, R. G. Edwards, B. Joo, M. J. Peardon, D. G. Richards and C. E. Thomas, *Isoscalar meson spectroscopy from lattice QCD*, *Phys. Rev.* **D83** (2011) 111502, [1102.4299].

[110] H.-Y. Cheng, *Revisiting Axial-Vector Meson Mixing*, *Phys. Lett.* **B707** (2012) 116–120, [1110.2249].

[111] M. Zanke, M. Hoferichter and B. Kubis, *On the transition form factors of the axial-vector resonance $f_1(1285)$ and its decay into e^+e^-*, *JHEP* **07** (2021) 106, [2103.09829].

[112] K.-C. Yang, *Light-cone distribution amplitudes of axial-vector mesons*, *Nucl. Phys. B* **776** (2007) 187–257, [0705.0692].

[113] P. A. Zyla et al., *Review of Particle Physics*, *Prog. Theor. Exp. Phys.* **2020** (2020) 083C01.

[114] K. Maltman and J. Kambor, *Decay constants, light quark masses and quark mass bounds from light quark pseudoscalar sum rules*, *Phys. Rev. D* **65** (2002) 074013, [hep-ph/0108227].

[115] B. Melic, D. Mueller and K. Passek-Kumericki, *Next-to-next-to-leading prediction for the photon to pion transition form-factor*, *Phys. Rev.* **D68** (2003) 014013, [hep-ph/0212346].

[116] J. Bijnens, N. Hermansson-Truedsson, L. Laub and A. Rodríguez-Sánchez, *The two-loop perturbative correction to the $(g-2)_\mu$ HLbL at short distances*, *JHEP* **04** (2021) 240, [2101.09169].

[117] J. Lüdtke and M. Procura, *Effects of longitudinal short-distance constraints on the hadronic light-by-light contribution to the muon $g-2$*, *Eur. Phys. J. C* **80** (2020) 1108, [2006.00007].

[118] G. Colangelo, F. Hagelstein, M. Hoferichter, L. Laub and P. Stoffer, *Short-distance constraints for the longitudinal component of the hadronic light-by-light amplitude: an update*, *Eur. Phys. J. C* **81** (2021) 702, [2106.13222].

[119] L. Cappiello, O. Catà and G. D'Ambrosio, *Scalar resonances in the hadronic light-by-light contribution to the muon $(g-2)$*, 2110.05962.

[120] D. K. Hong, D. Kim and S. Matsuzaki, *Holographic calculation of hadronic contributions to muon g-2*, *Phys. Rev. D* **81** (2010) 073005, [0911.0560].

[121] M. Stadlbauer, *Leading order HVP Contributions to the Anomalous Magnetic Moment of the Muon from Holographic QCD*, Master's thesis, TU Wien, 2020.

[122] J. Leutgeb, A. Rebhan and M. Stadlbauer, "Hadronic vacuum polarization contribution to the muon $g-2$ in holographic QCD." in preparation.

[123] H. Fritzsch and M. Gell-Mann, *Current algebra: Quarks and what else?*, *eConf* **C720906V2** (1972) 135–165, [hep-ph/0208010].

[124] H. Fritzsch and P. Minkowski, *Ψ Resonances, Gluons and the Zweig Rule*, *Nuovo Cim.* **A30** (1975) 393.

[125] R. Jaffe and K. Johnson, *Unconventional States of Confined Quarks and Gluons*, *Phys.Lett.* **B60** (1976) 201.

[126] A. M. Jaffe and E. Witten, *Quantum Yang-Mills theory*, .

[127] U. Wiedner, *Future Prospects for Hadron Physics at PANDA*, *Prog.Part.Nucl.Phys.* **66** (2011) 477–518, [1104.3961].

[128] F. Hechenberger, J. Leutgeb and A. Rebhan, "Radiative glueball decays." in preparation.

[129] R. C. Brower, S. D. Mathur and C.-I. Tan, *Glueball spectrum for QCD from AdS supergravity duality*, *Nucl.Phys.* **B587** (2000) 249–276, [hep-th/0003115].

[130] C. J. Morningstar and M. J. Peardon, *The Glueball spectrum from an anisotropic lattice study*, *Phys.Rev.* **D60** (1999) 034509, [hep-lat/9901004].

[131] N. R. Constable and R. C. Myers, *Spin-two glueballs, positive energy theorems and the AdS/CFT correspondence*, *JHEP* **9910** (1999) 037, [hep-th/9908175].

[132] C. Amsler and F. E. Close, *Is $f_0(1500)$ a scalar glueball?*, *Phys.Rev.* **D53** (1996) 295–311, [hep-ph/9507326].

[133] W.-J. Lee and D. Weingarten, *Scalar quarkonium masses and mixing with the lightest scalar glueball*, *Phys.Rev.* **D61** (1999) 014015, [hep-lat/9910008].

[134] F. E. Close and A. Kirk, *Scalar glueball $q\bar{q}$ mixing above 1 GeV and implications for lattice QCD*, *Eur.Phys.J.* **C21** (2001) 531–543, [hep-ph/0103173].

[135] C. Amsler and N. Törnqvist, *Mesons beyond the naive quark model*, *Phys.Rept.* **389** (2004) 61–117.

[136] F. E. Close and Q. Zhao, *Production of $f_0(1710)$, $f_0(1500)$, and $f_0(1370)$ in J/ψ hadronic decays*, *Phys.Rev.* **D71** (2005) 094022, [hep-ph/0504043].

[137] F. Giacosa, T. Gutsche, V. Lyubovitskij and A. Faessler, *Scalar nonet quarkonia and the scalar glueball: Mixing and decays in an effective chiral approach*, *Phys.Rev.* **D72** (2005) 094006, [hep-ph/0509247].

[138] M. Albaladejo and J. Oller, *Identification of a Scalar Glueball*, *Phys.Rev.Lett.* **101** (2008) 252002, [0801.4929].

[139] V. Mathieu, N. Kochelev and V. Vento, *The Physics of Glueballs*, *Int.J.Mod.Phys.* **E18** (2009) 1–49, [0810.4453].

[140] S. Janowski, F. Giacosa and D. H. Rischke, *Is $f_0(1710)$ a glueball?*, *Phys.Rev.* **D90** (2014) 114005, [1408.4921].

[141] H.-Y. Cheng, C.-K. Chua and K.-F. Liu, *Revisiting Scalar Glueballs*, *Phys. Rev.* **D92** (2015) 094006, [1503.06827].

[142] J.-M. Frère and J. Heeck, *Scalar glueballs: Constraints from the decays into η or η'*, *Phys. Rev.* **D92** (2015) 114035, [1506.04766].

[143] F. Brünner and A. Rebhan, *Nonchiral enhancement of scalar glueball decay in the Witten-Sakai-Sugimoto model*, *Phys. Rev. Lett.* **115** (2015) 131601, [1504.05815].

[144] F. Brünner and A. Rebhan, *Constraints on the $\eta\eta'$ decay rate of a scalar glueball from gauge/gravity duality*, *Phys. Rev.* **D92** (2015) 121902, [1510.07605].

[145] E. Klempt and A. Zaitsev, *Glueballs, Hybrids, Multiquarks. Experimental facts versus QCD inspired concepts*, *Phys.Rept.* **454** (2007) 1–202, [0708.4016].

[146] V. Crede and C. Meyer, *The Experimental Status of Glueballs*, *Prog.Part.Nucl.Phys.* **63** (2009) 74–116, [0812.0600].

[147] F. Brünner and A. Rebhan, *Holographic QCD predictions for production and decay of pseudoscalar glueballs*, *Phys. Lett.* **B770** (2017) 124–130, [1610.10034].

[148] S. Weinberg, *The U(1) Problem*, *Phys. Rev. D* **11** (1975) 3583–3593.

[149] G. 't Hooft, *Symmetry Breaking Through Bell-Jackiw Anomalies*, *Phys. Rev. Lett.* **37** (1976) 8–11.

[150] G. 't Hooft, *How Instantons Solve the U(1) Problem*, *Phys. Rept.* **142** (1986) 357–387.

[151] G. Veneziano, *U(1) Without Instantons*, *Nucl.Phys.* **B159** (1979) 213–224.

[152] E. Witten, *Current Algebra Theorems for the U(1) "Goldstone Boson"*, *Nucl.Phys.* **B156** (1979) 269.

[153] J. L. Barbon, C. Hoyos-Badajoz, D. Mateos and R. C. Myers, *The Holographic life of the η'*, *JHEP* **0410** (2004) 029, [hep-th/0404260].

[154] L. Bartolini, F. Bigazzi, S. Bolognesi, A. L. Cotrone and A. Manenti, *Theta dependence in Holographic QCD*, *JHEP* **02** (2017) 029, [1611.00048].

[155] P. Horava and E. Witten, *Eleven-dimensional supergravity on a manifold with boundary*, *Nucl. Phys. B* **475** (1996) 94–114, [hep-th/9603142].

[156] F. E. Close and N. A. Tornqvist, *Scalar mesons above and below 1-GeV*, *J. Phys. G* **28** (2002) R249–R267, [hep-ph/0204205].

[157] D. Bugg, *Four sorts of meson*, *Phys.Rept.* **397** (2004) 257–358, [hep-ex/0412045].

[158] Belle collaboration, S. Uehara et al., *High-statistics study of K^0_S pair production in two-photon collisions*, *PTEP* **2013** (2013) 123C01, [1307.7457].

[159] Particle Data Group collaboration, P. A. Zyla et al., *Review of Particle Physics*, *PTEP* **2020** (2020) 083C01.

[160] J. Polchinski, *String Theory: Volume 2, Superstring Theory and Beyond -*. Cambridge University Press, Cambridge, 1998.

[161] K. Becker, M. Becker and J. Schwarz, *String theory and M-theory: A modern introduction*, .

[162] C. Ewerz, M. Maniatis and O. Nachtmann, *A Model for Soft High-Energy Scattering: Tensor Pomeron and Vector Odderon*, *Annals Phys.* **342** (2014) 31–77, [1309.3478].

[163] P. Lebiedowicz, O. Nachtmann and A. Szczurek, *Exclusive central diffractive production of scalar and pseudoscalar mesons tensorial vs. vectorial pomeron*, *Annals Phys.* **344** (2014) 301–339, [1309.3913].

[164] P. Lebiedowicz, O. Nachtmann and A. Szczurek, *Central exclusive diffractive production of $\pi^+\pi^-$ continuum, scalar and tensor resonances in pp and $p\bar{p}$ scattering within tensor pomeron approach*, *Phys. Rev. D* **93** (2016) 054015, [1601.04537].

[165] P. Lebiedowicz, O. Nachtmann and A. Szczurek, *Searching for the odderon in $pp \to ppK^+K^-$ and $pp \to pp\mu^+\mu^-$ reactions in the $\phi(1020)$ resonance region at the LHC*, *Phys. Rev. D* **101** (2020) 094012, [1911.01909].

[166] S. Donnachie, H. G. Dosch, O. Nachtmann and P. Landshoff, *Pomeron physics and QCD*, vol. 19. Cambridge University Press, 12, 2004.

[167] P. Lebiedowicz, O. Nachtmann and A. Szczurek, *Towards a complete study of central exclusive production of K^+K^- pairs in proton-proton collisions within the tensor Pomeron approach*, *Phys. Rev. D* **98** (2018) 014001, [1804.04706].

[168] P. Lebiedowicz, O. Nachtmann and A. Szczurek, *Exclusive diffractive production of $\pi^+\pi^-\pi^+\pi^-$ via the intermediate $\sigma\sigma$ and $\rho\rho$ states in proton-proton collisions within tensor pomeron approach*, *Phys. Rev. D* **94** (2016) 034017, [1606.05126].

[169] P. Lebiedowicz, O. Nachtmann and A. Szczurek, *Central exclusive diffractive production of $p\bar{p}$ pairs in proton-proton collisions at high energies*, Phys. Rev. D **97** (2018) 094027, [1801.03902].

[170] P. Lebiedowicz, O. Nachtmann and A. Szczurek, *Central exclusive diffractive production of $K^+K^-K^+K^-$ via the intermediate $\phi\phi$ state in proton-proton collisions*, Phys. Rev. D **99** (2019) 094034, [1901.11490].

[171] P. Lebiedowicz, O. Nachtmann and A. Szczurek, *Extracting the pomeron-pomeron-$f_2(1270)$ coupling in the $pp \to pp\pi^+\pi^-$ reaction through angular distributions of the pions*, Phys. Rev. D **101** (2020) 034008, [1901.07788].

[172] N. Anderson, S. K. Domokos, J. A. Harvey and N. Mann, *Central production of η and η' via double Pomeron exchange in the Sakai-Sugimoto model*, Phys. Rev. **D90** (2014) 086010, [1406.7010].

[173] WA102 collaboration, D. Barberis et al., *A Measurement of the branching fractions of the f(1)(1285) and f(1)(1420) produced in central p p interactions at 450-GeV/c*, Phys. Lett. B **440** (1998) 225–232, [hep-ex/9810003].

[174] STAR collaboration, J. Adam et al., *Measurement of the central exclusive production of charged particle pairs in proton-proton collisions at $\sqrt{s} = 200$ GeV with the STAR detector at RHIC*, JHEP **07** (2020) 178, [2004.11078].

[175] M. B. Green, J. A. Harvey and G. W. Moore, *I-brane inflow and anomalous couplings on D-branes*, Class. Quant. Grav. **14** (1997) 47–52, [hep-th/9605033].

[176] O. Aharony and D. Kutasov, *Holographic Duals of Long Open Strings*, Phys.Rev. **D78** (2008) 026005, [0803.3547].

[177] K. Hashimoto, T. Hirayama, F.-L. Lin and H.-U. Yee, *Quark Mass Deformation of Holographic Massless QCD*, JHEP **0807** (2008) 089, [0803.4192].

[178] R. McNees, R. C. Myers and A. Sinha, *On quark masses in holographic QCD*, JHEP **0811** (2008) 056, [0807.5127].

[179] C. Amsler, *Nuclear and particle physics*. IOPP, 2015.